Methane Emissions and Isotopes of Northern Peatlands in a Global Vegetation Model

Inauguraldissertation

der Philosophisch–naturwissenschaftlichen Fakultät
der Universität Bern

vorgelegt von

Sibylle Zürcher

aus Trubschachen (BE)

Leiter der Arbeit:

Prof. Dr. Fortunat Joos
Prof. Dr. Hubertus Fischer

Abteilung für Klima– und Umweltphysik
Physikalisches Institut der Universität Bern

Methane Emissions and Isotopes of Northern Peatlands in a Global Vegetation Model

Inauguraldissertation

der Philosophisch–naturwissenschaftlichen Fakultät
der Universität Bern

vorgelegt von

Sibylle Zürcher

aus Trubschachen (BE)

Leiter der Arbeit:

Prof. Dr. Fortunat Joos
Prof. Dr. Hubertus Fischer

Abteilung für Klima– und Umweltphysik
Physikalisches Institut der Universität Bern

Von der Philosophisch–naturwissenschaftlichen Fakultät angenommen.

Bern, 19. September 2013

Der Dekan
Prof. Dr. Silvio Decurtins

„The fewer the facts, the stronger the opinion.“

(Arnold H. Glasow)

Contents

List of Figures

List of Tables

Thesis Summary

Methane is, after water vapor and carbon dioxide, the third most potent greenhouse gas in the atmosphere at present. Its concentration has strongly increased in the 20th century and reached a concentration exceeding any value ever measured over the last 800'000 years. For the effort to mitigate climate change, it is important to understand the dynamics leading to the atmospheric methane concentration. The atmospheric methane level is a balance between sources and sinks. While the present global total source and sink are relatively well known, the partition between the different contributors is not well understood. To be able to predict future CH_4 atmospheric levels it is important to understand the size of the different CH_4 sources and sinks and their reaction to climate change. As current observations are limited or only cover a small time window of climate and environmental change, past ice core observations in CH_4 and $\delta^{13}CH_4$ are of great value to validate models. Global wetlands are the largest natural emitters and very climate sensitive. Their feedback to a future warming is believed to be positive. Therefore, it is among many other things important to improve the process-based modelling of northern peatlands that are an important part of wetlands and a source of methane with a considerable uncertainty, variability and sensibility to climate change. Taking the isotopic composition of a source into account provides a further constraint in this difficult task. This thesis contributes to the effort of understanding the methane cycle by improving and enhancing a methane model embedded in a dynamic global vegetation model and by newly implementing and calibrating a methane isotope routine into this model framework.

This thesis is structured along 5 major chapters, while an outlook at the end of this thesis highlights research challenges and further topics to be addressed in future work.

Chapter 1 provides an introduction giving some general information about the global methane budget in the past and present, an overview on the important sources and sinks, and details on the role of wetlands and in particular peatlands. The processes leading to methane emissions in peatlands are discussed, as well as the importance of methane isotopes. The required notations are introduced as well.

In Chapter 2 an introduction to climate modelling is provided. Further, the model used in this thesis is presented in detail with a special focus on its methane routine and the implemented isotopes. At the end of the Chapter, site simulations are discussed in detail to illustrate the implemented mechanisms and explain the produced output like the methane emissions, isotopic signature or the soil profile. Note that for the simulations done during this thesis, two different versions of the model were used which are discussed separately. A first development step was to implement, improve and calibrate the methane module WHyMe (developed by R. Wania in Bristol) into Bern-LPJ. Bern-LPJ is a dynamic global vegetation model that simulates plant distribution and carbon stocks and flows. Methane isotopes were missing at that point. The simulations in the peer reviewed studies presented in Chapter 3, 4.1 and 4.2 were conducted with this model version (LPJ-Bern). A second version (called LPX) with general model improvements outside the methane routine as well as in the methane routine itself

including the implementation of methane isotopes was used for the simulations discussed at the end of Chapter 2 and in Chapter 5.

Chapter 3 presents a model application in a study about the impact of an abrupt cooling event on methane emissions in northern peatlands. Rapid changes in temperature and precipitation are paralleled with substantial variations in atmospheric methane concentrations as documented in ice cores. Most studies attribute a change in methane concentrations to emission changes from boreal and sub-tropical wetlands and boreal peatlands are believed to be the dominant and most directly responding ecosystem. The calibration of the model with modern site data is described (this was redone for LPX and summarized in the Appendix). The results of the methane emission simulations in reaction to an abrupt climate change are presented including sensitivity test to model parameters and climate input data. The main result is that if the simulated changes in climate are taken as an analogy to the 8.2 kyr event, boreal peatland emissions alone can only explain about 23% of the 80 ppb decline in atmospheric methane concentrations.

Chapter 4.1 shows the results of a model inter-comparison project (WETCHIMP) where the present ability to simulate wetland extend, characteristics and corresponding methane emissions is investigated. LPJ-Bern was one of ten models taking part in the comparison. A common experimental protocol was used to drive all models with the same climate forcings. Chapter 4.2 is the follow-up paper to the WETCHIMP paper and provides technical details for the six experiments that were conducted and about the models that took part in the study. The major conclusion is that the models demonstrate a great disagreement in their simulations of the wetland areal extend and methane emissions in space and time and it is stressed that we presently do not have sufficient wetland methane observations to evaluate model fluxes.

Chapter 5 presents applications of the implemented isotope routine. NH peatland runs for present day were performed and discussed. The sensitivity of the isotopic signature of methane emissions to the different plant types simulated in the peatland area are investigated as well as to input parameters like temperature or precipitation. Further, the correlation between the emitted signature and model parameters are investigated. The simulated emission signatures for present day are in the range of peatland methane emission measurements. Finally, a simulation of NH peatland methane emissions from the LGM till present was performed to assess the variability of $\delta^{13}CH_4$ and the possible contribution to the atmospheric signal during the Holocene.

Chapter 1

Introduction

1.1 Motivation

Methane (CH_4) is one of the most potent and influential greenhouse gases in the atmosphere at present. It traps heat by absorbing long wave radiation emitted from the ground and contributes ~20% (0.5 Wm^{-2}) to the total radiative forcing from all of the long-lived greenhouse gases (IPCC, 2007; Dlugokencky et al., 2011). Besides the direct effect, CH_4 also acts indirectly on Earth's temperature due to its chemical reactions, e.g. with the hydroxyl radical ·OH (~0.2 Wm^{-2}) (Dlugokencky et al., 2011; Hansen & Sato, 2001; Lelieveld et al., 1998).

Over the last 800 kyr, ice core records indicate that the abundance of CH_4 in the Earth's atmosphere fluctuated between lows of about 350 ppb during glacial periods to highs of about 750 ppb during interglacials (Loulergue et al., 2008; Spahni et al., 2005). Ongoing measurements show that the atmospheric CH_4 concentration has strongly increased during the 20th century (Fig. 1.1), reaching about 1800 ppb in 2008 (Dlugokencky et al., 2009; Forster et al., 2007), exceeding any of the peak concentrations during the past six glacial-interglacial cycles. In 2009-2011, the concentrations stayed almost constantly high at 1794 ±2 ppb (Kirschke et al., 2013) (Fig. 1.2).

Atmospheric CH_4 concentrations are a balance between CH_4 sources and sinks. The total global CH_4 source and sink is relatively well known but the strength of each source component and their trends are not (Forster et al., 2007). There are two different approaches to model CH_4 emissions for present day: bottom-up models that represent the processes leading to CH_4 emissions in a mechanistic way (e.g., Cao et al., 1996; Walter et al., 2001; Wania et al., 2010; Ringeval et al., 2010) and top-down or inverse models, which use observations of atmospheric CH_4 concentrations and transport models to quantify CH_4 emissions (e.g., Houweling et al., 1999; Pison et al., 2009; Bergamaschi et al., 2009). For past times, where no direct spatial monitoring is available, only bottom-up models can be applied. To better estimate the future level of atmospheric CH_4 it is - among other things - necessary to improve process-based modelling of the important CH_4 sources including their isotopic composition.

This chapter provides an introduction to the global CH_4 budget and the role that natural peatlands play within this budget. Further, background will be given about CH_4 emissions from natural peatland and their isotopic composition.

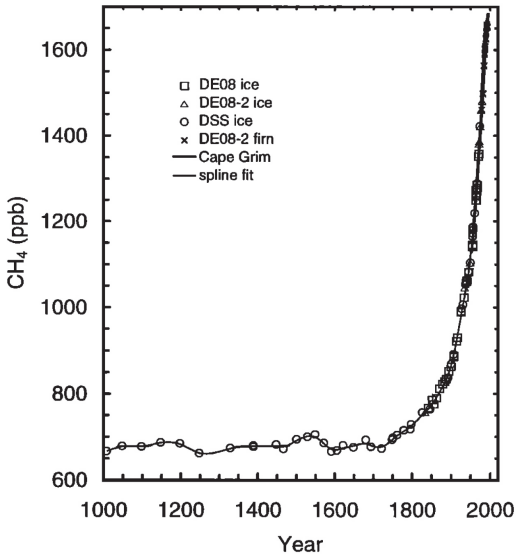

Figure 1.1: Atmospheric CH_4 concentration over the last 1000 years. Measurements overlap from recent atmospheric measurements (Cape Grim) via firn air (CE08-2 firn) to ice core samples from Law Dome (Etheridge et al., 1996).

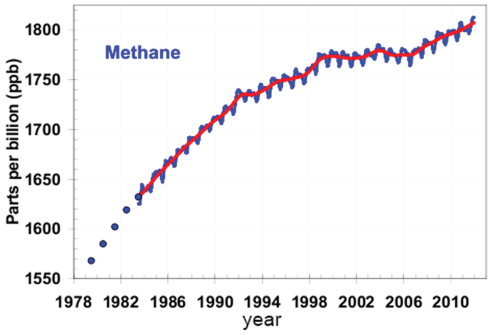

Figure 1.2: Rise of the atmospheric CH_4 concentrations from the Industrial Revolution till ∼2000 and stabilisation in the period 2000-2011 (NOAA global air sampling network).

1.2 Global methane budget

1.2.1 Present

CH_4 sources can be of anthropogenic and natural origin. The anthropogenic sources include rice agriculture, livestock, landfills and waste treatment, some biomass burning, and emissions related to fossil fuel exploration, distribution and combustion. Natural CH_4 is emitted from sources such as wetlands, forests, fire, termites and geological reservoirs. About half of the current CH_4 emissions are natural (40-51 %, see Fig. 1.3), while 49-60 % are anthropogenic (Kirschke et al., 2013).

Emissions of CH_4 from most of the biogenic sources involve ecosystem processes that result from complex sequences of events beginning with primary fermentation of organic macromolecules to acetic acid (CH_3COOH), other carboxylic acids, alcohols, CO_2 and hydrogen (H_2), followed by secondary fermentation of the alcohols and carboxylic acids to acetate, H_2 and CO_2, which are finally converted to CH_4 by the so-called methanogenic Archaea (Conrad, 1996). The two major pathways are acetate fermentation (eq. 1.1) and carbonate reduction (eq. 1.2):

$$CH_3COOH \rightarrow CH_4 + CO_2 \tag{1.1}$$

$$CO_2 + 4H_2 \rightarrow CH_4 + 2H_2O \tag{1.2}$$

Natural wetlands are the largest individual source, as well as the source with the largest uncertainty (Fig. 1.3). They are estimated to contribute 140 to 260 Tg CH_4 yr^{-1} to the annual global budget (Melton et al., 2013). Denman et al. (2007) estimate wetlands to contribute 15 to 40 % of the total present day source budget, Kirschke et al. (2013) estimate about 30 % in their synthesis of 9 inversion systems and 8 bottom-up models for wetland CH_4 emissions.

Sinks for CH_4 are the chemical oxidation in the troposphere (500 Tg CH_4 yr^{-1} or more, Denman et al., 2007), oxidation in aerated soils (30 Tg CH_4 yr^{-1}, Ridgwell et al., 1999; Curry,

2007) and loss to the stratosphere (40 Tg CH_4 yr^{-1}, Denman et al., 2007). Oxidation in the troposphere is by far the largest sink (∼90 %); CH_4 reacts with the hydroxyl radical (OH) and, after several intermediate reaction steps, ends up as either carbon monoxide or carbon dioxide (Lelieveld et al., 1998). The lifetime of CH_4 varies with the hydroxyl concentration in the troposphere. It is estimated to be 8.4 yr (Denman et al., 2007). Oxidation by chlorine atoms in the marine atmospheric boundary is suggested as an additional sink of possibly about 19 Tg CH_4 yr^{-1} (Denman et al., 2007). The chlorine sink varies seasonally with a minimum in the late summer mainly due to removal by the hydroxyl radical. The seasonal OH variation with minimum in winter can be related to annual and semiannual variations in ozone and water vapor, and to the annual variation in solar intensity due to the eccentricity of the Earth's orbit (Spivakovsky et al., 2000; Canty & Minschwander, 2002).

1.2.2 Past

Direct atmospheric measurements of CH_4 only started in 1978. But air enclosures in polar ice cores allow for the reconstruction of CH_4 variations in the past. They show that CH_4 has varied in synchrony with northern hemisphere temperature during glacial/interglacial transitions (Loulergue et al., 2008) as well as during rapid climate variations. Examples of abrupt variations are the 8.2 kyr event in the early Holocene (Blunier et al., 1995; Chappellaz et al., 1997; Spahni et al., 2003; Kobashi et al., 2007), the Dansgaard-Oeschger events (D-O-events) in the glacial period (Chappellaz et al., 1993; Brook et al., 2000; Blunier & Brook, 2001; Flückiger et al., 2004; Huber et al., 2006; Baumgartner et al., 2012) or the Younger Dryas (YD) cooling event (Chappellaz et al., 1993; Baumgartner et al., 2012). In warm interglacial or interstadial periods, atmospheric CH_4 concentration was high, while in cold glacial periods, atmospheric CH_4 concentration was low. The origin of atmospheric CH_4 variations is not completely clear. Most ice core studies attribute a change in CH_4 concentration in the past to a change in CH_4 emissions from both boreal and sub-tropical wet ecosystems (Chappellaz et al., 1997; Fischer et al., 2008). Part of the CH_4 concentration changes could also be explained by atmospheric sink changes. Sinks can modify the tropospheric CH_4 budget, as trace gases like volatile organic compounds are competing for the major reactant, the ·OH-radical. Additionally, the changing global atmospheric CH_4 concentration itself feeds back on its lifetime. For the period from the Last Glacial Maximum (LGM) to the pre-industrial era, the change in CH_4 is believed to be almost entirely source driven (Levine et al., 2011). Levine et al. (2011) examine with an atmospheric chemistry-transport model the main factors affecting OH during the LGM which is by far the greatest sink. These factors are assumed to depend only on air temperature and emissions of non-methane volatile organic compounds from vegetation. They find that their net effect is negligible, implying the change in CH_4 was almost entirely source driven. A concentration gradient with higher values in the northern hemisphere during warm stages was reconstructed from ice core data from Greenland and Antarctica. This gradient indicates stronger sources during warm periods located in the northern hemisphere (Baumgartner et al., 2012).

1.2.3 Future

The limitations of poorly quantified and characterised CH_4 source strengths inhibit the prediction of future CH_4 atmospheric concentrations (and hence its contribution to radiative forcing) for any given anthropogenic emission scenario, particularly since both natural emissions and the removal of CH_4 can be influenced substantially by climate change. Since CH_4 emissions from natural wetlands seem to play a key role in governing fluctuations of atmospheric CH_4 concentrations (Bousquet et al., 2006), it is important to improve the modelling

$TgCH_4/yr$	1980-89				1990-99				2000-09			
	Top-Down		Bottom-up		Top-Down		Bottom-up		Top-Down		Bottom-up	
Natural Sources	203	[150-267]	355	[229-451]	182	[167-197]	336	[215-450]	218	[179-273]	347	[223-469]
Natural Wetlands	167	[115-231][12,32,33]	225	[183-266][59,61]	150	[144-160][12,35,99]	206	[169-265][59,60,61]	175	[142-208][12,25,69,91,94,96,99]	217	[177-284][59,60,61]
Other Sources	36	[35-36][12,32,33]	130	[46-185]	32	[23-37][12,35,99]	130	[46-185]	43	[37-65][12,25,69,91,94,96,99]	130	[46-185]
Freshwater (lakes and rivers)			40	[8-73][46,57,90]			40	[8-73][46,57,90]			40	[8-73][46,57,90]
Wild animals			15	[-][36]			15	[-][36]			15	[-][36]
Wildfires			3	[1-5][36,66,93,95,97]			3	[1-5][36,66,93,95,97]			3	[1-5][36,66,93,95,97]
Termites			11	[2-22][36,67,93,102]			11	[2-22][36,67,93,102]			11	[2-22][36,67,93,102]
Geological (incl. oceans)			54	[33-75][54,93,102]			54	[33-75][54,93,102]			54	[33-75][54,93,102]
Hydrates			6	[2-9][36,55,92]			6	[2-9][36,55,92]			6	[2-9][36,55,92]
Permafrost (excl lakes & wetl)			1	[0-1][93]			1	[0-1][93]			1	[0-1][93]
Anthropogenic Sources	348	[305-383]	296	[304-310]	372	[290-453]	329	[274-392]	335	[273-409]	347	[296-399]
Agriculture&Waste	208	[187-220][12,32,33]	185	[-][42]	239	[180-301][12,35,99]	212	[187-255][42,43,44]	209	[180-241][12,25,69,91,94,96,99]	225	[195-263][42,43,44]
Biomass Burning (incl. Biofuels)	46	[43-55][12,32,33]	34	[31-37][98,101,102]	38	[26-45][12,35,99]	40	[35-	30	[24-45][12,25,69,91,94,96,99]	33	[31-
Fossil Fuels	94	[75-108][12,32,33]	77	[-][42]	95	[84-107][12,35,99]	77	[66-87][42,43,44]	96	[77-123][12,25,69,91,94,96,99]	89	[83-105][42,43,44]
Sinks												
Total Chemical Loss	490	[450-533][12,32,33]	539	[411-671][16,39,63,89]	525	[491-554][12,35,99]	571	[546-646][16,39,63,89]	518	[510-538][12,25,69,91,94,96,99]	604	[509-764][16,39,63,89]
Tropospheric OH			468	[382-567][63,53]			479	[457-501][63,53]			528	[454-617][46,53,89]
Stratospheric Loss			46	[16-67][16,63,89]			67	[51-83][16,63,89]			51	[16-84][16,63,89]
Tropospheric Cl			25	[13-37][39]			25	[13-37][39]			25	[13-37][39]
Soils	21	[10-27][12,32,33]	28	[9-47][37,61]	27	[-][12]	28	[9-47][37,61,105]	32	[26-42][12,25,69,91,94,96]	28	[9-47][37,61,105]
Totals												
Sum of sources	551	[500-592]	651		554	[529-596]	665		553	[526-569]	694	
Sum of sinks	511	[460-559]	539	[411-671]	542	[518-579]	596	[546-646]	550	[514-560]	630	[509-764]
Imbalance (Sources - Sinks)	30	[16-40]			12	[7-17]			3	[-4-19]		
Atmospheric Growth Rate	34				17				6			

Figure 1.3: Sources, sinks and atmospheric budgets of CH_4 ($Tg\,CH_4\ yr^{-1}$) summarized by Kirschke et al. (2013) from 9 top-down inversion and 8 bottom-up models for the last three decades.

of natural wetlands. The feedback between wetlands and climate - wetlands are believed to be sensitive to climate changes and wetlands influence climate by CH_4 emissions - has

led global wetlands to be highlighted as an area of concern for potential large increases in CH_4 emissions under future warming climates by the US Climate Change Science Program (CCSP, 2008).

1.3 Natural wetlands and peatlands

1.3.1 Wetlands

A wetland is a vegetated land area that is either permanently, seasonally or irregularly saturated with water. Wetlands can be distinguished from other landforms or water bodies by their water table that stands near the land surface and the types of plants that thrive within them. They arise when inundation produces soils dominated by anaerobic processes. This forces flora (particularly rooted plants) and fauna to adapt to flooding. Wetlands are found at every altitude and every climatic zone: they range from the high Arctic to the tropics and from low-lying coastal areas to high altitude plateaus. Floodplains, marshes, bogs, swamps, fens and shallow lakes and wet meadows all are examples of wetlands (Aselmann & Crutzen, 1989; Matthews & Fung, 1987). The water found in wetlands can be saltwater, freshwater, or brackish. The largest wetlands in the world include the Amazon River basin and the West Siberian Plain.

In the last three decades, different research groups have compiled information on wetland distribution, based on vegetation or soil types, lake distribution or landscape classification derived from satellite data (Matthews & Fung, 1987; Aselmann & Crutzen, 1989; Prigent et al., 2001; Tarnocai et al., 2009). More recent studies have reconstructed the location and initiation of peatlands in the past (MacDonald et al., 2006; Yu et al., 2010). Ground based monitoring of wetlands at present is difficult: the extent is subject to fluctuations due to seasonality and some wetlands are inaccessible or scattered. This makes surveys at ground level or from space, difficult, time-consuming and expensive. Nevertheless, recent studies by Prigent et al. (2007) and Papa et al. (2010) are promising and capture the distribution of inundated areas and their seasonality (Fig. 1.4).

1.3.2 Peatlands

The definitions of peatlands follows the definition of wetlands but includes additional qualifiers. First and foremost while wetlands can be seasonal or temporary, peatlands are permanent wetlands. The second requirement is that the soil accumulates organic matter at a higher rate than the rate of decomposition, so peatlands are building up soil (Wieder, 2006). In terms of areal coverage more than half of all wetlands are peatlands (Roulet, 2000; Gorham, 1991). They cover about 3-4 $\times$ $10^6\,km^2$ north of 40°N ($\sim$10% of the land) (Matthews & Fung, 1987; Aselmann & Crutzen, 1989). Fig. 1.5 shows a global map of peatland regions (Yu et al., 2010).
Peatlands are extremely important in terms of carbon storage. They contain 200-600 PgC or $\sim$10-20% of the total global soil carbon (Gorham, 1991; Roulet, 2000; MacDonald et al., 2006; Yu et al., 2010; Yu, 2012), almost entirely as peat (organic soil). Frolking & Roulet (2007) estimate the overall present day radiative effect of peatlands on the climate to be a net cooling between -0.2 and -0.5 Wm^{-2} as the sequestration of carbon outweighs the effect of the emitted CO_2 and CH_4.

Peat accumulation is mainly dependent on the water table position, the soil temperature and the net primary production (NPP) (Rouse et al., 1997). Peat deposits form under anaerobic conditions where decomposition rates are slower than accumulation rates. But it is not only the sequestration of carbon that makes peatlands interesting for climate science. There is

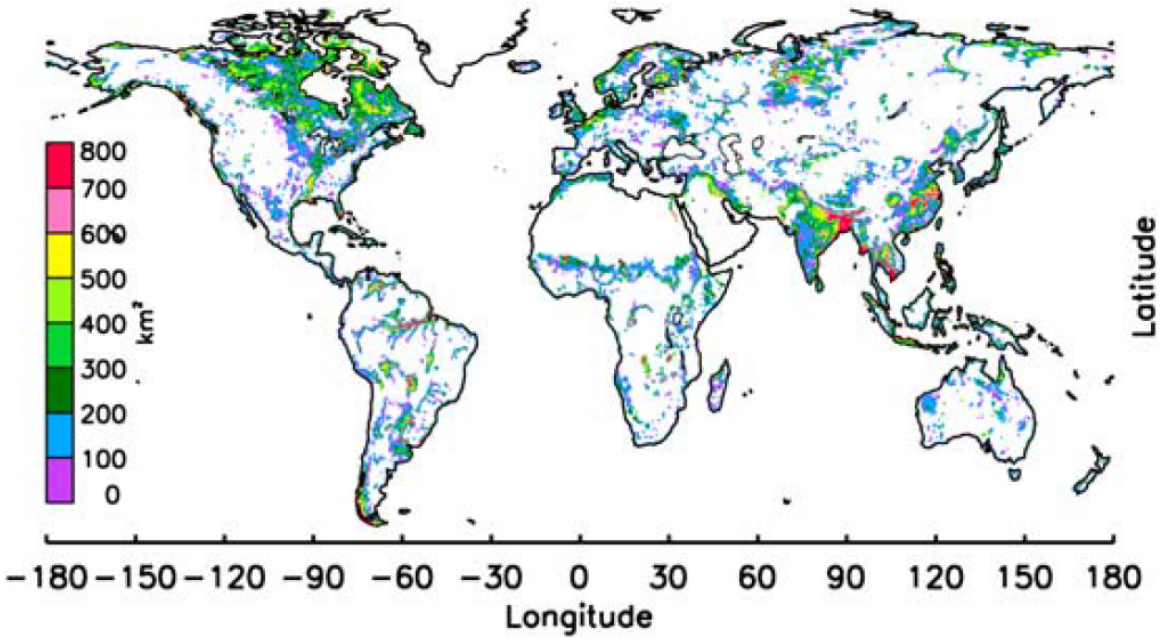

Figure 1.4: Global map of the annual maximum surface water extent (average over 1993-2004) derived from multisatellite method by Papa et al. (2010).

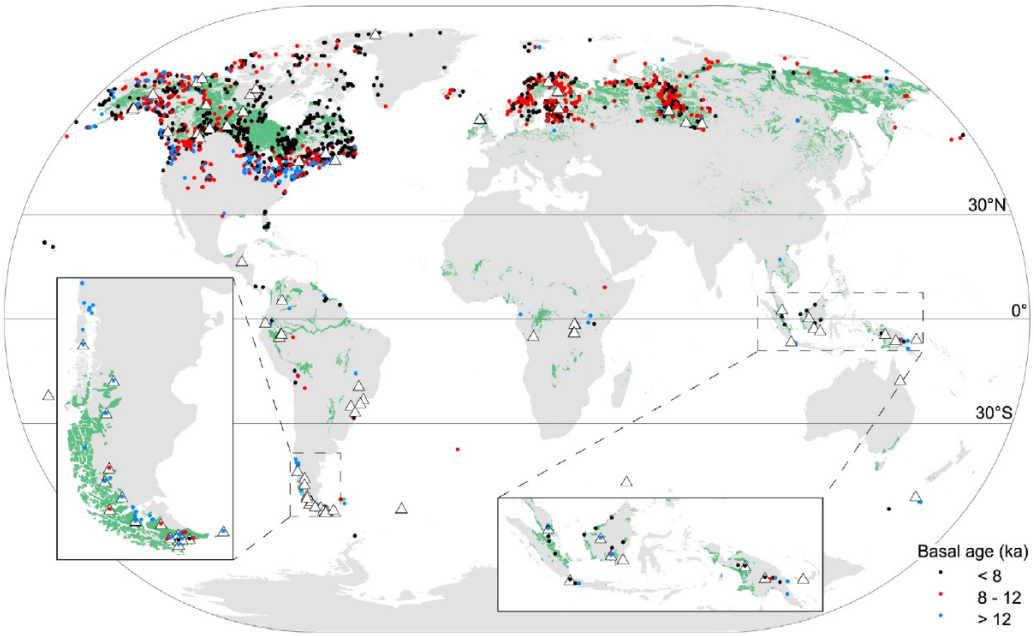

Figure 1.5: Global map of peatland regions and peatland study sites with basal peat ages found by Yu et al. (2010). Colors showing the ages of peatland initiation: black: <8 ka, red 8-12 ka and blue >12 ka.

also a large quantity of CH_4 emitted by peatlands. Zhuang et al. (2004) estimate the present emissions to 51 $TgCH_4$ yr^{-1} in high-latitude soils of the Northern Hemisphere and summarize recent studies that find 31 to 106 $TgCH_4$ yr^{-1}. Methane emissions from northern peatlands are predicted to rise under a future climate warming due to direct temperature effects on the production or indirect effects on vegetation, hydrology and thawing of permafrost.

Besides playing a key role in the global carbon cycle as one of the largest soil carbon stocks on Earth, peatlands are an important paleoenvironmental archive. They combine relatively rapid accumulation rates, copious in situ organic material, hydroclimatic sensitivity, and diverse paleoenvironmental proxies to provide a rich store of environmental history over much of the globe.

Two functional layers can be distinguished in peatlands: the uppermost layers with predominating oxic conditions and a lateral flow of water (acrotelm), have a higher biological activity than layers further down (catotelm) where the peat becomes anoxic and water is stagnant. The acrotelm is a thin layer of about <0.4 m overlaying a much thicker (usually several meters) catotelm (Hayward & Clymo, 1983; Clymo, 1984). On most peatlands the surface has a distinct microtopographical pattern of elevated hummocks alternating with depressions, in bogs designated as hollows and in patterned fens as flarks.
Bogs are ombrotrophic, which means they receive their water and nutrients from precipitation as they are hydrologically isolated. Since the rain is acidic and very low in nutrients, they are dominated by organisms such as *Sphagnum* mosses that are adapted to acidic, low-nutrient environments. In contrast, minerotrophic environments are those where the water supply comes mainly from streams and springs. They have a higher nutrient level and reduced acidity as the water has flown through rocks and other minerals, acquiring dissolved chemicals. Such mires are dominated by sedges, shrubs and *Sphagnum* mosses.

1.4 Methane emissions from peatlands

A dynamical balance between microbial CH_4 production and oxidation processes in different peat layers, as well as the transport in between the peat layers and into the atmosphere controls the CH_4 flux from wetlands (see Fig. 1.6). Climate is the main driver of CH_4 emissions. It influences soil temperature, thaw depth and water table position (WTP), and thus vegetation composition, net primary production (NPP) and heterotrophic respiration (RH). In order to model CH_4 emissions it is therefore important to understand vegetation dynamics, as well as water and heat transport in the soil.

Methane production requires a suitable carbon source (Valentine et al., 1994) and anaerobic conditions (Segers, 1998). The responsible microorganisms are methanogenic archaea (Whitman & Boone, 1992). It is valid to assume that methanogenesis in peatlands occurs universally below the WTP, as these microorganisms can also be found in oxic environments where they remain inactive until anoxic conditions dominate again. The produced CH_4 can be oxidised in the soil by methanotrophic bacteria above and slightly below the water table and near the roots. This process has a strong regulatory effect on CH_4 emissions. The root exudates by plants promote CH_4 production, which increases with the photosynthetic activity of plants (Whiting & Happell, 1991). Changes in substrate availability and redox conditions are suggested to control the growth and death of methanogenic bacteria. An increase in temperature enhances CH_4 production rate but the substrate availability strongly affects the temperature response (Valentine et al., 1994). Temperature control has been suggested to be less important for oxidation than for production (Dunfiel et al., 1993).
The organic substrate available to methanogens is a mixture of carbonaceous substances derived from the decomposition of root exudates, litter and soil carbon (Wania, 2007). The quality and quantity of the substrate is determined by the vegetation composition and productivity. The decomposition into CH_4 is dependent on the substrate and climatic conditions. Soil temperature regulates CH_4 emissions via the activity level of the bacteria for methanogenesis and oxidation, as well as via its influence on soil decomposition rates and transport

pathways (affecting the diffusivity of gases and concentration thresholds for ebullition). The vegetation is not only important for the substrate availability. It plays also an important role for the transport of CH_4 to the atmosphere and oxygen into the soil via aerenchyma (gas-conducting tissues) (Ding et al., 2005). There are two other possible ways for CH_4 to reach the atmosphere: diffusion through the soil and ebullition events (Chanton & Martens, 1988). Methane that is emitted via plant transport and diffusion can be oxidised on its way, while ebullition events represent a fast out-gassing.

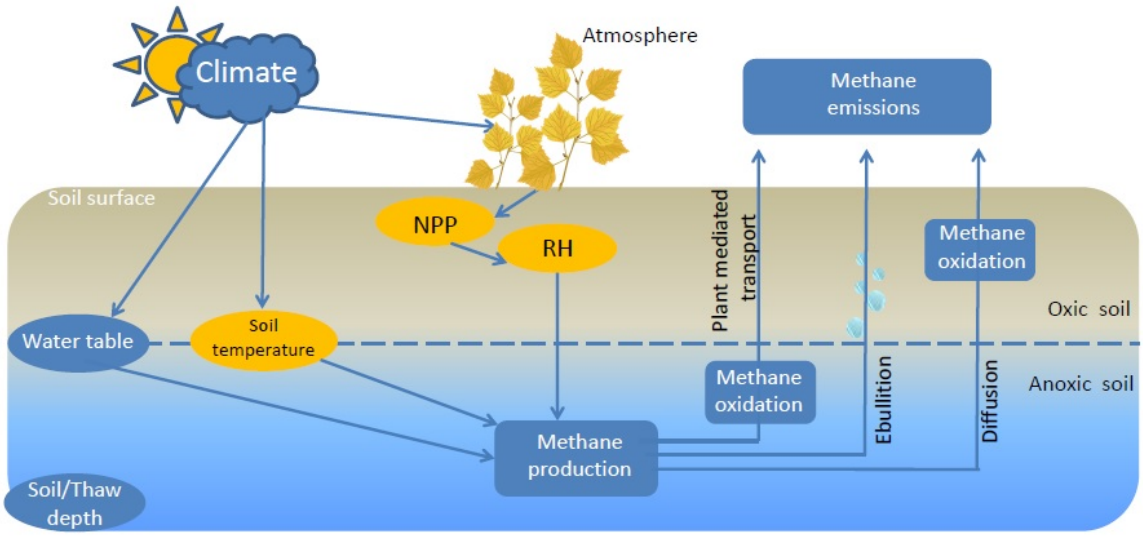

Figure 1.6: Schematic representation of CH_4 production, oxidation, different transport pathways and influencing factors. Adapted from Wania (2007).

1.5 Methane isotopes

Generally, CH_4 can be formed from organic matter or from inorganic matter in hydrothermal vents. There are two sources of natural CH_4: bacterial activity and thermogenic processes (for example geothermal vents, coal gases, biomass burning). The knowledge of the isotopic composition, also called signature, of the different CH_4 sources gives additional information about sources and flux strengths to better understand the global CH_4 cycle. The individual emission signatures of sources are determined by the physical and chemical processes that generate or transform them. By comparing the isotopic signature of the atmosphere with flux-weighted isotopic composition of the sources and sinks, one gets a further constraint on the individual source strength.

The isotopic signature or isotopic fingerprint is the ratio of stable or unstable isotopes of a particular element. The notation for the ^{13}C-signature of ^{12}C in this dissertation uses the following definition:

$$\delta^{13}C = \left(\frac{(^{13}C/^{12}C)_{sample}}{(^{13}C/^{12}C)_{PDB}} - 1\right) \times 1000 \tag{1.3}$$

where $(^{13}C/^{12}C)_{PDB} = 1123.75 \times 10^{-5}$ and PDB is the Pee Dee Belemnite carbonate standard. Values of $\delta^{13}C$ are conveniently given in permil (‰). A δ-value of a sample <0 stands for a depletion of the rare isotope in the sample relative to the international standard, while

a δ-value >0 represents an enrichment with respect to the international standard.

The separation of a compound of molecules into parts of heavier or lighter isotopic composition, where the heavier molecules are enriched and the lighter are depleted in heavy isotopes, is called fractionation. This separation can occur when molecules transfer into another compound or phase or are transported by diffusion and is described by the fractionation factor α.

$$\alpha_{B-A} = \frac{(^{13}C/^{12}C)_B}{(^{13}C/^{12}C)_A} \tag{1.4}$$

As isotope effects are rather small, $\alpha \sim 1$, a new term has been introduced, the fractionation ϵ [‰]:

$$\epsilon_{B-A} = (\alpha_{B-A} - 1) \cdot 1000 \tag{1.5}$$

ϵ , representing the new isotopic composition compared to the old, can be approximated as:

$$\epsilon \approx \delta_A - \delta_B = \epsilon \cdot (\frac{\delta_A}{1000} + 1) \tag{1.6}$$

Fractionation of stable isotopes in CH_4 in peatlands occurs at each stage of the process where either microorganisms, plants or physical diffusion are involved. CH_4 produced in wetlands has an extremely wide range of isotopic composition. δ^{13}C values range from -90‰ to -45‰ (Bowes & Hornibrook, 2006). Factors that affect the isotopic signature of biologically produced CH_4 are the isotopic composition of the starting material: C_3 plants have lower signature (-27.5 to -24 permil) than C_4 plants (-18.7 to -12.6 permil). Then the kinetic isotope effect (KIE). The KIE is the fraction of the rates of a reaction of the light isotope compared to the heavy isotope. Isotopic rate differences are most pronounced when the relative mass difference is greatest. Also temperature, which is correlated to the KIE, as heavier CH_4 is being emitted at higher temperatures, is a factor and finally, Gibb's free energy change (ΔG). The fractionation may be dependent on the reversibility of the enzymatic reactions involved. The more they are reversible, the more fractionation occurs (Gallego-Sala, 2010; Hornibrook, 2009). A further difference in the signatures of the produced CH_4 originates from the two different methanogenic pathways that occur in the soil: carbon dioxide reduction and acetate fermentation, which also depend on temperature, substrate availability and methanogenic community in the soil (Fey et al., 2004). CO_2 reduction (α_c = 1.031-1.082) fractionates much stronger than acetoclastic methanogenesis (α_a = 1 - 1.032) (Conrad, 2005). Depending on the transport pathways and oxidation, the isotopic composition is modified further on (Fey et al., 2004).
For example, minerotrophic mires produce CH_4 that is more ^{13}C enriched than ombrotrophic wetlands. Methane produced in ombrotrophic bogs is more depleted because of poor dissociation of acetic acid or absence of methanogenic archaea capable of metabolizing acetic acid under low pH conditions (Hornibrook & Bowes, 2007). The trends in ^{13}C-CH_4 values of CH_4 in pore water is that the signature becomes more positive with depth in rain-fed bogs and more negative with depth in fens. Hornibrook (2009) explain this by a predominance of acetoclastic methanogenesis in shallow peat in minerotrophic mires with greater ^{13}C-depletion of CH_4 occurring at depth because of a transition to CO_2/H_2 methanogenesis due to lower temperature and a lack of labile substrate. While CO_2/H_2 methanogenesis is prevalent in ombrotrophic bogs throughout the entire peat profile which explains the much smaller range of signatures and the more negative $\delta^{13}C(CH_4)$ values. The inverse trend in bogs is yet not completely understood - different plausible explanation exist (changes in signature due to unfavorable energetics and substrate availability, acidic conditions created by *Sphagnum* mosses

and the lack of buffering capacity of mineral-rich ground water, higher O_2 and SO_4^{2-} availability near the surface (Hornibrook, 2009)). The most important zone for methanogenesis is located at shallow depths in both types of peatland and consequently, ^{13}C values of CH_4 emitted from ombrotrophic bogs are more negative than from fens (Hornibrook & Bowes, 2007). An other reason for the more positive ^{13}C-CH_4 values in pore water in fens is the abundance of graminoids: they contribute to the enrichment through the release of root exudates which promotes acetoclastic methanogenesis, through rhizosphere oxidization of CH_4 causing localized enrichment of ^{13}C, and through the preferential export of $^{12}CH_4$ through aerenchyma, which also enriches pore water (Hornibrook, 2009). Penning et al. (2005) and Hornibrook (2009) note that the effect of a largely negative ΔG on CO_2 reduction (i.e. highly favorable energetic conditions) can make the resulting signatures indistinguishable from CH_4 formed by acetate fermentation and therefore, CO_2 reduction can not be totally excluded in fens.

The difference in ^{13}C for emissions of wetlands range from -100 permil (gas transported through aerenchyma of vascular plants) (Chanton et al., 2002), to -42 permil for residual CH_4 after loss of $^{12}CH_4$ due to methanotrophy or diffusion through plants (Hornibrook & Bowes, 2007). This large range can not only be explained by the difference from degradation of mostly C_3 plant material (-30 to -24 permil). The ^{13}C enrichment is dependent on the amount of oxidation and the distribution to the different transport pathways that have different fractionation factors.

While ^{13}C measurements help to separate between the different biogenic sources and between biogenic and other CH_4 sources, measurements of ^{14}C-CH_4 help to quantify the contribution of fossil CH_4 to the total source mix (Lassey et al., 2007).

1.6 Outline of the Thesis

Given the importance of simulating the contribution of global peatlands to the total CH_4 emissions in the past and in response to future climate change, this thesis describes the implementation and improvement of a CH_4 routine into LPJ-Bern, discusses applications and limitations and finally presents the implementation of CH_4 isotopes that give a further constraint to better understand the processes leading to CH_4 emissions in peatlands and to quantify the strength of this source.
The theory part in Chapter 2 gives a short overview of climate modeling in general and a description of the model used for the simulations presented in this thesis. Details about the CH_4 routine, as well as about the new implementation of the CH_4 isotopes are given. Site simulations are discussed to illustrate the implemented processes and compared to recent measurements. The third Chapter is about an application and test of the CH_4 routine: the simulation of CH_4 emissions during an abrupt climate change. It includes an evaluation and sensitivity test of the CH_4 routine. This application has been published in a paper in Biogeosciences. Chapter 4 present published results from a model intercomparison project (WETCHIMP) where the performances of 10 different CH_4 models are compared to estimate our present ability to simulate large scale wetland characteristics and corresponding CH_4. All models were driven with the same climate and CO_2 forcing datasets and the simulated global wetland extend and the corresponding CH_4 emissions were investigated. The fifth Chapter is about a model application for CH_4 isotopes. Global runs are performed and discussed and sensitivity tests are presented. To conclude, a short summary and an outlook is given.

Bibliography

Aselmann, I. & Crutzen, P., 1989. Global distribution of natural fresh-water wetlands and rice paddies, their net primary productivity, seasonality and possible methane emissions, *J. Atmos. Chem.*, **8**(4), 307–358.

Baumgartner, M., Schilt, A., Eicher, O., Schmitt, J., Schwander, J., Spahni, R., Fischer, H., & Stocker, T. F., 2012. High-resolution interpolar difference of atmospheric methane around the Last Glacial Maximum, *Biogeosciences*, **9**(10), 3961–3977.

Bergamaschi, P., Frankenberg, C., Meirink, J. F., Krol, M., Villani, M. G., Houweling, S., Dentener, F., Dlugokencky, E. J., Miller, J. B., Gatti, L. V., Engel, A., & Levin, I., 2009. Inverse modeling of global and regional CH_4 emissions using SCIAMACHY satellite retrievals, *J. Geophys. Res.*, **114**.

Blunier, T. & Brook, E., 2001. Timing of millennial-scale climate change in Antarctica and Greenland during the last glacial period, *Science*, **291**(5501), 109–112.

Blunier, T., Chappellaz, J., Schwander, J., Stauffer, B., & Raynaud, D., 1995. Variations in atmospheric methane concentration during the holocene epoch, *Nature*, **374**(6517), 46–49.

Bousquet, P., Ciais, P., Miller, J. B., Dlugokencky, E. J., Hauglustaine, D. A., Prigent, C., Van der Werf, G. R., Peylin, P., Brunke, E. G., Carouge, C., Langenfelds, R. L., Lathiere, J., Papa, F., Ramonet, M., Schmidt, M., Steele, L. P., Tyler, S. C., & White, J., 2006. Contribution of anthropogenic and natural sources to atmospheric methane variability, *Nature*, **443**(7110), 439–443.

Bowes, H. & Hornibrook, E., 2006. Emission of highly ^{13}C-depleted methane from an upland blanket mire, *Geophys. Res. Lett.*, (33), 1–4.

Brook, E., Harder, S., Severinghaus, J., Steig, E., & Sucher, C., 2000. On the origin and timing of rapid changes in atmospheric methane during the last glacial period, *Global Biogeochem. Cycles*, **14**(2), 559–572.

Canty, T. & Minschwander, K., 2002. Seasonal and solar cycle variability of oh in the middle atmosphere, *J. of Geophys. Res.-Atm.*.

Cao, M., Marshall, S., & Gregson, K., 1996. Global carbon exchange and methane emissions from natural wetlands: Application of a process-based model, *J. Geophys. Res.-Atm.*, **101**(D9), 14399–14414.

Chanton, J. & Martens, C., 1988. Seasonal variations in ebullitive flux and carbon isotopic composition of methane in a tidal freshwater estuary, *Global Biogeochem. Cycles*, (2), 289–298.

Chanton, J., Arkebauer, T., Harden, H., & Verma, S., 2002. Diel variation in lacunal CH_4 and CO_2 concentration and delta C-13 in Phragmites australis, *Biogeochemistry*, **59**(3), 287–301.

Chappellaz, J., Blunier, T., Raynaud, D., Barnola, J., Schwander, J., & Stauffer, B., 1993. Synchronous changes in atmospheric CH_4 and Greenland climate between 40-KYR AND 8-KYR BP, *Nature*, **366**(6454), 443–445.

Chappellaz, J., Blunier, T., Kints, S., Dallenbach, A., Barnola, J., Schwander, J., Raynaud, D., & Stauffer, B., 1997. Changes in the atmospheric CH_4 gradient between Greenland and Antarctica during the Holocene, *J. Geophys. Res.-Atm.*, **102**(D13), 15987–15997.

Clymo, R., 1984. The limits to peat bog growth, *Phil. Transactions of the Royal Society of London, Series B-Biological Sciences*, **303**(1117), 605–654.

Conrad, R., 1996. Soil microorganisms as controllers of atmospheric trace gases (H-2, CO, CH4, OCS, N2O, and NO), *Microbiological reviews*, **60**(4), 609+.

Conrad, R., 2005. Quantification of methanogenic pathways using stable carbon isotopic signatures: a review and a proposal, *Organic Geochemistry*, **36**(5), 739–752.

Curry, C. L., 2007. Modeling the soil consumption of atmospheric methane at the global scale, *Global Biogeochem. Cycles*, **21**(4).

Denman, K. L., Brasseur, G., Chidthaisong, A., Ciais, P., Cox, P. M., Dickinson, R. E., Hauglustaine, D., Heinze, C., Holland, E., Jacob, D., Lohmann, U., Ramachandran, S., da Silva Dias, P. L., Wofsy, S. C., & Zhang, X., 2007. Couplings Between Changes in the Climate System and Biogeochemistry, in *Climate Change 2007: The Physical Science Basis. Contribution of Working Group I to the Fourth Assessment Report of the Intergovernmental Panel on Climate Change*, pp. 499–587, eds Solomon, S., Qin, D., Manning, M., Chen, Z., Marquis, M., Averyt, K. B., Tignor, M., & Miller, H. L., Cambridge University Press, Cambridge, United Kingdom and New York, USA.

Ding, W., Cai, Z., & Tsuruta, H., 2005. Plant species effects on methane emissions from freshwater marshes, *Atmospheric environment*, **39**(18), 3199–3207.

Dlugokencky, E., Bruhwiler, L., White, J., Emmons, L., Novelli, P., Montzka, S., Masarie, K., Lang, P., Crotwell, A., Miller, J., & Gatti, L., 2009. Observational constraints on recent increases in the atmospheric CH_4 burden, *Geophys. Res. Lett.*, **36**(18), L18803 (5 pp.).

Dlugokencky, E. J., Nisbet, E. G., Fisher, R., & Lowry, D., 2011. Global atmospheric methane: budget, changes and dangers, *Philosophical transactions of the royal society A-Mathematical physical and engineering sciences*, **369**(1943), 2058–2072.

Dunfiel, P., Knowles, R., Dumont, R., & Moore, T., 1993. Methane production and consumption in temperate and sub-arctic peat soils - response to temperature and PH, *Soil Biology & Biochemistry*, **25**(3), 321–326.

Etheridge, D. M., Steele, L. P., Langenfelds, R. L., Francey, R. J., Barnola, J., & Morgan, V. I., 1996. Natural and anthropogenic changes in atmospheric CO_2 over the last 1000 years from air in Antarctic ice and firn, *J. Geophys. Res.*, **101**, 4115–4128.

Fey, A., Claus, P., & Conrad, R., 2004. Temporal change of ^{13}C isotope signatures and methanogenic pathways in rice field soil incubated anoxically at different temperatures, *Geochimica et Cosmochimica Acta*, (68), 293–306.

Fischer, H., Behrens, M., Bock, M., Richter, U., Schmitt, J., Loulergue, L., Chappellaz, J., Spahni, R., Blunier, T., Leuenberger, M., & Stocker, T. F., 2008. Changing boreal methane sources and constant biomass burning during the last termination, *Nature*, **452**(7189), 864–867.

Flückiger, J., Blunier, T., Stauffer, B., Chappellaz, J., Spahni, R., Kawamura, K., Schwander, J., Stocker, T., & DahlJensen, D., 2004. N_2O and CH_4 variations during the last glacial epoch: Insight into global processes, *Global Biogeochem. Cycles*, **18**(1).

Forster, P., Ramaswamy, V., Artaxo, P., Berntsen, T., Betts, R., Fahey, D. W., Haywood, J., Lean, J., Lowe, D. C., Myhre, G., Nganga, J., Prinn, R., Raga, G., Schulz, M., & Van Dorland, R., 2007. Changes in Atmospheric Constituents and in Radiative Forcing, in *Climate Change 2007: The Physical Science Basis. Contribution of Working Group I to the Fourth Assessment Report of the Intergovernmental Panel on Climate Change*, pp. 129–234, eds Solomon, S., Qin, D., Manning, M., Chen, Z., Marquis, M., Averyt, K. B., Tignor, M., & Miller, H. L., Cambridge University Press, Cambridge, United Kingdom and New York, USA.

Frolking, S. & Roulet, N. T., 2007. Holocene radiative forcing impact of northern peatland carbon accumulation and methane emissions, *Global change biology*, **13**(5), 1079–1088.

Gallego-Sala, A., 2010. Manuscript, *Dissertation*.

Gorham, E., 1991. Northern peatlands - role in the carbon-cycle and probable responses to climatic warming, *Ecological Applications*, **1**(2), 182–195.

Hansen, J. & Sato, M., 2001. Trends of measured climate forcing agents, *Preoceedings of the national academy of sciences or the United States of America*, **98**(26), 14778–14783.

Hayward, P. & Clymo, R., 1983. The Growth of spagnum - experiments on, and simulation of, some effects of light-flux and water-table depth, *Journal of Ecology*, **71**(3), 845–863.

Hornibrook, E., 2009. The stable carbon isotope composition of methane produced and emitted from northern peatlands, *Geophysical Monograph Series*, **184**.

Hornibrook, E. & Bowes, H., 2007. Trophic status impacts both the magnitude and stable carbon isotope composition of methane flux from peatlands, *Geophys. Res. Lett.*, (34), L21,401.

Houweling, S., Kaminski, T., Dentener, F., Lelieveld, J., & Heimann, M., 1999. Inverse modeling of methane sources and sinks using the adjoint of a global transport model, *J. Geophys. Res.*, **104**(D21), 26137–26160.

Huber, C., Leuenberger, M., Spahni, R., Fluckiger, J., Schwander, J., Stocker, T., Johnsen, S., Landals, A., & Jouzel, J., 2006. Isotope calibrated Greenland temperature record over Marine Isotope Stage 3 and its relation to CH_4, *Earth and Planetary Science Letters*, **243**(3-4), 504–519.

IPCC, 2007. *Climate Change 2007: The Scientific Basis. Contribution of Working Group I to the Fourth Assessment Report of the Intergovernmental Panel on Climate Change*, eds Solomon, S., Qin, D., Manning, M., Chen, Z., Marquis, M., Averyt, K. B., Tignor, M., & Miller, H. L., Cambridge University Press, Cambridge, United Kingdom and New York, USA.

Kirschke, S., Bousquet, P., Ciais, M., & et al., 2013. Three decades of global methane sources and sinks, *Nature Geoscience, in review*.

Kobashi, T., Severinghaus, J. P., Brook, E. J., Barnola, J.-M., & Grachev, A. M., 2007. Precise timing and characterization of abrupt climate change 8200 years ago from air trapped in polar ice, *Quaternary Science Reviews*, **26**(9-10), 1212–1222.

Lassey, K. R., Lowe, D. C., & Smith, A. M., 2007. The atmospheric cycling of radiomethane and the "fossil fraction" of the methane source, *Atmos. Chem. Phys.*, **7**, 2141–2149.

Lelieveld, J., Crutzen, P., & Dentener, F., 1998. Changing concentration, lifetime and climate forcing of atmospheric methane, *Tellus Series B-Chemical and Physical Meteorology*, **50**(2), 128–150.

Levine, J. G., Wolff, E. W., Jones, A. E., Sime, L. C., Valdes, P. J., Archibald, A. T., Carver, G. D., Warwick, N. J., & Pyle, J. A., 2011. Reconciling the changes in atmospheric methane sources and sinks between the Last Glacial Maximum and the pre-industrial era, *Geophys. Res. Lett.*, **38**.

Loulergue, L., Schilt, A., Spahni, R., Masson-Delmotte, V., Blunier, T., Lemieux, B., Barnola, J.-M., Raynaud, D., Stocker, T. F., & Chappellaz, J., 2008. Orbital and millennial-scale features of atmospheric CH_4 over the past 800,000 years, *Nature*, **453**(7193), 383–386.

MacDonald, G. M., Beilman, D. W., Kremenetski, K. V., Sheng, Y., Smith, L. C., & Velichko, A. A., 2006. Rapid Early Development of Circumarctic Peatlands and Atmospheric CH_4 and CO_2 Variations, *Science*, **314**(5797), 285–288.

Matthews, E. & Fung, I., 1987. Methane emissions from natural wetlands: Global distribution, area and environmental characteristics of sources, *Global Biogeochem. Cycles*, **1**, 61–86.

Melton, J. R., Wania, R., Hodson, E. L., Poulter, B., Ringeval, B., Spahni, R., Bohn, T., Avis, C. A., Beerling, D. J., Chen, G., Eliseev, A. V., Denisov, S. N., Hopcroft, P. O., Lettenmaier, D. P., Riley, W. J., Singarayer, J. S., Subin, Z. M., Tian, H., Zürcher, S., Brovkin, V., van Bodegom, P. M., Kleinen, T., Yu, Z. C., & Kaplan, J. O., 2013. Present state of global wetland extent and wetland methane modelling: conclusions from a model inter-comparison project (wetchimp), *Biogeosciences*, **10**(2), 753–788.

Papa, F., Prigent, C., Aires, F., Jimenez, C., Rossow, W. B., & Matthews, E., 2010. Interannual variability of surface water extent at the global scale, 1993-2004, *J. Geophys. Res.-Atmos.*, **115**.

Penning, H., Plugge, C., Galand, P., & Conrad, R., 2005. Variation of carbon isotope fractionation in hydrogenothrophic methanogenic microbial cultures and environmental samples at different energy status, *Global Change Biol.*, **11**, 2103–2113.

Pison, I., Bousquet, P., Chevallier, F., Szopa, S., & Hauglustaine, D., 2009. Multi-species inversion of CH_4, CO and H_2 emissions from surface measurements, *Atmospheric Chemistry and Physics*, **9**(14), 5281–5297.

Prigent, C., Matthews, E., Aires, F., & Rossow, W., 2001. Remote sensing of global wetland dynamics with multiple satellite data sets, *Geophys. Res. Lett.*, **28**(24), 4631–4634.

Prigent, C., Papa, F., Aires, F., Rossow, W. B., & Matthews, E., 2007. Global inundation dynamics inferred from multiple satellite observations, 1993-2000, *J. Geophys. Res.*, **112**(D12).

Ridgwell, A., Marshall, S., & Gregson, K., 1999. Consumption of atmospheric methane by soils: A process-based model, *Global Biogeochem. Cycles*, **13**(1), 59–70.

Ringeval, B., de Noblet-Ducoudre, N., Ciais, P., Bousquet, P., Prigent, C., Papa, F., & Rossow, W. B., 2010. An attempt to quantify the impact of changes in wetland extent on methane emissions on the seasonal and interannual time scales, *Global Biogeochem. Cycles*, **24**.

Roulet, N., 2000. Peatlands, carbon storage, greenhouse gases, and the Kyoto Protocol: Prospects and significance for Canada, *Wetlands*, **20**(4), 605–615.

Rouse, W., Douglas, M., Hecky, R., Hershey, A., Kling, G., Lesack, L., Marsh, P., McDonald, M., Nicholson, B., Roulet, N., & Smol, J., 1997. Effects of climate change on the freshwaters of arctic and subarctic North America, *Hydrological Processes*, **11**(8), 873–902, Symposium on Regional Assessment of Freshwater Ecosystems and Climate Change in North America, Leesburg, VA, OCT 24-26, 1994.

Segers, R., 1998. Methane production and methane consumption: a review of processes underlying wetland methane fluxes, *Biogeochemistry*, **41**(1), 23–51.

Spahni, R., Schwander, J., Fluckiger, J., Stauffer, B., Chappellaz, J., & Raynaud, D., 2003. The attenuation of fast atmospheric CH_4) variations recorded in polar ice cores, *Geophys. Res. Lett.*, **30**(11).

Spahni, R., Chappellaz, J., Stocker, T., Loulergue, L., Hausammann, G., Kawamura, K., Fluckiger, J., Schwander, J., Raynaud, D., Masson-Delmotte, V., & Jouzel, J., 2005. Atmospheric methane and nitrous oxide of the late Pleistocene from Antarctic ice cores, *Science*, **310**(5752), 1317–1321.

Spivakovsky, C., Logan, J., Montzka, S., Balkanski, Y., & Foreman-Fowler, M., 2000. Three-dimensional climatological distribution of tropospheric oh: Update and evaluation, *J. of Geophys. Res.-Atm.*.

Tarnocai, C., Canadell, J. G., Schuur, E. A. G., Kuhry, P., Mazhitova, G., & Zimov, S., 2009. Soil organic carbon pools in the northern circumpolar permafrost region, *Global Biogeochem. Cycles*, **23**.

Valentine, D., Holland, E., & Schimel, D., 1994. Ecosystem and physiological controls over methane production in northern wetlands, *J. Geophys. Res.- Atm.*, **99**(D1), 1563–1571.

Walter, B. P., Heimann, M., & Matthews, E., 2001. Modeling modern methane emissions from natural wetlands 1. Model description and results, *J. Geophys. Res.*, **106**(D24), 34189–34206.

Wania, R., 2007. *Modelling northern peatland land surface processes, vegetation dynamics and methane emissions*, Ph.D. thesis, University of Bristol.

Wania, R., Ross, I., & Prentice, I. C., 2010. Implementation and evaluation of a new methane model within a dynamic global vegetation model: LPJ-WHyMe v1.3.1, *Geosci. Model Dev.*, **3**(2), 565–584.

Whiting, G.J., C. J. B. D. & Happell, J., 1991. Relationships between CH4 emission, biomass, and CO2 exchange in a subtropical grassland, *J. Geophys. Res. - Atm.*, **96**(D7), 13067–13071.

Whitman, W.B., B. T. & Boone, D., 1992. *The methanogenic bacteria*, Springer-Verlag.

Wieder, R., 2006. *Peatlands and the boreal forest*, Springer-Verlag Berlin.

Yu, Z., 2012. Northern peatland carbon stocks and dynamics: a review, *Biogeosciences Discussions*, **9**, 5073–5107.

Yu, Z., Loisel, J., Brosseau, D. P., Beilman, D. W., & Hunt, S. J., 2010. Global peatland dynamics since the Last Glacial Maximum, *Geophys. Res. Lett.*, **37**.

Zhuang, Q., Melillo, J., Kicklighter, D., Prinn, R., McGuire, A., Steudler, P., Felzer, B., & Hu, S., 2004. Methane fluxes between terrestrial ecosystems and the atmosphere at northern high latitudes during the past century: A retrospective analysis with a process-based biogeochemistry model, *Global Biogeochem. Cycles*, **18**(3).

Chapter 2

Theory

2.1 Climate modeling

There are three different approaches to derive global CH_4 emissions: process-based modelling (bottom-up) (e.g., Cao et al., 1996; Walter et al., 2001; Wania et al., 2010; Ringeval et al., 2010), inverse modelling (top-down) (e.g., Houweling et al., 1999; Pison et al., 2009; Bergamaschi et al., 2009) and extrapolation from direct flux measurements. For top-down approaches, a series of assumptions and inputs are necessary to estimate the sinks and distinguish between different sources, while the other two approaches suffer from large uncertainties due to temporal and spatial variations of observed fluxes and prevalent conditions. Combining all methods helps to narrow down the uncertainties of global wet ecosystem CH_4 emissions (Spahni et al., 2011).
The first wetland CH_4 models were established about 25 years ago by Matthews & Fung (1987). They combined vegetation, soil and inundation maps with estimates of CH_4 flux intensity to estimate wetland emissions. Process-based modeling followed about 10 years later: For example, Cao et al. (1996) and Walter et al. (2001) modelled production, oxidation and transport pathways. At present, many different models attempt to simulate wetland and peatland characteristics and resulting CH_4 emissions mechanistically (see also Chap. 4.1 and 4.2). Various studies were conducted to investigate the recent past (Ringeval et al., 2010; Spahni et al., 2011), the distant past (Hopcroft et al., 2011; Singarayer et al., 2011) and to estimate future emissions in reaction to a climate change (Bohn et al., 2007; Ringeval et al., 2011; Stocker et al., 2013).

2.2 General model description

2.2.1 LPJ-Bern

For this thesis, LPJ-Bern, a dynamic global vegetation model was used and enhanced. It is a subsequent development of the Lund-Potsdam-Jena dynamic global vegetation model (LPJ DGVM Sitch et al., 2003; Gerten et al., 2004) that combines process-based, largescale representations of terrestrial vegetation dynamics and land-atmosphere carbon and water exchanges in a modular framework. The LPJ-Bern grid cell is applied on various resolutions: $3.75° \times 2.5°$, $1° \times 1°$, $0.5° \times 0.5°$. Vegetation is defined by plant functional types (PFTs) each with its own set of parameters describing growth, carbon uptake and mortality. PFTs, thus, occupy different environmental niches defined by bioclimatic limits and physiological optima and compete for resources such as light and water. This resource competition and differential responses to fire between PFTs determines the simulated vegetation composition year to year. The model includes feedbacks through canopy conductance between photosynthesis and transpiration. Interactive coupling between these and other ecosystem processes

such as resource competition, tissue turnover, population dynamics, soil organic matter and litter dynamics are included as well. Photosynthesis, evapotranspiration and soil water dynamics are modelled on a daily time step. In our version of LPJ, the calculation of the gross primary production (GPP), net primary production (NPP), heterotrophic respiration (RH) or the new CH_4 routine are also executed on a daily basis. Fig. 2.1 shows a flowchart describing the original LPJ version by Sitch et al. (2003). LPJ has been applied previously in paleo studies (e.g. Joos et al., 2004; Gerber et al., 2004) and in simulations assessing the anthropogenic climate perturbation and the impact of human induced landuse (e.g. Joos et al., 2001; Strassmann et al., 2008; Stocker et al., 2011).

2.2.2 Integration of LPJ-WhyMe into LPJ-Bern

A CH_4 module for boreal peatland based on LPJ-WhyMe (Wetland Hydrology and Methane; Wania et al., 2009a,b, 2010) was implemented. The following section was largely adopted from Wania (2007).

This new module simulates the peatland C-cycle and CH_4 emissions from peatlands. The CH_4 routine is a separate module coupled to the terrestrial C-cycle and derives all its input data directly from LPJ-Bern. LPJ-Bern itself needs spatially-resolved input data, such as a land mask, a soil type map, as well as monthly resolved climatic input for temperature, precipitation, cloud cover and number of wet-days per month. For the CH_4 simulations, a map with peatland distribution, given as the fraction of peatland per area, is additionally needed. Changes in vegetation composition or changes in decomposition rates affect the CH_4 routine. The basic concept of the CH_4 model is that a potential carbon pool for methanogens is created proportional to RH (Wania, 2007). For non-peatland grid cells, the decomposed carbon is directly turned into the atmospheric carbon flux as RH.
There are five carbon pools per PFT, representing leaves, sapwood, heartwood, fine roots and exudates. Further, there are an above-ground and a below-ground litter pool and two soil carbon pools, which receive input from litter of all PFTs. All this pools contribute to RH. The substrate for methanogenesis is then distributed over all soil layers, weighted by the root distribution. The C production flux is split into CO_2 and CH_4. In order to model CH_4 emissions in a mechanistic, process-based way, it requires the representation of the following key processes in soils after the allocation of the substrate: the production of CH_4, the oxidation of CH_4 and the transport of CH_4 to the atmosphere (described in Subsection 2.4.1).

New features for grid cells with a (prescribed) partition of peatland include the following changes in LPJ-Bern by including WhyMe (Wania et al., 2009a,b):

1. 8 soil layers for all soil types (mineral and peat soils) with depths of 0.1, 0.1, 0.1, 0.2, 0.2, 0.3, 0.5 and 0.5 m (total depth: 2 m)

2. permafrost dynamics with freezing and thawing and a soil temperature solver to simulate temperature as a function of depth, which is very important especially in permafrost area

3. a peatland hydrology: active layer depth, evapotranspiration and water table position (WTP); WTP can only fluctuate in the acrotelm (+10 to -30cm depth), the catotelm is assumed to be always water saturated

4. an improved snow module (now changes in snow thermal characteristics due to increases in snow density with snow age are taken into account)

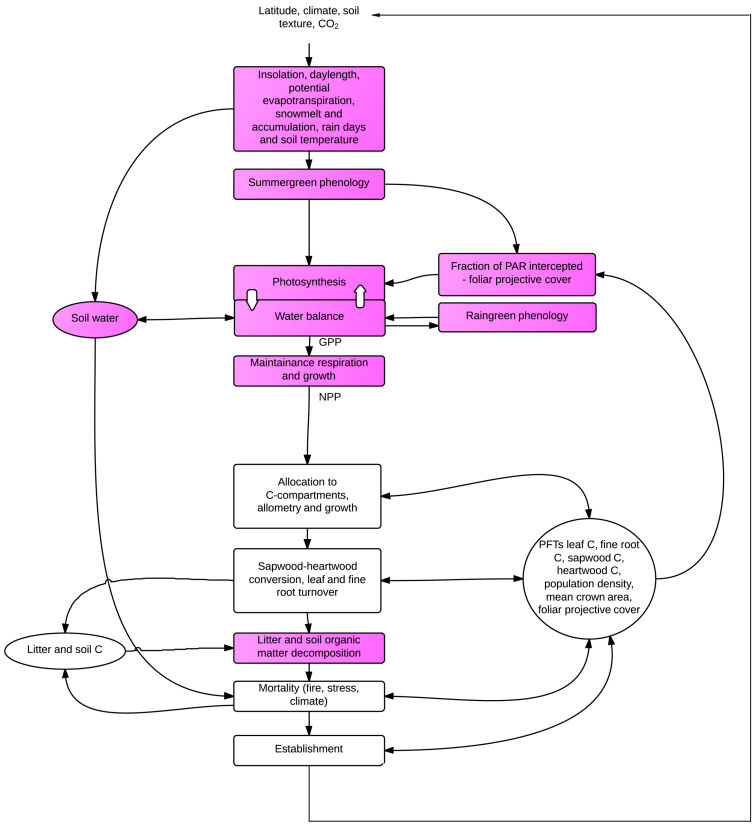

Figure 2.1: A flowchart describing the order of individual processes (modules) in LPJ performed in each grid cell during one year (Sitch et al., 2003). Shaded areas are called on a monthly or daily time step.

5. peatland vegetation as two additional PFTs for high-northern latitude peatlands: flood-tolerant C3 graminoids and *Sphagnum* moss that are adapted for water saturated or inundated environments (any generic PFT can establish in peatland depending on the inundation status)

6. a slow-down of decomposition under inundation

7. the addition of root exudates: after subtracting plant growth and maintenance respiration, a fraction (17.5 %) of C from NPP is transformed to exudates in the rhizosphere. The reduced NPP is then allocated to plant C pools as leaves and stems for *Sphagnum* mosses, leaves and roots for graminoids, and leaves, roots, sapwood and heartwood for trees

8. assignment of specific soil C pools to the acrotelm, a near surface soil layer with varying water table, and the catotelm, a deeper soil layer with permanent water saturation

9. simulation of the carbon balance of the peat, thus the soil carbon stock, carbon accumulation and decomposition rates

10. soil carbon serves as a substrate for methanogenesis parameterised as a fraction of soil heterotrophic respiration (RH). CH_4 is transported to the surface by plant mediated transport, by diffusion through the soil or by ebullition. CH_4 is oxidised under aerobic conditions in the soil layer and during diffusive transport

To this version, several changes and additions were made which will be described in the following paragraphs.

2.3 Modifications and improvements to LPJ-Bern - transition to LPX

The modifications to LPJ-Bern with integrated LPJ-WhyMe can be separated in two steps. In a first step, modifications to the CH_4 routine itself were made compared to the original LPJ-WHyMe version (Wania et al., 2010): A more mechanistic ebullition mechanism (see Chap. 2.4.1.6) that includes also the partial pressure of CO_2 for triggering an ebullition event was included and the carbon balance over all layers is now preserved after every gas diffusion time step (t=1/10 d), whereas in LPJ-WHyMe the carbon balance was closed at the end of the year with a correction factor. This version is called LPJ-Bern throughout this thesis and was used for the simulations presented in Chap. 3 for the simulation of an abrupt climate event (Zürcher et al., 2013), in Chap. 4.1 and 4.2. In a second step, a new peatland module was implemented in LPJ-Bern. It features a dynamic nitrogen cycle, a dynamic C transfer between peatland acrotelm (the upper oxic layer) and catotelm (deep anoxic layer), hydrology- and temperature-dependent respiration rates (Spahni et al., 2013). This version is called LPX and was used for the simulation in Chap. 2.6.2 and 5. In addition, further improvements to the CH_4 routine were added in LPX: the routine separates between dissolved and gaseous CH_4 for diffusion and ebullition processes and the ebullition parametrisation was changed. Further, the behavior during freezing was changed. In the old version, when a layer was frozen, the transport via diffusion for layers below was inhibited and the layer could stop the exchange of CH_4 for these layers below: In some cases, diffusion is the only transport pathway for the deeper layers: Ebullition and plant transport require positive temperatures, roots (for plant transport) and more (unfrozen) water content (for ebullition; see also Tab. 2.3). In the case the top layers were frozen, but not the layers beneath, it was possible in the model that CH_4 was still produced and could accumulate over time. Another case was that when production in the upper layer is high in summer and autumn, CH_4 gets transported via diffusion into the deeper layers which are still quite cold so as no other transport pathway is active and therefore accumulates there. To prevent this accumulation in (sporadically) frozen layers, a new daily check was added: if a layer is frozen, 90% of its gas content is added to the next unfrozen layer above. If no layer is thawed up to the surface, the flux is directly added to the atmosphere as ebullition (Mastepanov et al., 2008). Finally, the isotopic composition of CH_4 was included throughout the CH_4 routine including all relevant fractionation processes.

All changes in the CH_4 routine itself will be described in the next section (Chap. 2.4) which is separated in two parts. The first describes the CH_4 routine used in the model version of LPJ-Bern, the second the additional changes done in LPX. General changes throughout the whole programm (leading from LPJ-Bern to LPX) are discussed in the next subsection.

2.3.1 LPX

Fig. 2.2 shows a scheme of peatland carbon pools and associated C and N fluxes in LPX (Spahni et al., 2013). The substrate for CH_4 comes from NPP or organic matter turnover of both plant functional types: *Sphagnum* mosses and graminoids (including all other vascular plants). While in LPX leaf and wood turnover C enters the aboveground litter pool, root turnover C is added to the belowground litter pool. Thus, the fractional plant cover and related NPP of *Sphagnum* mosses versus graminoids directly modulate the proportion of C input to these two litter pools (Spahni et al., 2013). Both litter pools undergo oxic and anoxic organic matter decomposition, where C is partially respired to the atmosphere and partially moved to the soil C pools. For peatlands the acrotelm is identified as the intermediate soil C pool, while the anoxic catotelm is represented by the slow soil C pool. Aerobic and anaerobic decomposition of exudates, litter and soil C is parameterised by individual rates that are

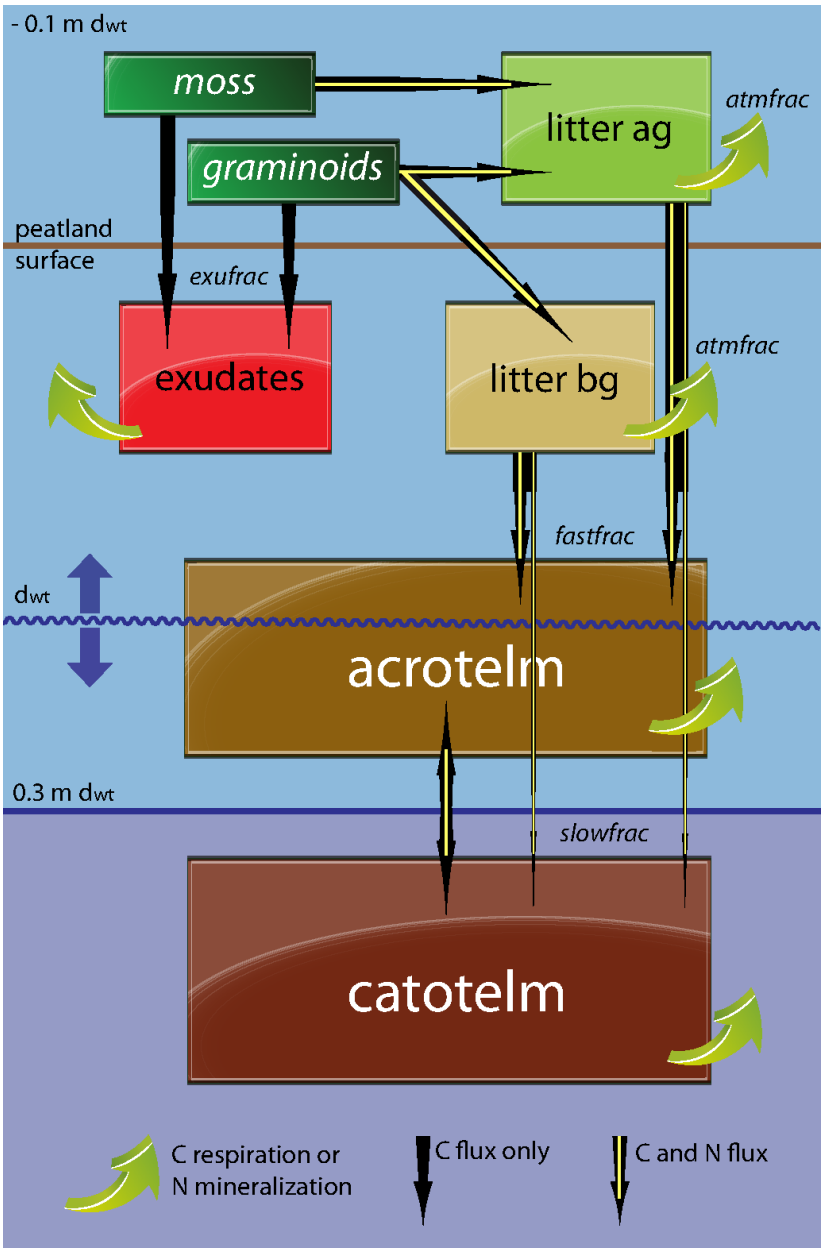

Figure 2.2: Scheme of peatland carbon pools and associated C and N fluxes in LPX (Spahni et al., 2013). There are two plant functional types (PFT): *Sphagnum* mosses and graminoids (including all other vascular plants). C fluxes originate from NPP or organic matter turnover of both PFTs. The water table varies in the range between acrotelm depth (0.3 m) and the maximum of standing water above the surface (0.1 m). For the litter pools "ag" and "bg" denote aboveground and belowground, respectively.

modified by soil temperature and water-filled pore space (Spahni et al., 2013), whereas the acrotelm decomposition rate is dependent on hydrology.

LPJ-WHyMe had a constant acrotelm-to-catotelm C transfer rate of 12 $\mathrm{gCm^{-2}yr^{-1}}$ (Wania et al., 2009b). The new version has a dynamic C transfer depending on actual accumulation and decomposition rates in the acrotelm described in Spahni et al. (2013). If the acrotelm C respires due to dry climatic conditions, the flux from acro-to-catotelm is negative and C is transferred from the catotelm to the acrotelm. Therefore, peatland can also shrink and could even disappear if conditions are too dry. Changes in peat bulk density and decom-

position rates of C returning from the catotelm compared to the overlying acrotelm layers are not considered. Simulated decadal acrotelm-to-catotelm C fluxes vary between -20 and $+50\,\mathrm{gCm^{-2}yr^{-1}}$ over the Holocene (Spahni et al., 2013).
LPX does not simulate lateral water transport within or between grid cells. Thus, no explicit distinction between fens and bogs are made. But atmospheric N deposition and an implicit N source as N input to peatlands are included. The latter can be interpreted as N_2 fixation and other N input processes that allow LPX to simulate conditions as in minerotrophic ecosystems (Spahni et al., 2013). Model simulations with the dynamic N cycle show a down-regulation of average modern NPP over peatlands by about 50%.

Fig. 2.3 shows the flowchart of LPX with the new modules.

2.4 Methane routine and improvements

2.4.1 The methane routine in LPJ-Bern

2.4.1.1 Overview of the routine

The important steps in the CH_4 routine are the allocation of available carbon substrate to methanogens, the production of CH_4 (and CO_2), the oxidation of CH_4 and the transport of CH_4, CO_2 and N_2 to the atmosphere and the transport of O_2 into the soil. The sequence in the code is the following:

1. CH_4 and CO_2 production
2. O_2 exchange between atmosphere and first soil layer
3. O_2 diffusion between soil layers (Crank-Nicolson-method)
4. O_2 transport through aerenchyma
5. CH_4 diffusion between soil layers
6. Oxidation $CH_4 + O_2 \rightarrow CO_2$
7. CH_4 exchange between atmosphere and first soil layer
8. CH_4 transport through aerenchyma
9. CO_2 diffusion among layers and atmosphere-first layer, plant transport
10. Ebullition of CH_4, CO_2 and N_2

All these processes are described in detail in the following sections (for CH_4 only; the processes for O_2 and CO_2 are implemented in the same way, but with their according constants). Production, oxidation and plant transport in LPJ-Bern (and LPX) are adapted from Wania et al. (2010); the diffusion routine is modified for LPX and the ebullition routine was completely exchanged first for LPJ-Bern and a second time for LPX. The description of the unmodified parts closely follows the description in Wania (2007).

2.4.1.2 Substrate for CH_4 production and production of CH_4 and CO_2

NPP of peatland vegetation is used as the exudates and biomass pool; part of the biomass is transferred into the litter pool; the exudates and litter pool are decaying into the RH pool which serves as the potential pool for methanogenesis. Parts of the decomposition of the litter pool directly go into the RH pool (70%), a smaller part (30%) flows into the fast and

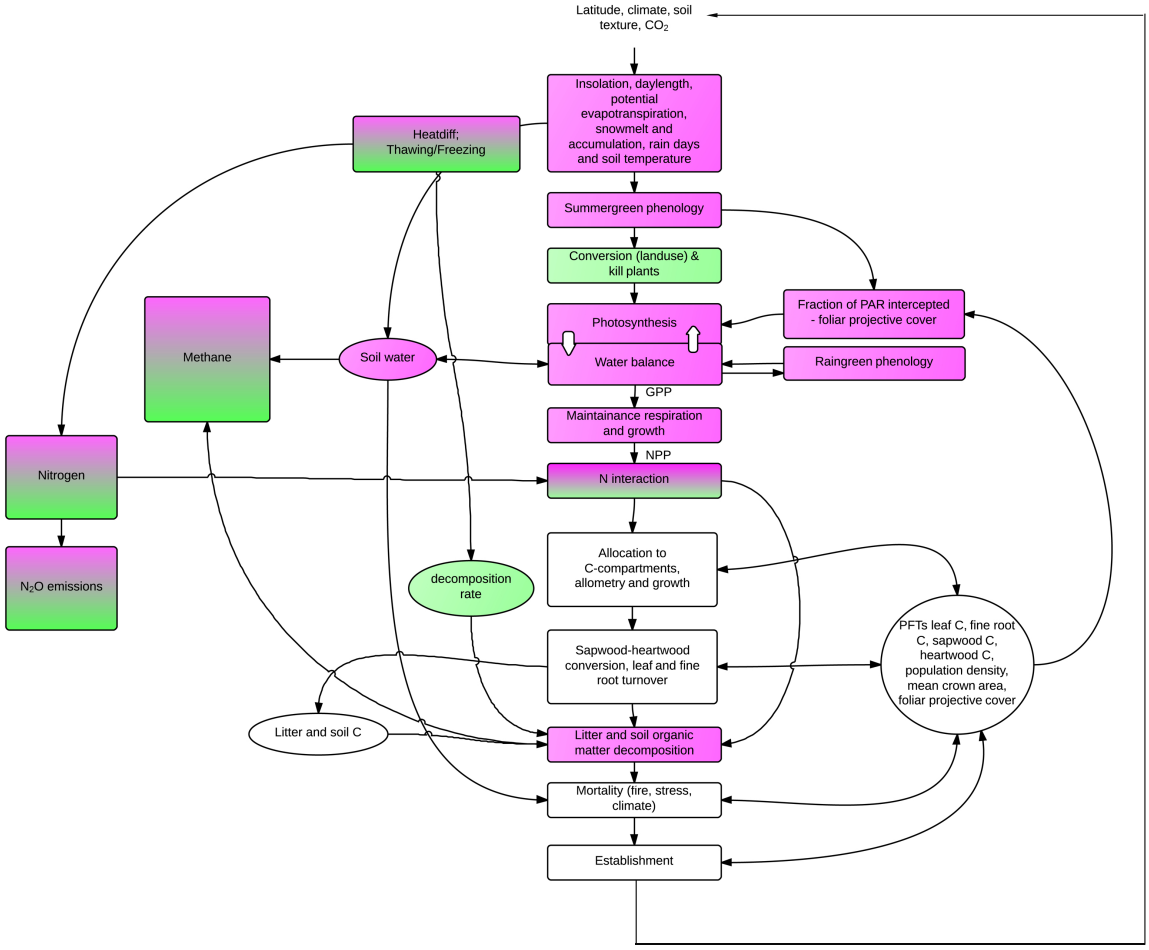

Figure 2.3: A flowchart showing the new modules (green) in LPX; subroutines with a daily timestep are indicated in pink; the interaction between the different subroutines is mostly daily, sometimes yearly: the first block (exchanging information on a daily basis) is calculation of GPP, soil temperature and albedo. The second is calculation of NPP, reproduction, turnover, litter degradation, RH.

slow carbon pools. RH is calculated based on the size of the litter and soil pools, regulated by soil moisture and soil temperature at a depth of 25 cm. It depends on the mass of each individual carbon pool and the associated turnover rates.

The pool for methanogenesis is then distributed to the 8 peat layers according to the root distribution (f_{root} = fraction of root biomass), where it is used to compute CH_4 production.

$$f_{root} = C_{root} e^{\frac{-z}{\lambda_{root}}} \tag{2.1}$$

z is the vertical coordinate increasing with depth, $\lambda_{root} = 25.17$ cm is the scaling length and $C_{root} = 0.025$ is a normalisation constant to give a total root biomass of 100 % within 2 m depth (Wania, 2007). If the first layer is frozen through the total year, no roots are allocated. Also, the allocation of roots to layers beneath frozen layers is prevented.
This dependence is also used for the flood-tolerant C_3 graminoid plant functional type to derive the root distribution needed for the plant transport of O_2, CO_2 and CH_4. The moss PFT does not have any roots and therefore does not contribute to the below ground litter pool (see also Fig. 2.2). Nevertheless, it contributes indirectly to the potential carbon pool for methanogenesis as it feeds into the exudates, above ground litter and soil carbon pools.

Therefore, the parametrisation in eq. 2.1 for the root distribution is here used to distribute all the RH (from graminoids and mosses). This is certainly a model simplification.

In each layer CH_4 production ($CH_{4(prod)}$) is calculated as the product of RH [$gCm^{-2}d^{-1}$], the root distribution f_{root}, the ratio of CH_4 to CO_2 production under anaerobic conditions ($f_{CH4/CO2}$), and the anoxity of the soil for each soil layer:

$$CH_{4(prod)} = RH \cdot f_{root} \cdot f_{CH4/CO2} \cdot anoxity \tag{2.2}$$

The decomposed carbon is mainly turned into CO_2, but a fraction is reduced to CH_4. The molar ratio between CH_4 and CO_2 production varies from 0.001 to 1.7 in anaerobic conditions and is difficult to predict (Segers, 1998). Therefore, $f_{CH4/CO2}$ is an adjustable parameter (Wania, 2007) which is determined via site evaluations (see Chap. 3). *anoxity* is defined as 1 - F_{air}, where F_{air} is the actual fraction of air in each layer. It is determined by the soil porosity and the fraction of water and ice in a layer (see also eq. 2.10). As the production factor is applied to anoxic conditions, *anoxity* weights the effect of the production factor for a mix of oxic and anoxic conditions.

In case a layer is completely frozen, the transport mechanisms, production and oxidation are prohibited. Nevertheless, the potential substrate is added to the next unfrozen layer above.

2.4.1.3 Methane oxidation

O_2 gets into the soil by diffusion and plant-mediated transport (described below). The transport depends on the WTP, the soil temperature, and the actual root distribution. The fraction of O_2 that can be used for oxidation (f_{O2}) is not fixed a priori and represents a second adjustable parameter. Microbiological activity attached to roots consumes oxygen itself and non-methanotrophic organisms can further reduce the amount of O_2 available for CH_4 oxidation.

It is assumed, that if enough oxygen is available (the stoichiometric balance requires two moles of oxygen for each mole of CH_4 oxidised: $CH_4 + 2\,O_2 \longrightarrow CO_2 + 2\,H_2O$), all of the CH_4 is oxidised within 1 day. If less O_2 is available than required, then all O_2 is used up in oxidising CH_4:

$$CH_{4(oxid)} = min(CH_4, 0.5 \cdot f_{O2} \cdot O_2 \cdot c_{mass}) \tag{2.3}$$

$CH_{4(oxid)}$ being the amount of oxidized CH_4 [$gCm^{-2}d^{-1}$ per layer], CH_4 the amount of CH_4 [gCm^{-2} per layer], O_2 the amount of oxygen [mol m^{-2} per layer], c_{mass} the molar mass of C (=12.01 g/mol).

2.4.1.4 Diffusion

Diffusion of O_2, CH_4 and CO_2 is simulated in the soil by numerically solving the diffusion equation for gas transport via molecular diffusion by a Crank-Nicolson numerical scheme (Wania, 2007). The time step in the Crank-Nicolson scheme is set to one tenth of a day.

If the gas volume per layer is less than 13 % of the total available layer volume (= porosity), the diffusivity of each gas is calculated in water (Lerman, 1979), otherwise in air (Broecker & Peng, 1974). The diffusion calculation itself does not separate between diffusion in water or air. In both cases, the surface available for the exchange is the same (the whole surface) and the concentration varies with the available, unfrozen water volume. To take account for the effect of porosity, the Millington-Quirk approach is used (Millington & Quirk, 1961; Iiyama

& Hasegawa, 2005; Wania, 2007) to modify the diffusivities respectively.

The Crank-Nicolson routine solves the following equation for each gas for the exchange between the soil layers:

$$\frac{\partial C}{\partial t} = \frac{\partial}{\partial z}(D(z)\frac{\partial C}{\partial z}) \tag{2.4}$$

with $C(z,t)$ being the concentration of a gas per unfrozen water volume [mol m^{-3}], D the diffusivity [m^2 d^{-1}], z the depth [m], t the time [d]. In the Crank-Nicolson discretisation, a forward Euler scheme (i.e. using values at the current timestep to calculate spatial derivatives) and a backwards Euler scheme (using values at the next timestep to calculate spatial derivatives) are calculated and the mean value of the two Euler schemes is used for the time derivative. A detailed description of the procedure can be found in Wania (2007).

The diffusivities per layer for CH_4 are calculated as follows (here in [$cm^2 s^{-1}$]) :

$$D_{CH4}^{air} = 0.1875 + 0.0013 \cdot T \qquad \text{(Lerman, 1979)} \tag{2.5}$$

$$D_{CH4}^{water} = (0.9798 + 0.02986 \cdot T + 0.0004381 \cdot T^2) \cdot 10^{-5} \qquad \text{(Broecker and Peng, 1974)} \tag{2.6}$$

where T is the temperature [K] in a soil layer.

In the acrotelm: If enough gas is present ($F_{air} > 0.13$, F_{air} the actual gas fraction per layer), the diffusivity is calculated via:

$$D_{CH4} = F_{air}^{\frac{10}{3}}/\Phi^2 \cdot D_{CH4}^{air} \tag{2.7}$$

with Φ being the overall porosity (Millington-Quirk model Millington & Quirk, 1961; Iiyama & Hasegawa, 2005).

Otherwise

$$D_{CH4} = D_{CH4}^{water} \tag{2.8}$$

In the catotelm:

$$D_{CH4} = D_{CH4}^{water} \tag{2.9}$$

Generally, the soil is divided into a fraction of ice (F_{ice}), (liquid) water (F_{water}) and air (F_{air}) per layer. These three fractions are equal to the porosity which is 0.9 in the acrotelm and 0.8 in the catotelm.

$$F_{air} + F_{water} + F_{ice} = \text{porosity} = 0.9 \text{ in acrotelm or } 0.8 \text{ in catotelm} \tag{2.10}$$

$$V_y = F_y \cdot D_z,\ y = \text{air, ice, water} \tag{2.11}$$

$$V_y' = \frac{V_y}{\text{m}^2} \tag{2.12}$$

The partition between water, ice and air is dynamic. D_z is the thickness of the according layer. V_y are the according volumes for these fractions in m^3, V_y' the same volumes per m^{-2}.

A difficult aspect of modelling gas diffusion is setting up boundary conditions at the water-air interface where diffusivities change by at least four orders of magnitude. A robust way to

calculate the flux F from the top water layer (or an unsaturated soil) into the overlying air layer is as

$$F = \frac{k_x}{d_z}(C_{surf,x} - C_{eq,x}) = -\frac{dC_x}{dt} \tag{2.13}$$

with k_x being the gas exchange coefficient with units of velocity [m d^{-1}] (piston velocity Wania, 2007), d_z [m] $= \frac{V_{available}}{1\,m^2}$ $[\frac{m^3}{m^2}]$, $V_{available}$ $(= F_{water} \cdot D_z)$ the water content per layer, $C_{eq,x}$ the equilibrium concentration [mol l^{-1}](Henry's Law) of a gas x in the atmosphere, $C_{surf,x}$ [mol l^{-1}] the concentration of the same gas measured in the surface water (McGillis et al., 2000). For simplicity, $C_{surf,x}$ is called C_t and the index x is not written in the following derivation; C_0 is a constant in [mol l^{-1}].

$$\frac{\Delta C}{\Delta t} = \frac{-k}{d_z}(C_t - C_{eq}) = \frac{C_{t+\Delta t} - C_t}{\Delta t} \tag{2.14}$$

$$C_{t+\Delta t} = C_0 e^{\frac{-k\cdot(t+\Delta t)}{d_z}} + C_{eq} \tag{2.15}$$

$$C_t = C_0 e^{\frac{-k\cdot t}{d_z}} + C_{eq} \tag{2.16}$$

$$\frac{C_{t+\Delta t} - C_{eq}}{C_t - C_{eq}} = \frac{e^{\frac{-k\cdot(t+\Delta t)}{d_z}}}{e^{\frac{-k\cdot t}{d_z}}} = e^{\frac{-k\Delta t}{d_z}} \tag{2.17}$$

Therefore, for each time step t, the new concentration for the uppermost layer is calculated as for gas x ($x = O_2$, CH_4 or CO_2):

$$C_{x,(t+\Delta t)} = C_{eq,x} + (C_{x,t} - C_{eq,x}) \cdot e^{\frac{-k_x}{d_z}\Delta t} \tag{2.18}$$

with

$$C_{eq,x} = \frac{P_{gas,x}}{H_x} \cdot RT$$

Eq. 2.18 is a stable analytical solution to eq. 2.13. The gas transfer velocity k_x [m d^{-1}] is calculated via the Schmidt number (Wania, 2007) and the equilibrium concentration via Henry's law. With $P_{gas,x}$ [Pa] the partial pressure of a gas x, P_{gas} [Pa] the total partial pressure and H_x the dimensionless Henry constant (ratio of aqueous to gaseous phase; see also Chap. 2.4.2.1), T the temperature [K] , R the universal gas constant.

In the LPJ-Bern version, the total CH_4 layer content diffuses (depending on the water content with a different diffusivity), while in the LPX version CH_4 is separated into dissolved and gaseous CH_4 content (see Chap. 2.4.2).

2.4.1.5 Plant transport

Another possible pathway to exchange CH_4, CO_2 and O_2 between the soil layers is transport through vascular plants. Vascular plants are adapted to inundation. They developed aerenchyma - gas filled tissue in roots, stems and leaves that enable the transport of CH_4 and carbon dioxide to the atmosphere as well as the delivering of oxygen to the roots. Here, only the dominant passive flux (gas flux follows the concentration gradient) is considered and not any active pumping (Cronk & Fennessy, 2001). The main factors for plant transport are the abundance of aerenchymatous plants, their biomass, the phenology of the plants and their rooting depths. In the model, plant-mediated transport only occurs via the flood-tolerant C_3 graminoid PFT, with the gas flux through vascular plants being related to the cross-sectional area of tillers available to transport gas. Estimates to determine the tiller radius (r_{tiller}) for the grass PFT are described in Wania (2007). As r_{tiller} controls the transport capacities of this pathway, it is the third sensitivity parameter in the CH_4 routine (see Chap. 3)

The new concentration in a layer is calculated similarly as described in the section about diffusion (Sec. 2.4.1.4; exchange between uppermost layer and atmosphere). Here, every soil layer is in direct contact with the atmosphere. For gas x ($x = O_2$, CH_4 or CO_2) as:

$$C_{x,(t+\Delta t)} = C_{eq,x} + (C_{x,t} - C_{eq,x}) \cdot e^{\frac{-k_x}{V_{available}/tillerarea}\Delta t} \tag{2.19}$$

The plant transport is weighted by the area of porous root cross-sections (Wania, 2007). $Tillerarea = (r_{tiller})^2 \cdot \pi$ [m^2]. For $C(t+1) > C_{eq}$, the calculated amount of exchanged gas is directly transported to the atmosphere.

2.4.1.6 Ebullition

Dissolved and gaseous CH_4 can escape to the atmosphere either by diffusion or through plant tissue (aerenchyma), which is also treated as a diffusive flux. Gaseous CH_4 can in addition reach the atmosphere by ebullition. The original ebullition routine from LPJ-WhyMe was completely replaced. The new CH_4 routine was recalibrated for 7 sites (described in Chap. 3) like in (Wania et al., 2010) after all major changes, which results in different values for the tuning parameters in the different versions, i.e. LPJ-WhyMe, LPJ-Bern and LPX (see Appendix).

Again, all calculations are done for each soil layer separately. The relevant variables are summarized in Tab. 2.1.

The existence of three gas species (CH_4, CO_2 and N_2) is assumed in the bubbles (Tokida et al., 2007).

The available volume per m^2, $V'_{available}$, is the layer height multiplied by the porosity and corrected for the frozen volume. Again, note that F_{air} (air fraction) and V_{air} (air volume) are not the same as F_{gas} and V_{gas} that are calculated within the CH_4 routine for the gaseous fraction and volume of CO_2, CH_4 and N_2 from $F_{available}$ ($= F_{water} \cdot D_z$) for the ebullition and diffusion routine.

$$V'_{available} = V'_{gas} + V'_{diss} = \rho \cdot D_z - V'_{ice} \quad [\frac{m^3}{m^2}] \tag{2.20}$$

The soil is separated in the acrotelm (defined as the upper 0.3 m which experiences a fluctuating water table) and the catotelm, the underlying permanently inundated layers with a fixed thickness of 1.7 m. The respective porosities are $\rho_{acro} = 0.9$ for the three first layers, $\rho_{cato} = 0.8$ for the 5 deeper layers. P_E is the environmental pressure and therefore the sum of the atmospheric pressure (101325 Pa) and the hydrostatic pressure.

Initial conditions: the gaseous volume of N_2 is assumed to be 1% (lower bound estimate, e.g. Shannon et al., 1996) of the available volume in a layer (liquid phase and gas phase).

$$n'_{CO2} = n'_{CH4} = 0 \tag{2.21}$$

$$V'_{\text{gas}} = 1\% V'_{\text{available}} \tag{2.22}$$

$$V'_{diss,N2} = 99\% V'_{available} \tag{2.23}$$

The amount of N_2 in each layer is then calculated via Henry's law (Tokida et al. (2007) or eq. 2.43).

$$n'_{N_2} = \frac{P_E \cdot (V'_{gas} + V'_{diss} \cdot H_{N_2})}{RT} \quad [\frac{mol}{m^2}] \tag{2.24}$$

x	gas species (CH_4, CO_2, N_2)
$V'_{available}$	available volume for CH_4, CO_2, N_2 (liquid and gas bubbles, not frozen) in a layer per m^2 [m]
V'_{gas}	total gas volume for CH_4, CO_2, N_2 per m^2 [m]
$V'_{diss,x}$	dissolved volume of species x per m^2 [m]
V'_{diss}	volume in which the gases can dissolve per m^2 [m]
V'_{ice}	frozen volume in a layer per m^2 [m]
ρ	porosity
T	temperature in a layer [K]
R	universal gas constant
D_Z	thickness of layer z [m]
P_E	pressure at depth of layer z [Pa]
H_x	dimensionless Henry constant (ratio of aqueous to gaseous phase) for gas x
n'_x	total number of moles of gas species x per m^2 [mol/m^2]
$V'_{gas,ebull}$	gas volume at threshold o ebullition [m]
$P_{gas,x}$	partial pressure of gas species x [Pa]
P_{gas}	total gas pressure [Pa]
$\Delta V'$	total gas volume lost through an ebullition event per m^2 [m]
$\Delta n'_x$	change in total amount of gas species x $[\frac{mol}{m^2}]$
$\Delta m'_x$	total mass change in gas species x $[\frac{g}{m^2}]$
M_x	molar mass of gas species x $[\frac{g}{mol}]$

Table 2.1: Overview of relevant variables in the ebullition routine.

Then, the produced or transported CH_4 and CO_2 is added to the layer (they are simulated in the model; in contrast to LPX, LPJ-Bern takes the whole CH_4 content as it can not separate between dissolved and gaseous CH_4) and recalculate the partial pressure for all gases (Tokida et al., 2007; Kellner et al., 2006; Yamamoto et al., 1976; Wiesenburg & Guinasso, 1979; Weiss, 1970):

$$n_{CO2}(t)' = n_{CO2}(t-1)' + \Delta n'_{CO2} \tag{2.25}$$
$$n_{CH4}(t)' = n_{CH4}(t-1)' + \Delta n'_{CH4} \tag{2.26}$$

$$n_{CH4}(t)' = n_{CH4}(t-1)' + \Delta n'_{CH4} \tag{2.27}$$

$$P_{x,i} = n'_{x,i} R T_i \left(V'_{\text{gas},i} + V'_{\text{diss},i} \cdot H_x\right)^{-1} \tag{2.28}$$

For the ebullition, assume a critical threshold for a gas volume that exceeds 15% of the available volume (FechnerLevy & Hemond, 1996; Rosenberry et al., 2003; Tokida et al., 2005)

$$V'_{gas} \geq 15\% V'_{available} \tag{2.29}$$

and compute $P_{gas,x}$.

$$P_{gas,x} = \frac{n'_x RT}{V'_{gas} + V'_{diss} \cdot H_x} = \frac{n'_x RT}{15\% V'_{availalbe} + 85\% V'_{available} \cdot H_x} \tag{2.30}$$

In the code, ebullition is triggered if the sum of all partial pressures is larger than the sum of atmospheric and hydrostatic pressure:

$$P_{gas} = \sum_x P_{gas,x} \geq P_E \tag{2.31}$$

The number of moles of CO_2 and CH_4 released per ebullition event is assumed to be 1% of the available volume times the CO_2 and CH_4 partial pressure divided by $R\,T_i$, respectively. In other words, a fifteenth of the CO_2 and CH_4 amount in the gas phase is released per ebullition event. This assumption and that the gas volume is equal to 15% of the available volume are not critical for the total emissions (see Chap. 3). Instead these parameters modulate the frequency and the magnitude of ebullition events on a short scale.

$$\Delta V' = 1\% V'_{available} \tag{2.32}$$

The change in the total amount of CO_2 and CH_4 is

$$\Delta n'_x = \frac{\Delta V' P_x}{RT} (mol\, m^{-2}) \tag{2.33}$$

$$\Delta m'_x = \Delta n'_x \cdot M_x (g\, m^{-2}) \tag{2.34}$$

while n'_{N2} is kept constant.

2.4.2 The methane routine in LPX

Differences in the CH_4 routine between LPJ-Bern and LPX are as mentioned before in the diffusion and the ebullition routine. The other parts and their order is as described in the previous sections for LPJ-Bern.

2.4.2.1 Partition between dissolved and gaseous CH_4 for diffusion

In LPX the amount of CH_4 existing in dissolved and in gas form is explicitly calculated. While in LPJ-Bern, the total amount of CH_4 is used in diffusion transport and only the diffusion constant is variable, CH_4 diffusion in LPX considers only the actual amount of CH_4 dissolved in water if the water phase is dominant for transport. The procedure in LPX is the following:

1. If the gas volume per layer is more than 13 % of the total available layer volume, it is assumed that CH_4 can diffuse through air in gas form which is much faster than through water. As long as a layer is not saturated with water, it is assumed that a new equilibrium between gas and water phase is reached instantaneously and all the CH_4 can be taken into account for diffusion. The diffusion constant is taken for gaseous CH_4.

2. If a layer is water saturated, only the dissolved part is taken into account for diffusion. The according diffusion constant is used.

The separation between gaseous and liquid CH_4 is also done in the new ebullition routine (Chap. 2.4.2.2): Only CH_4 in gas form is used in the ebullition calculation.

For diffusion and ebullition, the division between gaseous CH_4 and CH_4 dissolved in water is calculated numerically by solving eq. 2.43 daily for each layer. Henry's law (FechnerLevy & Hemond, 1996; Rosenberry et al., 2003; Tokida et al., 2005, 2007) relates the amount of dissolved and undissolved gases in each layer to the partial pressure of CH_4, CO_2 and N_2, available water and soil temperature.

$$n_{x,gas} = c_{x,gas} \cdot V_{gas} \tag{2.35}$$

$$n_{x,diss} = c_{x,diss} \cdot V_{diss} \tag{2.36}$$

$$H_x = \frac{c_{x,diss}}{c_{x,gas}} \tag{2.37}$$

$$\Rightarrow n_{x,diss} = c_{x,gas} \cdot H_x \cdot V_{diss} \tag{2.38}$$

$$n_x = n_{x,gas} + n_{x,diss} = c_{x,gas} \cdot (V_{gas} + H \cdot V_{diss}) \tag{2.39}$$

$$\text{with the ideal gas law:} \quad P_x = \frac{n_{gas} \cdot RT}{V_{gas}} = c_{gas} \cdot RT \tag{2.40}$$

$$\frac{P_x}{RT} = \frac{n_x}{V_{gas} + H \cdot V_{diss}} \tag{2.41}$$

$$P_{tot} = \sum_x P_x \tag{2.42}$$

P_{tot} [Pa] being the total partial pressure of CH_4, CO_2 and N_2, that is assumed to be equal to the environmental pressure at the start of the calculation; R is the universal gas constant, T the soil layer temperature [K]; n_x the total amount of gas x (x = CH_4, CO_2 or N_2) [mol]; V_{gas} the total gas volume of CH_4, CO_2 and N_2 [m^3] per layer, V_{diss} the dissolved (unfrozen) water volume [m^3] per layer, H_x the dimensionless Henry constant of gas x (ratio of aqueous to gas phase), $n_{x,gas}$ and $n_{x,diss}$ the total amount of gas x in gaseous or dissolved form [mol], c_{gas} and c_{diss} the concentration of gas x in gaseous or dissolved form [mol m^{-3}]. The previous calculations lead to Eq. 2.43:

$$\frac{P_{tot}}{RT} = \frac{n_{CH4}}{V_{gas} + V_{diss} \cdot H_{CH4}} + \frac{n_{CO2}}{V_{gas} + V_{diss} \cdot H_{CO2}} + \frac{n_{N2}}{V_{gas} + V_{diss} \cdot H_{N2}} \tag{2.43}$$

Eq. 2.43 leads to a cubic equation for V_{gas}, as the total amount of CH_4 and CO_2, the liquid (i.e. not frozen) water volume and the temperature are given. The water volume $V_{available}$ (=V_{gas}+V_{diss}) within each layer is given by the layer thickness and the porosity for fully water saturated conditions. The total amount of N_2 is assumed to be constant, since it is not simulated by our model. However, the change in the partitioning of N_2 being dissolved in water and gas form is considered.

Eq. 2.43 can be iteratively solved for V_{gas} starting with the assumption that the total gas pressure is in equilibrium with the external pressure (= atmospheric and hydrostatic pressure), and the following Henry constants depending on the soil temperature T (Yamamoto et al., 1976; Wiesenburg & Guinasso, 1979; Weiss, 1970):

$$H_{N2} = 1/exp(-59.6274 + \frac{85.7661 \cdot 100}{T} + 24.3696 \cdot \ln(\frac{T}{100})) \tag{2.44}$$

$$H_{CO2} = 1/exp(-58.0931 + \frac{90.5069 \cdot 100}{T} + 22.294 \cdot \ln(\frac{T}{100})) \tag{2.45}$$

$$H_{CH4} = 1/exp(-68.8862 + \frac{101.4956 \cdot 100}{T} + 28.731 \cdot \ln(\frac{T}{100})) \tag{2.46}$$

The iteration starts with $V_{gas} = 0.01\ V_{available}$ and the calculation of n_{N2} under this assumption and $P_{tot} = P_E$ (= hydrostatic and atmospheric pressure). n_x for CH_4 and CO_2 are set to 0. Then, a "running" total partial pressure p_{tot} is calculated for $0.1 \cdot n_{N2}$ and the resulting V_{gas}. Then, stepwise n_{CH4}, n_{CO2} and n_{N2} are added and the new V_{gas} is calculated and the total partial pressure p_{tot} adjusted (The procedure to built up the amount of CH_4, CO_2 and N_2 and the pressure is done to ensure to find the best, i.e. realistic solution with the cubic equation). This is iterated till all gas content is added and the result for V_{gas} is stable. If V_{gas}

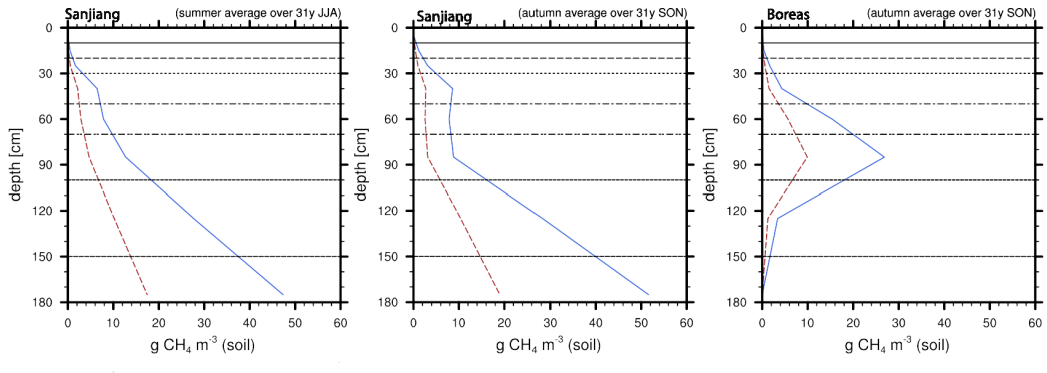

Figure 2.4: Example of partition into dissolved and gaseous CH_4 in LPX. Blue line: total CH_4 content per m^3 in a layer; red line: dissolved CH_4 content per m^3 in a layer; 1) Sanjiang (summer average over 1901-1930), 2) Sanjiang (autumn average over 1901-1930), 3) Boreas (autumn average over 1901-1930).

exceeds 20% of $V_{available}$, it is set to 20% of $V_{available}$ and the three gas species are divided into gaseous and liquid phase according to Henry's law. The excess volume is considered to be lost by ebullition. This partition between gaseous and dissolved CH_4 is used in the diffusion process and in the ebullition routine, where only the gaseous CH_4 is taken into account.

Glaser & Chanton (2009) estimate the gas volume of CH_4 to be 10-20% of the total soil volume within both deep and shallow peat strata, Comas et al. (2008) 0-20%. FechnerLevy & Hemond (1996) find that the mass of CH_4, stored in gas bubbles as much as 3 times the mass of dissolved CH_4, depending on the season and Schaefer et al. (2012) estimate that if the average gas volume is 5%, the average amount of CH_4 [gCH_4] in gas phase is 60% and 40% is dissolved. Fig. 2.4 illustrates the part of dissolved CH_4 simulated by LPX for test sides (input data described in Chap. 3, details about these simulations and results will be presented in Chap. 2.6.2 and 5). The average of simulations over 7 sites with LPX (description of the set-up in Chap. 3) in time and over all layers is about 17% gas volume and one quarter of CH_4 is in dissolved form and three quarters are in gas form. To save computing time, the old diffusion version from LPJ-Bern can be used. This leads in total to less diffusion due to a weaker concentration gradient between the soil layers.

2.4.2.2 Ebullition routine in LPX

The new ebullition mechanism calculates how much of the CH_4, CO_2 and N_2 actually is in gas phase and how much is dissolved as described above. The restriction that the gas volume can not exceed 20% of $V_{available}$ as described above holds also here.
In the ebullition version for LPJ-Bern, the gas volume was only reduced by constantly 1% of the water volume when it exceeded the threshold, regardless how much bigger the volume actually was. The modification in LPX now also takes into account by how much the threshold is exceeded:

if V_{gas} >0.15 $\cdot$ $V_{available}$ then

$\Delta V = (V_{gas}$ - 0.15 $\cdot$ $V_{available}) \cdot f_{ebull}$
$\Delta n_{CH4} = \Delta V \cdot P_{gas,CH4}$ / RT
$\Delta n_{CO2} = \Delta V \cdot P_{gas,CO2}$ / RT

with $P_{gas,CH4} + P_{gas,CO2} + P_{gas,N2} = P_{gas}$. f_{ebull} is set to 0.2 but can be changed (for example to 0.5) to modulate the magnitude and frequency of ebullition events.

Significant amounts of CH_4 can be stored as gas bubbles and the gas bubble volume is frequently large enough to serve as a significant buffer between microbial production of CH_4, and the release of CH_4 to the atmosphere (FechnerLevy & Hemond, 1996). Changes in atmospheric pressure, temperature, and water-table position may result in modulation of the ebullition CH_4 flux. Periods of rapidly rising atmospheric pressure or equivalent pressure changes due to water-table position are capable of arresting bubble volume growth, thereby halting CH_4 ebullition. Periods of rapid cooling of the bog could also temporarily halt ebullition, as thermally induced contraction of bubbles and dissolution of CH_4 offset bubble volume growth due to methanogenesis.

Glaser et al. (2004) suggest that the current estimates on northern peatland emissions (they are half of the worlds wetlands and contribute about a third or less of the total CH_4 emissions from all wetlands) need to be scaled up according to increasing data on the dynamics of CH_4 gas bubbles in peat deposits. They suggest that rates of methanogenesis may remain high in deep peat strata because of the downward transport of labile root exudates permitting the widespread production of gas bubbles. Their investigations using an array of methods have reported episodic ebullition fluxes exceeding $35\,\mathrm{g\,CH_4\ m^{-2}}$ per event. Gas bubbles accumulate in overpressured pockets that episodically rupture in response to steep declines in atmospheric pressure or declining water tables. Although these ebullition fluxes are highly variable in both time and space, they appear to dominate the annual CH_4 emissions from northern peatlands and represent a major and underappreciated element of the global CH_4 cycle (Glaser et al., 2004; Glaser & Chanton, 2009).

The tuning of all the adjustable parameters is described in Chap. 3 for LPJ-Bern and has been redone in the same way for LPX (see Appendix). Again, the choice of the threshold V_{gas} >0.15 $V_{available}$, ΔV and f_{ebull} in a reasonable range are not critical for the total yearly emissions. In most grid cells ebullition is the dominant pathway for CH_4 to escape (in all versions; see also Chap. 3). But the changes in the ebullition routine (especially when putting $f_{ebull} = 1$) have shifted the division between the three pathway by making especially plant transport weaker. Therefore, plant transport is now the least occurring pathway while before it was diffusion in most grid cells (see Chap. 2.6.2 for LPX and Chap. 3 for LPJ-Bern). LPX simulates for the 7 test sites plant transport from 5%-35% of the total CH_4 emissions, diffusion from 5-25% and ebullition 50-70% and for a global map (also driven with CRU data), the average partition is 16% plant transport, 21% diffusion and 63% ebullition. Bridgham et al. (2013) summarized the present findings in measurements for the importance of the different transportation pathways: the attribution to each of the three transportation pathways varies widely from measurement site. Plant transport is believed to be an important factor for emissions, but varies drastically depending on the system. For example, Dorodnikov et al. (2011) measured the plant-mediated CH_4 flux to account up to 30-50%. Also ebullition is believed to be very important for the emissions: Tokida et al. (2007) measure contributions from ebullition to be 50-65%.

2.5 Implementation of methane isotopes

The $\delta^{13}C(CH_4)$ values attributed to wetland emissions are ^{13}C-depleted relative to atmospheric CH_4 because the source is entirely biological. Fractionation of stable isotopes in CH_4 in peatlands occurs at each stage of the process where microorganisms or plants are involved (Gallego-Sala, 2010), i.e. during production, oxidation and transport. Also, the signature of the starting material is important. In the following, experimentally measured fractionations are listed as well as their implementation in the model. The atmospheric CH_4 signature is assumed to be constant at -47.7 permil for present day simulations and relevant for the diffusion process between the uppermost soil layer and the atmosphere.

2.5.1 Precursor material

The methanogenic pathway is crucial for the extent of carbon isotope fractionation, as methanogenesis by CO_2 reduction exhibits a much stronger fractionation factor than acetoclastic methanogenesis (Whiticar et al., 1986). For a long time, formation of wetland CH_4 has been attributed almost exclusively to methanogenic archaea that utilize the acetate fermentation pathway because of a long-standing assumption that acetoclastic methanogenesis dominates freshwater systems while CO_2/H_2 methanogenesis is most prevalent in marine sediments (Whiticar et al., 1986).

Northern wetland CH_4 exhibits a remarkable range of stable carbon isotope values considering that the gas is derived almost exclusively from degradation of C_3 plant material having a very limited range of $\delta^{13}C$ values (e.g., approximately -30 to -24 permil, Hornibrook et al., 2000). C_4 plants have a $\delta^{13}C$ of about -15 to -11 permil. Also LPX simulates different behaviour for ^{13}C in the photosynthesis process for C_3 and C_4 plants (Gerber et al., 2003). The $\delta^{13}C$ values reported to date for wetland CH_4 range from approximately -100 permil for gas transported through aerenchyma of vascular plants (Chanton et al., 2002) to approximately -42 permil for residual CH_4 after preferential loss of ^{12}C due to methanotrophy or diffusion through plant aerenchyma (Gerard & Chanton, 1993). These examples at the negative and positive ends of the $\delta^{13}C$ value range exhibited by wetland CH_4 are the result of secondary processes. Controls on primary $\delta^{13}C$ values of microbially formed CH_4 are similarly complex and include the biochemical pathway of methanogenesis (e.g., acetate fermentation or CO_2 reduction Whiticar et al., 1986), differences in the $\delta^{13}C$ composition of organic matter (Chanton et al., 1989), growth temperature (Whiticar, 1999), growth phase (Botz, 1996), and energetics of methanogenesis.

LPX uses a different atmospheric CO_2 concentration for mosses in the calculation of photosynthesis and GPP than for the grass PFT as mosses can access the CO_2 dissolved in acrotelm water (Wania, 2007; Smolders et al., 2001). For present day, this means instead of 340 ppm, mosses can see about up to 930 ppm. If the water table is high, mosses can access all of the acrotelm CO_2, but as the water table drops, the CO_2 concentrations available to mosses are a mixture between atmospheric CO_2 and acrotelm CO_2. Generally, the calculation of the fractionation of $\delta^{13}C$ in LPX during fixation in the leaf is based on a model by Lloyd & Farquhar (1994) which assigns the more positive values to the signature, the higher the CO_2 concentration is. This is not valid for mosses as it would lead to a signature for GPP coming from mosses of -12 permil. But typical values for moss biomass signature are -30 permil (Hornibrook et al., 2000; Markel et al., 2010). Therefore, it is assumed in LPX, that the Farquhar scheme holds not true for the additional CO_2 in water for the moss PFTs and the signature of moss GPP is set to constantly -30 permil. GPP coming from the grass PFT is simulated to be in average -25 permil which is in the range for C_3 plants. The average over all northern hemisphere peatland grid cells (see Chap. 5, present day simulation) for GPP

is about -27.6 permil. The averaged contribution to GPP from mosses is 53% and 47% from grasses, while the averaged fractional cover per grid cell is 36% grass, 64% moss.

2.5.2 Fractionation by process

2.5.2.1 Production

In peatlands, the prevalence of one of the two main methanogenic pathways seems to vary with the availability of labile substrates. The aceticlastic pathway is the most important near the surface while the hydrogenotrophic pathway predominates at depth, where more recalcitrant carbon is being utilised (Hornibrook et al., 1997). In peatlands of higher nutrient status, i.e. fens, there seems to be a greater dominance of the acetate fermentation pathway, while in bogs, the hydrogenotrophic pathway is the most important (Galand et al., 2005).

The plant matter (starting material) is decomposed by the fermentative bacteria and hydrolytic microorganisms, followed by syntrophic or homoacetogenic bacteria. Each of these processes has an intrinsic KIE (kinetic isotope effect; the KIE is the fraction of the rates of a reaction of a light isotope compared to the heavy isotope; see also Chap. 1.5) that imprints a stable isotope composition to the final material available to methanogens. The two main methanogenic pathways can be distinguished because CH_4 produced by the aceticlastic pathway tends to be ^{13}C-enriched, i.e. it has less negative δ^{13}C values (about -65 permil to -50 permil), than CH_4 produced by the carbon dioxide reduction pathway (δ^{13}C about -110 permil to -60 permil) (Whiticar et al., 1986; Gallego-Sala, 2010).

As LPX does not resolve CH_4 production on the microbial level, an empirical approach to simulate the isotopic signature of the CH_4 produced is applied. LPX changes the isotopic signature of CH_4 during production according to a logarithmic relation in dependance of the amount of the produced CH_4 (Hornibrook, 2009). The goal was to parameterise the production fractionation in such a way that it could reproduce in combination with all the other fractionations occurring, the relation between signature and amount of emitted CH_4 presented in (Hornibrook, 2009).

$$\delta^{13}C_{prod} = \delta^{13}C_{RH} + \epsilon_{prod} \tag{2.47}$$

$$\epsilon_{prod} = -c_1 \cdot log(^{12}C_{prod}) + c_2 \tag{2.48}$$

with $\delta^{13}C_{prod}$ and $\delta^{13}C_{RH}$ being the signatures of the produced CH_4 and the precursor material derived from RH [permil], $^{12}C_{prod}$ the amount of CH_4 [gCm^{-2} per layer per day]. c_1 and c_2 are chosen to agree with the findings of Hornibrook (2009).

2.5.2.1.1 Parametrisation

The parameters c_1 and c_2 for the fractionation during CH_4 production were chosen to reproduce approximately the relation between δ^{13}C values of CH_4 flux into the atmosphere and the logarithm of the CH_4 emission rate found by Hornibrook (2009), see Fig. 2.5.

Fig. 2.6 shows again this regression line ($y = 6.13 \ln(x) - 100.8$) together with model output from LPX simulations for a global run forced with CRU climate data with $c_1 = 6.13$ and $c_2 = -25$. Yearly output was taken and daily values over the 1991-2000 were calculated. The site measurements used in Hornibrook (2009) span over very different time intervals (from daily to yearly) and are performed at different times of the seasons (spanning from January to December). The sites that differ most from the regression line exhibit quite a cold climate,

have relatively low emissions and their emissions come mostly from only the uppermost layer via diffusion into the atmosphere.

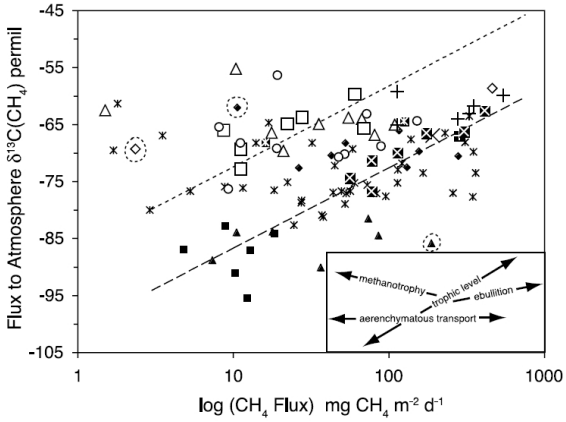

Figure 2.5: δ^{13}C values of CH_4 flux versus logarithm of CH_4 emissions rate Hornibrook (2009). The fine dashed line is the regression equation y = 14.18 log(x) - 86.6 permil (R^2=0.81) reported by Bellisario et al. (1999) determined from pore water $\delta^{13}C(CH_4)$ values and CH_4 flux rates. The coarse dashed line is the regression equation y = 6.13 ln(x) - 100.8 reported by Hornibrook & Bowes (2007) for flux rates of CH_4 emissions (R^2=0.63).

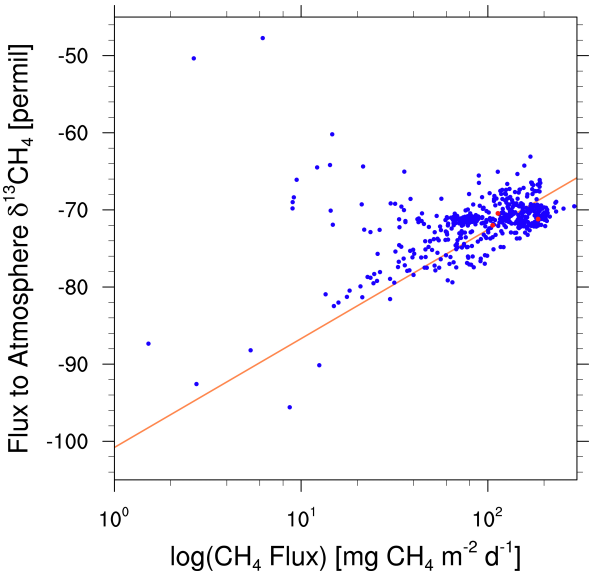

Figure 2.6: δ^{13}C values of CH_4 flux versus logarithm of CH_4 emissions rate in LPX. The line is the regression line found by Hornibrook (2009) with y = 6.13 ln(x) - 100.8. The blue dots are model output from a global LPX simulation over the active seasons (June-October) from 1991-2000 derived from monthly data; the dots highlighted in red are the three test sites.

2.5.2.2 Oxidation

Methane oxidation leads to a slight isotope fractionation because methanotrophs preferentially oxidize $^{12}CH_4$, leaving residual CH_4 enriched in ^{13}C. Values for the oxidation fractionation α_{ox} ranging from 1.008 (ϵ = 8 permil) (Bergamaschi et al., 1998), to 1.022 (Liptay et al., 1998), 1.022 - 1.025 (Reeburgh et al., 1997), 1.017 - 1.029 Tyler et al. (1994), to 1.025-1.049 (Chanton & Liptay, 2000) are reported.

LPX uses a constant fractionation effect of ϵ_{ox} = -20 permil.

$$\delta^{13}C_{oxid} = \delta^{13}C_{layer} + \epsilon_{ox} \tag{2.49}$$

with $\delta^{13}C_{oxid}$ being the signature of the oxidized CH_4, $\delta^{13}C_{layer}$ the signature of the CH_4 in the according layer of whom parts are oxidized. The signature of the layer after the oxidation is corrected accordingly:

$$\delta^{13}C_{layer,new} = \frac{\delta^{13}C_{layer,old} \cdot^{12} C_{layer,old} - \delta^{13}C_{oxid} \cdot^{12} C_{oxid}}{^{12}C_{layer,old} -^{12} C_{oxid}} \tag{2.50}$$

$\delta^{12}C_{layer,old}$ being the amount of CH_4 in a layer before oxidation [gCm^{-2}]and $\delta^{13}C_{layer,old}$ the according signature [permil], and $\delta^{12}C_{layer,new}$ and $\delta^{12}C_{layer,new}$ the amount and signature of CH_4 in a layer after oxidation.

2.5.2.3 Plant transport

Vascular plants may be responsible for a large fraction of the CH_4 emitted to the atmosphere from peatlands (Bowes & Hornibrook, 2006). During active transport by submerged plant tissue there is no fractionation. In contrast, during passive diffusion through vascular flora there is further fractionation of the CH_4 produced, and the emitted CH_4 is ^{13}C-depleted by $\sim$ 10 to 20 ‰ relative to CH_4 in the pore water pool (Hornibrook & Bowes, 2003; Bowes & Hornibrook, 2006). LPX uses a constant fractionation factor of ϵ_{plant} = -15 permil for the CH_4 that is emitted via plant transport.

$$\delta^{13}C_{plant} = \delta^{13}C_{layer} + \epsilon_{plant} \tag{2.51}$$

with $\delta^{13}C_{plant}$ being the signature of CH_4 leaving the layer via plant transport; at the same time the layer content of CH_4 is enriched in ^{13}C (analogue to eq. 2.50).

2.5.2.4 Diffusion

The ratio of the diffusion coefficient of $^{12}CH_4$ to the diffusion coefficient of $^{13}CH_4$, $\alpha_{diff,gas}$ was found experimentally to be 1.0178 ± 0.0009 in gas, close to the theoretically expected value of 1.0195 (De Visscher et al., 2004). From theoretical considerations, it can be expected that the binary diffusion coefficients of a mixture of two compounds A and B, is inversely proportional to the square root of the reduced mass, $M_A M_B/(M_A + M_B)$ (De Visscher et al., 2004). For water phase diffusion, $\alpha_{diff,diss}$ was measured to be 1.0012 (Knox et al., 1992).

$$D_{13CH4,water} = D_{12CH4,water} \cdot \alpha_{diff,water} \tag{2.52}$$

$$D_{13CH4,gas} = D_{12CH4,gas} \cdot \alpha_{diff,gas} \tag{2.53}$$

$D_{13CH4,water}$ and $D_{13CH4,gas}$ being the diffusivity for $^{13}CH_4$ [m^2 d^{-1}] in water or gas and $\alpha_{diff,gas}$ = 1.0178 for diffusion in gas phase, $\alpha_{diff,water}$ = 1.0012 for water phase.

Diffusion creates a secondary effect because some of the CH_4 is likely to be consumed by methanotrophs at the oxic-anoxic interface. The methanotrophs preferentially consume $^{12}CH_4$ and the CH_4 that remains and diffuses out to the atmosphere has therefore a more positive $\delta^{13}C$ value than primary CH_4 in the peat matrix.

LPX simulates the diffusion fractionation as all tracers ^{12}C, ^{13}C and ^{14}C diffuse separately (see Chap. 2.4.1.4) with a modified (eq. 2.52 and 2.53) diffusion coefficient. For perfect numerical match, a correction factor is applied to all layer contents after the diffusion process to ensure mass conservation (higher order numerical problem). Each species of CH_4 has its own correction factor which is in the order of 10^{-5}.

2.5.2.5 Diffusion air-water

The kinetic isotopic fractionation effect during gas exchange is $\alpha_{airwater} = 0.9992 \pm 0.0002$ or $\epsilon_{airwater} = 0.8$ permil (Knox et al., 1992). LPX has a constant $\epsilon_{airwater}$ of 1 permil.

2.5.2.6 Equilibrium fractionation air/water

Equilibrium fractionation due to partitioning between water and gas phase, or in other words the ratio of Henry's law constants of $^{12}CH_4$ and $^{13}CH_4$, was experimentally found to be very small (1.00033, (Fuex, 1980)), i.e. only a slightly higher amount of $^{13}CH_4$ than $^{12}CH_4$ is dissolved in water at equilibrium. Zhang & Krooss (2000) as well report that if a solubility fractionation exists, it is certainly much smaller than the fractionation effect resulting from diffusion and below the limit of detection for their methods. Therefore, LPX does not take this effect into account.

2.5.2.7 Ebullition

Ebullition is a fast process and one that does not result in a detectable fractionation (Gallego-Sala, 2010).

In summary, LPX simulates fractionation during production, oxidation and the plant and diffusive transport pathways. It also simulates the signature of the precursor material (RH coming from the moss and the grass PFT). But it does not directly differentiate between acetate fermentation or CO_2 reduction.

2.6 Soil profiles for δ^{13}C and δ^{12}C

2.6.1 Measurement examples

The δ^{13}C profile in the soil is dependent on the fractionation processes involved and the pathway of methanogenesis. Fig. 2.7 and Fig. 2.8 show two examples of measured profiles.

Fig. 2.7 is a profile measured in a landfill cover soil (De Visscher et al., 2004). De Visscher et al. (2004) demonstrated that not only oxidation is responsible for fractionation effects in landfill cover soils but also the transport of CH_4 through the soil. If oxidation was the only fractionating process (assuming the production signature is equal throughout the soil), the δ^{13}C value should increase as the gas moves up the soil and would be maximal at the soil surface. If there is fractionation due to diffusive transportation, the heavy isotope will diffuse out of the system more slowly and accumulate making δ^{13}C more negative closer at the surface. This will increase the concentration gradient for diffusive transport out of the soil until the increased gradient compensates the lower diffusion coefficient. This accumulation will lead to a maximum of the δ^{13}C value below the soil surface. The atmospheric CH_4 signature is about -47 permil (lighter than the CH_4 in the landfill cover soil) what influences the boundary value at the soil surface. Their measurements (see Fig. 2.7) illustrate the existence of fractionation during gas transport. They find stronger effects of transport fractionation in laboratory setups than in field measurements and attribute this to the presence of CO_2 (which is lacking in the laboratory setup) and fluctuating atmospheric pressure in reality which both lead to mixing and transport without fractionation.

Fig. 2.8 is a profile of a deep peat bog (Steinmann et al., 2008). Steinmann et al. (2008) explain the profile as follows: The isotopic composition of CH_4 and CO_2 traces the passage of respiration-derived CO_2 (from the near surface) through a shallow zone with methanogenesis of low isotopic fractionation (splitting of fermentation-derived acetate). This gas composition

then moves through the catotelm, where methanogenesis occurs by CO_2 reduction (large isotopic fractionation). In the upper part of the catotelm the ^{13}C-depleted respiration-derived CO_2 pool buffers the isotopic composition of CO_2; the δ^{13}C of CO_2 increases only slowly. At the same time strongly depleted CH_4 is formed as CO_2 reduction consumes the depleted CO_2. In the lower part of the catotelm, the respiration-derived CO_2 and shallow CH_4 become less important and CO_2 reduction is the dominant source of CH_4. The produced CH_4 in the peat bog has independent of the production pathway a more negative signature than the atmospheric CH_4. The contact of the uppermost soil region with the atmosphere therefore increases the signature in this region. In summary, they attribute the signature profile to the two different regimes of CH_4 production pathway and use only ebullition and advection in their transport model to explain the profile which both have an insignificant fractionation.

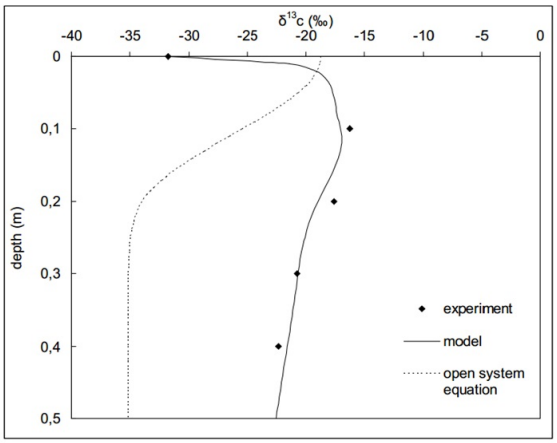

Figure 2.7: δ^{13}C-CH_4 vs. depth of landfill cover soils (De Visscher et al., 2004).

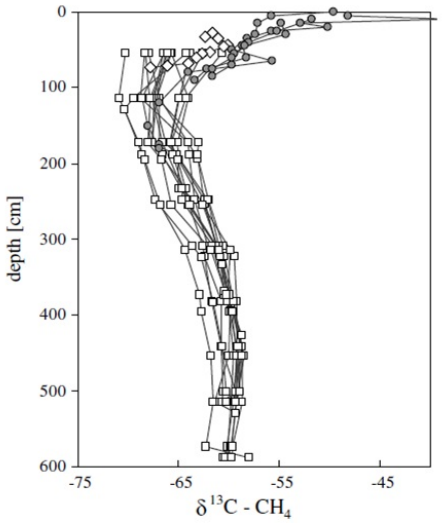

Figure 2.8: δ^{13}C-CH_4 vs. depth at Etang de la Gruyere (Steinmann et al., 2008). Squares represent measurements, diamonds are δ^{13}C values from a shallow profile. Circles are measurements from Sifton bog (Hornibrook et al., 1997).

2.6.2 Methane layer content of ^{12}C and ^{13}C in LPX

To illustrate the effect of the fractionation processes implemented in LPX on the ^{13}C soil profile, 3 sites with rather different climatic input (Tab. 2.2) are discussed in respect to ^{12}C and ^{13}C profiles and prevailing transportation pathways. The 3 sites are Boreas, Sanjiang and Abisko that were also used for the calibration of the methane routine (see Chap. 3 for details). They were forced with CRU climate data from 1901-2002 (with a 1000 years spin-up). The figures in this section either show one year (1990) or an average over 30 years (1971-2000).

Site	MAT	MAP	Info
Boreas	-2°C	480mm	deeper layers change between frozen/unfrozen
Sanjiang	2°C	620mm	never frozen in deeper layers
Abisko	-4°C	610mm	always frozen in deeper layers

Table 2.2: Average climatic input for the 3 test sites (1901-2002). MAT = Mean Annual Temperature; MAP: Mean Annual Precipitation. Modelled percentage of GPP coming from grasses: Boreas: 63%, Sanjiang 62%, Abisko 50%.

Fig. 2.9 shows the output for Boreas for the year 1990, Fig. 2.10 for Sanjiang and Fig. 2.11 for Abisko. The 4 columns represent the averages over the 4 seasons (DJF: December, January, February; MAM: March, April, May; JJA: June, July, August; SON: September, October, November). The first row shows the total and the dissolved CH_4 content per m^3 in a layer. Note that the layer contents are drawn in the middle of each layer and joined with a line for better visibility. The second row shows the CH_4 fluxes in (positive) and out (negative) of each layer [g CH_4 m^{-2} $month^{-1}$]. Values are only plotted if $|x| > 0.01$. Also fluxes into or out of a layer are plotted in the middle of the layer representing the change due to the fluxes for the whole box. Therefore, the lines do not represent fluxes through the boundary between two boxes; but the value in the middle of each box shows the change to the total layer content because of the according flux. In the case of diffusion between the layers, the plotted value is the sum of the fluxes into and from the layer above and below. Note that the representation of the diffusion from the uppermost layer to the atmosphere is drawn as a line in the first two layers and not only in the first one. This is done for better visibility. The third row shows the signature of the fluxes shown in the second row [permil] (see eq. 1.3). The fourth row presents the diffusive $^{13}CH_4$ flux [g CH_4 m^{-2} $month^{-1}$]. Finally, the fifth row shows the prevailing conditions in each layer: the water and ice content per layer, as well as the temperature [C]. F_{ice} and F_{water} are fractions (values between 0 and 1; see also eq. 2.10). Note the two different axis in this plot. LPX uses the units g CH_4 m^{-2} per layer for the layer content and g CH_4 m^{-2} per layer per day for fluxes. If not indicated otherwise, the layer contents are always plotted in units of g CH_4 m^{-3} (= model output corrected by layer thickness D_z: g CH_4 m^{-2} / D_z) and fluxes in g CH_4 m^{-2} per layer per day (or per month or year).

To interpret the different plots, it is crucial to note that the different processes have different thresholds for being active (see Tab. 2.3 and (Wania, 2007)) and to be aware of the order of the processes in the routine (see Chap. 2.4.1). Temperature and water content are the crucial factors to determine which processes are active. This again is crucial for the signature in the soil layers as each process has a different fractionation factor. Note that the production signature is kept constant for these first simulations here (ϵ_{prod} = -43 permil), while all other fractionation processes described in Chap. 2.5 are active.

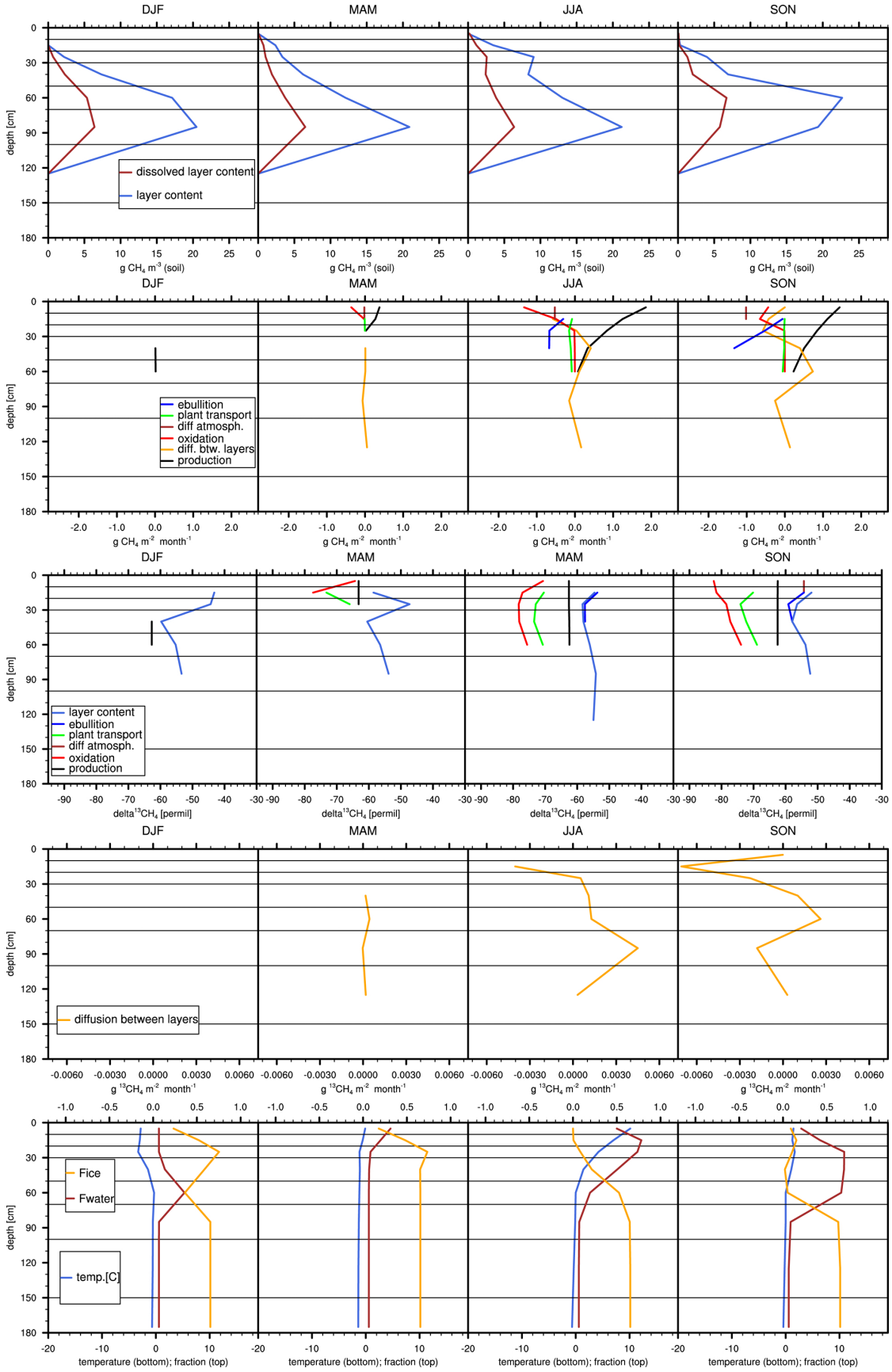

Figure 2.9: Seasonal layer content and fluxes of ^{12}C and ^{13}C, soil temperature and water content simulated for Boreas. Seasonal averages over all 3 month periods from 1901-1930 forced with CRU climate data (see Chap. 3. 1. row: soil content; 2. row: fluxes; 3. row: signature of fluxes; 4. row: ^{13}C diffusion flux; 5. row: climatic information (note that the axis is in Celsius for the temperature and unitless for the water and ice fraction (0-1)).

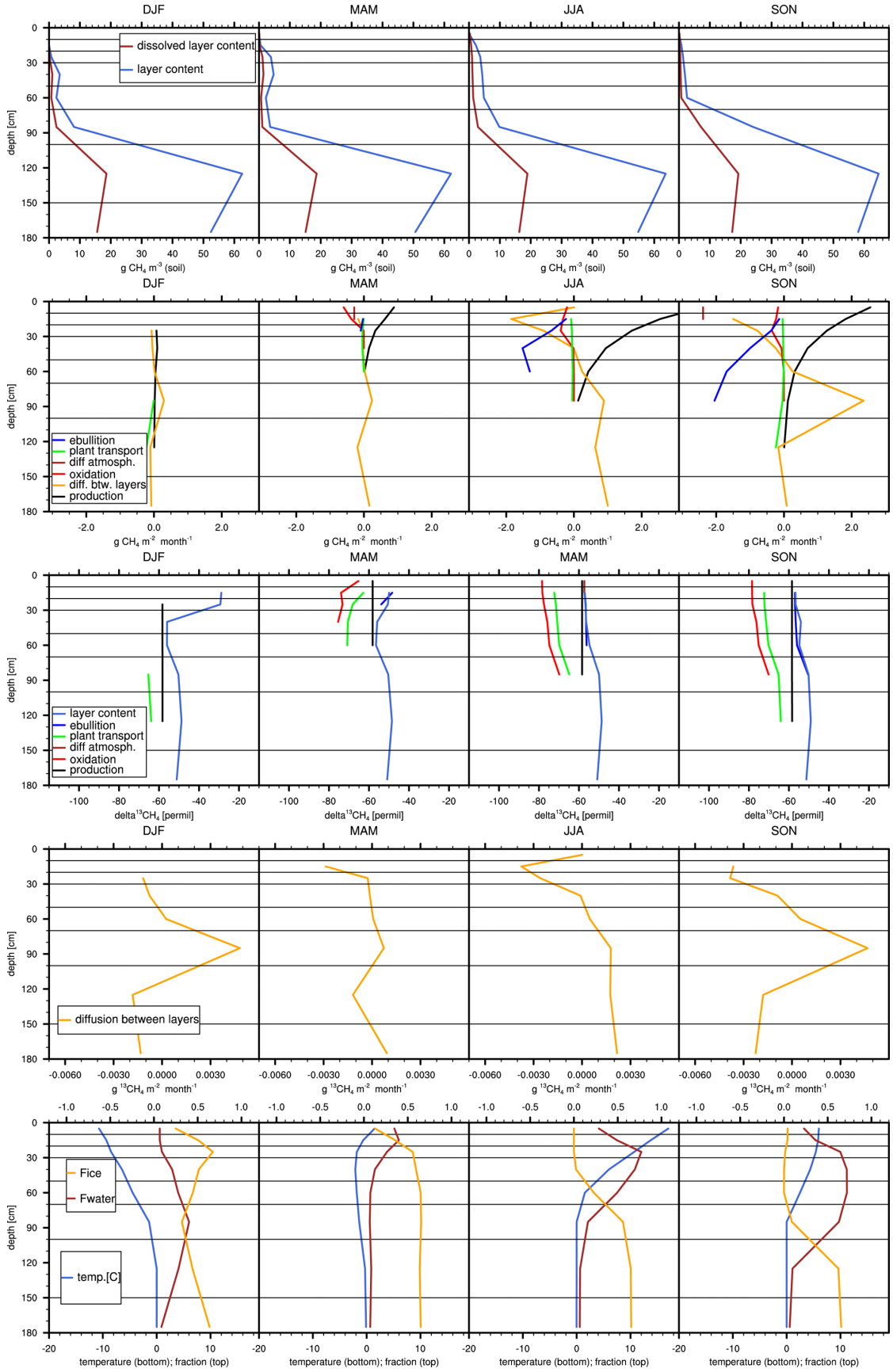

Figure 2.10: Seasonal layer content and fluxes of ^{12}C and ^{13}C, soil temperature and water content simulated for Sanjiang. Seasonal averages over all 3 month periods from 1901-1930 forced with CRU climate data (see Chap. 3).

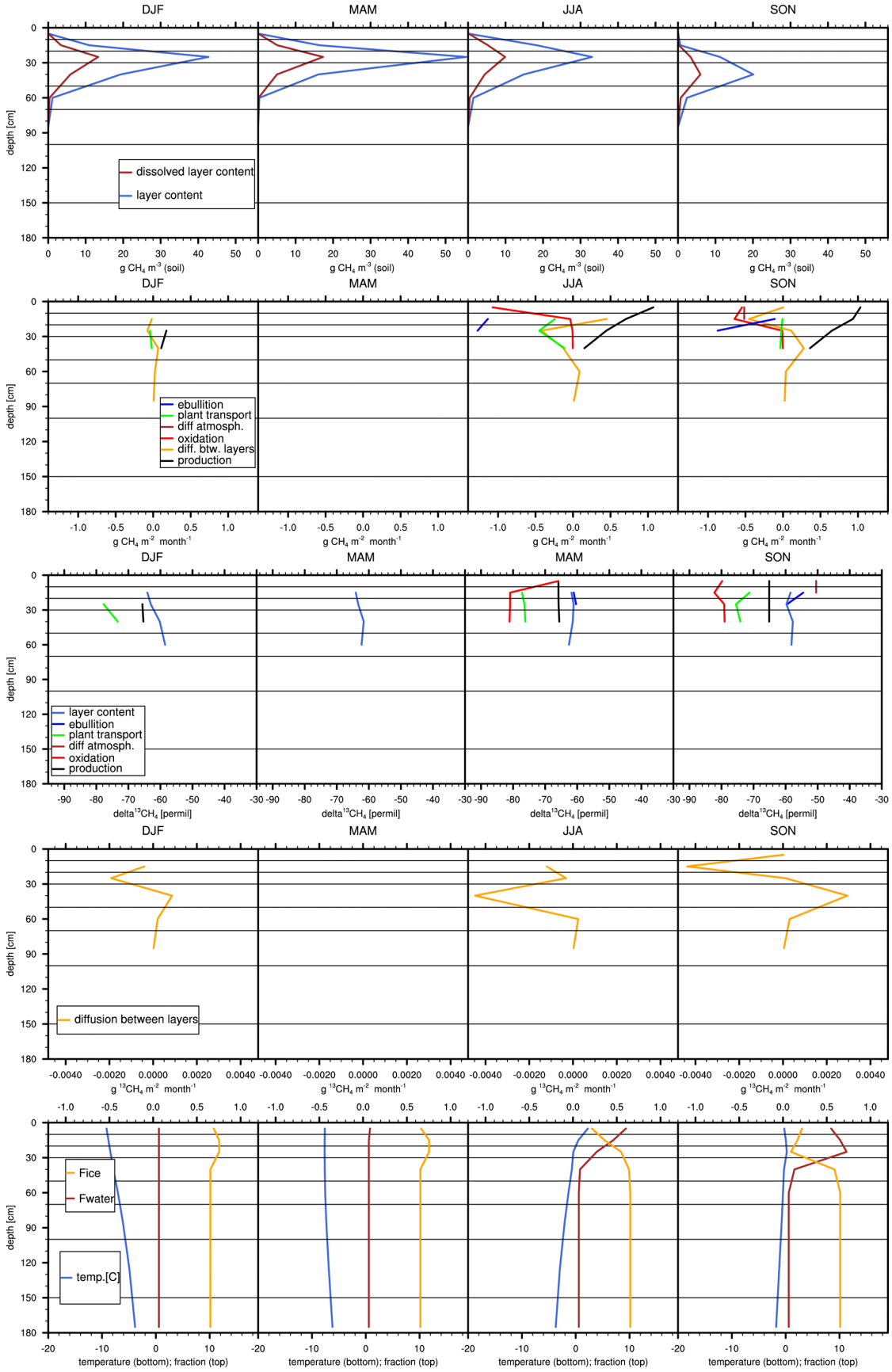

Figure 2.11: Seasonal layer content and fluxes of ^{12}C and ^{13}C, soil temperature and water content simulated for Abisko. Seasonal averages over all 3 month periods from 1901-1930 forced with CRU climate data (see Chap. 3).

Process	conditions
production	F_{water} >water minimum
diffusion	F_{water} >water minimum
	(and separation in diffusion in air or water depending on gas content)
oxidation	no further confinement (O_2 presence)
plant transport	F_{water} >water minimum and T >0°C
ebullition	F_{water} >0.3 and T >0°C

Table 2.3: Conditions for every process for being active; water minimum (=10% $\cdot V_{available}$) and F_{water} are fractions per layer volume.

Abisko is only active in the uppermost five layers. The lower layers are always inactive as the average temperature in every season stays clearly below zero and the non frozen water content never exceeds the minimum water content. Boreas is similar to Abisko but the temperatures are a bit higher, allowing diffusion to be active in short periods also in the deeper layers. Sanjiang in contrast has over an extended period and deep down a water content above the minimum and almost never negative temperatures, wherefore production and all transport pathways are active throughout almost all layers and the whole year (see also the 30 year average shown in Fig. 2.12-2.14): some CH_4 accumulates in deeper layers but part of it is also transported into the atmosphere later. Without the outgassing during freezing (mechanism described in Chap. 2.3), Boreas would accumulate much larger quantities of CH_4 than Sanjiang: During summer and autumn, production is high in the upper layers and diffusion transports CH_4 into the deeper layers. Slightly negative temperatures inhibit ebullition and plant transport but not diffusion. CH_4 could accumulate without the new mechanism of outgassing. In Abisko no accumulation is possible in the deeper layers because the soil temperature stays too negative throughout the whole year. Even diffusion is practically inhibited.

If the conditions are too cold and dry, nothing happens. If the conditions are warm and wet, all processes can be active: a lot of CH_4 is transported in both directions and most different fractionations take place. For the conditions between the two extremes, diffusion is the most important process and its fractionation dominant for the modification of the signature in the soil. As the deeper layers are water saturated, the fractionation for diffusion in water is taken (0.9988; see Chap. 2.5.2.4), which does only slightly change the signature.

The order of the processes is crucial (see Chap. 2.4.1). First, CH_4 gets produced. Then, diffusion reallocates CH_4 more uniformly between the layers, adding distortions to the isotope profile. If only diffusion is active in deeper layers, then CH_4 isotopes are depleted with depth. This is followed by oxidation and plant transport that are predominantly in the upper layer and that isotopically enrich the layers. Ebullition transports the biggest amount of CH_4 but does not change the signature of the CH_4 involved.

Note again that the first plots here are for one specific year only and that the budget for the layers (fluxes in and out) do not have to be zero as the layer content can still change over time. Especially Sanjiang has larger variations in the attribution and strength of the different processes. This ist visible in Fig. 2.16 and Fig. 2.17 - the signature fluctuates even in the deeper layers. For example, the trend (gain or loose) through diffusion in the deeper layers in the summer and autumn season is not always the same. For the comparison plot (Fig. 2.15) of all three sites together and a more general discussion, the 30 year average was taken to better capture the overall trends. Fig. 2.12-2.14 are basically the same as Fig. 2.9-2.11, except for the time period and that the production fractionation is not constant anymore.

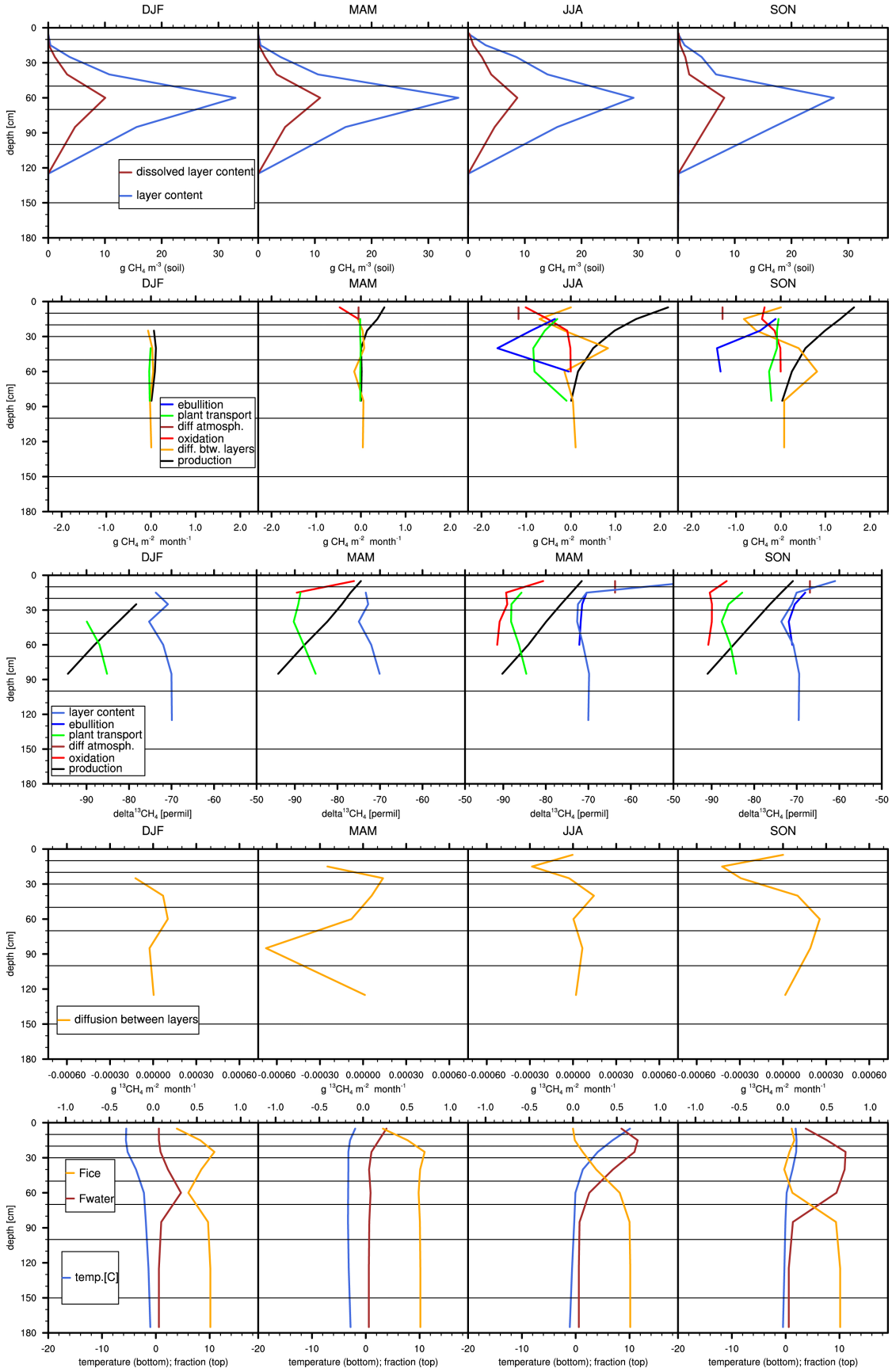

Figure 2.12: Seasonal layer content and fluxes of ^{12}C and ^{13}C, soil temperature and water content simulated for Boreas. Seasonal averages over all 3 month periods from 1971-2000 forced with CRU climate data (see Chap. 3).

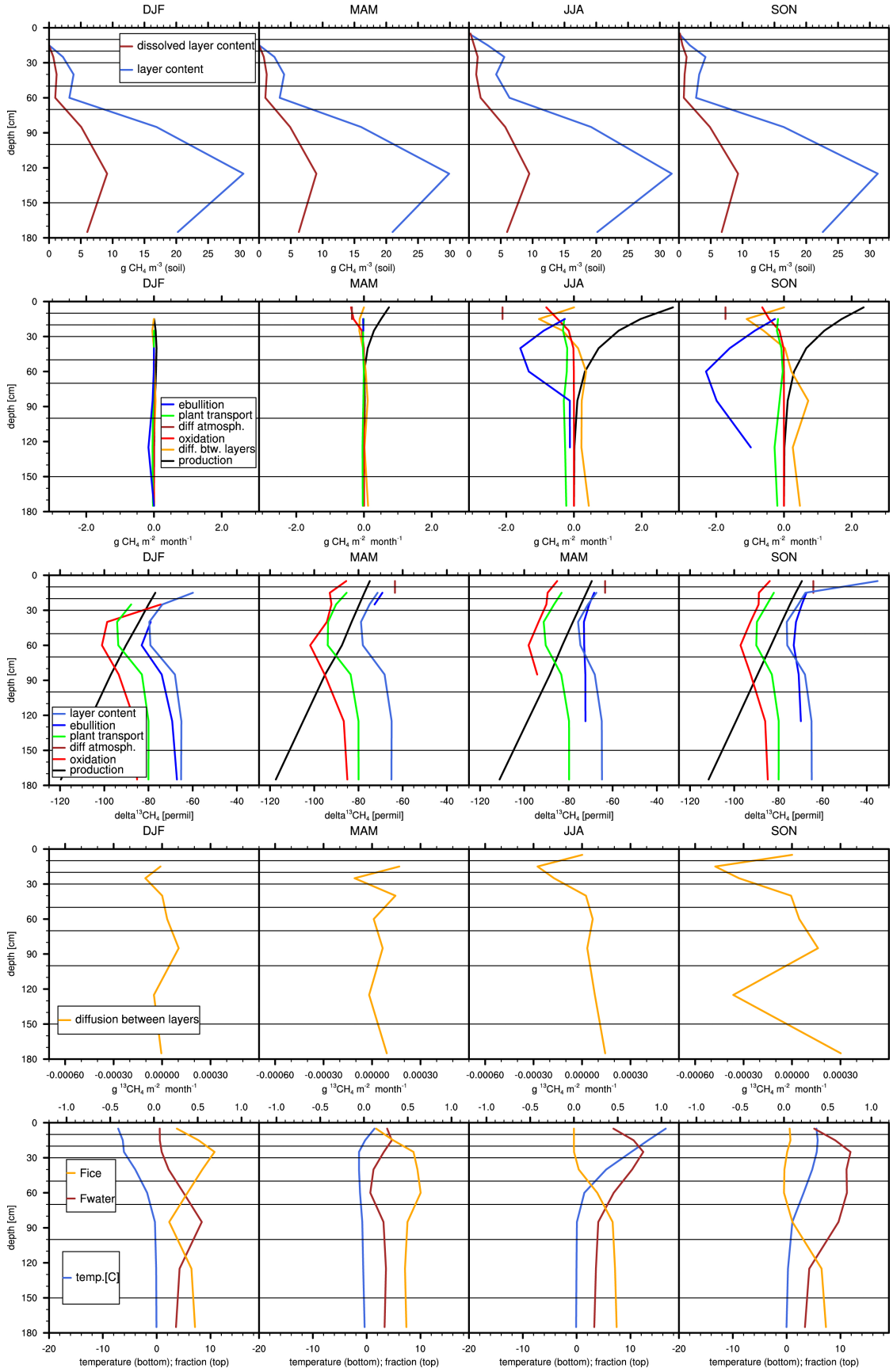

Figure 2.13: Seasonal layer content and fluxes of ^{12}C and ^{13}C, soil temperature and water content simulated for Sanjiang. Seasonal averages over all 3 month periods from 1971-2000 forced with CRU climate data (see Chap. 3).

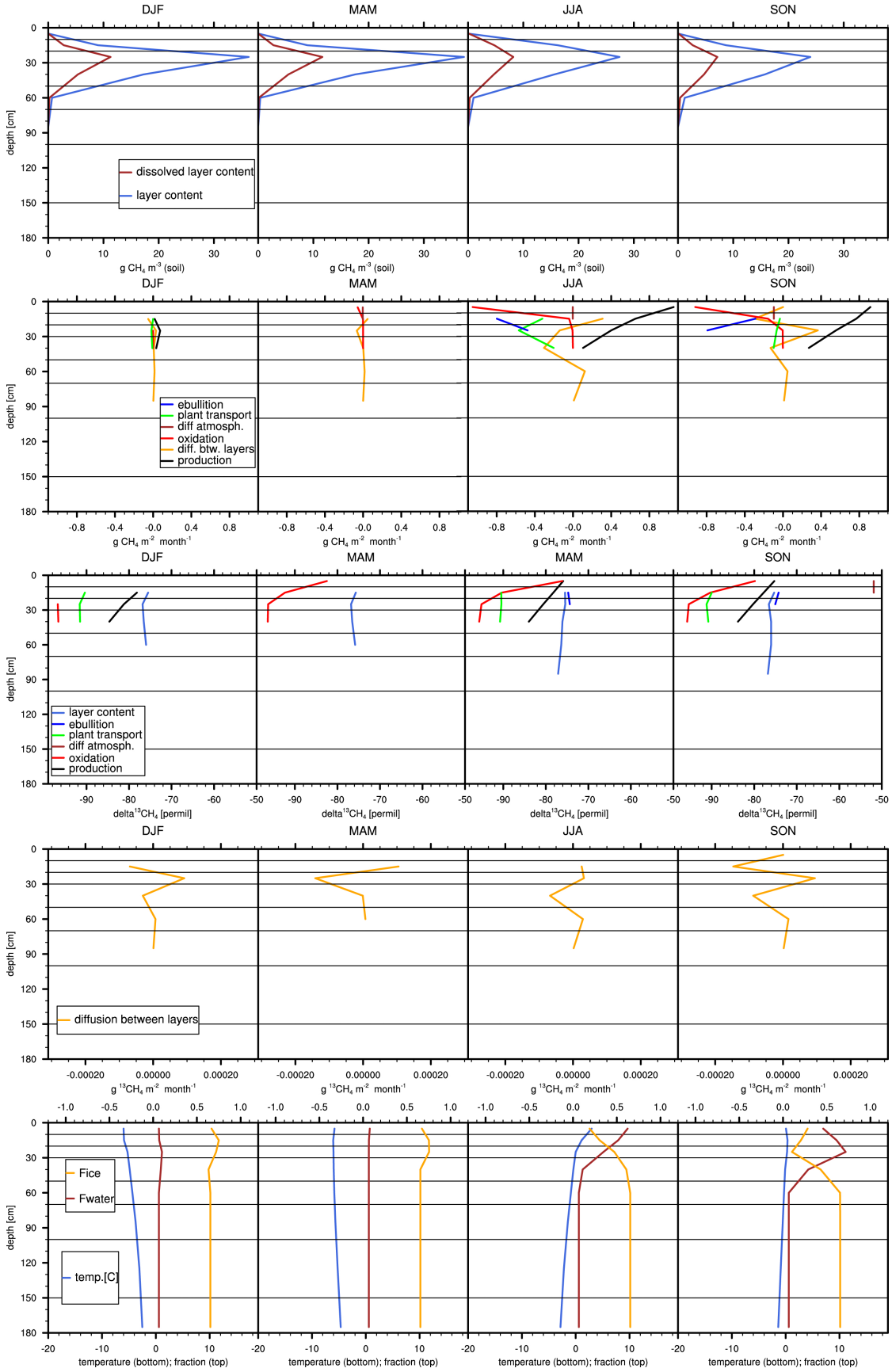

Figure 2.14: Seasonal layer content and fluxes of ^{12}C and ^{13}C, soil temperature and water content simulated for Abisko. Seasonal averages over all 3 month periods from 1971-2000 forced with CRU climate data (see Chap. 3.

The main reason that the deepest layers in Sanjiang are isotopically a bit more positive than Boreas is that only a small amount of CH_4 is transported downwards in Boreas. This makes the signature more negative with depth. In Sanjiang diffusion transports larger amounts of CH_4 downwards which then is released via plant transport making the remaining CH_4 heavier again (even if ebullition is the main transport pathway). In the middle layers, the opposite effect occurs. Both sites have diffusion of CH_4 into these layers but in Sanjiang, CH_4 mostly is transported to the atmosphere via ebullition, while in Boreas, plant transport is also an active transport way that is making the remaining CH_4 heavier. Therefore, Boreas middle layers are isotopically heavier than Sanjiangs'.

Fig. 2.15 shows the layer content for the autumn and winter season in $^{12}CH_4$ and $^{13}CH_4$ for Boreas, Sanjiang and Abisko as above (but values are already plotted if > 0.001) and in comparison to various measurements (see Tab. 2.4).

Generally, most papers published before 2007 assume that most of the CH_4 in the soils is dissolved. Therefore, they only measured the dissolved CH_4. Conrad (2005) state that it is not possible for them to quantify the relative contribution of the major methanogenic pathways by environmental data and Schaefer et al. (2012) report that soil and climate parameters do not have a simple correlation.

Paper	Site	Period	WTP	Info	diss./gas
Glaser, 09	Minnesota	1990+91, average	-	34 bogs&fens	porewater profile (assumed to be total)
Schäfer, 12	Jutland	Summer 2000	-30cm	3 temperate grassland	both (N-a Block)
Knorr, 08	Bayern	300d in 2008	-10cm	temperate fen; peatcore treatments	gas phase (W-V long term)
Steinmann, 08	CH	July 1999-Aug.2001	-15cm	peat bog	porewater profile
Popp, 99	Alberta	Aug.-Nov.1996	10cm	fen	porewater profile
Knorr, 08	Bayern	300d in 2008	-10cm	temp. fen; peatcore treatments	gas phase

Table 2.4: Details for measurements used for comparison with simulated soil profiles. (N-a is a specification of the measurement site (N = the one most north) and the block number (a); W-V stands for wet-vegetation and is a specification of the treatment of the block.)

Measurements of CH_4 emissions from ombrotrophic bogs typically come to -74.9 $\pm$ 9.8 permil, while values from fens are -64.8 $\pm$ 4.0 permil (Hornibrook, 2009). The model emissions from the three test sides (averaged over 1971-2000) are -62 permil for Boreas (with emissions of 11% from plant transport, 28% diffusion and 61% ebullition), -61 permil for Sanjiang (with emissions of 9% from plant transport, 38% diffusion and 53% ebullition) and -65 permil for Abisko (15% plant transport, 13% diffusion, 72% ebullition) with the constant production fractionation of -43 permil (as used in the simulations in Chap. 2.6.2) and -69 for Boreas, -67 for Sanjiang and -75 for Abisko with the parametrisation of the production discussed in Sec. 2.5.2.1 (c_1 = 6.13 and c_2 = -25).

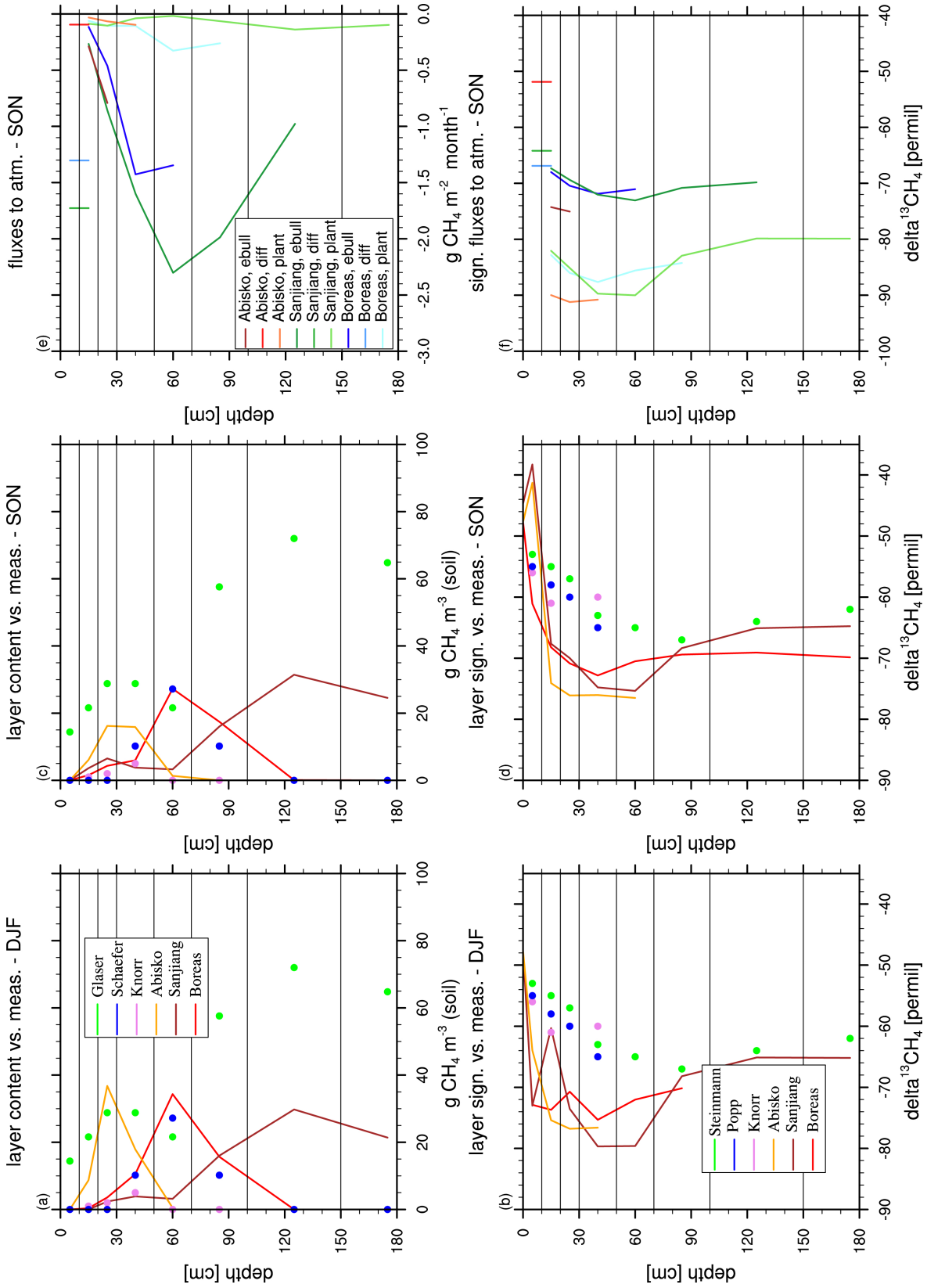

Figure 2.15: Seasonal layer content of ^{12}C (a for winter and c for autumn) and ^{13}C (b for winter and d for autumn) simulated for Boreas, Sanjiang and Abisko compared to measurements. $^{12}CH_4$ amounts (with corresponding signatures) are only plotted when they are greater than 0.0001 $\frac{g}{m^3}$. Plots e and f show the fluxes from plant transport, diffusion to the atmosphere and ebullition for the three sites with their signatures in autumn.

To understand the form of the signature soil profiles and the emission signals, it is important to know the proportion of the three different transport pathways in the soil layers. Another factor playing an important role for the CH_4 emission signature is the fractionation during production that is dependent on the amount of produced CH_4, i.e. sites with high production tend to have heavier emissions (see Chap. 2.5.2.1). Further, the composition of the starting material, i.e. sites with a higher contribution from mosses to RH have a slightly lighter signature in the starting material (see Chap. 2.5.1) and the fraction of oxidized CH_4 influence the δ^{13}C profile and emissions.

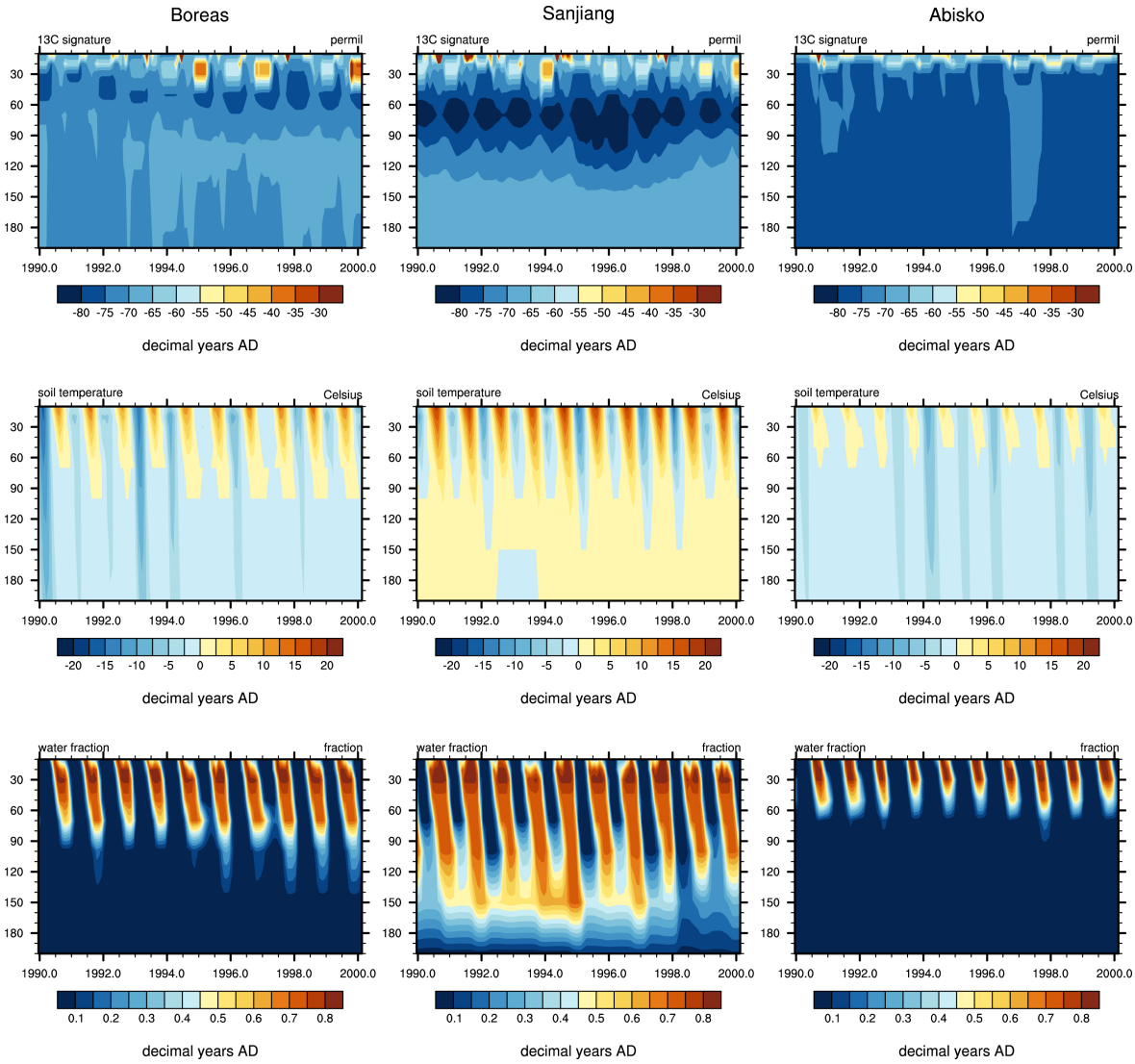

Figure 2.16: Isopleth diagram showing the δ^{13} values for CH_4 in the three test sites Boreas, Sanjiang and Abisko. The first row shows the monthly layer signature over 10 years (CRU input data), the second and third row the soil temperature and the water content as fraction of the soil volume.

Fig. 2.16 illustrates the monthly CH_4 signature in the soil over time (1990-2000; CRU data) for the three sites, Fig. 2.17 shows yearly averages over the time period of 100 years. For the deeper layers, CH_4 concentrations do not vary much over the seasonal cycle whereas the upper layers are more strongly affected by seasonal variation of transportation and oxidation. The signature (and CH_4 content) in the upper three layers (0-30 cm) is fluctuating in concert with temperature and non frozen water content: in summer and autumn, when the

temperatures in the soil are higher and the soil is more moist, signatures are higher. Note that the drastic signature rises are associated with almost empty layers. The signature as well as the ^{12}C content in the deeper 5 layers stays quite constant through the seasonal cycles and over many years in Abisko and Boreas. The soil profile of Sanjiang varies more as even the processes in the deeper layers are rarely shut down and change over time. Looking at the budget for the layers in Sanjiang before has already hinted to the fact that the profile will change over time.

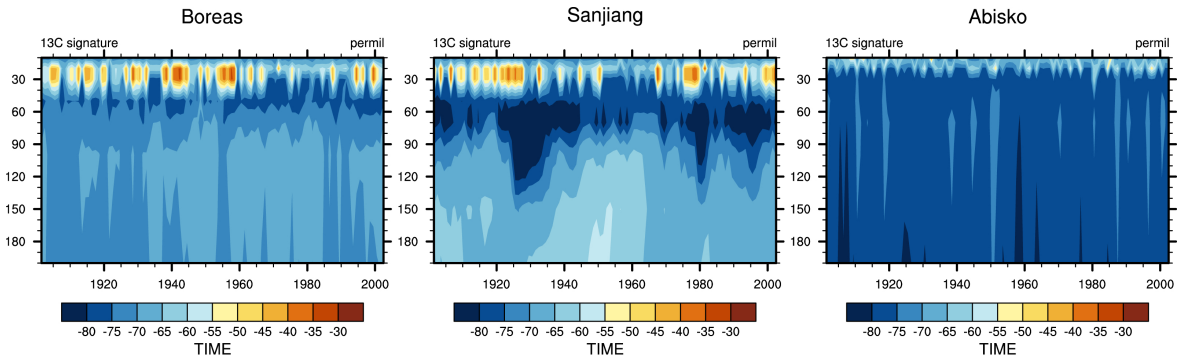

Figure 2.17: Isopleth diagram showing the δ^{13} values for CH_4 in the three test sites over a century. Note that signatures are also plotted for very small CH_4 content.

2.6.3 Effects by process

For the better illustration of the effect of every single fractionation process, the fractionations are turned on step-wise and discussed for the fall season of the test site Sanjiang and shown in Fig. 2.18. Picture a) shows again the ^{12}C fluxes. All soil layers are unfrozen (see Fig. 2.16). Ebullition that does not fractionate in LPX is the most dominant transportation pathway, followed by diffusion. Note that diffusion for ^{13}C is always active. The fractionation during diffusion can be turned off, but as soon as a gradient in the signature through another process is present, diffusion can further modify the profile. Picture b) shows the signature of the different fluxes and the layer content when the starting material's signature is constantly set to -21 permil and the production fractionation constantly to ϵ_{prod} = -43 permil, while all other fractionations are turned off, i.e., no fractionation during oxidation (ϵ_{oxid} = 0), diffusion (α_{diff} = 1) and plant transport (ϵ_{plant} = 0). There is the same concentration gradient between the layers for the diffusion in ^{12}C and ^{13}C when the production, oxidation or plant transport do not change the signature, therefore both isotopes diffuse likewise and the diffusion process does not change the relation between ^{12}C and ^{13}C. Picture c) shows what happens when the fractionation for production is turned on (see eq. 2.5.2.1; $\epsilon_{prod} = 6.13 \ln(x)$ - 25). We now have a different gradient in the ^{12}C and ^{13}C layer content throughout the soil profile, therefore, diffusion will also start to modify the profile further. The first 5 layers loose CH_4 through diffusion, making the layer isotopically more positive. The biggest gain has layer 3. Relevant amounts of CH_4 are only produced up to the 5th layer. The deeper layers inherit their CH_4 via diffusion through water, therefore the signature stays almost the same as in the 5th layer. Picture d) shows the effect, when we consider the fractionation during diffusion (to make the effect more visible, a slightly higher fractionation constant during diffusion was used here, namely the one for air than water; if the layer is water saturated, the diffusion in water is dominant which has only a small fractionation effect). The changes to picture c) are not that large, as $\alpha_{diff,gas}$ = 1.0178 for diffusion in gas phase, $\alpha_{diff,water}$ = 1.0012 for water phase. Picture e): In a next step, the oxidation fractionation is turned

on (ϵ_{oxid} = -25). Oxidation occurs in this example mostly in the second layer. Thus, the signature of the according layer is shifted to a heavier signature. Picture f): Finally, the plant fractionation is also turned on (ϵ_{plant} = -15) which results in the final situation illustrated. The plant transport is quite weak in this example - but still present. A small shift of the layer signatures to more positive values can be seen.

The budget in each layer (change in content = flux$_{in}$-flux$_{out}$) is preserved on a daily, monthly and yearly time level. As an example, the budget of fluxes and layer content changes of one specific day in Sanjiang is presented in Fig. 2.19.

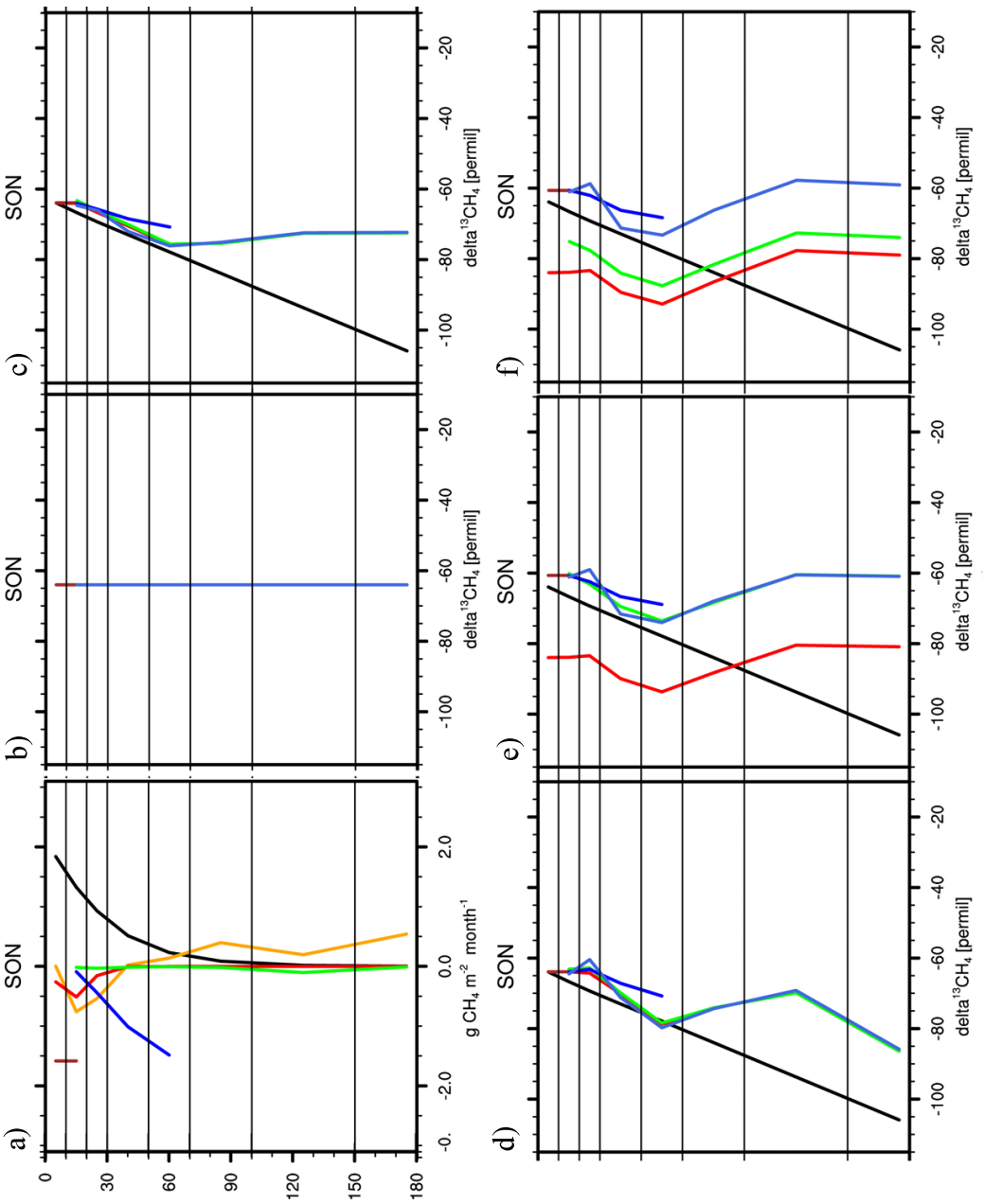

Figure 2.18: ^{12}C fluxes of CH_4 (Fig. a) and isotopic signature of CH_4 fluxes (Fig. b-f) as simulated for Sanjiang and averaged over September, October and November. b) without fractionation in the CH_4 routine; stepwise adding c) fractionation in the production; d) fractionation in the diffusion; e) fractionation in oxidation; f) fractionation in plant transport. Again, the production is plotted in black, diffusion between the layers in orange, oxidation in red, diffusion into the atmosphere in claret-red, plant transport in green, ebullition in dark blue and the layer content or signature in light blue.

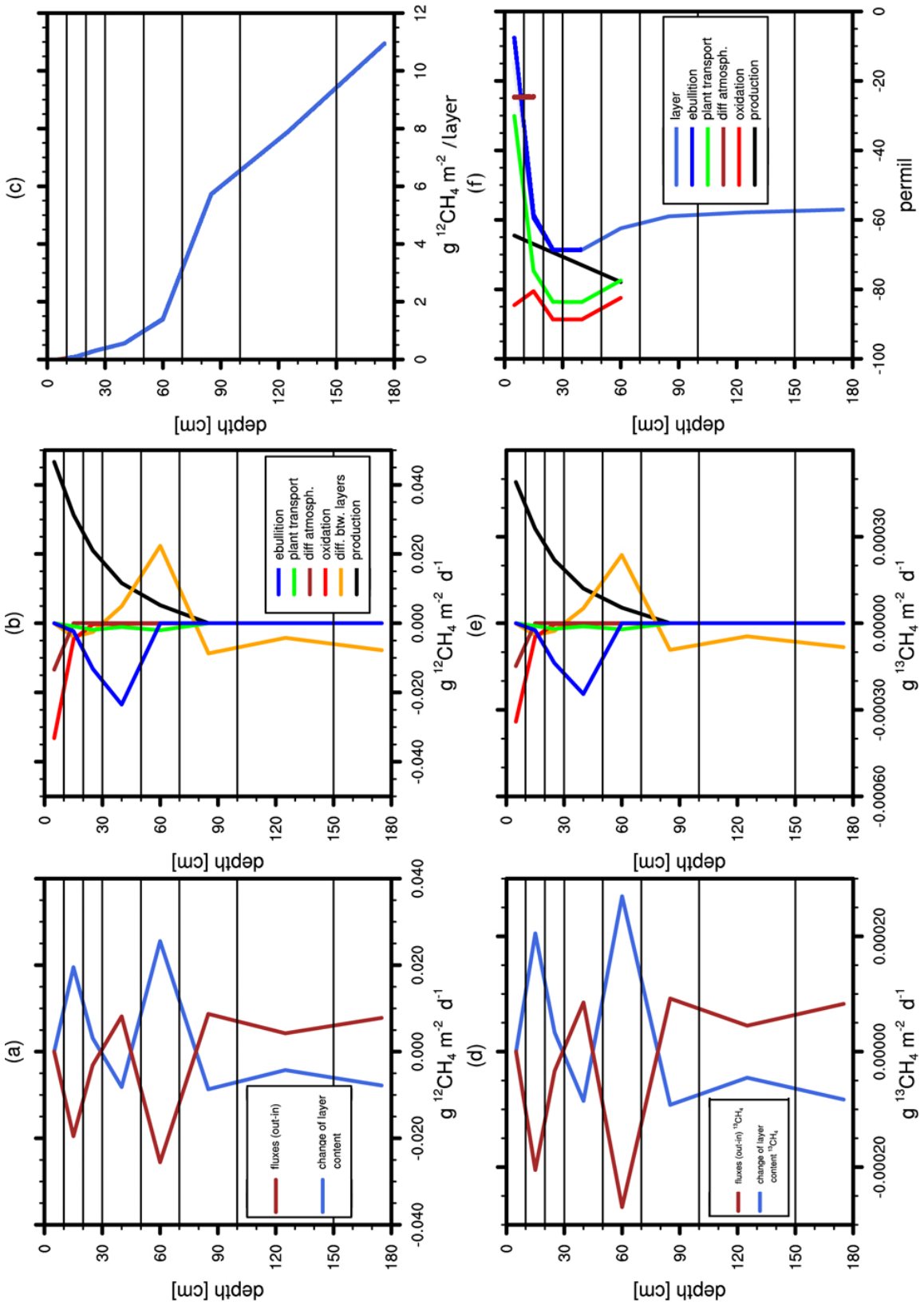

Figure 2.19: Example of a daily budget (Sanjiang, day 200 in 1989), (a) blue: change of the layer content from the beginning of the day to the end of the day after all processes are executed ($CH_{4\ end}$-$CH_{4\ beginning}$), red: budget of the fluxes -(F_{in}-F_{out}) in a day. The red and the blue line add up to zero. (b) $^{12}CH_4$ fluxes in and out the layers during the day; (c) $^{12}CH_4$ content of the soil at the beginning of the day (note: the units are per m^2 per layer and not as before per m^3. (d) same as Figure a) but for $^{13}CH_4$; again, the budget is perfectly closed. (e) same as Figure b) but for $^{13}CH_4$. f) signature of each flux. Note that the ebullition signature (no fractionation) is equal to the layer signature at the end of the day and therefore not visible in the plot.

Bibliography

Bellisario, L., Bubier, J. L., Moore, T., & Chanton, J. P., 1999. Controls on CH_4 emissions from a northern peatland, *Global Biochem. Cyc.*, **13**, 81–91.

Bergamaschi, P., Lubina, C., Konigstedt, R., Fischer, H., Veltkamp, A., & Zwaagstra, O., 1998. Stable isotopic signatures (δ^{13}C, δ D) of methane from European landfill sites, *J. Geophys. Res. - Atm.*, **103**, 8251–8265.

Bergamaschi, P., Frankenberg, C., Meirink, J. F., Krol, M., Villani, M. G., Houweling, S., Dentener, F., Dlugokencky, E. J., Miller, J. B., Gatti, L. V., Engel, A., & Levin, I., 2009. Inverse modeling of global and regional CH_4 emissions using SCIAMACHY satellite retrievals, *J. Geophys. Res.*, **114**.

Bohn, T., Lettenmaier, D., Sathulur, K., Bowling, L., Podest, E., McDonald, K., & Friborg, T., 2007. Methane emissions from Western Siberian wetlands: heterogeneity and sensitivity to climate change, *Environ. Res. Lett.*, **2**.

Botz, R., 1996. Carbon isotope fractionation during bacterial methanogenesis by co_2 reduction, *Org. Geochem.*, **25**, 255–262.

Bowes, H. & Hornibrook, E., 2006. Emission of highly ^{13}C-depleted methane from an upland blanket mire, *Geophys. Res. Lett.*, (33), 1–4.

Bridgham, S., Cadillo-Quiroz, H., Keller, J., & Zhuang, Q., 2013. Methane emissions from wetlands: biogeochemical, microbial, and modeling perspectives from local to global scales, *Global Change Biol.*, **19**, 1325–1346.

Broecker, W. & Peng, T., 1974. Gas-exchange rates between air and sea, *Tellus*, **26**(1-2), 21–35.

Cao, M., Marshall, S., & Gregson, K., 1996. Global carbon exchange and methane emissions from natural wetlands: Application of a process-based model, *J. Geophys. Res.-Atm.*, **101**(D9), 14399–14414.

Chanton, J. & Liptay, K., 2000. Seasonal variation in methane oxidation in a landfill cover soil as determined by an in situ stable isotope technique, *Global Biochem. Cyc.*, **14**, 51–60.

Chanton, J., Crill, P., Bartlett, K., & Martens, C., 1989. Amazon capims (floating grassmats): A source of ^{13}C enriched methane to the troposphere, *Geophys. Res. Lett.*, **16**, 799–802.

Chanton, J., Arkebauer, T., Harden, H., & Verma, S., 2002. Diel variation in lacunal CH_4 and CO_2 concentration and delta C-13 in Phragmites australis, *Biogeochemistry*, **59**(3), 287–301.

Comas, X., Slater, L., & Reeve, A., 2008. Seasonal geophysical monitoring of biogenic gases in a northern peatland: Implications for temporal and spatial variability in free phase gas production rates, *J. of Geophys. Res.- Biogeosciences*, **113**(G1).

Conrad, R., 2005. Quantification of methanogenic pathways using stable carbon isotopic signatures: a review and a proposal, *Organic Geochemistry*, **36**(5), 739–752.

Cronk, J. & Fennessy, M., 2001. Wetland plants: biology and ecology, *CRC Press LLC*.

De Visscher, A., De Pourcq, I., & Chanton, J., 2004. Isotope fractionation effects by diffusion and methane oxidation in landfill cover soils, *J. Geophys. Res. - Atm.*, **109**(D18).

Dorodnikov, M., Knorr, K. H., Kuzyakov, Y., & Wilmking, M., 2011. Plant-mediated CH_4 transport and contribution of photosynthates to methanogenesis at a boreal mire: a C-14 pulse-labeling study, *Biogeosciences*, **8**(8), 2365–2375.

FechnerLevy, E. & Hemond, H., 1996. Trapped methane volume and potential effects on methane ebullition in a northern peatland, *Limnology and Oceanography*, **41**(7), 1375–1383.

Fuex, A., 1980. Experimental evidence against an appreciable isotopic fractionation of methane during migration, *Physics and Chemistry of the Earth*, **12**, 725–732.

Galand, P., Fritze, H., Conrad, R., & Yrjala, K., 2005. Pathways for methanogenesis and diversity of methanogenic archaea in three boreal peatland ecosystems, *Applied and Environmental Microbiology*, **71**, 2195–2198.

Gallego-Sala, A., 2010. Manuscript, *Dissertation*.

Gerard, G. & Chanton, J., 1993. Quantification of Methane Oxidation in the Rhizosphere of emergent aquatic macrophytes - defining upper limits, *Biogeochemistry*, **23**, 79–97.

Gerber, S., Joos, F., & Prentice, I. C., 2004. Sensitvity of a dynamic global vegetation model to climate and atmospheric CO_2, *Global Change Biol.*, **10**, 1223–1239.

Gerber, S., Joos, F., Brugger, P., Stocker, T., Mann, M., Sitch, S., & Scholze, M., 2003. Constraining temperature variations over the last millennium by comparing simulated and observed atmospheric CO_2, *Climate Dynamics*, **20**(2-3), 281–299.

Gerten, D., Schaphoff, S., Haberlandt, U., Lucht, W., & Sitch, S., 2004. Terrestrial vegetation and water balance - hydrological evaluation of a dynamic global vegetation model, *J. Hydrology*, **286**(1-4), 249–270.

Glaser, P. & Chanton, J., 2009. Methane accumulation and release from deep peat: Measurements, conceptual models, and biogeochemical significance, in carbon cycling in northern peatlands, *Geophys. Monogr.*, **184**, 145–158.

Glaser, P., Chanton, J., Morin, P., Rosenberry, D., Siegel, D., Ruud, O., Chasar, L., & Reeve, A., 2004. Surface deformations as indicators of deep ebullition fluxes in a large northern peatland, *Global Biochem. Cycle*, **18**(1).

Hopcroft, P. O., Valdes, P. J., & Beerling, D. J., 2011. Simulating idealized Dansgaard-Oeschger events and their potential impacts on the global methane cycle, *Quaternary Science Reviews*, **30**(23-24), 3258–3268.

Hornibrook, E., 2009. The stable carbon isotope composition of methane produced and emitted from northern peatlands, *Geophysical Monograph Series*, **184**.

Hornibrook, E. & Bowes, H., 2003. The stable isotope signature of ch4 emissions from northern wetlands, *Geochimica et Cosmochimica Acta*, **67**, A158–A158.

Hornibrook, E. & Bowes, H., 2007. Trophic status impacts both the magnitude and stable carbon isotope composition of methane flux from peatlands, *Geophys. Res. Lett.*, (34), L21,401.

Hornibrook, E., Longstaffe, F., & Fyfe, W., 1997. Spatial distribution of microbial methane production pathways in temperate zone wetland soils: Stable carbon and hydrogen isotope evidence., *Geochimica et Cosmochimica Acta*, **61**, 745–753.

Hornibrook, E., Longstaffe, F., & Fyfe, W., 2000. Evolution of stable carbon isotope compositions for methane and carbon dioxide in freshwater wetlands and other anaerobic environments, *Geochimica et Cosmochimica Acta*, **64**, 1013–1027.

Houweling, S., Kaminski, T., Dentener, F., Lelieveld, J., & Heimann, M., 1999. Inverse modeling of methane sources and sinks using the adjoint of a global transport model, *J. Geophys. Res.*, **104**(D21), 26137–26160.

Iiyama, I. & Hasegawa, S., 2005. Gas diffusion coefficient of undisturbed peat soils, *Soil Sci. Plant Nutr.*, **51**, 431–435.

Joos, F., Prentice, I. C., Sitch, S., Meyer, R., Hooss, G., Plattner, G.-K., Gerber, S., & Hasselmann, K., 2001. Global warming feedbacks on terrestrial carbon uptake under the Intergovernmental Panel on Climate Change (IPCC) emission scenarios, *Global Biogeochem. Cycles*, **15**, 891–907.

Joos, F., Gerber, S., Prentice, I., Otto-Bliesner, B., & Valdes, P., 2004. Transient simulations of Holocene atmospheric carbon dioxide and terrestrial carbon since the Last Glacial Maximum, *Global Biogeochem. Cycles*, **18**(2).

Kellner, E., Baird, A. J., Oosterwoud, M., Harrison, K., & Waddington, J. M., 2006. Effect of temperature and atmospheric pressure on methane (CH_4) ebullition from near-surface peats, *Geophys. Res. Lett.*, **33**(18).

Knox, M., Quay, P., & Wilbur, D., 1992. Kinetic isotopic fractionation during air-water gas transfer of o_2, n_2, ch_4 and h_2, *J. Geophys. Res.*.

Lerman, A., 1979. *Geochemical processes: Water and sediment environments*, Wiley (New York).

Liptay, K., Chanton, J., Czepiel, P., & Mosher, B., 1998. Use of stable isotopes to determine methane oxidation in landfill cover soils, *J. Geophys. Res. - Atm.*, **103**, 8243–8250.

Lloyd, J. & Farquhar, G., 1994. C-13 Discrimination during CO_2 Assimilation by the terrestrial biosphere, *Oecologia*, **99**(3-4), 201–215.

Markel, E., Booth, R., & Qin, Y., 2010. Testate amoebae and δ^{13}C of *Sphagnum* as surface-moisture proxies in Alaskan peatlands, *Holocene*.

Mastepanov, M., Sigsgaard, C., Dlugokencky, E. J., Houweling, S., Strom, L., Tamstorf, M. P., & Christensen, T. R., 2008. Large tundra methane burst during onset of freezing, *Nature*, **456**(7222), 628–U58.

Matthews, E. & Fung, I., 1987. Methane emissions from natural wetlands: Global distribution, area and environmental characteristics of sources, *Global Biogeochem. Cycles*, **1**, 61–86.

McGillis, W., Dacey, J. W. H., Frew, N. M., Bock, E., & Nelson, R., 2000. Water-air flux of dimethylsulfide, *J. Geophys. Res.*, **105**, 1187–1193.

Millington, R. & Quirk, J., 1961. Permeability of porous solids, *Trans. Faraday Soc.*, **57**, 1200–1207.

Pison, I., Bousquet, P., Chevallier, F., Szopa, S., & Hauglustaine, D., 2009. Multi-species inversion of CH_4, CO and H_2 emissions from surface measurements, *Atmospheric Chemistry and Physics*, **9**(14), 5281–5297.

Reeburgh, W., Hirsch, A., Sansone, F., Popp, B., & Rust, T., 1997. Carbon kinetic isotope effect accompanying microbial oxidation of methane in boreal forest soils, *Geochimica et Cosmochimica Acta*, **61**, 4761–4767.

Ringeval, B., de Noblet-Ducoudre, N., Ciais, P., Bousquet, P., Prigent, C., Papa, F., & Rossow, W. B., 2010. An attempt to quantify the impact of changes in wetland extent on methane emissions on the seasonal and interannual time scales, *Global Biogeochem. Cycles*, **24**.

Ringeval, B., Friedlingstein, P., Koven, C., Ciais, P., & de Noblet-Ducoudre, N., a. C. P., 2011. Climate-CH_4 feedback from wetlands and its interaction with the climate CO_2 feedback, **8**.

Rosenberry, D., Glaser, P., Siegel, D., & Weeks, E., 2003. Use of hydraulic head to estimate volumetric gas content and ebullition flux in northern peatlands, *Water Resources Research*, **39**(3).

Schaefer, C. M., Elsgaard, L., Hoffmann, C. C., & Petersen, S. O., 2012. Seasonal methane dynamics in three temperate grasslands on peat, *Plant and Soil*, **357**(1-2), 339–353.

Segers, R., 1998. Methane production and methane consumption: a review of processes underlying wetland methane fluxes, *Biogeochemistry*, **41**(1), 23–51.

Shannon, R., White, J., Lawson, J., & Gilmour, B., 1996. Methane efflux from emergent vegetation in peatlands, *Journal of Ecology*, **84**(2), 239–246.

Singarayer, J. S., Valdes, P. J., Friedlingstein, P., Nelson, S., & Beerling, D. J., 2011. Late Holocene methane rise caused by orbitally controlled increase in tropical sources, *Nature*, **470**(7332), 82–U91.

Sitch, S., Smith, B., Prentice, I. C., Arneth, A., Bondeau, A., Cramer, W., Kaplan, J. O., Levis, S., Lucht, W., Sykes, M. T., Thonicke, K., & Venevsky, S., 2003. Evaluation of ecosystem dynamics, plant geography and terrestrial carbon cycling in the LPJ dynamic global vegetation model, *Global Change Biol.*, **9**, 161–185.

Smolders, A., Tomassen, H., Pijnappel, H., Lamers, L., & Roelof's, J., 2001. Substrate-derived CO_2 is important in the development of *Sphagnum Spp.*, *New Phytologist*, **152**, 325–332.

Spahni, R., Joos, F., Stocker, B., Steinacher, M., & Yu, C., 2013. Transient simulations of the carbon and nitrogen dynamics in northern peatlands: from the last glacial maximum to the 21st century, *Clim. Past*, **9**(3), 1287–1308.

Spahni, R., Wania, R., Neef, L., van Weele, M., Pison, I., Bousquet, P., Frankenberg, C., Foster, P. N., Joos, F., Prentice, I. C., & van Velthoven, P., 2011. Constraining global methane emissions and uptake by ecosystems, *Biogeosciences*, **8**(6), 1643–1665.

Steinmann, P., Eilrich, B., Leuenberger, M., & S.J., B., 2008. Stable carbon isotope composition and concentrations of co_2 and ch_4 in the deep catotelm of a peat bog, *Geochimica et Cosmochimica Acta*, **72**, 6015–6026.

Stocker, B., Roth, R., Joos, F., Spahni, R., Steinacher, M., Zaehle, S., Bouwman, L., Xu-Ri, & Prentice, C., 2013. Multiple greenhouse-gas feedbacks from the land biosphere under future climate change scenarios, *Nature Climate Change*.

Stocker, B. D., Strassmann, K., & Joos, F., 2011. Sensitivity of Holocene atmospheric CO_2 and the modern carbon budget to early human land use: analyses with a process-based model, *Biogeosciences*, **8**(1), 69–88.

Strassmann, K. M., Joos, F., & Fischer, G., 2008. Simulating effects of land use changes on carbon fluxes: past contributions to atmospheric CO_2 increases and future commitments due to losses of terrestrial sink capacity, *Tellus B*, **60**(4), 583–603.

Tokida, T., Miyazaki, T., & Mizoguchi, M., 2005. Ebullition of methane from peat with falling atmospheric pressure, *Geophys. Res. Lett.*, **32**(13).

Tokida, T., Miyazaki, T., Mizoguchi, M., Nagata, O., Takakai, F., Kagemoto, A., & Hatano, R., 2007. Falling atmospheric pressure as a trigger for methane ebullition from peatland, *Global Biochem. Cycles*, **21**(2).

Tyler, S., Crill, P., & Brailsford, G., 1994. $^{13}c/^{12}c$ fractionation of methane during oxidation in a temperate forested soil, *Geochimica et Cosmochimica Acta*, **58**, 1625–1633.

Walter, B. P., Heimann, M., & Matthews, E., 2001. Modeling modern methane emissions from natural wetlands 1. Model description and results, *J. Geophys. Res.*, **106**(D24), 34189–34206.

Wania, R., 2007. *Modelling northern peatland land surface processes, vegetation dynamics and methane emissions*, Ph.D. thesis, University of Bristol.

Wania, R., Ross, I., & Prentice, I. C., 2010. Implementation and evaluation of a new methane model within a dynamic global vegetation model: LPJ-WHyMe v1.3.1, *Geosci. Model Dev.*, **3**(2), 565–584.

Wania, R., Ross, I., & Prentice, I. C., 2009a. Integrating peatlands and permafrost into a dynamic global vegetation model: 1. Evaluation and sensitivity of physical land surface processes, *Global Biogeochem. Cycles*, **23**.

Wania, R., Ross, I., & Prentice, I. C., 2009b. Integrating peatlands and permafrost into a dynamic global vegetation model: 2. Evaluation and sensitivity of vegetation and carbon cycle processes, *Global Biogeochem. Cycles*, **23**.

Weiss, R., 1970. Solubility of Nitrogen, Oxygen and Argon in Water and Seawater, *Deep-sea research*, **17**(4), 721–&.

Whiticar, M., 1999. Carbon and hydrogen isotope systematics of bacterial formation and oxidation of methane, *Chem. Geol.*, **161**, 291–314.

Whiticar, M., Faber, E., & Schoell, M., 1986. Biogenic methane formation in marine and fresh-water environments - co_2 reduction vs. acetate fermentation isotope evidence, *Geochimica et Cosmochimica Acta*, **50**, 693–709.

Wiesenburg, D. & Guinasso, N., 1979. Equilibrium Solubilities of Methane, Carbon-Monoxide and Hydrogen in Water and Sea-Water, *Journal of Chemical and Engineering Data*, **24**(4), 356–360.

Yamamoto, S., Alcauskas, J., & Crozier, T., 1976. Solubility of methane in distilled water and seawater, *Journal of Chemical and Engineering Data*, **21**(1), 78–80.

Zhang, T. & Krooss, B., 2000. Experimental investigation on the carbon isotope fractionation of methane during gas migration by diffusion through sedimentary rocks at elevated temperature and pressure, *Geochimica et Cosmochimica Acta*, **65**, 2273–2742.

Zürcher, S., Spahni, R., Joos, F., Steinacher, M., & Fischer, H., 2013. Impact of an abrupt cooling event on interglacial methane emissions in northern peatlands, *Biogeosciences*, **10**, 1963–1981.

Chapter 3

Impact of an abrupt climate cooling event on interglacial methane emissions in northern peatlands

S. Zürcher, R. Spahni, F. Joos, M. Steinacher, H. Fischer

Published in Biogeosciences, 10, 1963-1981 , 2013

doi:10.5194/bg-10-1963-2013

Impact of an abrupt cooling event on interglacial methane emissions in northern peatlands

S. Zürcher[1,2], R. Spahni[1,2], F. Joos[1,2], M. Steinacher[1,2], and H. Fischer[1,2]

[1]Climate and Environmental Physics, Physics Institute, University of Bern, Sidlerstrasse 5, 3012 Bern, Switzerland
[2]Oeschger Centre for Climate Change Research, University of Bern, Zähringerstrasse 25, 3012 Bern, Switzerland

Correspondence to: S. Zürcher (zuercher@climate.unibe.ch)

Received: 18 July 2012 – Published in Biogeosciences Discuss.: 25 September 2012
Revised: 18 January 2013 – Accepted: 25 February 2013 – Published: 20 March 2013

Abstract. Rapid changes in atmospheric methane (CH_4), temperature and precipitation are documented by Greenland ice core data both for glacial times (the so called Dansgaard-Oeschger (D-O) events) as well as for a cooling event in the early Holocene (the 8.2 kyr event). The onsets of D-O warm events are paralleled by abrupt increases in CH_4 by up to 250 ppb in a few decades. Vice versa, the 8.2 kyr event is accompanied by an intermittent decrease in CH_4 of about 80 ppb over 150 yr. The abrupt CH_4 changes are thought to mainly originate from source emission variations in tropical and boreal wet ecosystems, but complex process oriented bottom-up model estimates of the changes in these ecosystems during rapid climate changes are still missing. Here we present simulations of CH_4 emissions from northern peatlands with the LPJ-Bern dynamic global vegetation model. The model represents CH_4 production and oxidation in soils and transport by ebullition, through plant aerenchyma, and by diffusion. Parameters are tuned to represent site emission data as well as inversion-based estimates of northern wetland emissions. The model is forced with climate input data from freshwater hosing experiments using the NCAR CSM1.4 climate model to simulate an abrupt cooling event. A concentration reduction of ~ 10 ppb is simulated per degree K change of mean northern hemispheric surface temperature in peatlands. Peatland emissions are equally sensitive to both changes in temperature and in precipitation. If simulated changes are taken as an analogy to the 8.2 kyr event, boreal peatland emissions alone could only explain 23 % of the 80 ppb decline in atmospheric methane concentration. This points to a significant contribution to source changes from low latitude and tropical wetlands to this event.

1 Introduction

CH_4 is a greenhouse gas contributing to the ongoing global warming. CH_4 concentrations have increased from their preindustrial value of ~ 700 ppb to approximately 1800 ppb in 2008 (Dlugokencky et al., 2009) due to anthropogenic CH_4 emissions. Air enclosures in polar ice cores allow for the reconstruction of methane variations in the past and show that CH_4 changed in concert with Northern Hemisphere temperature during the glacial/interglacial transitions (Loulergue et al., 2008) as well as during rapid climate variations. Examples of abrupt CH_4 variations recorded in Greenland ice cores are the 8.2 kyr event in the early Holocene (Fig. 1) (Blunier et al., 1995; Chappellaz et al., 1997; Spahni et al., 2003; Kobashi et al., 2007), the Dansgaard-Oeschger events (D-O-events) in the glacial period (Chappellaz et al., 1993; Brook et al., 2000; Blunier and Brook, 2001; Flückiger et al., 2004; Huber et al., 2006; Baumgartner et al., 2012) or the Younger Dryas (YD) cooling event (Chappellaz et al., 1993; Baumgartner et al., 2012). During the last glacial period Greenland temperature and CH_4 are found to covary within ~ 30 yr, which is the limit of ice core data resolution and the width of the age distribution of air enclosed in bubbles in that ice (Huber et al., 2006). This suggests that CH_4 sources responded synchronously to the rapid climate changes. The nominal sensitivity of methane concentration variations on changes in Greenland temperature derived from ice cores is about ~ 22 ppb K^{-1} for the 8.2 kyr event (Kobashi et al., 2007), ~ 7–16 ppb K^{-1} for onsets of D-O events (Huber et al., 2006) and ~ 9 ppb K^{-1} for the beginning and end of the YD (Severinghaus et al., 1998; Brook et al., 2000; Grachev and Severinghaus, 2005). Note, however, that temperature changes

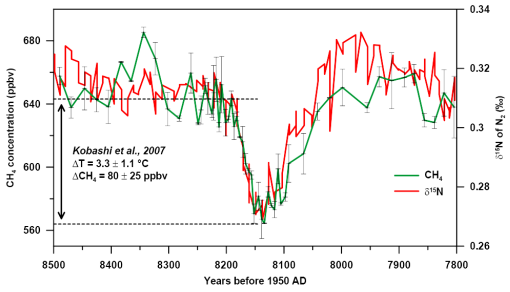

Fig. 1. Evolution of Greenland temperature and atmospheric methane concentration during the 8.2 kyr event. The measured $\delta^{15}N$ signature allows for a quantitative temperature reconstruction and represents a temperature change of about 3 °C over Central Greenland which is accompanied by an 80 ppb decline in atmospheric CH_4 (Kobashi et al., 2007).

recorded in Greenland are not necessarily representative for the temperature changes in boreal and even less in tropical wetland sources nor for precipitation changes.

While the origin of the abrupt climate variations can be explained by a shut-down or resumption of the North Atlantic thermohaline circulation (Vellinga and Wood, 2002; McManus et al., 2004; Ellison et al., 2006), the origin of atmospheric methane variations is much less clear and abrupt climate variations are still not well understood (Clement et al., 2008). Most ice core studies attribute a change in methane concentration to a change in methane emissions from both boreal and sub-tropical to tropical wet ecosystems (Chappellaz et al., 1997; Fischer et al., 2008). The interpolar concentration gradient (IPG) was reconstructed from ice core methane data from Greenland and Antarctica (Brook et al., 2000; Baumgartner et al., 2012). This gradient together with methane isotopic information indicates important sources during both warm and cold periods located in high northern latitudes with a tendency to a higher IPG during interstadials (Bock et al., 2010; Brook et al., 2000; Dallenbach et al., 2000). For the 8.2 kyr event, the interpolar gradient suggests that the CH_4 emissions must have been reduced in the early phase of the 8.2 kyr event in the Northern Hemisphere, followed by sub-tropical and tropical emission reductions (Spahni et al., 2003). However, a quantitative estimate of the response of boreal CH_4 sources on rapid climate changes based on the IPG is subject to large uncertainties due to the transient character of the changes and the simplified models used in this approach.

The dominant and most directly responding type of methane emitting ecosystems in the northern high latitudes, i.e., the latitudes with the strongest temperature response to rapid changes in the Atlantic Meridional Overturning Circulation (AMOC), are boreal peatlands (Dallenbach et al., 2000; Baumgartner et al., 2012). Northern high-latitude peatland and permafrost soils are associated with large carbon stocks that serve as a substrate for microbial methane production (Gorham, 1991; Roulet, 2000). For the understanding of the covariations of atmospheric methane and climate during abrupt events it is, thus, crucial to investigate the carbon cycle of northern high-latitude peatlands (northern peatlands hereafter). The carbon cycle response of northern peatlands regulates the peatland methane emissions and thus directly affects the global methane concentration within its atmospheric mixing and lifetime of ~ 2 and ~ 10 yr, respectively (Lelieveld et al., 1998; Denman et al., 2007; Prather, 2012; Levine et al., 2011). Accordingly, the goal of this study is to investigate the CH_4 sensitivity of the northern peatlands to rapid climate cooling.

There are two different approaches to model methane emissions from wet ecosystems for present day: bottom-up models that represent the processes leading to methane emissions in a mechanistic way (e.g. Cao et al., 1996; Walter et al., 2001a; Wania et al., 2010; Ringeval et al., 2010) and top-down or inverse models which use observations of atmospheric methane concentrations and transport models to quantify methane emissions (e.g. Houweling et al., 1999; Pison et al., 2009; Bergamaschi et al., 2009). Combining both methods can help to narrow down the uncertainties of global wet ecosystem methane emissions (Spahni et al., 2011).

For past time periods, before the start of direct atmospheric methane monitoring in the 1980s, the spatially available CH_4 data is restricted to firn and ice core data from Greenland and Antarctica. Global inversions from atmospheric concentrations to emissions using atmospheric chemistry transport models are, thus, not applicable for past time periods. Ice-core based top-down approaches using simple box models (e.g. Fischer et al., 2008) can only explain the inter-hemispheric gradient, but not distributions within a hemisphere. Accordingly, biogeochemical process modelling of methane emissions and comparisons of resulting atmospheric concentrations to ice core data are the only way to estimate natural methane emission distributions.

Previous paleo-modelling studies have shown that simple methane models are capable of simulating emissions on long-term glacial-interglacial time scales (Valdes et al., 2005; Kaplan et al., 2006; Weber et al., 2010; Singarayer et al., 2011) and are also able to capture methane emissions during abrupt events (van Huissteden, 2004; Hopcroft et al., 2011), but find it difficult to replicate the magnitude of change in atmospheric CH_4 for abrupt events. Hopcroft et al. (2011) can not explain the full magnitude or rapidity of methane emission changes during D-O-events and believe their model to be too insensitive for abrupt events or to be missing important mechanism. van Huissteden (2004) finds doubled methane fluxes from northern European wetlands during interstadials, but attributes big uncertainties to the peatland area. The long-term simulations confirm the finding that atmospheric methane concentrations parallel temperature reconstructions from Antarctic ice cores also on glacial-interglacial time

scales of the past 800 000 yr (Spahni et al., 2005; Loulergue et al., 2008). A drawback of previous paleo-modelling studies for methane is the limited representation of processes and interactions related to the interplay of vegetation and soil dynamics, soil temperature, soil hydrology, permafrost thawing, methane production, oxidation and transport from the soils to the atmosphere by a variety of mechanisms. For example, Kaplan et al. (2006) calculate the methane emissions as a fixed ratio of the heterotrophic respiration. Valdes et al. (2005); Kaplan et al. (2006); Singarayer et al. (2011) consider changes in the atmospheric CH_4 lifetime in order to explain glacial-interglacial changes in CH_4. According to the latest chemistry model studies these changes in CH_4 lifetime appear to be very limited (Levine et al., 2011).

Here, we further develop and apply a process-oriented CH_4 module (Wania et al., 2009a,b, 2010) within the Bern version of the LPJ dynamic global vegetation model. Soil temperature at different depths, including freeze-thaw cycles and water table position is explicitly calculated and CH_4 transport by soil diffusion, ebullition and through plant aerenchyma is simulated mechanistically. The LPJ land model is forced with the climate output from idealised freshwater hosing experiments with the NCAR CSM1.4 climate model. Freshwater is added in the model to the preindustrial northern North Atlantic surface ocean. In response, the Atlantic Overturning Circulation collapses and surface air temperature in the Northern Hemisphere is reduced. We will discuss the results of our idealised simulations in relation to the 8.2 kyr event, but we emphasise that a direct comparison between model results and proxy data for the 8.2 kyr event is hampered as environmental conditions at 8.2 kyr ago and before the onset of the industrialisation were different. For the early Holocene, the initiation of boreal peatlands is reasonably well known from recent observations (Yu et al., 2010). Since peatland initiation peaks at 10 kyr BP we apply present day boreal peatland distribution (Tarnocai et al., 2009). A comparison of this distribution with the ice cover-age 8200 yr ago (Peltier, 2004) shows that only very small areas of present day peatlands were covered by land ice at that time. Additionally, the warm Holocene climate conditions prevailed already for more than 1000 yr allowing for an initiation of peat expansion to interglacial conditions.

The outline of this paper is as follows. In Sects. 2.1 and 2.2, we describe the LPJ-Bern global dynamic vegetation model (Sitch et al., 2003; Joos et al., 2004; Gerber et al., 2003; Strassmann et al., 2008; Stocker et al., 2011), the implementation and improvements to LPJ-WHyMe (Wania et al., 2009a,b) and a recently developed methane module (Wania et al., 2010). Section 2.3 presents the calibration of the model with modern site data and describes the experimental setup for control simulations and for simulations forced with climate input from an ensemble of freshwater hosing model experiments (Bozbiyik et al., 2011). Results are presented in Sect. 3 and include simulated changes in CH_4 emissions for the set of freshwater hosing experiments, the attribution of change in CH_4 emissions to temperature and precipitation variations, and sensitivity to model parameters.

2 Model description and set-up

2.1 LPJ-Bern

The LPJ-Bern (hereafter LPJ) model is a subsequent development of the Lund-Potsdam-Jena dynamic global vegetation model (LPJ-DGVM; Sitch et al., 2003) that combines process-based, large-scale representations of terrestrial vegetation dynamics and land-atmosphere carbon and water exchanges in a modular framework. Vegetation is defined by plant functional types (PFTs) each with its own set of parameters describing growth, carbon uptake and mortality. LPJ has been applied previously in paleo studies (e.g. Joos et al., 2004; Gerber et al., 2004) and in simulations assessing the anthropogenic climate perturbation and the impact of human induced landuse (e.g. Joos et al., 2001; Strassmann et al., 2008; Stocker et al., 2011).

For this study we implemented the boreal peatland and methane module based on LPJ-WHyMe (Wetland Hydrology and Methane, Wania et al., 2009a,b, 2010) that derives its input data from the LPJ. It includes new features for grid cells with a (prescribed) partition of peatland: 8 soil layers, permafrost dynamics with freezing and thawing (including a soil temperature solver to simulate temperature as a function of depth), peatland hydrology (active layer depth and water table position), peatland vegetation as two additional PFTs (flood-tolerant C_3 graminoids and *Sphagnum* moss), a slow-down of decomposition under inundation and the addition of root exudates (Wania et al., 2009a,b).

The main differences between our methane routine and the original LPJ-WHyMe version 1.3.1 (Wania et al., 2010) is a more mechanistic ebullition mechanism that includes also the partial pressure of CO_2 for triggering an ebullition event (see Sect. 2.2). The carbon balance over all layers is now preserved after every gas diffusion time step, whereas in LPJ-WHyMe the carbon balance was closed at the end of the year with a correction factor.

2.2 Methane routine in peatlands of LPJ-Bern

The carbon module simulates carbon allocation in vegetation, above and below ground litter and fast and slow soil carbon pools, as well as soil organic matter dynamics (Sitch et al., 2003). Heterotrophic respiration (HR) is calculated based on the size of the litter and soil pools, regulated by soil moisture and soil temperature at a depth of 25 cm. HR is then distributed to 8 peat layers according to the root distribution, where it is used to compute methane production. In each layer methane production is calculated as the product of HR, the ratio of CH_4 to CO_2 production under anaerobic

conditions (f_{CH_4/CO_2}), and the anoxity of the soil for each soil layer (Wania et al., 2010).

Depending on the water table position, the soil temperature and the presence of O_2, the produced methane can be oxidised to CO_2, accumulated or transported to other layers or released to the atmosphere. The three implemented transport processes are plant-mediated transport, diffusion and ebullition. Plant-mediated transport is implemented as described in (Wania et al., 2010): the flood-tolerant C_3 graminoids (one of two PFTs growing in peatlands) are adapted to inundation by the presence of aerenchyma, gas-filled tissue, through which gas can be transported by diffusion. Plant-mediated transport depends on temperature, water content and the actual gradients of CH_4, CO_2 or O_2. The tiller radius r_{tiller} defines the open area available for plant-mediated transport and is a tunable parameter.

Diffusion transports O_2, CO_2 and CH_4 between the 8 soil layers. The temperature-dependent diffusion coefficients of all gases are set to their molecular diffusivities in air or water (Lerman, 1979; Broecker and Peng, 1974), depending on the water table position in the acrotelm (top 30 cm of soil). Peatland soil layers below that horizon are assumed to be completely water saturated (catotelm). Water can freeze if the soil layer temperature falls below 0 °C and all transport mechanisms are prohibited. CH_4 is not incorporated into the ice during freezing leading to an enrichment of CH_4 in the remaining water and an eventual release by ebullition.

The new ebullition mechanism calculates how much of the CH_4, CO_2 and N_2 is in the gas phase and how much is dissolved. Following Henry's law (FechnerLevy and Hemond, 1996; Rosenberry et al., 2003; Tokida et al., 2005, 2007) the amount of dissolved gases in each layer depends on partial pressure of CH_4, CO_2 and N_2, hydrostatic pressure and soil temperature. The available volume ($V_{\text{available}}$) within each layer i is given by the layer thickness and the porosity for fully water saturated conditions. The total amount of N_2 is assumed to be constant, since it is not simulated by our model. However, the partitioning of N_2 between water and soil air changes. Assuming the gaseous volume of N_2 to be 1 % (lower bound estimate, e.g. Shannon et al., 1996) of the available volume in a layer (liquid phase and gas phase), we calculate with Henry's law the amount of N_2 dissolved in each layer (Tokida et al., 2007). We then add the produced or transported CH_4 and CO_2 to the layer and recalculate the partial pressure for all gases (Eq. 1, Tokida et al., 2007; Kellner et al., 2006):

$$P_{x,i} = n_{x,i} R T_i \left(V_{g,i} + \frac{V_{w,i}}{H_x} \right)^{-1} \quad (1)$$

where $P_{x,i}$ is the partial pressure of gas species x in layer i, $n_{x,i}$ is the total number of moles of gas x, $V_{g,i}$ is the gas volume, $V_{w,i}$ is the volume of liquid water, H_x is the dimensionless Henry's law constant for gas x (Yamamoto et al., 1976; Wiesenburg and Guinasso, 1979; Weiss, 1970), R is the universal gas constant, and T_i is the temperature in layer i (see Appendix A). We assume that during ebullition the gas volume, $V_{g,i}$, is equal to 15 % and the liquid water volume, $V_{w,i}$, 85 % of the available volume (FechnerLevy and Hemond, 1996; Rosenberry et al., 2003; Tokida et al., 2005). In the code, ebullition is triggered if the sum of all partial pressures ($pN_2 + pCO_2 + pCH_4$) (Eq. 1 with $V_{g,i} = 15\,\% \cdot V_{\text{available}}$) is larger than the sum of atmospheric and hydrostatic pressure. The number of moles of CO_2 and CH_4 released per ebullition event is assumed to be 1 % of the available volume times the CO_2 and CH_4 partial pressure divided by $R\ T_i$, respectively. In other words, a fifteenth of the CO_2 and CH_4 amount in the gas phase is released per ebullition event. This assumption and that the gas volume is equal to 15 % of the available volume are not critical for the total emissions. Instead these parameters modulate the frequency and the magnitude of ebullition events on a short scale (see parameter tuning, Sect. 3.4).

Oxygen is transported into soils by diffusion through open soil pores and through the aerenchyma of the flood tolerant graminoids. Only a fraction (f_{oxid}) of the available oxygen is used to oxidise CH_4 to CO_2. The remaining O_2 is assumed to be consumed by other electron acceptors. Again f_{oxid} is a tunable model parameter.

2.3 Calibration and site validation

The implementation of LPJ-WHyMe into the LPJ-Bern, the code improvements and the adaption of the ebullition scheme calls for a re-evaluation of flux densities at the site level and a retuning of model parameters. We compare simulated CH_4 emissions to flux measurement at 7 sites. A detailed description of the sites and their environmental conditions can be found in Wania et al. (2010). Measured seasonal methane fluxes over a specific year are available for each site (see Fig. 2) (Bubier et al., 1998; Ding et al., 2004; Saarnio et al., 1997; Alm et al., 1999; Granberg et al., 2001; Johansson et al., 2006; Jackowicz-Korczynski et al., 2010; Shannon and White, 1994; Dise, 1993). We force LPJ with local temperature and precipitation for the sites in Abisko and Sanjiang and we use CRU-data (Climate Research Unit's (CRU) TS 2.1, climatology from 1901 to 2002, (New et al., 1999; Mitchell and Jones, 2005)) of the corresponding grid cell and year for the other sites for the calibration. LPJ is forced with monthly climate data, i.e., temperature (Fig. 4b), precipitation (Fig. 4c) and cloud cover, which are interpolated to daily values. The climate records include seasonal and interannual variability and are repeated over the spin-up period to reach a stable steady state.

The three most important factors for total methane emissions and the attribution to each emission pathway in the model turned out to be (i) the CH_4/CO_2-factor f_{CH_4/CO_2}, followed by (ii) the oxidation fraction f_{oxid} and (iii) the tiller radius r_{tiller} of peatland grasses. Other factors controlling methane emissions are the exudate turnover rate, the moisture response, which is also used to calculate decomposition

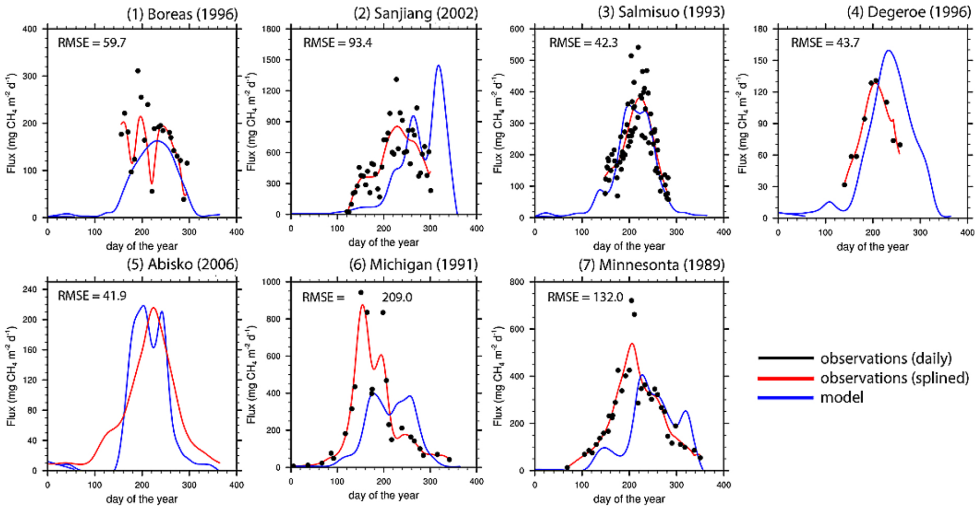

Fig. 2. Daily methane emissions measured at seven sites compared to LPJ model output analogue to a previous model calibration (Wania et al., 2010). All our model runs use the same optimised parameter set for all sites. The respective root-mean-square errors (RMSE) calculated from daily differences between spline fits through the measurements and model output over the period where the measurements exist are given in the top left corner of each box. Note that at the Degeroe site ebullition was not measured and was, therefore, also excluded in the model output. The Abisko record is the only one with daily measurements and only the spline fit is plotted for the purpose of better clarity. Model results are plotted as smoothing spline function with a cut-off period of two months (blue line), observations are plotted as daily values (black dots) and a smoothing spline function with a cut-off period of two months (red line). Note the different scales on the y-axes.

rates, the leaf-to-root ratio, which influences the cross-sectional area of aerenchyma available for plant-mediated gas transport, the tiller porosity which influences the area for plant-mediated transport and parameters regulating the frequency when ebullition occurs and the volume released in a single ebullition event. Except for the two new parameters of our ebullition routine, we use the same values as (Wania et al., 2010) for these six parameters that have proven to be less important.

The CH_4/CO_2-factor, linking heterotrophic respiration and CH_4 production, directly affects the total production of CH_4 and, thus, total annual emissions. The oxidation fraction is the percentage of available O_2 that is used to oxidise CH_4 in each layer. Its effect is similar to the CH_4/CO_2-factor, but weaker. The tiller radius of peatland grasses influences directly the plant-mediated transport of O_2, CO_2 and CH_4. These three parameters were varied over the range of values found in the literature and chosen to minimise the root-mean-square error between model results and data for the seven sites. Data and model results were smoothed using a spline approximation (Enting, 1987) with a cut-off period of two months. The spline covers the time period where the respective measurements exist. Nominal daily data were applied to compute that root-mean-square error for each site between splined measurements and splined model output. The root-mean-square error for all sites is computed from the time period weighted (spanned by measurements) site errors. Local methane emissions for the best parameter set in this sensitivity study are shown in Fig. 2, together with the site measurements and the RMSE as computed from the spline fits. These optimised parameter set is then used to simulate global CH_4 emissions in the model experiment. The same set of parameters is used across all sites although a better fit with observational data could be achieved when parameters would be adjusted for each site individually. We find a slightly improved agreement between model and observations compared to results presented by (Wania et al., 2010) (see Appendix B). This is likely related to the elimination of some coding errors and the improved representation of ebullition.

The optimised parameters are $0.17\,\mathrm{g\,C\,(g\,C)^{-1}}$ for the ratio of CH_4/CO_2 production under anaerobic conditions, 0.5 for the oxidation fraction, i.e., the fraction of available oxygen used for methane oxidation, and 0.0035 m for the tiller radius. Further, we make the assumptions that ebullition occurs when 15 % of the available pore volume is gas and that 1 % of the available volume is released as gas in a single ebullition event. The influence of these parameters on modelled changes in methane emissions after a climate perturbation will be presented in the result section.

It is possible to get similar root-mean-square deviations between model results and observations with different combinations for the production ratio and the oxidation fraction. Very different fractions of oxygen consumption by methanogenesis have been reported, reaching from 0.2 to 1 (Wania, 2007; Frenzel and Rudolph, 1998; Strom et al., 2005). Therefore, we set our oxidation fraction according to literature values and in agreement with Wania et al. (2010) to the value 0.5. Changing parameters, governing plant-mediated transport or ebullition, changes the attribution to the different pathways, but does only weakly influence the total emission per unit area. To quantify the distribution better, either more site measurements would be needed or some further constraints like the ^{13}C signature of the total emissions.

Despite a rather well representation of the amplitude in CH_4 emissions in the course of the year a significant phase lag between observed and modelled CH_4 emissions is found for some sites as illustrated in Fig. 2. This may be partly attributed to the coarse resolution of the CRU data that drives the model for Boreas, Salmisuo, Degeroe, Michigan and Minnesota. In these cases CRU data are not necessarily representing the local conditions. For example, a delayed rise in spring temperature leads to a time lag in soil thawing and, thus, methane production and emissions. Effects like water runoff from other regions are not taken into account either. However, even if we use site climate data at Sanjiang, emissions show a phase lag. This indicates that the seasonal change in the different emission processes is not accurately reflected by our model for all sites. The mismatch may be related to a possible neglect of heterotrophic respiration at shallow soils that thaw early in the season. The methane routine distributes substrate for methanogenesis derived from the total heterotrophic respiration according to the root distribution. In case a layer is still frozen, the substrate is put into the next unfrozen layer above. Analysis of the model output for Sanjiang shows that the soil thawing in deep layers has not began when the measured emissions should start and the substrate for production is transferred to upper layers where it is almost completely oxidised. The HR is directly correlated to temperature in LPJ and the simulated temperature profile seems to have a lag respective to the site profile.

Our sensitivity simulations presented in Sect. 3.4, also show that the partitioning between the different emission pathways (diffusion, plant transport, ebullition) has an influence on the seasonality of the emissions and is sensitive on the choice of model parameters, however, the total annual emission is not. As illustrated in Fig. 3, the time-integrated CH_4 flux is well represented by the model across the different sites and a tight correlation ($R^2 = 0.92$) is found between simulated and measured cumulative site emissions. This indicates that the model has a good skill in representing annual emissions across a wide range of environmental conditions in the boreal zone. In conclusion, total annual emissions are simulated well across the different sites, while deviations between simulated and observed seasonal cycles remain (see also Wania, 2007).

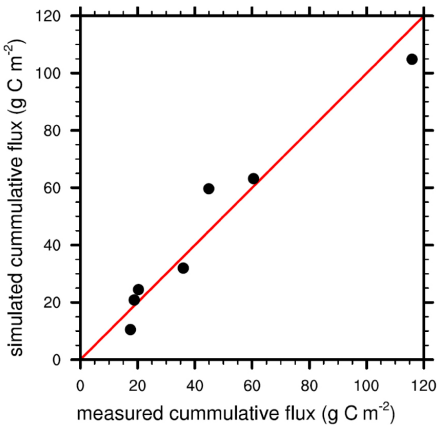

Fig. 3. Measured versus simulated cumulative methane emissions for each site. Emissions for each site are integrated over the time spanned by the measurements. The errors of the measurements (mostly per hour) are up to 50 %.

2.3.1 Input data, spin-up, and setup for transient experiments

Spatially-resolved input data include the global land mask, the soil type (Zobler, 1986) (always "organic" on peatland) and a map of present day peatlands, here on a resolution of 3.75° longitude and 2.5° latitude. We prescribe the distribution and fraction of peatland area per grid cell (Tarnocai et al., 2009). The Tarnocai NCSCD dataset (Tarnocai et al., 2007) includes histels and histosols that were rasterised and regridded to the model resolution (Fig. 4a), and scaled globally to match an area of 1.048 million km^2 in the permafrost affected region in North America (Tarnocai et al., 2009). This scaling results in a Northern Hemisphere peatland area of 2.81 million km^2. This area is larger than the 2.06 million km^2 derived from the IGBP-DIS map as used in (Wania et al., 2010). The number of wet days per month is prescribed from the CRU climatology (New et al., 1999; Mitchell and Jones, 2005). Atmospheric CO_2 is set to a constant value of 279 ppm as found in ice cores for preindustrial conditions (Monnin et al., 2004).

LPJ is forced with monthly data of temperature (Fig. 4b), precipitation (Fig. 4c) and cloud cover. Here, climate output from a control run and a 3-member ensemble of freshwater hosing simulations recently conducted with the Climate System Model, version 1.4, (CSM1.4) of the National Centre for Atmospheric Research (NCAR) (Bozbiyik et al., 2011) is applied to simulate methane emissions and emission changes in northern peatlands during a cooling event

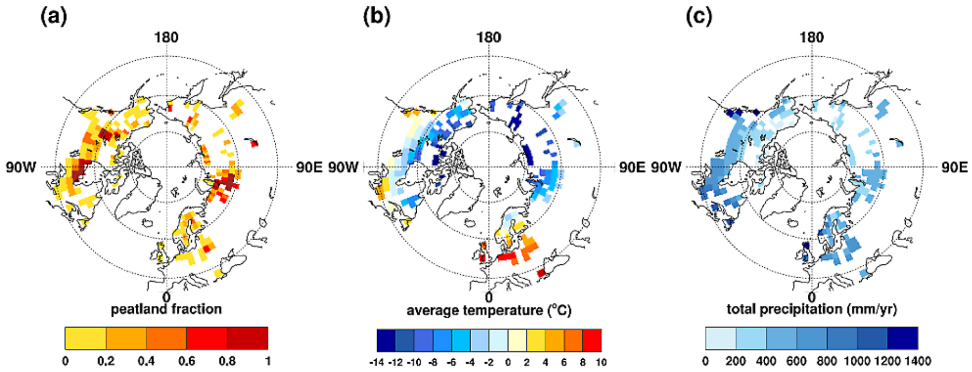

Fig. 4. Distribution and grid cell fraction of peatlands based on (Tarnocai et al., 2009) for present conditions **(a)**; Northern Hemisphere climate patterns averaged over 1961–1990 CRU data (New et al., 1999; Mitchell and Jones, 2005) for temperature **(b)** and precipitation **(c)**, at the peatland grid cells.

similar to the 8.2 kyr event with respect to temperature change over Greenland and Northern Hemisphere land area (Fig. 1). All CSM1.4 freshwater hosing simulations branch from the control simulations that features a stable climate and a constant freshwater input flux anomaly of 1 Sv (1 Sverdrup = 106 $m^3 s^{-1}$) is applied over 100 yr in the Northern North Atlantic. Freshwater input starts 126, 263 and 305 yr after the start of the control in ensemble simulation s1, s2 and s3 and simulations are continued for several centuries. We run several ensembles with the same forcing to distinguish between forced changes and changes that are related to internal climate variability such as the Arctic Oscillation.

The monthly temperature and precipitation data of each CSM1.4 simulation are splined for each grid cell and each calendar month separately, using a 20-yr cut-off frequency (Enting, 1987) (Fig. 5). Anomalies for each month relative to the corresponding monthly mean of the CSM1.4 control run are computed. Monthly anomalies are then added to the CRU climatology (New et al., 1999; Mitchell and Jones, 2005). As the LPJ model is sensitive to the absolute input climatology, this procedure eliminates biases of the NCAR CSM 1.4 (Kiehl et al., 2006) for modern climate relative to the CRU dataset and, thus, corrects for climate-related biases in grid cell vegetation distribution and carbon stocks.

All LPJ simulations are driven with a combination of the repeated 31-yr cycle of CRU data (TS 2.1, detrended climatology from 1960 to 1990, New et al., 1999; Mitchell and Jones, 2005) as a baseline and monthly anomalies from the NCAR CSM 1.4 model under preindustrial conditions. The spin-up is done for all runs with the CRU climatology and the anomalies from the control run and is 1000 yr long. To accelerate the spin-up procedure, equilibrium soil carbon stocks are computed after 400 yr based on average input fluxes and decomposition rates. Then spin-up is continued for another 600 yr.

Simulated annual boreal methane emissions are scaled to 30 Tg CH_4 yr^{-1} for the end of the spin-up period, which is a reasonable value for the present day and the preindustrial (Spahni et al., 2011, and therein). The scaling factor is 0.6. Since the area of effective methane emissions is highly heterogeneous, the simulated emissions have to be scaled accordingly. The prescribed peatland map only indicates the location of peat and the total area, but not its small scale structure. Peat layers on hummocks are emitting much less than peat layers in lawns. Accordingly, a perfect match of the total modelled peatland emission with best estimates from observations cannot be expected.

3 Results and model sensitivity

3.1 Preindustrial emissions from boreal peatlands and interannual variability

There is significant year-to-year climate variability and boreal methane emissions vary accordingly in the control simulation (Fig. 6). The range in annual emissions lies between 27 and 37 Tg CH_4 yr^{-1} and the standard deviation of annual emissions around the long-term mean is $\pm$ 1.8 Tg CH_4 yr^{-1} in the control. The spread in annual emission of 27 to 37 Tg CH_4 yr^{-1} may be compared with the spread of 29 to 37 Tg CH_4 yr^{-1} for Northern Hemisphere extratropical wetlands found by Chen and Prinn (2006) or 25 to 34 Tg CH_4 yr^{-1} by Spahni et al. (2011). Clearly, boreal wetland emissions have the potential to influence interannual variations in atmospheric methane by a few ppb.

Multi-year average methane emissions from peatlands are simulated to typically range between 0 to 50 g C m^{-2} yr^{-1}

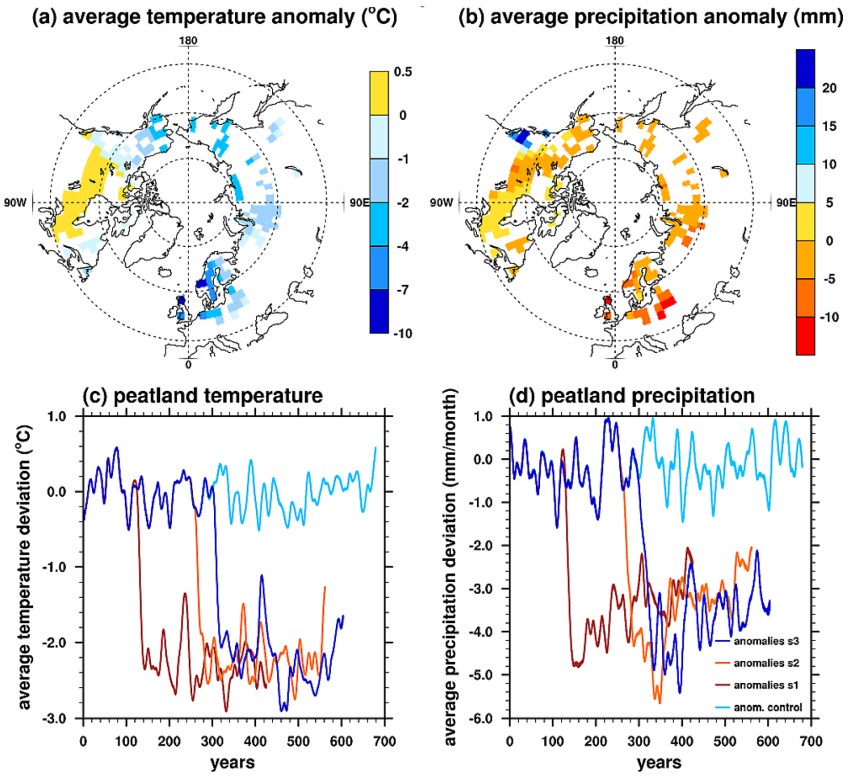

Fig. 5. Temperature and precipitation anomalies in boreal peatlands simulated by NCAR CSM 1.4 in response to freshwater hosing in the North Atlantic. Top: anomalies represent the differences in 50 yr averages of monthly data before and after the freshwater release of ensemble run 1. Bottom: anomalies represent spatial-averages using peatland area of each grid cell as weights and with respect to the mean of the control simulation (2 months running average).

(Fig. 7a) for the control. In general, emissions per unit area are relatively high in Northern Europe and in grid cells along the southern boundary of the peat zone in North America. Relatively low emissions per unit area are simulated in the Canadian Arctic and parts of Siberia, reflecting a generally short growing season and harsh climatic conditions (Fig. 4).

3.2 Temporal and spatial changes in methane emissions after a climate perturbation

We next turn to the response to the simulation of an idealised abrupt cooling event. The additional freshwater flux applied in the NCAR CSM1.4 ensemble simulations results in a collapse of the Atlantic Meridional Overturning Circulation and of the associated northward heat transport into the North Atlantic region with no sign of recovery until the end of the simulations. In return, simulated temperature and precipitation in the North Atlantic and over the adjacent continents decrease relative to the stable CSM1.4 control run (Fig. 5). On annual and spatial average, using peatland area of each grid cell as weights, temperature over peatlands (40–90° N) decrease by about 2.5 °C within decades after adding the freshwater and remain low until the end of the simulations (Fig. 5c). Largest temperature anomalies over peatlands are simulated for the British Isles and Scandinavia, whereas simulated temperature changes remain small in northern North America and the Siberian lowland, except in near-costal regions (Fig. 5a). A slight warming is even simulated for the major peat regions in North America. On average, precipitation drops over peatland areas by 3 to 5 mm per month (Fig. 5d), with largest changes again on the British Isles (Fig. 7b).

While the moss PFT was slightly dominant before the start of the freshwater input (foliar projective cover of 55 % for the moss PFT and 45 % for the grass PFT), it suffers more under the dryer and cooler conditions (∼ 43 % both afterwards).

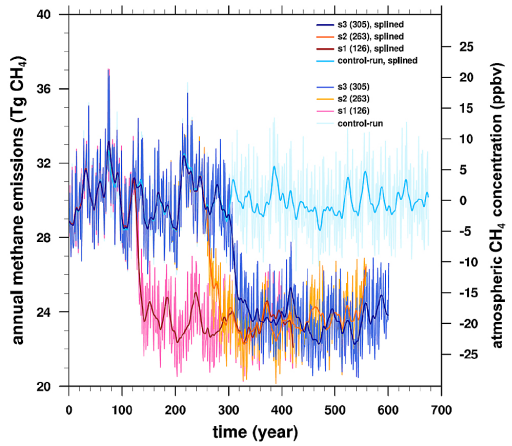

Fig. 6. Total methane emission from northern peatlands for the ensemble runs with freshwater input forcing (s1 to s3) and the control run (cyan). The resulting total methane flux was scaled to reach an average value of 30 Tg CH_4 per year during the control run. Annual emissions are shown by light colours and splines through the annual data by dark colours.

The biggest changes are in the Atlantic regions and the retreat of the sum of both PFTs is about 10 %.

In response to the widespread decrease in temperature and precipitation, peatland CH_4 emissions are reduced by about 19 % compared to the control run. In accordance with the evolution of climate, emissions do not recover in the centuries after the perturbation (Fig. 6). The spatial pattern of response reflects the change in climate with largest decrease in emissions per unit area of up to 25 g C m^{-2} yr^{-1} in Northern Europe and small changes in Eastern North America and in the Siberian lowlands (Fig. 7b). A slight increase in emissions is even found south of Hudson Bay, where an increase in temperature and small precipitation changes are simulated after the freshwater perturbation.

The results are consistent across the three ensemble members. The signal from the freshwater hosing is much larger than internal variability and, therefore, we will rely on run 1 for further discussion. The decrease in emissions from boreal peatlands by 6 Tg CH_4 yr^{-1} corresponds to a decrease of 18 ppb in atmospheric methane (assuming a lifetime of 8.4 yr (Stevenson et al., 2006; Prinn, 1994; Lelieveld et al., 1998; Levine et al., 2011), and a unit conversion factor of 2.78 Tg CH_4 ppb^{-1}).

3.3 Influence of changes in temperature and precipitation on emission changes

Next, we investigate the sensitivity of methane emission changes to changes in individual climatic drivers. This is done by factorial simulations, where either precipitation anomalies or temperature anomalies from the NCAR CSM1.4 simulations are applied. The results show that the changes in the amount of precipitation and in temperature are about equally responsible for the drop in the total methane emissions from the northern peatlands (Fig. 8a); total emission decreases by about 4 Tg CH_4 yr^{-1} in each simulation. The combined effect of temperature and precipitation is not the sum of the individual contributions to the CH_4 emission response. The main reason for this is that cells where the production and transport of methane is already inhibited by low temperatures cannot further be reduced in their activity by missing water and vice versa; grid cells with no activity due to too dry conditions are inactive independent of a further decrease in temperature. In conclusion, both temperature and precipitation changes influence CH_4 emissions significantly.

3.4 Governing processes and their sensitivity to model parameters

We now turn our attention to the importance of individual processes for methane emissions from boreal peatlands. Gross primary productivity (GPP) of the two plant functional types existing on boreal peatlands decreases by 14 % from 1460 to 1260 Tg C yr^{-1} as evaluated by average values before and after the freshwater pulse. This sustained decrease is of the same order as interannual variability in GPP of $\pm$ 80 Tg C yr^{-1} ($\pm$ 1 sdv). Net primary productivity (NPP) drops by 12 % from 840 to 740 Tg C (interannual: $\pm$ 40 Tg C) and total (aerobic and anaerobic) heterotrophic respiration (HR) by 13 % from 840 to 730 Tg C (interannual: $\pm$ 30 Tg C). This decrease is driven by the general decrease in temperature and precipitation in roughly equal parts as inferred from the factorial simulations described above. In turn, the simulated total soil carbon inventory in boreal peatlands of 536 Pg C (interannual: $\pm$ 0.1), including the litter above and below ground, the exudates, and a fast and a slowly decaying soil carbon pool, remains virtually unchanged (532 $\pm$ 0.1 Pg C ($-$1 %)). The changes in the fast carbon pools only (exudates, litter and fast soil pool) are 2.6 %. The decrease in respiration is, thus, the result of a decrease in the mean decomposition rate of organic material and not a decrease in soil carbon inventory. Note that the temperature and precipitation changes in the area of large soil carbon stocks are moderate (Figs. 9 and 5a,b). The soil carbon inventory is in a steady state under preindustrial conditions and realistic compared to available data (MacDonald et al., 2006; Yu et al., 2010; Tarnocai et al., 2009). The average yearly water table position over all peatland gridcells drops from 4 mm below the surface to 6 mm. The biggest changes are in the Atlantic regions and the adjacent areas with up to 110 mm change in the annual mean.

In our model, production of methane is linearly scaled with the rate of heterotrophic respiration and total preindustrial emissions from peatlands are scaled to 30 Tg CH_4 yr^{-1} as

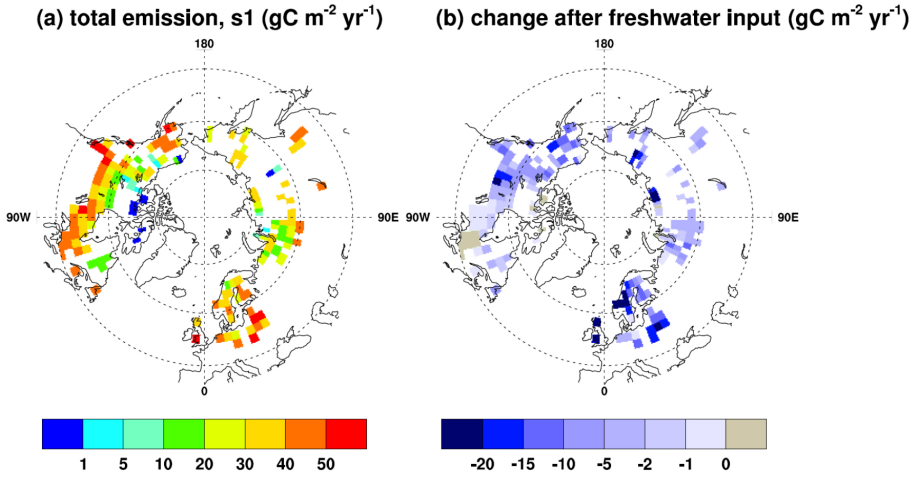

Fig. 7. (a) Spatial distribution of methane emissions ($g C m^{-2} yr^{-1}$ per wetland area) from the sum of plant-mediated transport, diffusion and ebullition averaged over the first fifty years of the control run. **(b)** Difference in methane emission ($g C m^{-2} yr^{-1}$) in 50-yr averages of monthly data before and after the freshwater release of ensemble run 1. Note that fluxes per unit area always denote fluxes per wetland area, not grid cell area.

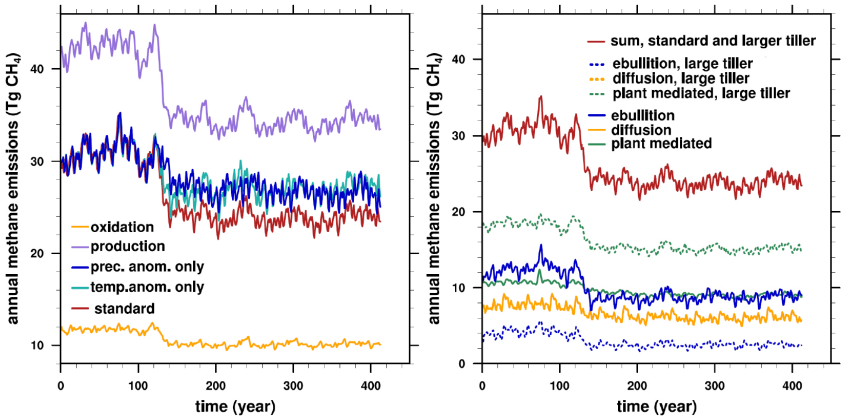

Fig. 8. (a) Total annual methane emission from northern peatlands in the standard scenario (red) compared to factorial runs where only changes in temperature (cyan) or only in precipitation (blue) were taken in account. The total annual methane production rate (violet) and soil oxidation rate (yellow) is plotted as well for the standard scenario. **(b)** Contribution of the three different transport pathways to the total emissions. Results are obtained with the best fitting parameters (solid lines) and a run with a doubled tiller-radius (dashed lines). The total emissions and emissions by diffusion are identical for the standard run and the doubled tiller-radius run, whereas there is a redistribution of plant-mediated emissions and emissions by ebullition. Climate forcing data are from ensemble simulation s1 and model output is smoothed with a spline.

described in the method section. For the standard set of parameters, preindustrial total methane production amounts to 42 ± 2 Tg CH_4 yr^{-1} of which 29 % (12 ± 1 Tg CH_4 yr^{-1}) are removed within the soil by oxidation. After the freshwater pulse, production drops on average to 35 ± 2 Tg CH_4 yr^{-1} of which again about 31 % (11 ± 1 Tg CH_4 yr^{-1}) are oxidised and 69 % emitted (Fig. 8a). 5.0 % of total NPP and HR is converted into methane (42 Tg C/840 Tg C) under preindustrial

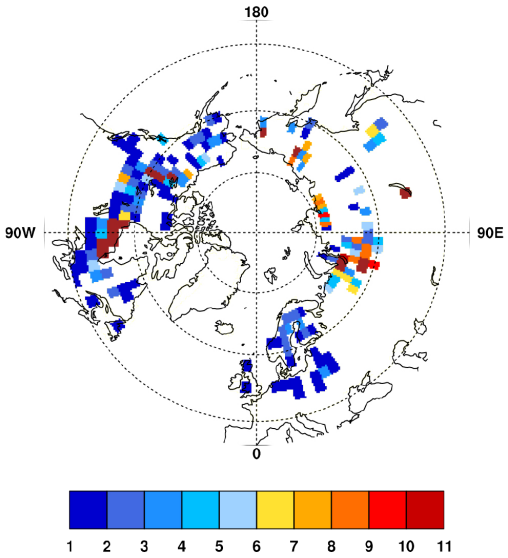

Fig. 9. Peatland soil carbon stocks at the end of the spin-up [Tg C per grid-cell area]

conditions. These fractions stay almost the same (4.7 %) under the climate prevailing after the freshwater input. A simple approach using the decline in RH as a scaling for the drop-down in methane would lead to only a decline in methane emissions by about 13 % as mentioned above, while we find a decline of about 19 % with the coupled process modelling approach (Table 1). This suggests that a fixed scaling of CH_4 emissions to total heterotrophic respiration may not be adequate to simulate variations in CH_4 emissions under varying climate conditions such as reconstructed for Dansgaard-Oeschger events or glacial-interglacial cycles.

The total methane emission flux is the sum of plant transport, diffusion and ebullition. For the standard parameter choice, ebullition and plant transport are the dominant transport pathways (solid lines in Fig. 8b) and each contribute about 35 to 40 % to the total emission. The percentage contribution of these pathways to total emissions remains roughly constant after the climatic perturbation. The fraction of methane that is oxidised remains also fairly constant.

Next, we analyse the sensitivity of the simulated emissions and their changes to the choice of model parameters in the methane module (Table 1). In a suite of sensitivity experiments, a parameter is varied individually around its standard value. Each run is rescaled with the same factor that scales the standard parameter run to 30 Tg CH_4 yr^{-1} at the end of the spin-up. Parameters varied are the CH_4/CO_2 production factor, the oxidation factor, i.e., the percentage of available O_2 that is used to oxidise CH_4 in each layer, and the tiller

Table 1. Average methane emissions before perturbation (EBP) and after perturbation (EAP) from northern peatland; standard parameters: f_{CH_4/CO_2} = 0.17 g C g C^{-1}, f_{oxid} = 0.5, tiller radius r_{tiller} = 0.0035 m, V_{gas} (fraction of gas from actual water volume) = 0.15, ΔV (fraction for ebullition) = 0.01

Parameter	value	EBP [Tg CH_4 yr^{-1}]	EAP [Tg CH_4 yr^{-1}]	reduction in %
standard parameters		30.00	24.42	−18.6 %
f_{oxid}	0.2	35.48	29.48	−16.9 %
f_{oxid}	0.3	33.16	27.37	−17.5 %
f_{oxid}	0.4	31.38	25.77	−17.9 %
f_{oxid}	0.6	28.77	23.43	−18.6 %
r_{tiller}	0.00175	30.11	24.67	−18.7 %
r_{tiller}	0.007	29.56	24.12	−18.4 %
V_{gas}	0.2	29.97	24.50	−18.4 %
ΔV	0.05	30.02	24.60	−18.5 %

radius of the peatland grass PFT and the two parameters controlling the ebullition mechanism.

The CH_4/CO_2 production factor and the oxidation fraction (range 0.2 to 0.6) scale the total methane emissions from boreal wetlands almost linearly under preindustrial conditions. Changing the parameters governing methane transport to reduce a specific methane emission pathway usually leads to an increased flux by the other two pathways as a compensation. However, large reductions in emissions through one pathway would lead to different emissions. This has two reasons: On one hand CH_4 oxidation is different for each pathway, on the other hand high CH_4 amounts can build up in the soil in case of limited transport capacities. For illustration Fig. 8b shows a comparison between the standard run and a run with a doubled tiller radius. As shown by Wania et al. (2010), an increase in the tiller radius leads to more plant-mediated transport and in turn to a lower ebullition flux (Fig. 8b), whereas the diffusive flux to the atmosphere remains practically unchanged. A larger tiller radius increases O_2 diffusion into the soil and, thus, potentially favours oxidation. At the same time, a larger tiller radius also favours a larger methane efflux to the atmosphere (Wania et al., 2010). We find that the fraction of produced methane that is oxidised in the soil increases from 30 to 32 % when the tiller radius is doubled.

It is interesting to analyse how the drop in emission for the simulated climate anomaly depends on the choice of parameters. The reduction in methane emissions after the freshwater perturbation barely depends on the oxidation fraction (Table 1). The reduction in emissions is only 16.9 % when the oxidation fraction is set to 0.2 compared to a reduction by −18.6 % for the standard value of 0.5. Correspondingly, the reduction in emissions becomes slightly larger if a larger fraction of available oxygen is used for methane oxidation. Changes in the tiller radius and in the parameters

governing ebullition also have a small influence on the simulated change in emission (Table 1).

4 Discussion and conclusions

Various climate input scenarios and parameter sets were used to model methane emissions during a freshwater experiment under interglacial climate conditions, reflecting conditions to some degree similar to the 8.2 kyr event. How well does the simulated climate pattern fit with reconstructions of the climate anomaly about 8.2 kyr BP?

The Greenland temperature in our input data drops by almost 4 °C over 20 yr, whereas Kobashi et al. (2007) estimate a cooling by 3.3 ± 1 °C during the 8.2 kyr event from ice-core measurements, revising previous less accurate estimates of 6 °C (Alley et al., 1997) and 7.4 °C (5.4–11.7 °C; Leuenberger et al., 1999). Kobashi et al. (2007) suggest a drying, especially surrounding the North Atlantic area, and an average northern (30–90° N) temperature cooling by 1–2 °C during the 8.2 kyr event. This agrees with findings from many paleo-data from Europe (Wiersma et al., 2006) and also fits with our input data (see Fig. 5). Morrill et al. (2005) present data from paleoclimate proxy records for the 8.2 kyr event from 52 site measurements in Greenland, Europe, America and Africa. The magnitude of their reconstructed temperature drops in Northern Germany, Estonia, Greenland and Norway compare very well to our input data. Also Alley et al. (2005) simulate a similar temperature change pattern to our input (Fig. 6), while LeGrande et al. (2008) find a bit lower surface temperature drops in North America (−0.6 °C), Middle Europe (−1.4 °C), Scandinavia and Siberia compared to our input data. Tindall et al. (2011) simulate maximum temperature anomalies of −1.33 °C in Siberia, −4 °C in Scandinavia and no changes in Middle Europe and wide parts of North America. Further, they find generally a slight precipitation decline of 17 % at maximum, but much less in the area where we simulate peatlands. The precipitation change in our input data is in most grid cells between 1 % and 5 %. In summary we can conclude that even though we use climate input data from simulations at pre-industrial conditions, the patterns and amplitudes of changes in temperature and precipitation are comparable to what is known about the 8.2 kyr event. However, the seasonal temperature and precipitation variability might be different in the input data compared to the variability at 8.2 kyr BP.

For the period 8.2 kyr ago, the location and initiation of boreal peatlands is reasonably well known from peat data (Yu et al., 2010). We used the present day boreal peatland distribution in our simulations based on a map by Tarnocai et al. (2009). This approach appears to be justified, because the comparison of the recent peatland distribution with the ice coverage 8.2 kyr ago (Peltier, 2004) shows that only very small areas of present day peatlands were covered by land ice at that time. Warm Holocene climate conditions prevailed already for more than 1000 yr at that time allowing for an initiation of peat expansion to interglacial conditions (Renssen et al., 2012; Seppä et al., 2009). A sensitivity test in a simulation with ice masking out peatlands 8.2 kyr ago only shows a reduction of 6 % in the simulated emissions and no change to the sensitivity at all. The presence of remnants of the Laurentide ice sheet, thus, appears to have only a minor effect on our boreal CH_4 emissions.

Beside climate input data and ice sheet configuration other uncertainties arise from the preindustrial conditions used in our simulations. The soil carbon inventory in our simulations is in steady state under preindustrial conditions and realistic compared to available data (Yu et al., 2010; Tarnocai et al., 2009). Therefore, it is higher than at the beginning of the 8.2 kyr event. In addition the different solar insolation and CO_2-level may have an influence on the seasonality, the climate response to the freshwater forcing, as well as on the vegetation productivity. The effects on the latter are of opposite direction. While higher solar insolation at high latitudes favours plant growth during the 8.2 kyr event, higher CO_2 levels during the pre-industrial period have a larger fertilisation effect on plant productivity.

Knowing the above limitations, we can compare our results from the freshwater experiment to the 8.2 kyr event. We find that the decrease of 18 ppb in our simulation could explain about 23 % of the 80 ppb reduction during the 8.2 kyr event observed in ice core records (Fig. 1). This would suggest that variations in emissions from boreal peatlands contributed significantly to the CH_4 variations recorded in ice cores, but that other boreal and especially tropical CH_4 sources must have varied much stronger. Evidence for an attribution of reduced CH_4 emissions to tropical wetlands is suggested in Spahni et al. (2003). Part of the CH_4 concentration changes could also be explained by atmospheric sink changes. However, Levine et al. (2011) find that the change in CH_4 from the Last Glacial Maximum to the pre-industrial era was almost entirely source driven. It is, thus, not very likely that the smaller climate changes at the 8.2 kyr event lead to drastic sink changes.

We find that peatland CH_4 emissions drop by 19 %, caused by a reduction in precipitation of only 3 mm per month and a cooling of about 2.5 °C averaged over 50 yr. In addition the emission reduction is not very sensitive to the selection of most parameters in our model. The driving factor for the total magnitude of the modelled emissions is the production. Changes in the model parameters that describe the different transport mechanisms only influence the seasonal timing of the emissions and the attribution to the different transport pathways. The type and rate of CH_4 transport by diffusion in pore water or plants is important on whether CH_4 is directly moved to the atmosphere or gets stored in the soil. In the latter case it stays until it reaches the threshold for ebullition, which is the fastest and most efficient transport pathway. Therefore, the corresponding model parameters have an effect on the intraannual variability of CH_4 emissions.

On top of the variability of CH_4 transport and storage, the CH_4 production also changes significantly from year to year in our model. The modeled interannual variability in CH_4 emissions is on the order of $10\,Tg\,CH_4\,yr^{-1}$ (27–$37\,Tg\,CH_4\,yr^{-1}$), which is comparable to the variability found by Chen and Prinn (2006) and Spahni et al. (2011). This interannual variability amounts to a third of the average peatland emissions of $30\,Tg\,CH_4\,yr^{-1}$ and is also comparable in size to the average and sustained decline in CH_4 emissions found during our freshwater hosing experiment.

It is, thus, plausible that a decline in peatland CH_4 emissions occurred during the 8.2 kyr event similar to the decline simulated during the freshwater hosing event in our model and that this decline was at least partly caused by a direct, fast response of the existing peatland ecosystems to climate change. The observed emission decline during the 8.2 kyr event occurred on time scales of decades, similarly as the simulated decrease in our experiments, and again showing that existing peatlands are able to respond quickly and sensitively to changing climate boundary conditions. Thus, we conclude that a sustained change in peatland emissions on the order of $10\,Tg\,CH_4\,yr^{-1}$ does not require a much slower climate induced geographical relocation of peatlands or a change in peatland ecosystem structure, such as a transgression from fens to bogs, but can be entirely explained by CH_4 emission changes that are comparable to current year-to-year emission variations.

A dynamic relocation or aging of peatlands is not yet included in our model, but would become important for the simulation of glacial CH_4 emissions or during transient Holocene climate conditions on time scales of millennia, where peatland location, structure and ecosystem composition can change. For example, during glacial times northern boreal wetlands were most likely displaced southwards compared to the Holocene in response to the widespread cooler conditions and the ice cover by the Laurentide and Fennoscandinavian ice sheets (Weber et al., 2010). For the 8.2 kyr event itself, which lasted only about 150 yr, a peatland relocation in response to the cooling appears to be unlikely as the time scale for peat development is much longer (Yu et al., 2010; Spahni et al., 2012).

The total average CH_4 emissions of $30\,Tg\,CH_4\,yr^{-1}$ are based on results from Spahni et al. (2011), compatible with Chen and Prinn (2006) for current conditions, but are at the lower end compared to the survey of Zhuang et al. (2004). Zhuang et al. (2004) summarised the recent literature and found that emission estimates for the pan-Arctic region from eleven studies ranged from 31 to $106\,Tg\,CH_4\,yr^{-1}$, although the upper end of their range is incompatible with ice core observations on the interhemispheric CH_4 gradient (Brook et al., 2000; Baumgartner et al., 2012). MacDonald et al. (2006) also suggests that boreal wetland CH_4 emissions might have been higher at 8 kyr BP than today although peat extent was lower. The reason for this is that the emissions from minerotrophic fens that dominated early during peat formation are much higher than from the currently predominant ombrotrophic sphagnum bogs that only developed over time. They suggest that the northern peatland complex was likely at 20 % of its current areal extent at the end of the YD and expanded to about 50 % by 8 ka. On the basis of current estimates of overall CH_4 production from northern peatlands, they may have contributed 12 to $27\,Tg\,CH_4\,yr^{-1}$ by 8 ka. However, taking the higher CH_4 emission rates of early fens into account, MacDonald et al. (2006) speculate that the emissions before the 8.2 kyr event may have been also considerably larger. Accordingly this would then also imply a larger drop in CH_4 concentrations during the 8.2 kyr event. Brook et al. (2000) and Baumgartner et al. (2012) estimate the total CH_4 source strength in the Northern Hemisphere to be 60–$70\,Tg\,CH_4\,yr^{-1}$ for the early Holocene. This estimate includes all extratropical CH_4 sources (e.g., ruminants, wet soils, thawing of submerged permafrost, thermokarst lakes etc.). If we set the annual average peatland emissions to 50 instead of $30\,Tg\,CH_4\,yr^{-1}$, we could explain a 30 ppb change during our freshwater hosing experiment. This could still only explain about 40 % of the observed CH_4 decrease during the 8.2 kyr event. Accordingly, a substantial contribution of tropical and other boreal sources to this event remains most likely.

The simulated CH_4 emission reduction (19 %) is generally within the range of other estimates and ice core observations. Kobashi et al. (2007) find that total CH_4 emissions decreased by 15 ± 5 % during the 8.2 kyr event, while Walter et al. (2001b) and Christensen et al. (2003) find that a global temperature change of ± 1 °C leads to about 20 % changes in methane emissions.

Changes in CH_4 emissions are still subject to considerable uncertainties with respect to the total peatland CH_4 emissions as well as the processes on the soil and ecosystem level. To constrain the parameters further, additional information from field data and potentially from isotopic information are required. Moreover, CH_4 emissions of peatland ecosystems also vary over time. As outlined above the temporal transgression of peatlands from minerotrophic fens to ombrotrophic bogs is not yet included in our model. Sowers (2010) measured a decreasing trend in $\delta^{13}C$ throughout the Holocene beginning at −46.4 ‰ 11 kyr BP and decreasing to −48.4 ‰ at 1 ka. He suggests that the 2 ‰ $\delta^{13}C$ drop is likely to be a combination of increased CH_4 emissions from Arctic lakes and wetlands, an increase in the ratio of C_3/C_4 plants in wetlands and an increase in methanogenic communities utilising the CO_2 reduction pathway as compared to the acetate fermentation pathway. In particular, the latter process would be directly related to the transgression of fens to bogs and could explain the $\delta^{13}CH_4$ shift observed in ice cores (Sowers, 2010) in the first half of the Holocene.

Generally, model improvements could be made by a carbon allocation to the different layers instead of an overall total number for HR given to the methane routine, a more sophisticated parameterisation of the soil anoxity that regulates

the production, a changing ratio of CH_4 production and HR in transient simulations and by including a dynamic peatland distribution. The simulations done for this study could be improved by choosing more specific boundary conditions for the 8.2 kyr event (such as an improved peatland distribution map, the climate influence of the ice sheet remnants and the choice of orbital parameters and CO_2 concentrations at the time of the 8.2 kyr event) instead of preindustrial conditions as used in these simulations. There are also uncertainties to which extent the NCAR climate input is appropriate to do a 8.2 kyr event-like simulation. To improve the model calibration more site measurements would be needed and some further constraints like the ^{13}C signature would give additional constraints for the attribution to the different processes. However, despite these limitations, our model experiments and sensitivity tests indicate that it is most unlikely for the CH_4 drop observed in ice cores during the 8.2 kyr event to be solely due to changes in peatland CH_4 emissions.

Appendix A

Ebullition routine

We assume the existence of three gas species CH_4, CO_2 and N_2 in the bubbles (Tokida et al., 2007). All calculations are done for each soil layer separately.

x	gas species (CH_4, CO_2, N_2)	
$V_{\text{available}}$	available volume (liquid and gas bubbles, not frozen) in a layer per m^2	[m]
V_{gas}	total gas volume per m^2	[m]
$V_{\text{diss},x}$	dissolved volume of species x per m^2	[m]
V_{diss}	volume in which the gases can dissolve per m^2	[m]
V_{ice}	frozen volume in a layer per m^2	[m]
ρ	porosity	
T	temperature in a layer	[°C]
R	universal gas constant	
D_Z	thickness of layer z	[m]
P_{E}	pressure at depth of layer z	[Pa]
H_x	dimensionless Henry constant (ratio of aqueous to gaseous phase) for gas x	
n_x	total number of moles of gas species x per m^2	[mol m^2]
$V_{\text{gas, ebull}}$	gas volume at threshold o ebullition	[m]
$P_{\text{gas},x}$	partial pressure of gas species x	[Pa]
P_{gas}	gas pressure	[Pa]
ΔV	total gas volume lost through an ebullition event per m^2	[m]
Δn_x	change in total amount of gas species x	$[\frac{\text{mol}}{\text{m}^2}]$
Δm_x	total mass change in gas species x	$[\frac{\text{g}}{\text{m}^2}]$
M_x	molar mass of gas species x	$[\frac{\text{g}}{\text{mol}}]$

The available volume per m^2, $V_{\text{available}}$, is the layer height multiplied by the porosity and corrected for the frozen volume.

$$V_{\text{available}} = V_{\text{gas}} + V_{\text{diss}} = \rho \cdot D_z - V_{\text{ice}} \quad [\frac{\text{m}^3}{\text{m}^2}] \tag{A1}$$

The soil in wetlands is divided in the acrotelm (defined as the upper 0.3 m which experiences a fluctuating water table) and the catotelm, the underlying permanently inundated layers with 1.7 m thickness. This assumption is justified as the model simulates only for very few sites ever an acrotelm to catotelm boundary below 30 cm when this boundary is not fixed. The respective porosities are $\rho_{\text{acro}} = 0.9$ for the three first layers, $\rho_{\text{cato}} = 0.8$ for the 5 deeper layers.
P_{E} is the environmental pressure and, therefore, the sum of the atmospheric pressure (101 325 Pa) and the hydrostatic pressure.
Initial conditions:

$$n_{CO_2} = n_{CH_4} = 0 \tag{A2}$$

$$V_{\text{gas}} = 1\,\% V_{\text{available}} \tag{A3}$$

$$V_{\text{diss},N_2} = 99\,\% V_{\text{available}} \tag{A4}$$

We assume the gaseous volume of N_2 to be 1 % (see Sect. 2.3) of the available volume. This assures a minimum gas volume independent of the variables CH_4 and CO_2.
With Eq. (1) (ideal gas law and mass balance) we can calculate the total amount of N_2

$$n_{N_2} = \frac{P_{\text{E}} \cdot (V_{\text{gas}} + \frac{V_{\text{diss}}}{H_{N_2}})}{RT} \quad [\frac{\text{mol}}{\text{m}^2}] \tag{A5}$$

Now we add CH_4 and CO_2 as they are simulated in the model.

$$n_{CO_2}(t) = n_{CO_2}(t-1) + \Delta n_{CO_2} \tag{A6}$$

$$n_{CH_4}(t) = n_{CH_4}(t-1) + \Delta n_{CH_4} \tag{A7}$$

$$n_{CH_4}(t) = n_{CH_4}(t-1) + \Delta n_{CH_4} \tag{A8}$$

For the ebullition criterion we assume that it is critical if the gas volume exceeds 15 % of the available volume

$$V_{\text{gas}} \geq 15\,\% V_{\text{available}} \tag{A9}$$

and compute $P_{\text{gas},x}$.

$$P_{\text{gas},x} = \frac{n_x RT}{V_{\text{gas}} + \frac{V_{\text{diss}}}{H_x}} = \frac{n_x RT}{15\,\% V_{\text{availalbe}} + \frac{85\,\% V_{\text{available}}}{H_x}} \tag{A10}$$

If $P_{\text{gas}} \geq P_{\text{E}}$, ebullition is triggered:

$$P_{\text{gas}} = \sum_x P_{\text{gas},x} \geq P_{\text{E}} \tag{A11}$$

We assume that a fifteenth of the total gas volume bubbles out. The assumption is not critical (see Sect. 3.4)

$$\Delta V = 1\,\% V_{\text{available}} \tag{A12}$$

Therefore, the change in the total amount of CO_2 and CH_4 is

$$\Delta n_x = \frac{\Delta V P_x}{RT} (\mathrm{mol\,m^{-2}}) \quad \text{(A13)}$$

$$\Delta m_x = \Delta n_x \cdot M_x (\mathrm{g\,m^{-2}}) \quad \text{(A14)}$$

while n_{N_2} is kept constant.

Appendix B

RMSE between splined measurements and simulations

RMSE of spline functions (as in Figs. 2 and Wania et al., 2010):

Site	Wania et al. (2010)	our calibration	improvement
Michigan	226.4	209.0	8 %
Minnesota	146.7	132.0	10 %
Salmisuo	75.4	42.3	44 %
Degeroe	50.7	43.7	14 %
Boreas	61.3	59.7	3 %
Abisko	62.8	41.9	33 %

If we weight each site with the time length of the measurement we get an improvement of 30 % for the site evaluation.

Acknowledgements. Financial support for this study was provided by the European Research Council advanced grant MATRICs (ERC grant agreement no. 226172) under the European Community's Seventh Framework Programme. We appreciate support by the Swiss National Science Foundation through the National Centre of Competence in Research (NCCR) Climate and its grant of the Division of Climate and Environmental Physics, and by the European Commission through the FP7 project Past4Future (grant no. 243908), and the Swiss National Supercomputing Centre (CSCS) in Manno, Switzerland, for coupling support.

Edited by: G. Wohlfahrt

References

Alley, R. B., Mayewski, P. A., Sowers, T., Stuiver, M., Taylor, K. C., and Clark, P. U.: Holocene climatic instability: A prominent, widespread event 8200 yr ago, Geology, 25, 483-486, doi:10.1130/0091-7613(1997)025, 1999.

Alley, R. B. and Agustsdottir, A. M :The 8k event: cause and consequences of a major Holocene abrupt climate change, Quat. Sci. Rev., 24, 1123–1149, doi:10.1016/j.quascirev.2004.12.004, 2005

Alm, J., Saarnio, S., Nykanen, H., Silvola, J., and Martikainen, P.: Winter CO_2, CH_4 and N_2O fluxes on some natural and drained boreal peatlands, Biogeochemistry, 44, 163–186, doi:10.1023/A:1006074606204, 1999.

Baumgartner, M., Schilt, A., Eicher, O., Schmitt, J., Schwander, J., Spahni, R., Fischer, H., and Stocker, T. F.: High-resolution interpolar difference of atmospheric methane around the Last Glacial Maximum, Biogeosciences, 9, 3961–3977, doi:10.5194/bg-9-3961-2012, 2012.

Bergamaschi, P., Frankenberg, C., Meirink, J. F., Krol, M., Villani, M. G., Houweling, S., Dentener, F., Dlugokencky, E. J., Miller, J. B., Gatti, L. V., Engel, A., and Levin, I.: Inverse modelling of global and regional CH_4 emissions using SCIAMACHY satellite retrievals, J. Geophys. Res., 114, D22301, doi:10.1029/2009JD012287, 2009.

Blunier, T. and Brook, E.: Timing of millennial-scale climate change in Antarctica and Greenland during the last glacial period, Science, 291, 109–112, doi:10.1126/science.291.5501.109, 2001.

Blunier, T., Chappellaz, J., Schwander, J., Stauffer, B., and Raynaud, D.: Variations in atmospheric methane concentration during the holocene epoch, Nature, 374, 46–49, doi:10.1038/374046a0, 1995.

Bock, M., Schmitt, J., Moeller, L., Spahni, R., Blunier, T., and Fischer, H.: Hydrogen isotopes preclude marine hydrate CH_4 emissions at the onset of Dansgaard-Oeschger events, Science, 328, 1686–1689, doi:10.1126/science.1187651, 2010.

Bozbiyik, A., Steinacher, M., Joos, F., Stocker, T. F., and Menviel, L.: Fingerprints of changes in the terrestrial carbon cycle in response to large reorganizations in ocean circulation, Clim. Past, 7, 319–338, doi:10.5194/cp-7-319-2011, 2011.

Broecker, W. and Peng, T.: Gas-exchange rates between air and sea, Tellus, 26, 21–35, 1974.

Brook, E., Harder, S., Severinghaus, J., Steig, E., and Sucher, C.: On the origin and timing of rapid changes in atmospheric methane during the last glacial period, Global Biogeochem. Cy., 14, 559–572, doi:10.1029/1999GB001182, 2000.

Bubier, J. L., Crill, P. M., Varner, R. K., and Moore, T. R.: BOREAS TGB-01/TGB-03 CH4 chamber flux data: NSA Fen. Data set, available online: http://www.daac.ornl.gov from Oak Ridge National Laboratory Distributed Archive Center, Technical report, Oak Ridge, Tennessee, USA, (last access: 24 September 2012), 1998.

Cao, M., Marshall, S., and Gregson, K.: Global carbon exchange and methane emissions from natural wetlands: application of a process-based model, J. Geophys. Res., 101, 14399–14414, doi:10.1029/96JD00219, 1996.

Chappellaz, J., Blunier, T., Raynaud, D., Barnola, J., Schwander, J., and Stauffer, B.: Synchronous changes in atmospheric CH_4 and Greenland climate between 40-KYR AND 8-KYR BP, Nature, 366, 443–445, doi:10.1038/366443a0, 1993.

Chappellaz, J., Blunier, T., Kints, S., Dallenbach, A., Barnola, J., Schwander, J., Raynaud, D., and Stauffer, B.: Changes in the atmospheric CH_4 gradient between Greenland and Antarctica during the Holocene, J. Geophys. Res., 102, 15987–15997, doi:10.1029/97JD01017, 1997.

Chen, Y.-H. and Prinn, R. G.: Estimation of atmospheric methane emissions between 1996 and 2001 using a three-dimensional global chemical transport model, J. Geophys. Res., 111, D10307, doi:10.1029/2005JD006058, 2006.

Christensen, T. R., Ekberg, A., Ström, L., and Mastepanov, M.: Factors controlling large scale variations in methane emissions from wetlands, Geophys. Res. Lett., 30, 1414, doi:10.1029/2002L016848, 2003.

Clement, A. and Peterson, L.: Mechanisms of Abrupt Climate Change of the Last Glacial, Period. Rev. Geophys., 46, RG4002,

doi:10.1029/2006RG000204, 2008.

Dallenbach, A., Blunier, T., Fluckiger, J., Stauffer, B., Chappellaz, J., and Raynaud, D.: Changes in the atmospheric CH_4 gradient between Greenland and Antarctica during the Last Glacial and the transition to the Holocene, Geophys. Res. Lett., 27, 1005–1008, doi:10.1029/1999GL010873, 2000.

Denman, K. L., Brasseur, G., Chidthaisong, A., Ciais, P., Cox, P., Dickinson, R. E., Hauglustaine, D., Heinze, C., Holland, E., Jacob, D., Lohmann, U., Ramachandran, S., da Silva Dias, P. L., Wofsy, S. C., and Zhang, X.: Chapter 7: Couplings between changes in the climate system and biogeochemistry, in: Climate Change 2007: The Physical Science Basis. Contribution of Working Group I to the Fourth Assessment Report of the Intergovernmental Panel on Climate Change, edited by: Solomon, S., Qin, D., Manning, M., Chen, Z., Marquis, M., Averyt, K., Tignor, M., and Miller, H., Cambridge Univ. Press, UK and New York, NY, USA, 499–588, 2007.

Ding, W., Cai, Z., and Wang, D.: Preliminary budget of methane emissions from natural wetlands in China, Atmos. Environ., 38, 751–759, doi:10.1016/j.atmosenv.2003.10.016, 2004.

Dise, N.: Methane emission from Minnesota peatlands – spatial and seasonal variability, Global Biogeochem. Cy., 7, 123–142, doi:10.1029/92GB02299, 1993.

Dlugokencky, E., Bruhwiler, L., White, J., Emmons, L., Novelli, P., Montzka, S., Masarie, K., Lang, P., Crotwell, A., Miller, J., and Gatti, L.: Observational constraints on recent increases in the atmospheric CH_4 burden, Geophys. Res. Lett., 36, L18803, doi:10.1029/2009GL039780, 2009.

Ellison, C., Chapman, M., and Hall, I.: Surface and deep ocean interactions during the cold climate event 8200 years ago, Science, 312, 1929–1932, doi:10.1126/science.1127213, 2006.

Enting, I.: On the use of smoothing splines to filter CO_2 data, J. Geophys. Res., 92, 10977–10984, doi:10.1029/JD092iD09p10977, 1987.

FechnerLevy, E. and Hemond, H.: Trapped methane volume and potential effects on methane ebullition in a northern peatland, Limnol. Oceanogr., 41, 1375–1383, 1996.

Fischer, H., Behrens, M., Bock, M., Richter, U., Schmitt, J., Loulergue, L., Chappellaz, J., Spahni, R., Blunier, T., Leuenberger, M., and Stocker, T. F.: Changing boreal methane sources and constant biomass burning during the last termination, Nature, 452, 864–867, doi:10.1038/nature06825, 2008.

Flückiger, J., Blunier, T., Stauffer, B., Chappellaz, J., Spahni, R., Kawamura, K., Schwander, J., Stocker, T., and DahlJensen, D.: N_2 and CH_4 variations during the last glacial epoch: insight into global processes, Global Biogeochem. Cy., 18, GB1020, doi:10.1029/2003GB002122, 2004.

Frenzel, P. and Rudolph, J.: Methane emission from a wetland plant: the role of CH_4 oxidation in Eriophorum, Plant Soil, 202, 27–32, doi:10.1023/A:1004348929219, 1998.

Gerber, S., Joos, F., Brugger, P., Stocker, T., Mann, M., Sitch, S., and Scholze, M.: Constraining temperature variations over the last millennium by comparing simulated and observed atmospheric CO_2, Clim. Dyn., 20, 281–299, doi:10.1007/s00382-002-0270-8, 2003.

Gerber, S., Joos, F., and Prentice, I. C.: Sensitvity of a dynamic global vegetation model to climate and atmospheric CO_2, Global Change Biol., 10, 1223–1239, 2004.

Gorham, E.: Northern peatlands – role in the carbon-cycle and probable responses to climatic warming, Ecol. Appl., 1, 182–195, doi:10.2307/1941811, 1991.

Grachev, A. M. and Severinghaus, J. P.: A revised $+10 \pm 4$ °C magnitude of the abrupt change in Greenland temperature at the Younger Dryas termination using published GISP2 gas isotope data and air thermal diffusion constants, Quat. Sci. Rev., 24, 513–519, doi:10.1016/j.quascirev.2004.10.016, 2005.

Granberg, G., Ottosson-Lofvenius, M., Grip, H., Sundh, I., and Nilsson, M.: Effect of climatic variability from 1980 to 1997 on simulated methane emission from a boreal mixed mire in Northern Sweden, Global Biogeochem. Cy., 15, 977–991, doi:10.1029/2000GB001356, 2001.

Hopcroft, P. O., Valdes, P. J., and Beerling, D. J.: Simulating idealised Dansgaard-Oeschger events and their potential impacts on the global methane cycle, Quat. Sci. Rev., 30, 3258–3268, doi:10.1016/j.quascirev.2011.08.012, 2011.

Houweling, S., Kaminski, T., Dentener, F., Lelieveld, J., and Heimann, M.: Inverse modelling of methane sources and sinks using the adjoint of a global transport model, J. Geophys. Res., 104, 26137–26160, 1999.

Huber, C., Leuenberger, M., Spahni, R., Fluckiger, J., Schwander, J., Stocker, T., Johnsen, S., Landals, A., and Jouzel, J.: Isotope calibrated Greenland temperature record over Marine Isotope Stage 3 and its relation to CH_4, Earth Planet. Sc. Lett., 243, 504–519, doi:10.1016/j.epsl.2006.01.002, 2006.

Jackowicz-Korczynski, M., Christensen, T. R., Backstrand, K., Crill, P., Friborg, T., Mastepanov, M., and Strom, L.: Annual cycle of methane emission from a subarctic peatland, J. Geophys. Res.-Biogeosci., 115, G02009, doi:10.1029/2008JG000913, 2010.

Johansson, T., Malmer, N., Crill, P. M., Friborg, T., Akerman, J. H., Mastepanov, M., and Christensen, T. R.: Decadal vegetation changes in a northern peatland, greenhouse gas fluxes and net radiative forcing, Global Change Biol., 12, 2352–2369, doi:10.1111/j.1365-2486.2006.01267.x, 2006.

Joos, F., Prentice, I. C., Sitch, S., Meyer, R., Hooss, G., Plattner, G.-K., Gerber, S., and Hasselmann, K.: Global warming feedbacks on terrestrial carbon uptake under the Intergovernmental Panel on Climate Change (IPCC) emission scenarios, Global Biogeochem. Cy., 15, 891–907, 2001.

Joos, F., Gerber, S., Prentice, I., Otto-Bliesner, B., and Valdes, P.: Transient simulations of Holocene atmospheric carbon dioxide and terrestrial carbon since the Last Glacial Maximum, Global Biogeochem. Cy., 18, GB2002, doi:10.1029/2003GB002156, 2004.

Kaplan, J. O., Folberth, G., and Hauglustaine, D. A.: Role of methane and biogenic volatile organic compound sources in late glacial and Holocene fluctuations of atmospheric methane concentrations, Global Biochem. Cy., 20, GB2016, doi:10.1029/2005GB002590, 2006.

Kellner, E., Baird, A. J., Oosterwoud, M., Harrison, K., and Waddington, J. M.: Effect of temperature and atmospheric pressure on methane (CH_4) ebullition from near-surface peats, Geophys. Res. Lett., 33, L18405, doi:10.1029/2006GL027509, 2006.

Kiehl, J. T., Shields, C. A, Hack, J. J., and Collins, W.: The Climate Sensitivity of the Community Climate System Model version 3 (CCSM3), J. Climate, 19, 2584–2596, 2006.

Kobashi, T., Severinghaus, J. P., Brook, E. J., Barnola, J.-M., and Grachev, A. M.: Precise timing and characterization of abrupt climate change 8200 years ago from air trapped in polar ice, Quat. Sci. Rev., 26, 1212–1222, doi:10.1016/j.quascirev.2007.01.009, 2007.

LeGrande, A. and Schmidt, G.:Ensemble, water isotope-enabled, coupled general circulation modelling insights into the 8.2 ka event, Paleoceanography, 23, PA3207, doi:10.1029/2008PA001610, 2008.

Lelieveld, J., Crutzen, P., and Dentener, F.: Changing concentration, lifetime and climate forcing of atmospheric methane, Tellus B, 50, 128–150, doi:10.1034/j.1600-0889.1998.t01-1-00002.x, 1998.

Lerman, A.: Geochemical Processes: Water and Sediment Environments, Wiley, New York, 1979.

Leuenberger, M. C., Lang, C., and Schwander, J.: Delta(15)N measurements as a calibration tool for the paleothermometer and gas-ice age differences: A case study for the 8200 BP event on GRIP ice, J. Geophys. Res.-Atmos., 104, 22163–22170, doi:10.1029/1999JD900436, 1999.

Levine, J. G., Wolff, E. W., Jones, A. E., Sime, L. C., Valdes, P. J., Archibald, A. T., Carver, G. D., Warwick, N. J., and Pyle, J. A: Reconciling the changes in atmospheric methane sources and sinks between the Last Glacial Maximum and the pre-industrial era, Geophys. Res. Lett., 38, L23804, doi:10.1029/2011GL049545, 2011.

Loulergue, L., Schilt, A., Spahni, R., Masson-Delmotte, V., Blunier, T., Lemieux, B., Barnola, J.-M., Raynaud, D., Stocker, T. F., and Chappellaz, J.: Orbital and millennial-scale features of atmospheric CH_4 over the past 800 000 years, Nature, 453, 383–386, doi:10.1038/nature06950, 2008.

MacDonald, G. M., Beilman, D. W., Kremenetski, K. V., Sheng, Y., Smith, L. C., and Velichko, A. A.: Rapid early development of circumarctic peatlands and atmospheric CH_4 and CO_2 variations, Science, 314, 285–288, doi:10.1126/science.1131722, 2006.

McManus, J., Francois, R., Gherardi, J., Keigwin, L., and Brown-Leger, S.: Collapse and rapid resumption of Atlantic meridional circulation linked to deglacial climate changes, Nature, 428, 834–837, doi:10.1038/nature02494, 2004.

Mitchell, T. D. and Jones, P. D.: An improved method of constructing a database of monthly climate observations and associated high-resolution grids, Int. J. Climatol., 25, 693–712, doi:10.1002/joc.1181, 2005.

Monnin, E., Steig, E., Siegenthaler, U., Kawamura, K., Schwander, J., Stauffer, B., Stocker, T., Morse, D., Barnola, J., Bellier, B., Raynaud, D., and Fischer, H.: Evidence for substantial accumulation rate variability in Antarctica during the Holocene, through synchronization of CO_2 in the Taylor Dome, Dome C and DML ice cores, Earth and Planet. Sci. Lett., 224, 45–54, doi:10.1016/j.epsl.2004.05.007, 2004.

Morrill, C. and Jacobsen, R. M.: How widespread were climate anomalies 8200 years ago?, Geophys. Res. Lett., 32, L19701, doi:10.1029/2005GL023536, 2005.

New, M., Hulme, M., and Jones, P.: Representing twentieth-century space-time climate variability. Part I: Development of a 1961–90 mean monthly terrestrial climatology, J. Climate, 12, 829–856, 1999.

Peltier, W.: Ice-age paleotopography, Science, 265, 195–201, doi:10.1126/science.265.5169.195, 1994.

Peltier, W.: Global glacial isostasy and the surface of the ice-age Earth: the ICE-5G (VM2) model and GRACE, Annu. Rev. Earth Pl. Sc., 32, 111–149, 2004.

Pison, I., Bousquet, P., Chevallier, F., Szopa, S., and Hauglustaine, D.: Multi-species inversion of CH_4, CO and H_2 emissions from surface measurements, Atmos. Chem. Phys., 9, 5281–5297, doi:10.5194/acp-9-5281-2009, 2009.

Prather, M. J., Holmes, C. D., and Hsu, J.: Reactive greenhouse gas scenarios: systematic exploration of uncertainties and the role of atmospheric chemistry, Geophys. Res. Lett., 39, L09803, doi:10.1029/2012GL051440, 2012.

Prinn, R.: The interactive atmosphere – global atmospheric-biospheric chemistry, Ambio, 23, 50–61, 1994.

Renssen, H., Seppä, H., Crosta, X., Goose, H., and Roche, D. M.: Global characterization of the Holocene Thermal Maximum, Quat. Sci. Rev., 48, 7–19, doi:10.1016/j.quascirev.2012.05.022, 2012.

Ringeval, B., de Noblet-Ducoudre, N., Ciais, P., Bousquet, P., Prigent, C., Papa, F., and Rossow, W. B.: An attempt to quantify the impact of changes in wetland extent on methane emissions on the seasonal and interannual time scales, Global Biogeochem. Cy., 24, GB2003, doi:10.1029/2008GB003354, 2010.

Rosenberry, D., Glaser, P., Siegel, D., and Weeks, E.: Use of hydraulic head to estimate volumetric gas content and ebullition flux in northern peatlands, Water Resour. Res., 39, 1066, doi:10.1029/2002WR001377, 2003.

Roulet, N.: Peatlands, carbon storage, greenhouse gases, and the Kyoto Protocol: prospects and significance for Canada, Wetlands, 20, 605–615, doi:10.1672/0277-5212(2000)020[0605:PCSGGA]2.0.CO;2, 2000.

Saarnio, S., Alm, J., Silvola, J., Lohila, A., Nykanen, H., and Martikainen, P.: Seasonal variation in CH_4 emissions and production and oxidation potentials at microsites on an oligotrophic pine fen, Oecologia, 110, 414–422, doi:10.1007/s004420050176, 1997.

Seppä, H., Bjune, A. E., Telford, R. J., Birks, H. J., and Veski, S.: Last nine-thousand years of temperature variability in Northern Europe, Clim. of the Past, 5, 523–535, 2009.

Severinghaus, J., Sowers, T., Brook, E., Alley, R., and Bender, M.: Timing of abrupt climate change at the end of the Younger Dryas interval from thermally fractionated gases in polar ice, Nature, 391, 141–146, doi:10.1038/34346, 1998.

Shannon, R. and White, J.: 3-year study of controls on methane emissions from 2 Michigan peatlands, Biogeochemistry, 27, 35–60, 1994.

Shannon, R., White, J., Lawson, J., and Gilmour, B.: Methane efflux from emergent vegetation in peatlands, J. Ecol., 84, 239–246, doi:10.2307/2261359, 1996.

Singarayer, J. S., Valdes, P. J., Friedlingstein, P., Nelson, S., and Beerling, D. J.: Late Holocene methane rise caused by orbitally controlled increase in tropical sources, Nature, 470, 82–91, doi:10.1038/nature09739, 2011.

Sitch, S., Smith, B., Prentice, I. C., Arneth, A., Bondeau, A., Cramer, W., Kaplan, J. O., Levis, S., Lucht, W., Sykes, M. T., Thonicke, K., and Venevsky, S.: Evaluation of ecosystem dynamics, plant geography and terrestrial carbon cycling in the LPJ dynamic global vegetation model, Glob. Change Biol., 9, 161–185, 2003.

Sowers, T.: Atmospheric methane isotope records covering the Holocene period, Quat. Sci. Rev., 29, 213–221, doi:10.1016/j.quascirev.2009.05.023, 2010.

Spahni, R., Schwander, J., Fluckiger, J., Stauffer, B., Chappellaz, J., and Raynaud, D.: The attenuation of fast atmospheric CH_4 variations recorded in polar ice cores, Geophys. Res. Lett., 30, 1571, doi:10.1029/2003GL017093, 2003.

Spahni, R., Chappellaz, J., Stocker, T., Loulergue, L., Hausammann, G., Kawamura, K., Fluckiger, J., Schwander, J., Raynaud, D., Masson-Delmotte, V., and Jouzel, J.: Atmospheric methane and nitrous oxide of the late Pleistocene from Antarctic ice cores, Science, 310, 1317–1321, doi:10.1126/science.1120132, 2005.

Spahni, R., Wania, R., Neef, L., van Weele, M., Pison, I., Bousquet, P., Frankenberg, C., Foster, P. N., Joos, F., Prentice, I. C., and van Velthoven, P.: Constraining global methane emissions and uptake by ecosystems, Biogeosciences, 8, 1643–1665, doi:10.5194/bg-8-1643-2011, 2011.

Spahni, R., Joos, F., Stocker, B. D., Steinacher, M., and Yu, Z. C.: Transient simulations of the carbon and nitrogen dynamics in northern peatlands: from the Last Glacial Maximum to the 21st century, Clim. Past Discuss., 8, 5633–5685, doi:10.5194/cpd-8-5633-2012, 2012.

Stevenson, D., Dentener, F., Schultz, M., Ellingsen, K., van Noije, T., Wild, O., Zeng, G., Amann, M., Atherton, C., Bell, N., Bergmann, D., Bey, I., Butler, T., Cofala, J., Collins, W., Derwent, R., Doherty, R., Drevet, J., Eskes, H., Fiore, A., Gauss, M., Hauglustaine, D., Horowitz, L., Isaksen, I., Krol, M., Lamarque, J.-F., Lawrence, M., Montanaro, V., Muller, J.-F., Pitari, G., Prather, M., Pyle, J., Rast, S., Rodriguez, J., Sanderson, M., Savage, N., Shindell, D., Strahan, S., Sudo, K., and Szopa, S.: Multimodel ensemble simulations of present-day and near-future tropospheric ozone, J. Geophys. Res., 111, D08301, doi:10.1029/2005JD006338, 2006.

Stocker, B. D., Strassmann, K., and Joos, F.: Sensitivity of Holocene atmospheric CO_2 and the modern carbon budget to early human land use: analyses with a process-based model, Biogeosciences, 8, 69–88, doi:10.5194/bg-8-69-2011, 2011.

Strassmann, K. M., Joos, F., and Fischer, G.: Simulating effects of land use changes on carbon fluxes: past contributions to atmospheric CO_2 increases and future commitments due to losses of terrestrial sink capacity, Tellus B, 60, 583–603, doi:10.1111/j.1600-0889.2008.00340.x, 2008.

Strom, L., Mastepanov, M., and Christensen, T.: Species-specific effects of vascular plants on carbon turnover and methane emissions from wetlands, Biogeochemistry, 75, 65–82, doi:10.1007/s10533-004-6124-1, 2005.

Tarnocai, C., Swanson D., Kimble J., and Broll G.: Northern Circumpolar Soil Carbon Database, Digital Database, Research Branch, Agriculture and Agri-Food Canada, Ottawa, Canada, available at: http://wms1.agr.gc.ca/NortherCircumpolar/northercircumpolar.zip (last access: September 2012), 2007.

Tarnocai, C., Canadell, J. G., Schuur, E. A. G., Kuhry, P., Mazhitova, G., and Zimov, S.: Soil organic carbon pools in the northern circumpolar permafrost region, Global Biogeochem. Cy., 23, GB2023, doi:10.1029/2008GB003327, 2009.

Tindall, J. C. and Valdes, P. J.: Modeling the 8.2 ka event using a coupled atmosphere-ocean GCM, Glob. Planet. Change, 79, 312–321, doi:10.1016j.gloplacha.2011.02.004/, 2011.

Tokida, T., Miyazaki, T., and Mizoguchi, M.: Ebullition of methane from peat with falling atmospheric pressure, Geophys. Res. Lett., 32, L13823, doi:10.1029/2005GL022949, 2005.

Tokida, T., Miyazaki, T., Mizoguchi, M., Nagata, O., Takakai, F., Kagemoto, A., and Hatano, R.: Falling atmospheric pressure as a trigger for methane ebullition from peatland, Global Biochem.Cy., 21, GB2003, doi:10.1029/2006GB002790, 2007.

Valdes, P., Beerling, D., and Johnson, C.: The ice age methane budget, Geophys. Res. Lett., 32, L02704, doi:10.1029/2004GL021004, 2005.

van Huissteden, J.: Methane emission from northern wetlands in Europe during Oxygen Isotope Stage 3, Quat. Sci. Rev., 23, 1989–2005, doi:10.1016/j.quascirev.2004.02.015, 2004.

Vellinga, M. and Wood, R.: Global climatic impacts of a collapse of the Atlantic thermohaline circulation, Climatic Change, 54, 251–267, doi:10.1023/A:1016168827653, 2002.

Walter, B. P., Heimann, M., and Matthews, E.: Modeling modern methane emissions from natural wetlands 1. model description and results, J. Geophys. Res., 106, 34189–34206, 2001a.

Walter, B. P., Heimann, M., and Matthews, E.: Modeling modern methane emissions from natural wetlands 2. Interannual variations 1982–1993, J. Geophys. Res., 106, 34207–34219, 2001b.

Wania, R.: Modelling northern peatland land surface processes, vegetation dynamics and methane emissions, Ph. D. thesis, University of Bristol, 25 pp., available at: http://www.wania.net/docs/Wania-PhD-thesis.pdf (last access: 15 March 2013), 2007.

Wania, R., Ross, I., and Prentice, I. C.: Integrating peatlands and permafrost into a dynamic global vegetation model: 1. Evaluation and sensitivity of physical land surface processes, Global Biogeochem. Cy., 23, GB3014, doi:10.1029/2008GB003412, 2009a.

Wania, R., Ross, I., and Prentice, I. C.: Integrating peatlands and permafrost into a dynamic global vegetation model: 2. Evaluation and sensitivity of vegetation and carbon cycle processes, Global Biogeochem. Cy., 23, GB3015, doi:10.1029/2008GB003413, 2009b.

Wania, R., Ross, I., and Prentice, I. C.: Implementation and evaluation of a new methane model within a dynamic global vegetation model: LPJ-WHyMe v1.3.1, Geosci. Model Dev., 3, 565–584, doi:10.5194/gmd-3-565-2010, 2010.

Weber, S. L., Drury, A. J., Toonen, W. H. J., and van Weele, M.: Wetland methane emissions during the Last Glacial Maximum estimated from PMIP2 simulations: climate, vegetation, and geographic controls, J. Geophys. Res.-Atmos., 115, D06111, doi:10.1029/2009JD012110, 2010.

Weiss, R.: Solubility of nitrogen, oxygen and argon in water and seawater, Deep-Sea Res., 17, 721–735, doi:10.1016/0011-7471(70)90037-9, 1970.

Wiersma, A. P., Renssen, H., Goosse, H., and Fichefet, T.: Evaluation of different freshwater forcing scenarios for the 8.2 ka BP event in a coupled climate model, Clim. Dynam., 27, 831–849, doi:10.1007/s00382-006-0166-0,2006

Wiesenburg, D. and Guinasso, N.: Equilibrium solubilities of methane, carbon-monoxide and hydrogen in water and sea-water, J. Chem. Eng. Data, 24, 356–360, doi:10.1021/je60083a006, 1979.

Yamamoto, S., Alcauskas, J., and Crozier, T.: Solubility of methane in distilled water and seawater, J. Chem. Eng. Data, 21, 78–80, doi:10.1021/je60068a029, 1976.

Yu, Z., Loisel, J., Brosseau, D., Beilman, D., and Hunt, S.: Global peatland dynamics since the Last Glacial Maximum, Geophys. Res. Lett., 37, L13402, doi:10.1029/2010GL043584, 2010.

Zhuang, Q., Melillo, J., Kicklighter, D., Prinn, R., McGuire, A., Steudler, P., Felzer, B., and Hu, S.: Methane fluxes between terrestrial ecosystems and the atmosphere at northern high latitudes during the past century: a retrospective analysis with a process-based biogeochemistry model, Global Biogeochem. Cy., 18, GB3010, doi:10.1029/2004GB002239, 2004.

Zobler, L.: A World Soil File for Global Climate Modelling, NASA Technical Memorandum 87802, 1986.

Chapter 4

A model intercomparison project (WETCHIMP)

This Chapter presents the results of a model inter-comparison project (WETCHIMP) where the present ability to simulate wetland extent, characteristics and corresponding methane emissions is investigated. As global wetlands are the largest natural emitters and very climate sensitive, their feedback to a future warming is important to predict as it is believed to be positive. LPJ-Bern was one of ten models taking part in the comparison. Northern peatlands were simulated as described in this thesis. For inundated areas, a parametrisation was used to calculate emissions from inundated mineral soils. And a unique parametrisation was used to simulate emissions beside the ones from peatland and inundated areas: emissions from wet mineral soils (see Spahni et al. (2011)).

The 10 models covered the spectrum from simple to complex CH_4 emission parameterizations and being tailored for either regional or global simulations. A common experimental protocol was used to drive all models with the same climate forcings. Some models were able to simulate the wetland extent, others used remotely sensed inundation datasets.

The major conclusions were that the models demonstrate a great disagreement in their simulations of the wetland areal extend and methane emissions in space and time. Better agreement was achieved in comparing zonally summed emissions. All models showed a strong positive reaction from methane emissions and wetland area to increased atmospheric carbon dioxide concentrations. It was stressed that we presently do not have sufficient wetland methane observations to evaluate model fluxes for a spatial scale comparable to model grid cells, which is a severe restriction for a reliable modelling of emissions. The large disagreement in emission rates suggests that large uncertainties exist in the model parameters and structure.

Chapter 4.2 is the follow-up paper to the WETCHIMP paper in Chap. 4.2 and provides technical details for the six experiments that were conducted and about the models that took part in the study.

4.1 Present state of global wetland extent and wetland methane modelling: conclusions from a model intercomparison project (WETCHIMP)

J. R. Melton, R. Wania, E. L. Hodson, B. Poulter, B. Ringeval, R. Spahni, T. Bohn, C. A. Avis, D. J. Beerling, G. Chen, A. V. Eliseev, S. N. Denisov, P. O. Hopcroft, D. P. Lettenmaier, W. J. Riley, J. S. Singarayer, Z. M. Subin, H. Tian, S. Zürcher, V. Brovkin, P. M. van Bodegom, T. Kleinen, Z. C. Yu, and J. O. Kaplan

Published in Biogeosciences, 10, 753-788, 2013

doi:10.5194/bg-10-753-2013

Present state of global wetland extent and wetland methane modelling: conclusions from a model inter-comparison project (WETCHIMP)

J. R. Melton[1,*], R. Wania[2,], E. L. Hodson[3,***], B. Poulter[4], B. Ringeval[4,5,6], R. Spahni[7], T. Bohn[8], C. A. Avis[9], D. J. Beerling[10], G. Chen[11], A. V. Eliseev[12,13], S. N. Denisov[12], P. O. Hopcroft[5], D. P. Lettenmaier[8], W. J. Riley[14], J. S. Singarayer[5], Z. M. Subin[14], H. Tian[11], S. Zürcher[7], V. Brovkin[15], P. M. van Bodegom[16], T. Kleinen[15], Z. C. Yu[17], and J. O. Kaplan[1]**

[1]ARVE Group, École Polytechnique Fédérale de Lausanne, Switzerland
[2]Institut des Sciences de l'Evolution (UMR 5554, CNRS), Université Montpellier 2, Place Eugène Bataillon, 34090 Montpellier, France
[3]Swiss Federal Research Institute WSL, Switzerland
[4]Laboratoire des Sciences du Climat et de l'Environment, CNRS-CEA, UVSQ, Gif-sur Yvette, France
[5]BRIDGE, School of Geographical Sciences, Univerity of Bristol, UK
[6]VU University Amsterdam, Department of Earth Sciences, Amsterdam, The Netherlands
[7]Climate and Environmental Physics, Physics Institute & Oeschger Centre for Climate Change Research, University of Bern, Switzerland
[8]Dept. of Civil and Environmental Engineering, University of Washington, USA
[9]School of Earth and Ocean Sciences, University of Victoria, Canada
[10]Dept. of Animal and Plant Sciences, University of Sheffield, Sheffield S10 2TN, UK
[11]International Center for Climate and Global Change Research and School of Forestry and Wildlife Sciences, Auburn University, Auburn, AL 36849, USA
[12]A.M. Obukhov Institute of Atmospheric Physics, Russian Academy of Sciences, Russia
[13]Kazan (Volga Region) Federal University. Kazan, Russia
[14]Earth Sciences Division (ESD) Lawrence Berkeley National Lab, USA
[15]Max Planck Institute for Meteorology, Hamburg, Germany
[16]Department of Ecological Sciences, VU University, Amsterdam, The Netherlands
[17]Department of Earth and Environmental Sciences, Lehigh University, USA
[*]now at: Canadian Centre for Climate Modelling and Analysis, Environment Canada, Victoria, BC, V8W 2Y2, Canada
[**]Lanser Strasse 30, 6080 Igls, Austria
[***]now at: AAAS Science and Technology Policy Fellow, Office of Climate Change Policy and Technology, US Department of Energy, USA

Correspondence to: J. R. Melton (joe.melton.sci@gmail.com)

Received: 30 July 2012 – Published in Biogeosciences Discuss.: 27 August 2012
Revised: 10 December 2012 – Accepted: 12 December 2012 – Published: 4 February 2013

Abstract. Global wetlands are believed to be climate sensitive, and are the largest natural emitters of methane (CH_4). Increased wetland CH_4 emissions could act as a positive feedback to future warming. The Wetland and Wetland CH_4 Inter-comparison of Models Project (WETCHIMP) investigated our present ability to simulate large-scale wetland characteristics and corresponding CH_4 emissions. To ensure inter-comparability, we used a common experimental protocol driving all models with the same climate and carbon dioxide (CO_2) forcing datasets. The WETCHIMP experiments

were conducted for model equilibrium states as well as transient simulations covering the last century. Sensitivity experiments investigated model response to changes in selected forcing inputs (precipitation, temperature, and atmospheric CO_2 concentration). Ten models participated, covering the spectrum from simple to relatively complex, including models tailored either for regional or global simulations. The models also varied in methods to calculate wetland size and location, with some models simulating wetland area prognostically, while other models relied on remotely sensed inundation datasets, or an approach intermediate between the two.

Four major conclusions emerged from the project. First, the suite of models demonstrate extensive disagreement in their simulations of wetland areal extent and CH_4 emissions, in both space and time. Simple metrics of wetland area, such as the latitudinal gradient, show large variability, principally between models that use inundation dataset information and those that independently determine wetland area. Agreement between the models improves for zonally summed CH_4 emissions, but large variation between the models remains. For annual global CH_4 emissions, the models vary by $\pm 40\,\%$ of the all-model mean ($190\,\mathrm{Tg\,CH_4\,yr^{-1}}$). Second, all models show a strong positive response to increased atmospheric CO_2 concentrations (857 ppm) in both CH_4 emissions and wetland area. In response to increasing global temperatures ($+3.4\,^{\circ}\mathrm{C}$ globally spatially uniform), on average, the models decreased wetland area and CH_4 fluxes, primarily in the tropics, but the magnitude and sign of the response varied greatly. Models were least sensitive to increased global precipitation ($+3.9\,\%$ globally spatially uniform) with a consistent small positive response in CH_4 fluxes and wetland area. Results from the 20th century transient simulation show that interactions between climate forcings could have strong non-linear effects. Third, we presently do not have sufficient wetland methane observation datasets adequate to evaluate model fluxes at a spatial scale comparable to model grid cells (commonly 0.5°). This limitation severely restricts our ability to model global wetland CH_4 emissions with confidence. Our simulated wetland extents are also difficult to evaluate due to extensive disagreements between wetland mapping and remotely sensed inundation datasets. Fourth, the large range in predicted CH_4 emission rates leads to the conclusion that there is both substantial parameter and structural uncertainty in large-scale CH_4 emission models, even after uncertainties in wetland areas are accounted for.

1 Introduction

Global wetlands are an important component of the hydrologic and carbon cycles. Wetlands influence groundwater recharge, gross water balance, flood response, and river flow variability including base and low flows (Bullock and Acreman, 2003). Geographically, about 44 % of global wetlands occur in the high northern latitudes (OECD, 1996) where they can be influenced by permafrost controls on hydrology (Woo and Winter, 1993; Woo and Young, 2006). The remainder of global wetlands are primarily located in the tropical and subtropical humid regions; of those, about 30 % occur in arid and sub-arid areas (OECD, 1996). The slow decomposition rates of organic matter in wetlands allow accumulation of carbon in the soil. Thus, while wetlands cover about 6 %–7 % of the Earth's surface (OECD, 1996; Lehner and Döll, 2004), they account for a disproportionate share of the terrestrial soil carbon pool. The vast majority of this wetland carbon is stored in peatland soils, primarily in the northern boreal and sub-arctic regions where estimated peat carbon stocks range between ~ 270 and $\sim 600\,\mathrm{Pg\,C}$ (Gorham, 1991; Turunen et al., 2002; Yu et al., 2010; Yu, 2012), with some important locations in the tropics estimated to contain a further $\sim 90\,\mathrm{Pg\,C}$ (Page et al., 2011). Wetlands, especially eutrophic and mesotrophic wetlands, are also often more productive than other ecosystems in the same climatic zone. For example, Peregon et al. (2008) estimated average net primary productivity (NPP) for wetlands of the West Siberian Lowlands to be $\sim 400\,\mathrm{g\,C\,m^2\,yr^{-1}}$, which is higher than the average NPP of boreal forests (about $200\text{–}250\,\mathrm{g\,C\,m^2\,yr^{-1}}$; Prentice et al., 2001).

While wetland vegetation takes up and stores carbon, its decomposition releases carbon dioxide (CO_2) and methane (CH_4). Methane production is promoted by saturated or flooded conditions in wetlands leading to limited oxygen availability for soil microbes and anaerobic decomposition (Whiticar, 1999). Wetlands play a dominant role in the global methane budget with a contribution estimated to be between 15 and 40 % of the total source budget (Denman et al., 2007). Methane is an important greenhouse gas, with an estimated global radiative forcing of $0.48\,\mathrm{W\,m^{-2}}$ since the start of the Industrial Era (ca. 1750), roughly 30 % that of CO_2 ($1.66\,\mathrm{W\,m^{-2}}$) (Denman et al., 2007). Although wetland CH_4 influences climate, wetlands themselves are believed sensitive to climate changes and have been implicated in past changes in global atmospheric CH_4 concentration following abrupt (Chappellaz et al., 1997; Brook et al., 2000; Huber et al., 2006) and glacial/interglacial climate changes (Loulergue et al., 2008). This apparent feedback between wetlands and climate has led global wetlands to be highlighted as an area of concern for potential large increases in CH_4 emissions under future warming climates by the US Climate Change Science Program (CCSP, 2008). The CCSP (2008) report suggests that wetland modelling should aim to quantify the impact of climate changes on CH_4 emissions, and to improve representation of wetland biogeochemistry, hydrology, and permafrost dynamics in both Earth system and global climate models, for a greater understanding of the risk this hypothesized positive climatic feedback poses.

Wetland CH_4 modelling began twenty-five years ago with Matthews and Fung (1987) combining vegetation, soil and fractional inundation maps, along with estimates of CH_4 flux intensity, to generate a map of global wetland distribution and an estimate of wetland CH_4 emissions. More process-based modelling of CH_4 production, oxidation, and transport soon followed (Christensen and Cox, 1995; Christensen et al., 1996; Cao et al., 1996; Walter et al., 1996; Potter, 1997; Walter and Heimann, 2000), with much recent work devoted to improving these parameterizations (Segers and Leffelaar, 2001; van Bodegom and Goudriaan, 2001; van Bodegom et al., 2001; Zhuang et al., 2006) and using models to investigate the recent past (Ringeval et al., 2010; Hodson et al., 2011; Spahni et al., 2011), more distant past climates (Kaplan, 2002; van Huissteden, 2004; Valdes et al., 2005; Kaplan et al., 2006; Beerling et al., 2011; Hopcroft et al., 2011; Singarayer et al., 2011), and to project responses to future climate change (Shindell et al., 2004; Gedney et al., 2004; Bohn et al., 2007; Bohn and Lettenmaier, 2010; Ringeval, 2011).

Given the importance of accurately simulating global wetland CH_4 emissions response to climate change, it is important to assess how well the models perform and to evaluate our current understanding. The WETland and wetland CH_4 Inter-comparison of Models Project (WETCHIMP) was initiated to coordinate and facilitate the systematic study of wetland and wetland methane models for simulations of large-scale wetland characteristics and corresponding CH_4 emissions. To accomplish this goal, the project was designed around a standard set of simulations performed by each participating global or large-scale regional model. These simulations were run over the modern instrumental period because acceptable quality climate, observational data, topography, land cover, and soil data exist for this period. The standard simulations examined model responses to selective forcing inputs (such as precipitation, temperature, and atmospheric CO_2 mixing ratios) to enable easier comparison between models. For full details of the modelling protocol, as well as a detailed analysis of the methodological differences between models, see Wania et al. (2012). The WETCHIMP participating models and simulations performed are described in Sect. 2. Model performance for wetland location determination is discussed in Sect. 3.1, wetland CH_4 emissions in Sect. 3.2, and Sect. 3.3 discusses the sensitivity test results. The final section describes the project conclusions.

2 Methods and participating models

2.1 Wetland definition

For the purposes of regional- to global-scale modelling, wetlands are defined as grid cells, or fractions thereof, where the land surface has inundated, or saturated, conditions. The presence of the water table above, or close to the surface (on the order of centimetres), allows for anaerobic conditions to develop. Anaerobic conditions combined with decomposition of organic matter permits methanogenic CH_4 production. Varying amounts of CH_4 are emitted to the atmosphere dependent upon transport and consumption mechanisms as well as characteristics of a location such as vegetation present, plant root depth, water table position, and temperature. Following the National Wetlands Working Group (1988) classification, wetlands comprise three general types: peatlands (including bogs and fens), mineral wetlands (which includes swamps and marshes), and shallow water (National Wetlands Working Group, 1988).

Each wetland type has distinct characteristics. Peatlands have fixed extents, at least on timescales of decades, and contrasting hydrologic and nutrient regimes between dry nutrient-poor bogs and wet nutrient-rich fens. Mineral wetlands are dominated by vascular plants that facilitate CH_4 transport through their roots and, along with shallow waters, strong interactions with water tables. These wetland types can be modelled explicitly or treated as a generic wetland type (where no distinction is made between the hydrologic regime, plant communities, and nutrient dynamics of the different wetlands); the latter is the general state of global wetland modelling with the exception of a few peatland specific models developed for the boreal region. LPJ-WHyMe, UW-VIC, and LPJ-Bern (which embeds LPJ-WHyMe as a submodel) are the only participating models to model a wetland type (peatlands) explicitly (Bohn et al., 2007; Wania et al., 2009a,b; Bohn and Lettenmaier, 2010). Besides simulating peatlands and inundated areas, the LPJ-Bern model includes a unique parameterization of CH_4 emissions from wet mineral soils. These areas are not wetlands, according to our definition as outlined above, but are argued to be an important source; they are simulated to emit low flux densities but over large areas (Spahni et al., 2011).

Generally excluded from consideration by large-scale wetland models are lakes, rivers, rice agriculture, saline estuaries, salt marshes, and reservoirs. The carbon, hydrologic, and anthropogenic management and plant community dynamics of these water bodies are considered to be distinct from those of natural wetlands. Saline systems, in particular, may involve processes that are missing in freshwater wetland models such as sulphate reduction (Bartlett et al., 1987). In practice however, the models are commonly not able to distinguish between wetlands and these other non-wetland water bodies; thus exclusion of these systems is commonly accomplished through masking of the grid cells with observational datasets (Table A1).

2.2 Participating models and project simulations

2.2.1 Participating models

This paper describes the first iteration of WETCHIMP. Ten models participated (Table 1), eight of which are global in

Table 1. List of WETCHIMP participating models. Not all models contributed results to all experiments. The conceptualized, general description of net methane flux, F, by each model is adapted from Table 5 in Wania et al. (2012). This formulation is for illustrative purposes; thus the main variables and parameters used in CH_4 production are detailed, but oxidation, O, and atmospheric oxidation, O_{atm}, are not. For all results presented in this paper, all O_{atm} values were set to 0, allowing comparison of modelled gross fluxes. All variables listed are described in the table footnotes. Note that identical parameters/variables for different models do not imply identical values used in the models. A full listing of contributed experiments and model set-ups for the experiments, as well as greater detail on the models' methane flux parameterizations, is provided in Wania et al. (2012).

Model	Resolution (long. × lat.)	Coverage	Wetland determination scheme	CH_4 flux parameterization (see table footnotes)**	Principal references
CLM4Me	2.5° × 1.9°	Global	Model-simulated runoff and water table depth used in diagnostic equation that was parameterized for best fit to the GIEMS dataset.	$F = (R_{het} r_{CH4:C} f_{pH} f_{pE} Q_{10} - O) f_{transport} - O_{atm}$	Riley et al. (2011)
DLEM	0.5° × 0.5°	Global	Maximal extents from inundation dataset with simulated intra-annual dynamics.	$F = (P_{max} C_{labile} f_T f_{pH} f_\Theta - O_{trans} - O_{soil}) f_{transport} - O_{atm}$	Tian et al. (2010, 2011); Xu and Tian (2012)
IAP-RAS	0.5° × 0.5°	Global	Prescribed extents from land cover dataset (CDIAC NDP017).	$F = f_T f_\Theta Q_{10}$	Mokhov et al. (2007); Eliseev et al. (2008)
LPJ-Bern	0.5° × 0.5°	Global	Prescribed peatlands and monthly inundation. Simulated dynamic wet mineral soils (saturated, non-inundated).	Peat: $F = (R_{het} r_{CH4:C} f_{root} f_{WTP} - O) f_{transport}$ Wetlands: $F = R_{het} r_{CH4:C}$ Wet soils: $F = R_{het} r_{CH4:C} f_\Theta - O_{atm}$	Spahni et al. (2011)
LPJ-WHyMe	0.5° × 0.5°	Peatlands (> 35° N)	Prescribed peatland extents (Tarnocai et al., 2009) with simulated saturated/unsaturated conditions.	$F = (R_{het} r_{CH4:C} f_{root} f_{WTP} - O) f_{transport}$	Wania et al. (2009a,b, 2010)
LPJ-WSL	0.5° × 0.5°	Global	Prescribed from monthly inundation dataset.	$F = R_{het} r_{CH4:C} f_{ecosys}$	Hodson et al. (2011)
ORCHIDEE	1.0° × 1.0°	Global	Mean yearly extent over 1993–2004 period scaled to that of inundation dataset with model calculated intra- and inter-annual dynamics.	$F = (R_0 C_{labile} f_{WTP} f_T Q_{10} - O) f_{transport}$	Ringeval et al. (2010, 2011) Ringeval (2011) Ringeval et al. (2012)
SDGVM	0.5° × 0.5°	Global	Independently simulated extents.	$F = R_{het} r_{CH4:C} f_{WTP} f_T Q_{10} - O$	Hopcroft et al. (2011) Singarayer et al. (2011)
UVic-ESCM	3.6° × 1.8°	Global	Independently simulated extents.	n.a.	Avis et al. (2011)
UW-VIC	100 km*	W. Siberian lowlands	Prescribed peatland extents with inundation dataset dynamics modulated by internally calculated saturated/unsaturated conditions.	$F = (R_0 f_{NPP} f_{root} f_T Q_{10} - O) f_{transport}$	Bohn et al. (2007); Bohn and Lettenmaier (2010)

* 100 km polar azimuthal equal-area grid (EASE grid), resampled to 0.5° × 0.5°.
** Summary of variable names: C_{labile}: labile carbon pool; O_{soil}: oxidation in the soil pore water; O_{trans}: oxidation associated with transport through plants; P_{max}: maximum CH_4production; Q_{10}: factor describing dependence on temperature; R_{het}: heterotrophic respiration; R_0: CH_4 production rate; f_{ecosys}: function of ecosystem type; f_{NPP}: function of the ratio of monthly to annual net primary production (NPP); f_{pE}: function of alternative electron acceptors; f_{pH}: function of pH value; f_{root}: function of vertical root distribution; f_T: function of temperature; f_Θ: function of soil moisture; $f_{transport}$: function of CH_4 transport; f_{WTP}: function of water table position; and $r_{CH4:C}$: fraction of C converted to CH_4.

extent with two additional models specific to smaller regions (LPJ-WHyMe and UW-VIC). One model, UVic-ESCM, simulates the global wetland area but does not presently contain a parameterization for methane emissions. The general UW-VIC model set-up is described here, but a detailed treatment of UW-VIC's results will be discussed in a follow-up paper (Bohn et al., 2013). Of the participating models, there is a large variation in complexity and how comprehensive the models have attempted to be in characterizing wetland extent and CH_4 emission processes.

The participating models use three general approaches for determining wetland areal extents: prescribed extents, parameterization/forcing with a remotely sensed inundation dataset, or independent wetland location determination via the model's hydrological model. Models with prescribed extents include LPJ-WHyMe (peatlands), LPJ-Bern (peatlands), IAP-RAS (global wetlands), and UW-VIC (peatlands). Models that used a remotely sensed inundation dataset include CLM4Me, DLEM, ORCHIDEE, LPJ-Bern, UW-VIC, and LPJ-WSL. To ensure inter-comparability, these six models used the Global Inundation Extent from Multi-Satellites (GIEMS) dataset (Prigent et al., 2007; Papa et al., 2010) (Fig. 1d). Two models, SDGVM and UVic-ESCM, used solely their internal hydrological model to determine wetland locations. Masking of rice agriculture areas, large lakes, and large rivers was done by several models (Table A1).

The models that used the GIEMS dataset to aid determination of wetland location adopted different procedures. CLM4Me used the GIEMS dataset from 1993–2000 (as reported in Prigent et al., 2007) to constrain a diagnostic inundated fraction that is used for CH_4 and O_2 reaction transport. The water table in the diagnostic fraction is either model-generated or at the surface. DLEM limits their simulated annual maximal wetland extent to the GIEMS dataset but independently simulates intra-annual wetland dynamics. The mean simulated wetland areal extent of ORCHIDEE is scaled to match that of the GIEMS dataset, with simulated intra- and inter-annual variability otherwise unchanged from the model's TOPMODEL-based

approach (Beven and Kirkby, 1979). LPJ-WSL directly used the GIEMS dataset to determine wetland extent.

The CH_4 emission parameterizations embedded within the models also have varying levels of complexity. The models use wetland (DLEM, UW-VIC, LPJ-Bern – peatlands, and LPJ-WHyMe) and/or upland (CLM4Me, DLEM, SDGVM, LPJ-Bern – non-peatlands, LPJ-WSL, ORCHIDEE, IAP-RAS) plant functional types (PFTs) to estimate NPP. The PFT fractional cover is either prescribed (ORCHIDEE, IAP-RAS, CLM4Me, UW-VIC) or determined dynamically within the model (LPJ-Bern, LPJ-WHyMe, LPJ-WSL, SDGVM, DLEM, UVic-ESCM). Most models then relate CH_4 emissions to NPP with the exception of IAP-RAS. IAP-RAS has a simple methane parameterization that is sensitive to temperature, but considers carbon substrates to be non-limiting in wetlands. Due to the simplicity of its approach, IAP-RAS is applicable only for annual CH_4 fluxes. In other models, relating NPP to CH_4 emissions is done via production of exudates or litter and soil carbon to yield heterotrophic respiration estimates (Table 1). A proportion of the heterotrophic respiration estimate is then taken to be CH_4 production. Some models explicitly simulate oxidative loss during transport of the CH_4 from site of production to the atmosphere (CLM4Me, LPJ-Bern – peatlands, LPJ-WHyMe, and UW-VIC) or assign a fixed proportion of loss (LPJ-WSL, SDGVM, LPJ-Bern – non-peatlands, ORCHIDEE, DLEM, and IAP-RAS). A few models also simulate aerobic soil uptake of CH_4 from the atmosphere (CLM4Me, DLEM, and LPJ-Bern). The WETCHIMP results presented here are simulated gross wetland CH_4 emissions (thereby excluding soil uptake of atmospheric CH_4 in both wetland and upland ecosystems). The full differences between the models' wetland and CH_4 production schemes are described in detail in Wania et al. (2012).

2.2.2 Project simulations

Six experiments were performed for WETCHIMP. The suite of experiments were designed to investigate model performance under transient conditions, as well as equilibrium state simulations with step changes in climate forcing. The first experiment was an equilibrium simulation under a repeating 1901–1931 climate and a carbon dioxide concentration ($[CO_2]$) of 303 ppm. The second experiment was a transient simulation from 1901–2009 using observed climate and $[CO_2]$ values (all datasets used and full experiment details are described in Wania et al., 2012). One exception to the project protocol was CLM4Me, which kept a constant $[CO_2]$ across the simulation period of Experiment 2 (303 ppm). The comparison period of 1993–2004 was chosen due to the overlap with the GIEMS dataset, allowing the models that require an inundation dataset to be forced with observed values. A third experiment was run with similar constraints as the second experiment, but the models were allowed to run in user-defined optimal conditions (Wania et al., 2012). The third experiment allowed participants to investigate the impact of using their optimized forcing data for comparison against the results of Experiment 2. Since Experiment 2 allows for better inter-comparability between the models, all transient results presented here are from Experiment 2.

From each model's equilibrium state (Experiment 1) (Fig. A1), model atmospheric $[CO_2]$ was instantaneously increased to 857 ppm (SRES A2 year 2100 levels IPCC, 2000, Experiment 4). The simulation was then run until the model had reached a new equilibrium state (number of years was model dependent). Experiment 5 investigated the effect of an instantaneous increase of $+3.4\,^{\circ}C$ in surface air temperature (SAT). The magnitude of this $+3.4\,^{\circ}C$ increase was taken from the SRES A2 year multi-model mean SAT warming for 2090 to 2099 relative to 1980 to 1999 (Meehl et al., 2007). However, in our simulations this $+3.4\,^{\circ}C$ increase was applied to the mean climate of 1901–1931, and not to 1980–1999, thus causing a slightly smaller influence than it would have had against the climate of 1980–1999. The final experiment (#6) examined model response to changes in precipitation with an instantaneous increase of $+3.9\,\%$ (SRES A2 2100 level; 30 yr global average for 2071–2100 relative to 1961–1990) (Prentice et al., 2001). Both the SAT and precipitation sensitivity tests were applied to all months and grid cells uniformly. While the magnitudes of the step increases were chosen to be of a similar magnitude to projected future climate changes, the uniform application of these changes is unrealistic but suitable for the purpose of the sensitivity tests, where we are most interested in the relative responses from the models rather than projecting absolute responses to future climate changes. Step changes were adopted, rather than transient simulations, to allow for simpler interpretation of the results and the differences between model responses. For statistical analysis of the model results, all Spearman correlation coefficients and percentile distributions (quantile function, type = 8, 5 %, 25 %, 75 %, and 95 % distributions) were calculated using the R statistical package (v. 2.10.1).

2.2.3 Wetland observational datasets

Observational datasets of wetlands are used to both parameterize and evaluate wetland CH_4 models. The observational datasets presently available fall into two main categories: remotely sensed inundation datasets (such as GIEMS; Prigent et al., 2007; Papa et al., 2010, or Schroeder et al., 2010) and wetland and land cover mapping products (including MODIS: ORNL DAAC, 2000, Lehner and Döll, 2004; and Kaplan 2007 in Bergamaschi et al., 2007). In this study, we have compared the simulated wetland extent to two observationally based datasets. The first dataset is the remotely sensed inundation product, GIEMS (Prigent et al., 2007; Papa et al., 2010), and the second is the Kaplan 2007 wetland mapping product (hereafter referred to as K07) (Fig. 1c), which was originally presented and described in Bergamaschi et al. (2007). Each dataset has

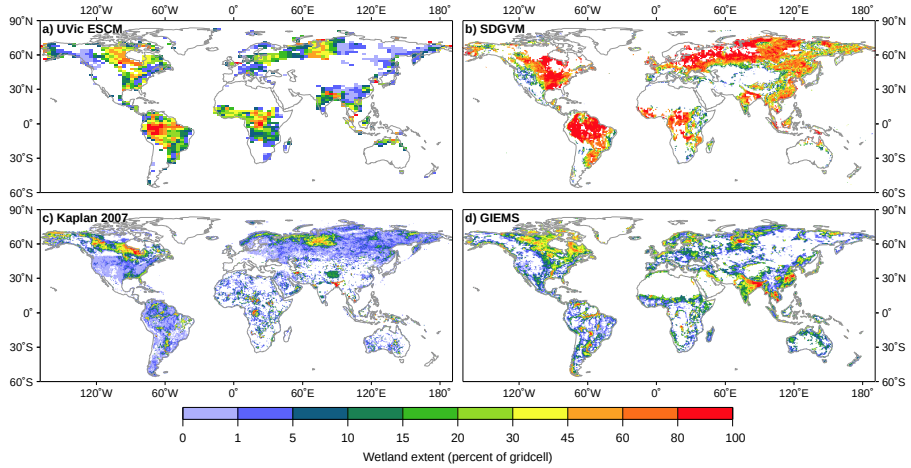

Fig. 1. Simulated mean annual maximal wetland extent for 1993–2004. The SDGVM and UVic-ESCM model results are from Experiment 2-Transient. The GIEMS inundation dataset is plotted as the mean annual maximum value across all years (1993–2004).

particular strengths and weaknesses for application in wetland modelling studies.

Wetland mapping products like K07 and GLWD-3 (Lehner and Döll, 2004) are based on aggregating regional and global wetland and land cover maps. Wetland mapping products have the advantage of only selecting wetlands for inclusion, excluding other water bodies like lakes and rice agriculture. However, they also might overestimate some wetlands, such as in arid or semiarid regions where intermittent wetlands' frequency of turning into actual wetlands could be extremely rare (Lehner and Döll, 2004). These mapping products are also static in time, not allowing for seasonal dynamics, and could be outdated given that wetland ecosystems are highly impacted by humans. For example, it is roughly estimated that up to half of the world's wetlands have been drained for disease vector control or agriculture, at a rate that has increased in recent times, making it difficult for the map production to keep pace (Dugan, 1993). Remotely sensed inundation datasets, such as GIEMS, have the advantage of being more up-to-date, allowing at least monthly resolution, and have close to global coverage. Problems with the use of these datasets for wetland modelling relates to the non-specific measurement of inundation, i.e. no information about depth of water ponding; ambivalence to type of water body (thus necessitating masking of non-wetlands); and presently available datasets are limited to detecting standing water at the surface. Given that many wetlands will continue to produce CH_4 at depth even if there is no standing water, detection of saturated, non-inundated conditions is also important.

Before we use these two datasets to evaluate simulated wetland extents, we should note there is a fair amount of discrepancy between the inundation (GIEMS; Fig. 1d) and the wetland mapping (K07; Fig. 1c) datasets that complicates our evaluation. The major areas of disagreement are around Labrador and Nunavut in the Canadian Arctic (GIEMS shows more wetlands), the Hudson Bay Lowlands (HBL) (K07 shows more wetlands), and in Europe (GIEMS shows extensive inundation while K07 shows few wetlands). As well, both GIEMS and K07 show relatively small wetland extents in the humid tropics. These characteristics of the datasets appear to be related to four main issues.

First, in boreal and Arctic Canada, the GIEMS inundation dataset appears to detect the many small lakes present and classify these as inundated land (Walker et al., 2005). While correct in principle, these areas are not commonly defined as wetlands due to the differing hydrologies, carbon dynamics, and plant communities. Thermokarst lakes are an important example of a lake system that produces methane from carbon sources and processes distinct from those of arctic wetland complexes (Walter Anthony et al., 2008; van Huissteden et al., 2011) and would not be adequately captured if modelled as a wetland system. Thus, while it is perhaps reasonable for an inundation dataset to not distinguish small lakes from wetlands if the dataset is principally designed to detect standing water, this has important implications for the use of these datasets for wetland simulations. These lakes are explicitly not included in the K07 wetland mapping dataset.

Second, the extensive peatland complexes of the HBL are not adequately resolved by the inundation dataset, as many of these areas have a high water table that is below the peatland surface, but retain saturated conditions and the ability to produce CH_4 at depth (Bellisario et al., 1999). In the

West Siberian Lowlands, the GIEMS dataset gives higher inundation values in non-forested regions, and lower values in forested regions, than another remotely sensed dataset (Schroeder et al., 2010). For this region, after comparison with high-resolution Phased-Array L-Band Synthetic Aperature Radar (PALSAR), it appears GIEMS underestimates inundation in forested areas in this region (T. Bohn, personal communication, 2012).

Third, Europe appears to have large inundated areas in the GIEMS dataset, but very few wetlands with the K07 dataset. Many of these inundated areas could be flooded agricultural fields and not actual wetland complexes. Given the population density and well-mapped nature of Europe, it is unlikely that the wetland mapping products are greatly in error.

Finally, both the inundation and wetland mapping datasets appear to be missing large areas of wetlands in the humid tropics. The presence of these wetlands can be inferred from SCIAMACHY satellite data indicating wide-spread high CH_4 emissions in the tropics, e.g. over the Amazon region (Frankenberg et al., 2008). Aerobic CH_4 production from plants appears to be a minor source (Houweling et al., 2006; Kirschbaum et al., 2006; Ferretti et al., 2007), thus the dominant source of the CH_4 should be saturated soils or wetlands. For example, Miller et al. (2007) estimated wetlands to emit around 70 % of total CH_4 emissions in eastern Amazonia, yet the GIEMS dataset shows relatively little inundated area in the region. Other indirect evidence comes from the GIEMS dataset's high inundation reported along the northern Saharan vegetation border in Africa, dropping off rapidly inside the tropical forest cover (Fig. 1d). The remotely sensed GIEMS datasets could have difficulty detecting inundated areas under the dense forest canopies of the region (similar to the low inundation reported in the West Siberian Lowlands, as discussed earlier). While Prigent et al. (2007) state that the remote sensing approach allows for penetration of the vegetation to a certain extent, it is possible that the dense canopy of the tropical regions does not allow adequate penetration of the microwave emissivities and backscatter coefficients. Wetland mapping datasets, like K07, rely upon land surveys to determine the land cover type – an approach possibly hampered by sparse or incomplete information for remote regions.

Problems of consistency and accurate coverage are not limited to the K07 and GIEMS datasets, as other well-known datasets are also problematic. The Matthews and Fung (1987) dataset has been used in several forward and inverse CH_4 modelling studies (Fung et al., 1991; Cao et al., 1996; Hein et al., 1997). The Matthews and Fung (1987) dataset has been suggested to be poorly suited for modelling of wetland CH_4 emissions as the dataset contains salt marshes (similar to GLWD-3; Lehner and Döll, 2004) and denotes wetlands based on indirect criteria (soils, vegetation and inundation) (Sanderson, 2001). Additionally, the Matthews and Fung (1987) dataset has been shown (Sanderson, 2001) to be missing large areas of wetlands that are documented in other databases such as the Ramsar database (Wetlands International, 2002), a deficiency shared with other databases including Cogley (1994) and GLCC (Loveland et al., 2000). On a regional scale, remote peatland regions appear to be problematic for both wetland mapping and inundation datasets as reported by Frey and Smith (2007) . They collected field ground cover observations over an area of $\sim 10^6\,\mathrm{km}^2$ in West Siberia and compared them to four remotely sensed datasets and wetland mapping products for permanent wetlands, finding an agreement of only between 2 and 56 %, depending on the dataset (although it should be noted that neither K07 nor GIEMS was part of their comparison) (Frey and Smith, 2007).

Table 2 shows a three-fold difference between various observational-based estimates of global wetland area; some of this difference can be related to earlier estimates not including transient wetlands (Lehner and Döll, 2004), however the magnitude and spatial differences between datasets remains large and presents difficulties for appropriate parameterization of wetland models, and evaluation of model outputs.

3 Results and discussion

3.1 Wetland areal extent

3.1.1 Maximal wetland areal extent

The mean annual maximal wetland extent was calculated for the models over the period 1993–2004 for Experiment 2 (see Sect. 2 for description), correlating to the same time period as the GIEMS dataset. The K07 dataset possibly contains some wetlands mapped over that same time period but is composed primarily of wetlands mapped during earlier periods. The results for the SDGVM and UVic-ESCM models, the only models that are not parameterized with an inundation dataset or prescribed extents, and the K07 and mean annual maximal wetland areal extent of GIEMS are shown in Fig. 1.

Looking first at the overall pattern of modelled maximal wetland extent, the SDGVM model generally simulates greater wetland area than UVic-ESCM along with higher saturation of wetlands in grid cells with wetland cover. For both models there is a tendency for large areas to be simulated as almost 100 % wetland cover (though the grid cell size of UVic-ESCM is larger at $3.6^\circ \times 1.8^\circ$ compared to $0.5^\circ \times 0.5^\circ$ for SDGVM), which is not apparent in the wetland mapping and inundation datasets.

Regionally, SDGVM simulates more wetland area than UVic-ESCM across large areas of the Eastern US and Eastern Eurasia. The greatest similarity in modelled wetland extents is for the western Amazon and Congo regions, with both models showing large areas of high wetland extents (approaching 100 % of grid cell area). Both models show little wetlands in normally arid regions like Central Australia,

Table 2. Mean annual maximum wetland extent for participating models over the period 1993–2004 (Experiment 2-Transient). For a description of how each model determines wetland extent, see Table 1 and Wania et al. (2012). GLCC is the USGS Global Land Cover Characteristics database (Loveland et al., 2000). MODIS is the MODerate resolution Imaging Spectroradiometer land cover product (ORNL DAAC, 2000). Some of the observational estimates do not include transient wetlands (GLCC & MODIS), and are not specific to the 1993–2004 period with the exception of the GIEMS dataset.

Model	Global ($10^6\,km^2 \pm 1\sigma$)	Tropics (30° S–30° N) ($10^6\,km^2 \pm 1\sigma$)	Extratropics (> 35° N)[a] ($10^6\,km^2 \pm 1\sigma$)
CLM4Me	8.8 ± 1.5	2.6 ± 0.2	5.1 ± 1.4
DLEM	7.1 ± 1.1	3.1 ± 0.4	3.3 ± 0.8
IAP-RAS	20.3	1.3	18.9
LPJ-Bern[a]	81.7 ± 2.4	38.8 ± 1.8	36.4 ± 2.8
	(7.9 ± 0.8)[b]	(2.7 ± 0.2)[b]	(4.5 ± 0.6)[b]
LPJ-WHyMe	2.7[c]	.n.a.	2.7[c]
LPJ-WSL	9.0 ± 1.1	3.8 ± 0.3	4.2 ± 0.9
ORCHIDEE	8.6 ± 0.9	4.3 ± 0.3	3.4 ± 0.7
SDGVM	26.9 ± 3.6	13.2 ± 1.1	12.0 ± 3.8
UVic-ESCM	16.3 ± 1.4	10.6 ± 0.4	5.0 ± 1.2
Observational estimates:			
Matthews and Fung (1987)	5.3		
Williams (1991)[d]	8.6		
Cogley (1994)	4.3		
Stillwell-Soller et al. (1995)	4.8		
GLCC[d]	10.9		
MODIS[d]	12.9		
Finlayson et al. (1999)	min. 12.8		
Mitsch and Gosselink (2000)[d]	7.0–9.0		
GLWD-3 in Lehner and Döll (2004)	9.2		
Gross wetlands map in Lehner and Döll (2004)[e]	11.7		
K07 in Bergamaschi et al. (2007)	6.2	2.8	2.8
GIEMS[f]	12.6 ± 0.8	6.0 ± 1.4	5.2 ± 1.2

[a] This includes the area of wet mineral soils in addition to peatlands and masked inundated areas.
[b] This includes only the masked inundated areas and peatlands.
[c] The LPJ-WHyMe model considers only northern peatlands.
[d] As summarized in Lehner and Döll (2004).
[e] This estimate is derived in Lehner and Döll (2004) as the maximum wetland area per grid cell in either Matthews and Fung (1987), Cogley (1994), Stillwell-Soller et al. (1995), GLCC, or MODIS.
[f] The GIEMS inundation dataset has not had any masking applied. Removing areas of rice agriculture gives the same magnitude of extent as LPJ-WSL.

the Western US, western South Africa, and desert regions. The eastern Canadian Arctic (> 65° N) differs between the models with UVic-ESCM simulating much higher wetland extents than SDGVM and with an opposite pattern in Eastern Siberia with more wetlands simulated by SDGVM than UVic-ESCM. These high latitude differences are likely due to the model treatment of permafrost and soil freezing. UVic-ESCM has fully dynamic permafrost regions with freezing and thawing of soil layers, which influence soil hydrology. Conversely, SDGVM has relatively simple precipitation-evaporation/water table functions that do not allow freezing of the soil water. Both of these models, and indeed all models in WETCHIMP, do not have lateral flow of water between grid cells, which limits their ability to simulate hydrologic conditions in regions where large contributions of water flow into a region from upland areas via rivers into floodplains.

The overall pattern of wetland locations for the UVic-ESCM model compares well to the K07 dataset, with the exception of more wetlands in Eastern Europe and much more in the Congo for UVic-ESCM. Comparing UVic-ESCM to the GIEMS dataset shows reasonable general agreement with the exception of greater wetland extents in Eastern Siberia and Southern Australia in the GIEMS dataset. For SDGVM, while it simulates a larger wetland extent globally, there are some areas where SDGVM simulates less wetlands than the observational datasets. Two examples include Scandinavia, which has more wetlands in both GIEMS and K07, and the Canadian areas of Labrador and Nunavut, which appear prominently in the GIEMS dataset, but not in the K07 dataset. Both of these higher latitude sites could be poorly resolved by SDGVM due to its simple soil model and inability to simulate permafrost.

Comparing maximal wetland extent modelled by SDGVM and UVic-ESCM with the observational datasets shows a general tendency of these models to estimate relatively large global wetland extents (Table 2). UVic-ESCM has a larger tropical wetland area than subtropical, while SDGVM has more similar extents. The other models are about evenly split with almost half the models simulating a larger extratropical wetland area, and the other half simulating a larger tropical wetland area (Table 2). The observational datasets, K07 and GIEMS, give maximal wetland extents of 6.2×10^6 and 12.6×10^6 km^2, respectively, with both datasets showing similar wetland extents in the extratropics and tropics. SDGVM simulates a global wetland area of 26.9×10^6 km^2 and UVic-ESCM simulates 16.9×10^6 km^2. Previous observationally based studies would suggest that global wetland extent is in the range of 6–13 $\times 10^6$ km^2 (Table 2), possibly in the upper part of that range (Lehner and Döll, 2004). The apparent overestimate of wetland extents by SDGVM is a result of the binary nature of its wetland determination scheme. This overestimate will not necessarily carry over into its estimated CH_4 emissions, as once a wetland grid cell is identified by SDGVM, the CH_4 emissions are calculated using simulated water table position (WTP), not wetland area, and are corrected for sub-grid orography. Some of the UVic-ESCM model's overestimation could be due to the model being parameterized to the internal UVic-ESCM-modelled climate, with its associated biases, and not to the observed climate used in this inter-comparison. As well, UVic-ESCM uses only two parameters to define wetland locations: soil moisture and slope. It appears that this simple approach results in overestimated wetland extent in regions not influenced by permafrost dynamics, which is where the model was originally intended to be applied (Avis et al., 2011).

The other models participating in WETCHIMP either have static wetland extents (IAP-RAS and LPJ-WHyMe) or have been parameterized to yield a similar magnitude of annual wetland extent to the GIEMS dataset (Table 2). One other model, LPJ-Bern, has a wetland extent considerably higher than K07 and GIEMS. The wet mineral soils parameterization of LPJ-Bern results in very large areas of wet mineral soils, non-inundated water saturated regions, that are assumed capable of CH_4 production. This large area (81.7×10^6 km^2) is not readily comparable to the other models, or the observational datasets, and is unique to LPJ-Bern. This "wet mineral soils" source should not be confused with "mineral wetlands", a wetland type identified by the National Wetlands Working Group (1988) as described in Sect. 2.1.

3.1.2 Inter- and intra-annual variability of wetland areal extent

Simulated changes in wetland areal inter- and intra-annual extent are compared for the period 1993–2004 for six models in Fig. 2 (SDGVM, UVic-ESCM, CLM4Me LPJ-Bern, DLEM and ORCHIDEE). The GIEMS dataset, without any masking for lakes and rice agriculture applied, is included in the normalized plot (Fig. 2g) for comparison against an observational dataset, with the caveats as described in Sect. 2.2.3, and the additional consideration that the GIEMS dataset represents inundated area, which is not necessarily the same as wetland area. It is assumed that the temporal pattern of inundated area is likely to correspond reasonably with the temporal pattern of wetland area (see wetland definition in Sect. 2.1). The K07 dataset can not be used here for comparison as it is a static distribution. A discussion of each model's simulated changes in wetland areal extents is included in Appendix A1.

If the GIEMS inundation dataset is assumed to be an accurate proxy for global wetland area, the models that most closely, on average, reproduce its annual cycle are CLM4Me and SDGVM, and to a lesser extent DLEM. The relative difference between maximum and minimum global wetland extents for the GIEMS dataset is much larger than LPJ-Bern and UVic-ESCM results, again more in line with CLM4Me and SDGVM, and to a lesser extent DLEM. The model distribution (grey area in Fig. 2g) shows that, on average, the models simulate an earlier peak in wetland extent than the inundated area peak in the GIEMS dataset, outside of the models' 5th percentile distribution for the months of May and June. If it is correct that the GIEMS dataset is underestimating inundated area in the tropics as suggested earlier, global wetland extent from GIEMS would be biased to the northern high latitudes. This could cause a later peak in global wetland extent as the region is slow to lose snow cover and allow inundation to develop.

Papa et al. (2010) found a ~ 5.7 % reduction in mean annual maximum inundation across the 1993–2004 period, located mostly in the tropics. This reduction is not evident in the models' results (see Figs. 2 and 7), with the exception of DLEM whose annual maximum is prescribed to be the same as the GIEMS dataset. The lack of trend in the simulated wetland extents could be due to several possible reasons: (1) the models are inadequately simulating inundation and saturated conditions, (2) modelled wetland extent, which can include both saturated/inundated and unsaturated areas (model dependent, see Wania et al., 2012), does not correlate to inundated area, (3) the assumption that wetland area is proportional to inundated area is false, (4) the models' inability to laterally transfer water between grid cells produces erroneous lowland wetland extents, and (5) the trend observed in the GIEMS dataset is due to artefacts in data retrieval and processing although the decrease in global extent occurred primarily in the 1990s, the years of the GIEMS record with the highest confidence (Papa et al., 2010).

Zonal sums of the mean annual maximal wetland extent for all models show relatively poor agreement between the models (Fig. 3). The area of best agreement is the high northern latitudes (north of 45° N). CLM4Me predicts a prominent peak in wetland extent above 60° N. These wetlands form in CLM4Me due to impeded drainage on frozen soils

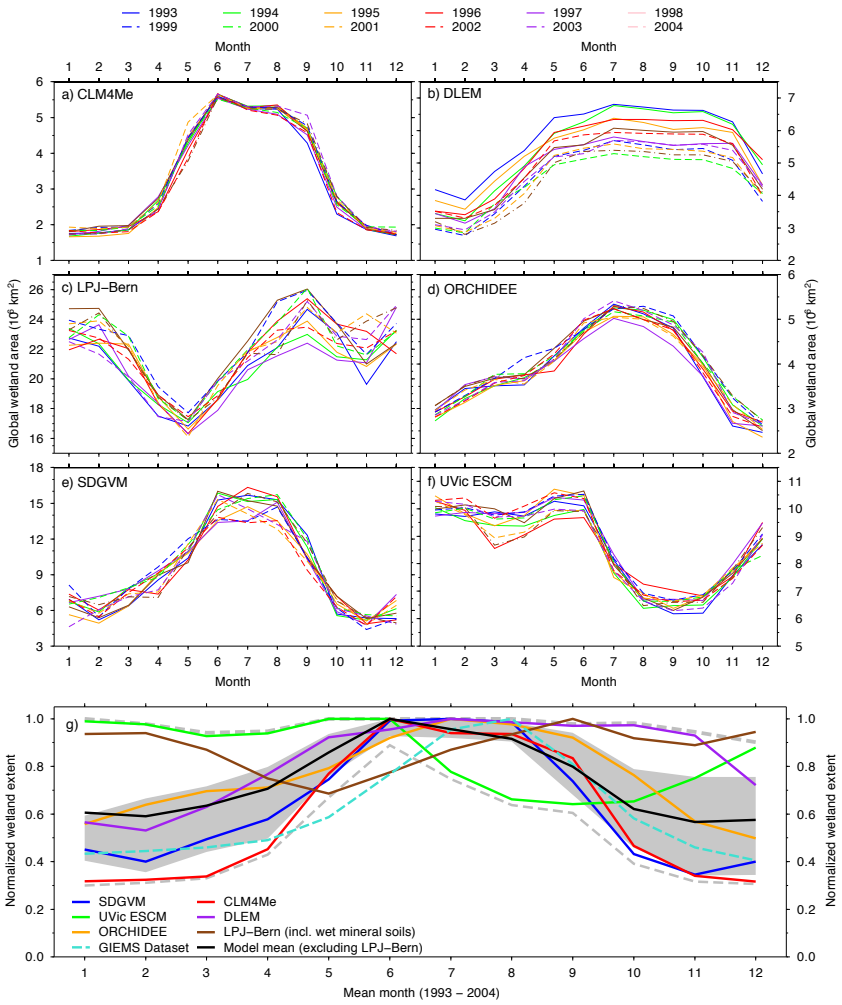

Fig. 2. Monthly global wetland extent for 1993–2004 for all models that do not use an external dataset for calculation of intra- and/or inter-annual variability. Plot **(g)** is the normalized monthly global wetland extent for all models in plots **(a)–(f)**, the unaltered GIEMS inundation dataset, as well as the mean extent of the models (excluding LPJ-Bern due to its wet mineral soils parameterization). The grey shading denotes the 25th and 75th percentiles of the model distribution (excluding LPJ-Bern). The grey dashed lines are the 5th and 95th percentiles.

(Riley et al., 2011). SDGVM has a much larger boreal peak than the other models as a result of its simple soil model and binary wetland parameterization, as discussed earlier. Farther south, CLM4Me, SDGVM, and the GIEMS dataset have a peak in wetland extent around 20°–30° N. This is a prominent rice agriculture band, and the rice growing regions have been masked out of other models, reducing the natural wetland extent in these areas (Table A1). Around the equator, the use of the GIEMS inundation dataset by models is especially apparent. Both SDGVM and UVic-ESCM show very large wetland extents around the equator larger than (UVic-ESCM), or similar in size (SDGVM) to, the high northern latitude peaks. The other models simulate a smaller equatorial wetland peak extent than the area above 45° N.

Comparing the models' mean value (which excludes LPJ-Bern's wet mineral soils) to the K07 and GIEMS datasets shows a general agreement in pattern, but the model mean (and percentile distribution) is higher in most latitudes. The

general agreement in spatial pattern is expected considering that several of the models either use directly, or are parameterized to scale with, the GIEMS dataset. Monthly zonally averaged wetland area plots for 1993 to 2004 for each model are discussed in Appendix A1.

Several conclusions can be drawn from the simulated wetland extents. First, there is little agreement between the models for the magnitude of maximal wetland extent, with an almost four-fold difference across the suite of models (excluding here the wet mineral soils of LPJ-Bern). Estimates from inundation and wetland mapping datasets constrain the observed maximal wetland extent to the lower range of the model estimates, but those observational datasets have several discrepancies that make their use problematic. Additionally, there is little agreement between the published wetland extent estimates, with an almost three-fold difference between them (Table 2). Second, the models have best agreement zonally in the high northern latitudes above 45° N. The greatest differences are in the equatorial band, with models that use the inundation dataset simulating a much smaller peak in wetlands than those that find wetland extents independently. Third, the seasonal dynamics of wetland extent also do not show a strongly consistent pattern between the models. A general pattern of higher wetland extent in the boreal summer is supported by most models, however the months, and magnitude, of peak wetland extent are not consistent. The models also fail to produce a trend in wetland area across 1993 to 2004 as is reported for global inundation (Papa et al., 2010). Lastly, our present uncertainties in modelling global wetland dynamics will only magnify uncertainties in the methane emissions simulated from those wetlands.

3.2 Simulated methane emissions

3.2.1 Annual CH_4 emissions

Annual global methane emitted to the atmosphere for the period 1993–2004 is estimated by the models to be between about 140 and 260 $\mathrm{Tg\,CH_4\,yr^{-1}}$ with a mean value of $\sim 190\,\mathrm{Tg\,CH_4\,yr^{-1}}$ (Table 3). The basic parameterization of each model's CH_4 scheme is listed in Table 1, with greater detail provided in Wania et al. (2012). The WETCHIMP model estimates generally fall within the range of inverse model estimates and are bracketed by some of the early forward-model results. The WETCHIMP models estimate a slightly higher fraction of CH_4 emissions to come from the tropics (66 %) and less from the extratropics (27 %) than the recent inverse modelling results of Bloom et al. (2010) (55 % and 42 %, respectively) and are similar to Bousquet et al. (2006, 2011) ($\sim$ 63 % and $\sim$ 30 %, respectively). While this seems reassuring that different model techniques (forward and inverse) yield reasonably close estimates, the convergence of these estimates provides no proof of their accuracy. Indeed, neither modelling approaches are independent of assumptions (priors for the inverse models and tuning for the forward models), so similar results are expected.

To compare the simulated CH_4 emissions to observationally based estimates, we require datasets that are of similar temporal and spatial scale. The temporal scale of the emissions presented here are monthly to annual, thus we require observational datasets to span similar periods of time. The spatial scale of the observational datasets is especially important as the smallest grid size presented here is $0.5° \times 0.5°$. Many observational studies of CH_4 emissions are for point locations (e.g. Moore and Roulet, 1990; Chasar et al., 2000) or take an approach of upscaling from sparse measurements (e.g. Smith et al., 2000; Melack et al., 2004). Upscaling of point measurements introduces large uncertainties due to the influence of spatial heterogeneity, as well as uncertainties around accurately capturing emissions from ebullition, diffusion, and plant-mediated transport (van Bodegom et al., 2002). Ideally, to ensure a consistent spatial reference, we require measurements conducted over broad areas such as airmass back trajectory analysis, aircraft or large flux tower datasets, or concurrent chamber observations across relevant spatially heterogenous terrain features. Specifically, the areas should be large enough to encompass several grid cells to reduce the influence of inaccuracies in the model inputs (such as soil texture, climate, vegetation, and topography). With these constraints, we are not aware of any studies conducted in the tropics that would allow comparison with our model results, although it does appear that some promising projects are currently underway (Guerrero et al., 2011). This lack of comparative datasets is a major deficiency in our ability to evaluate the models' performance in the regions that contribute the largest share of global CH_4 emissions (Denman et al., 2007) (Table 3).

The boreal region is better studied on large spatial scales. The HBL (Harriss et al., 1994; Roulet et al., 1994; Worthy et al., 2000; Pickett-Heaps et al., 2011) and West Siberian Lowlands (Winderlich et al., 2010; Glagolev et al., 2011), in particular, have several large-scale studies that estimate annual emissions. Focusing on the HBL (the West Siberian Lowlands will be discussed in a follow-up paper, Bohn et al., 2013 in preparation), the most recent analysis estimated annual emissions for the period 2004–2008 using ARC-TAS and pre-HIPPO aircraft campaigns in May–July 2008 and long-term monitoring from two sites located north (Alert, Northwest Territories) and south (Fraserdale, Ontario) of the HBL. These observations were interpreted with wetland bottom-up modelling integrated into a global chemical transport model (GEOS-CHEM). From this approach, the mean CH_4 emissions were estimated to be $2.3 \pm 0.3\,\mathrm{Tg\,yr^{-1}}$ (Pickett-Heaps et al., 2011). This estimate is larger than a previous estimate of $0.5 \pm 0.3\,\mathrm{Tg\,CH_4\,yr^{-1}}$ from the ABLE-3B/NOWES surface and aircraft field study from July 1990 (Harriss et al., 1994; Roulet et al., 1994). The differences in these estimates demonstrates some of the challenges of up-scaling measurements to large regions, as was done in

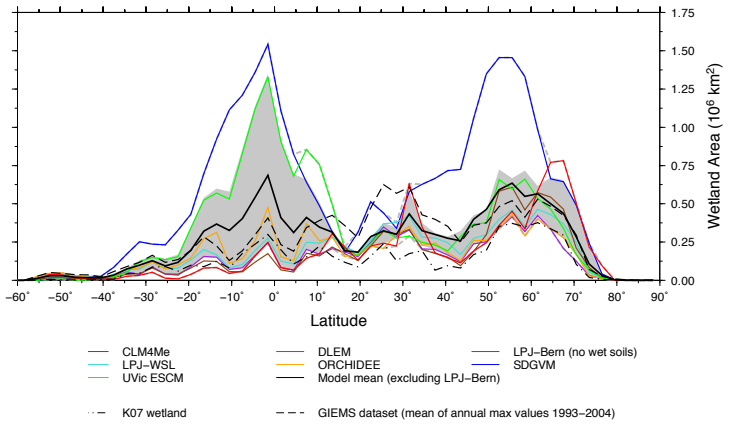

Fig. 3. Zonal sum of mean annual maximal wetland area for 1993–2004 for all models that have dynamic wetland extents. LPJ-Bern is plotted here excluding its wet mineral soils (keeping inundated areas and peatlands). Also included are the K07 and GIEMS datasets. The grey shading denotes the 25th and 75th percentiles of the model distribution (excluding LPJ-Bern); the grey dashed lines the 5th and 95th. The wetland extents are summed across 3° bins.

the ABLE-3B/NOWES studies (Harriss et al., 1994; Roulet et al., 1994), with much of the difference due to spatial heterogeneity across the HBL region. From the same two sites used by Pickett-Heaps et al. (2011), an earlier study by Worthy et al. (2000) used inverse methods to estimate an annual CH_4 flux of 0.2–0.5 Tg yr^{-1} for the HBL.

Table 3 lists the simulated mean CH_4 emissions over the period 1993–2004. The wetland models on average estimate CH_4 emissions for the HBL a little over double that of Pickett-Heaps et al. (2011) and an order of magnitude greater than the estimates of Harriss et al. (1994), Roulet et al. (1994), and Worthy et al. (2000).

It is surprising for SDGVM to have a relatively low HBL CH_4 flux estimate but be on the high end of global CH_4 estimates. For the HBL, the soil texture information used by SDGVM could be part of the reason, as only part of the region is found to be wetlands by the SDGVM dynamic wetlands scheme. The largest CH_4 flux is simulated by LPJ-Bern. This value is related to peaks in CH_4 emission for the 1998, 1999, and 2001 simulation years and is a model artefact (full description in Wania et al., 2012). Outside of these years, LPJ-Bern simulates a mean HBL CH_4 flux of 7.2 ± 1.7 Tg yr^{-1}. An additional reason the models could be high compared to these other estimates is the influence of 1998 on the mean of 1993–2004, which was a year of of exceptional warmth and moisture in the boreal region that has been suggested to have greatly increased boreal CH_4 emissions (see discussion in Sect. 3.2.3).

3.2.2 Methane emissions spatial distribution

The mean spatial distribution of CH_4 emissions with meridional and zonal sums for 1993–2004 are shown in Fig. 4. The spatial pattern of CH_4 emissions per model is obviously dependent upon the presence or absence of wetlands, yet the intensity of emissions reflects internal model dynamics.

The models, taken as a whole, simulate the strongest methane fluxes in the tropical regions with a general, non-uniform decline into higher latitudes. The meridional sums of the models have a common pattern of a large peak corresponding to the longitudes of the Amazon. The models also generally simulate a small peak at longitudes corresponding to the Congo region of Africa and a moderate peak for Southeast Asia. These patterns show large variability amongst the models, with a general tendency for models with smaller wetland areas simulating higher methane fluxes. Further discussion on the differences between models can be found in Appendix A2.

Plotting the zonal sums of the models together shows reasonable agreement between the models (Fig. 5). The models generally simulate a large peak of CH_4 emission in the tropics (as is also evident in Table 3) and smaller secondary peaks centred on 25° N and 55° N. The peak around 25° N is likely slightly overestimated due to some models not masking rice agriculture that is present in that region (Leff et al., 2004) (Table A1). ORCHIDEE stands out with prominent peaks in the Southern Hemisphere that are also simulated by IAP-RAS, as well as a lower latitude boreal peak around 45° N. IAP-RAS's boreal CH_4 emissions are well within the models' 25th to 75th percentile distribution, but outside of this region IAP-RAS is commonly an outlier. This relates to the

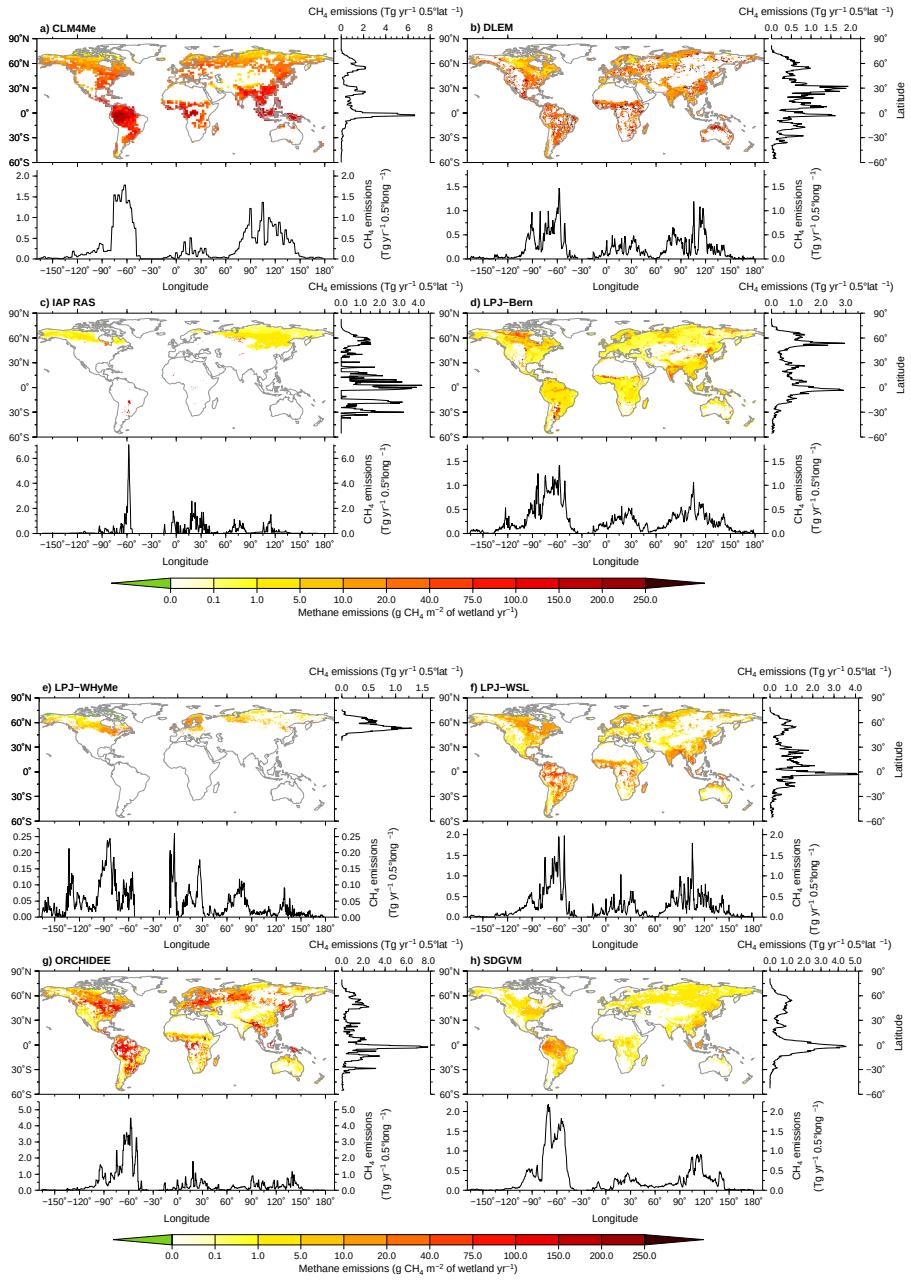

Fig. 4. Global maps of mean annual CH_4 flux intensity per meter squared of wetland with meridional and zonal emission sums for 1993 to 2004. The zonal and meridional sums are per 0.5° of latitude/longitude. The CLM4Me and ORCHIDEE models were interpolated to a 0.5° grid to allow inter-comparison with the other models.

Table 3. Simulated annual mean total methane emitted to atmosphere from natural wetlands for 1993–2004. All units are $\mathrm{Tg\,CH_4\,yr^{-1}} \pm 1\sigma$, where the standard deviation represents the inter-annual variation in the model estimates. Note that estimates from some other reference studies are not for the same time period, or are for slightly different geographic regions. These exceptions are noted in the table footnotes.

Model	Global	Tropics (30° S–30° N)	Extratropics (> 35° N)[a]	HBL[b]
LPJ-Bern[c]	181 ± 15	106 ± 2	65 ± 13	11.3 ± 7.9
CLM4Me	206 ± 6	134 ± 5	62 ± 6	3.4 ± 0.3
DLEM	141 ± 11	85 ± 7	39 ± 3	2.9 ± 0.2
IAP-RAS	164 ± 4	115 ± 2	43 ± 2	4.7 ± 1.1
LPJ-WHyMe			27 ± 2	5.5 ± 1.0
LPJ-WSL	174 ± 10	122 ± 7	42 ± 2	3.9 ± 0.3
ORCHIDEE	264 ± 12	184 ± 11	71 ± 4	9.1 ± 1.7
SDGVM	199 ± 5	135 ± 6	59 ± 3	2.2 ± 0.2
Mean $\pm 1\sigma$	190 ± 39	126 ± 31	51 ± 15	5.4 ± 3.2
Forward model estimates:				
Fung et al. (1991)			35[d]	
Cao et al. (1996)	92	55	30	
Walter et al. (2001)[e]	260		~ 65	
Inverse model estimates:				
Hein et al. (1997)	231 ± 27			
Worthy et al. (2000)				0.2–0.5
Houweling et al. (2000)[f]	163 ± 16			
Wang et al. (2004)[g]	176 ± 10			
Mikaloff Fletcher et al. (2004)[h]	231 ± 46			
Chen and Prinn (2006)[i]	145 ± 28			
Reference scenario Bousquet et al. (2006) and Bousquet et al. (2011)[j]	145 ± 10	91 ± 11	43 ± 4	
Mean of alternate scenarios in Bousquet et al. (2011)[j]	151 ± 10	97 ± 10	43 ± 4	
Bloom et al. (2010)[k]	165 ± 50	91 ± 28	69 ± 20	4.9 ± 1.4[l]
Observation-based estimates:				
Pickett-Heaps et al. (2011)				2.3 ± 0.3

[a] Northern extratropical region low latitude limit chosen to coincide with the low latitude limit of the peatland distribution in Tarnocai et al. (2009) used by the LPJ-WHyMe model.
[b] Hudson Bay lowland region is included to allow direct comparison to independent estimates from Pickett-Heaps et al. (2011) and encompasses 50° N–60° N and 75° W–96° W.
[c] Excluding CH_4 emissions from wet mineral soils for LPJ-Bern gives lower estimates of global (93 ± 14), tropical (41 ± 1), extratropical (48 ± 13) and HBL (11.1 ± 7.9) CH_4 emissions.
[d] Wetlands and tundra CH_4 emissions > 50° N.
[e] For the period 1982–1993, and extratropical wetlands are considered > 30° N.
[f] Value is for the pre-industrial period (pre-1850).
[g] Value is for the period 1988–1997.
[h] Swamps, bogs, and tundra for 1998–2000.
[i] This estimate implicitly includes rice emissions.
[j] Values are a 2012 update for the reference scenario (P. Bousquet, personal communication, 2012).
[k] Estimate is an average of years 2003 and 2004. Mean values for the five year period, 2003–2007, are 171 ± 52 (global), 92 ± 28 (tropics), 74 ± 22 (extratropics), and 5.1 ± 1.5 (HBL).
[l] Estimate corresponds to roughly the same area but on the original 3° grid.

sparse wetlands, outside of the boreal region, that are prescribed for IAP-RAS. DLEM is also commonly outside of the models' 25th to 75th percentile distribution, particularly close to the equator.

The relative latitudinal contributions and seasonal timing of CH_4 fluxes varies greatly between the models (see Fig. 6 with further discussion in Appendix A1). There is, however a consistent pattern of peak global CH_4 emissions in boreal summer across all models. The principal contributing latitudinal band of that increase is 40°–90° N.

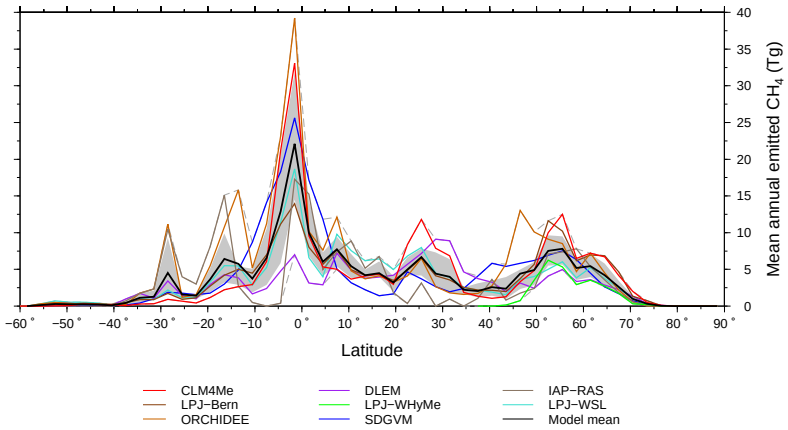

Fig. 5. Zonally summed mean annual CH_4 emissions for 1993–2004. The grey shading denotes the limits of the 25th and 75th percentile of the model distribution. Grey dashed lines are the 5th and 95th percentile limits. The CH_4 emissions are summed across 3° bins.

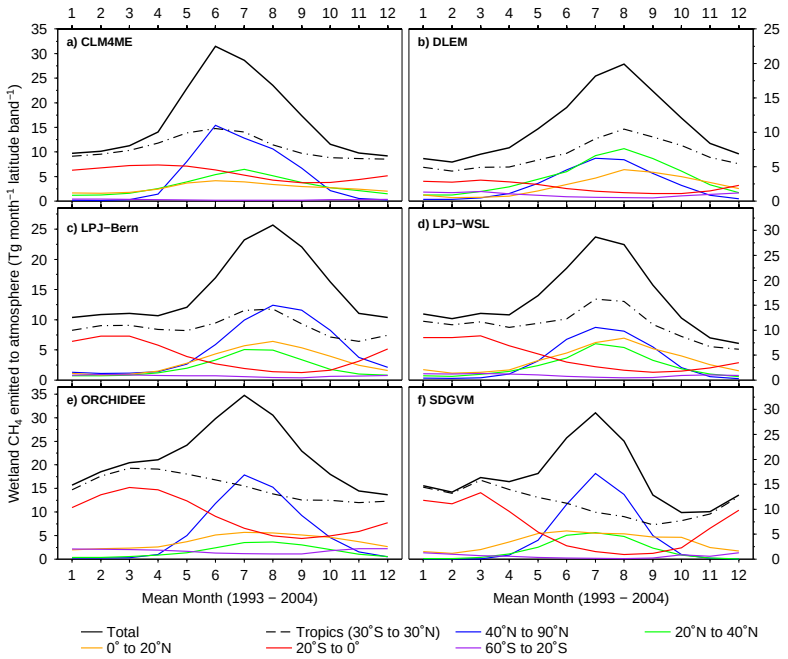

Fig. 6. Mean monthly simulated methane emissions by latitudinal band for 1993–2004 for all models with monthly emissions and global extent. Note the magnitude of the y-axes differs between models.

Table 4. Spearman correlation coefficients (ρ) for monthly wetland area and CH_4 emissions over the period 1993–2004 (see Figure 7). The model mean excludes LPJ-Bern due to its wet mineral soils parameterization.

Model	Global	Tropics (30° S–30° N)	Extratropics (> 35° N)[a]
LPJ-Bern[b]	0.067	0.511	0.267
CLM4Me	0.931	0.247	0.980
DLEM	0.885	0.877	0.848
LPJ-WSL	0.910	0.798	0.990
ORCHIDEE	0.920	0.508	0.944
SDGVM	0.845	0.910	0.979
Model Mean (excl. LPJ-Bern)	0.898	0.668	0.948

[a] Northern extratropical region low latitude limit chosen to coincide with the low latitude limit of the peatland distribution in Tarnocai et al. (2009) used by the LPJ-WHyMe model.
[b] Excluding the wet mineral soils of LPJ-Bern results in ρ values of 0.843 (global), 0.908 (tropics), and 0.940 (extratropics).

3.2.3 Simulated wetland areal extent and CH_4 emissions for the 1993–2004 period

Normalizing the monthly global wetland areal extent and CH_4 fluxes facilitates a comparison between model responses to inter-annual and intra-annual changes in climate (left-hand column of Fig. 7). To normalize each model, all values were divided by the maximum value for that model over the period 1993–2004, giving a fractional value between 0 and 1. The models have some striking differences in both the magnitude and timing of CH_4 emissions relative to wetland area. CLM4Me has a strong early peak in CH_4 emissions that declines in magnitude before the decline of the wetland extent in most years (Fig. 7a). This early boreal summer peak in CH_4 flux, that drops before wetland extent, is also a prominent feature of LPJ-Bern (Fig. 7c), however LPJ-Bern also has a strong secondary peak in wetland/wet soils extent that only slightly increases CH_4 emissions. This secondary peak is driven by the low CH_4 producing wet mineral soils parameterization (Fig. 2c).

CLM4Me also has a similar relative change in emissions and wetland extent over the course of a year, indicating that wetland area explains a large amount of the model's CH_4 variations. Indeed, the global Spearman correlation coefficient (ρ), calculated between global monthly wetland extent and CH_4 emissions, for CLM4Me is 0.931 with the extratropics even higher (0.980), and the tropics weaker (0.247) (Table 4). Conversely, DLEM simulates much larger relative changes in CH_4 fluxes than wetland extent, indicating other factors strongly influence CH_4 emissions in their model (Fig. 7b). DLEM also commonly has its methane emissions peak at the peak of wetland extent, not biased towards the early part of the wetland extent peak as in CLM4Me or LPJ-Bern. The correlation between wetland extent and CH_4 emissions for DLEM is similar to the model mean with a similar value between the tropics and extratropics. LPJ-Bern has the smallest relative changes in wetland/wet soils area of $\sim 30\,\%$, again due to the wet mineral soils parameterization, but the relative changes in CH_4 emissions are still relatively large at $\sim 40\,\%$. LPJ-Bern has no correlation between global wetland area and CH_4 emissions (0.067), but removing consideration of wet mineral soils raises the global ρ value to 0.843, well in line with the other models. LPJ-WSL simulates a consistent pattern of similar magnitude relative changes in wetland extent and CH_4 emissions (Fig. 7d). A slightly larger drop in CH_4 emissions relative to wetland extent is simulated during the boreal winter for most years. The ORCHIDEE relationship between wetland area and CH_4 emissions is slightly above average (0.920) with a global value similar to the all-model mean (0.898), though with less correlation in the tropics (0.508) than the mean of the models (0.668). SDGVM also has close links between the timing and magnitude of wetland extent and CH_4 emissions (Fig. 7f) similar to CLM4Me and LPJ-WSL.

The relative changes in wetland area and CH_4 emissions inter-annually show good similarity between the models (righthand side of Fig. 7). All models simulate 1998 to be a year of high CH_4 emissions over the 1993–2004 period. DLEM and LPJ-WSL simulate total CH_4 emissions for 1998 to be less than 1993 and 1994; both years have higher wetland extent in the GIEMS dataset. ORCHIDEE simulates slightly less CH_4 emissions in 1998 than 2000. LPJ-Bern has a very prominent 1998 peak in CH_4 emissions. This peak corresponds to a large release of CH_4 in the boreal regions as has been discussed earlier and is likely an overestimate (see Wania et al., 2012, for full discussion). All models show smaller CH_4 emissions in 1997 than 1998. This period is of interest as it covers the largest magnitude El Niño on record. Dlugokencky et al. (2001) report a significant increase in the global atmospheric [CH_4] growth rate corresponding to an additional $24\,Tg\,CH_4\,yr^{-1}$ imbalance in the sources and sinks of CH_4 for 1998 compared to the previous three years. They used a version of the Walter (1998) model to estimate a global wetland CH_4 flux increase of 7.3 % for 1998 over 1997. The WETCHIMP models, on average, estimate a 6 % increase in global CH_4 emissions for 1998 over 1997 (excluding LPJ-Bern this increase drops to 4.5 %). Chen and Prinn (2006) used an inverse model to estimate a slightly higher wetland CH_4 flux increase ($\sim 10\,\%$) between the same two years. An increase in wetland CH_4 emissions for 1998 was also found by Mikaloff Fletcher et al. (2004) using a $^{13}CH_4/^{12}CH_4$ and [CH_4]-informed inverse model for 1998–1999. They estimated the wetland contribution for 1998 was $40\,Tg\,CH_4\,yr^{-1}$ (or $\sim 20\,\%$) larger than 1999. The WETCHIMP models estimate a more modest mean difference of 4.1 % ($\sim 5\,Tg\,yr^{-1}$, 3 % excluding LPJ-Bern) for 1998 over 1999, suggesting the Mikaloff Fletcher et al. (2004) value is an overestimate. Not all studies find large changes. For example, Bousquet et al. (2006) used an

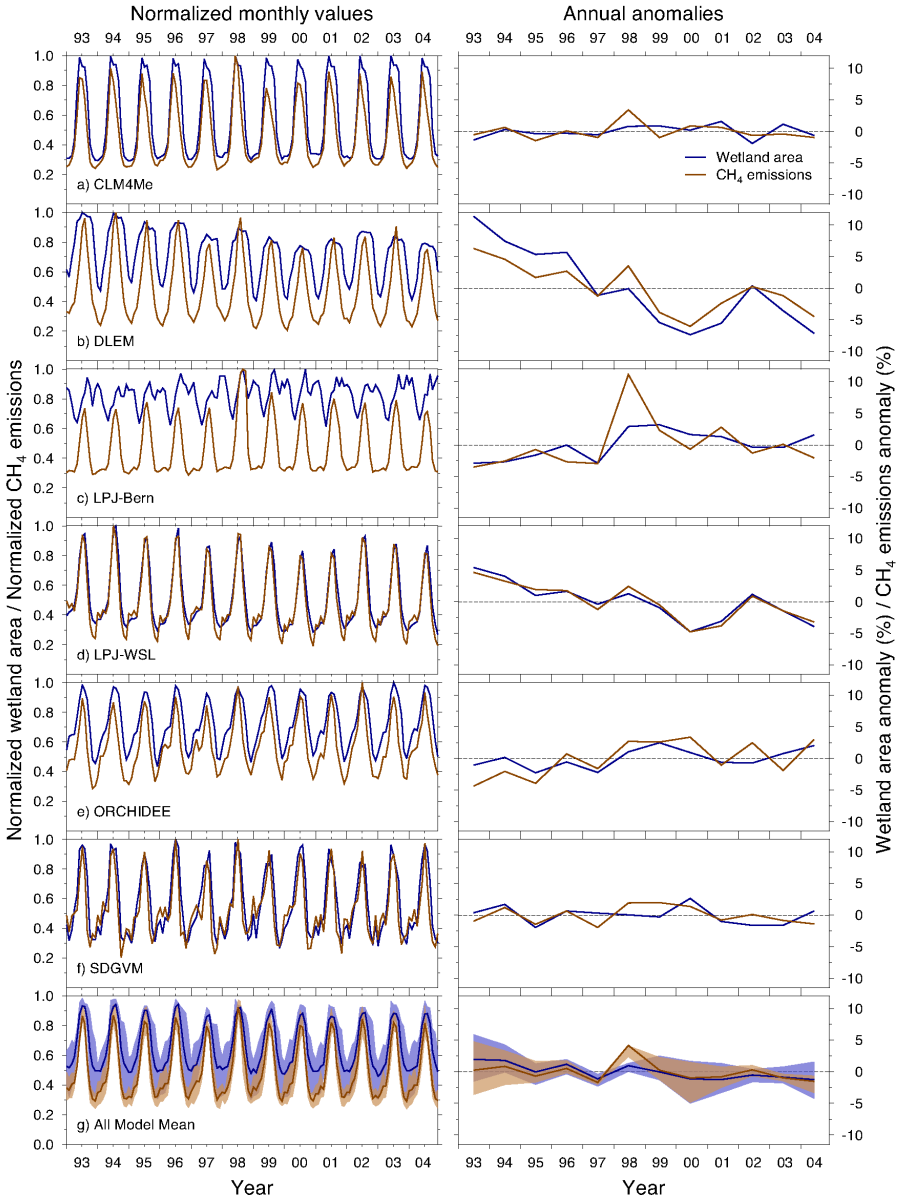

Fig. 7. Global normalized monthly wetland area and CH_4 emissions (left column) and global annual CH_4 emissions and wetland area percent anomalies (right column) for 1993–2004. The Spearman correlation coefficients are listed in Table 4. Anomalies are calculated relative to the maximal value of 1993–2004 for each model, where the maximal value is set to 1 and the other values scale between 0 and 1. The model mean value includes all models. Shading indicates the models' 25th and 75th percentile distributions.

inverse model to estimate generally stable natural wetland CH_4 emissions over the 1997–1998 period, with a drop in northern wetland CH_4 emissions in 1997 and an increase in southern emissions in 1998. Bousquet et al. (2006) also show a consistent trend of declining wetland emissions after 1998, coinciding with the smaller inundated area globally as observed by Papa et al. (2010). There is not a consistent pattern of maximal wetland extent corresponding with the peak in CH_4 emissions in 1998, however all models do show 1997 to have below average wetland extent for the period. The WETCHIMP models also do not show a trend in wetland area over the 1993–2004 period (the two models with a strong trend, LPJ-WSL and DLEM, have their annual maximal wetland extent set to the GIEMS dataset).

Importantly, the models do not appear to respond solely to warmer temperatures, as 2002 and 2003 were essentially as warm as 1998 (Hansen et al., 2010), but the models do not show elevated CH_4 fluxes as in 1998. The main difference between 2002/2003 and 1998 are that 1998 was a very strong El Niño year while 2002 and 2003 had much milder El Niño conditions. Global precipitation for 1998 was high, particularly in the northern extratropics with record levels in those regions (latitude bands spanning 85° N–55° N and 55° N–30° N), while 2002 and 2003 were both below the 1961–1990 global average (NOAA National Climatic Data Center, 2003).

We can conclude four main points about the WETCHIMP models' simulated methane emissions. First, the models' simulated global total CH_4 emissions are in-line with previous estimates from both forward and inverse models, a result that is expected given the assumptions inherent to both techniques. However, given the large range between the models ($\sim \pm 40$ % of the models' mean), forward models, at present, appear unable to further narrow the uncertainty of global wetland CH_4 emissions. Regionally, we lack appropriate observational datasets to evaluate the models. For one well-studied area, the HBL, many models appear to overestimate emissions, sometimes several-fold over previous estimates. Second, the models have similar disagreement in the relative timing of emissions throughout the year as they do for periods of maximum wetland extent. Given that the models' mean global correlation ρ value between CH_4 emissions and wetland extent is 0.898, it is evident that errors in the timing and spatial extent of wetlands will strongly impact predicted CH_4 emissions, as has been shown before (Petrescu et al., 2008). Third, model agreement for zonal methane emissions has better internal agreement between the models than the simulated wetland extent, with most models showing a large tropical and smaller boreal CH_4 emissions peak. Lastly, the models estimate a mean increase in global wetland CH_4 for 1998 over 1997 of about 4.5 %, on the low-end of inverse and observationally based estimates. This increase corresponds to one of the strongest El Niños on record demonstrating the models' sensitivity to transient warm and wet events.

3.3 Sensitivity tests

3.3.1 Sensitivity of CH_4 emissions and wetland area to increased atmospheric CO_2 concentrations

The change in simulated wetland extent and CH_4 emissions from equilibrium due to increasing $[CO_2]$ (step increase from ~ 300 to 857 ppm) is shown in Fig. 8 and annual percent change in Table 5. All models estimate a significant increase in global, tropical, and extratropical CH_4 emissions and global wetland extent under elevated $[CO_2]$. While, globally, the net change is an increase in CH_4 flux and wetland area, spatially, some models show areas of decreasing wetland extent, especially ORCHIDEE, but also SDGVM and CLM4Me. The model with the largest sensitivity to increased $[CO_2]$ is ORCHIDEE, with a ~ 160 % increase in global CH_4 flux. Excluding ORCHIDEE, the mean globally integrated increase drops from 73.2 ± 49.1 % to 55.4 ± 25.5 %. ORCHIDEE, while having the strongest response in CH_4 emissions, simulates only the third largest increase in wetland area. This reflects the more mixed pattern of increase and decrease in wetland extent for ORCHIDEE (Fig. 8d).

The increase in global wetland areal extent was highest for UVic-ESCM at ~ 13 %. Increases in UVic-ESCM wetland area, and indeed the rest of the models as well, are likely due to reduced evapotranspiration (ET). Elevated $[CO_2]$ allows plants to increase stomatal closure, reducing water loss by the plant. The decreased water loss reduces water demand from the soil, increasing soil moisture and thus increasing wetland extent. For UVic-ESCM, the model ET parameterization is strongly sensitive to CO_2, and the wetland determination scheme is directly derived from soil moisture, so the model responds strongly to increasing $[CO_2]$. While the wetland determination of UVic-ESCM is directly related to soil moisture, the mechanism of wetland areal extent expansion due to reduced ET is common to the models.

The general increase in CH_4 emissions under elevated $[CO_2]$ is also due to CO_2 fertilization promotion of higher NPP. Large increases in modelled NPP under increased $[CO_2]$ is commonly reported, including a study of eleven coupled climate–carbon models as part of C^4MIP (Friedlingstein et al., 2006). Observations have shown that with higher NPP, more plant photosynthates are allocated to the rhizosphere where the root exudates provide increased carbon for soil microbial communities' reduction to CH_4 (Chanton et al., 1995; Vann and Megonigal, 2003; Whiting and Chanton, 1993). Few models explicitly simulate exudates (Wania et al., 2012), so in the majority of models, the linkage between the CO_2 enrichment and enhanced CH_4 emissions comes from prescribing CH_4 emissions as a direct fraction of NPP, or prescribing emissions as a fraction of heterotrophic respiration (R_h), which is related to NPP (Table 1). This difference between the model approaches could be important, as there is presently no consensus on changes in

the ratio between NPP and R_h under future climate changes (Friedlingstein et al., 2006).

Most models show a stronger enhancement in CH_4 emissions under elevated $[CO_2]$ for the tropics over the extratropics. The stronger response from the tropics is primarily due to a greater change in NPP for the region over the extratropics. NPP enhancement is a strong lever on CH_4 emissions, as ORCHIDEE's strong NPP enhancement under elevated $[CO_2]$ partially explains its strong increase in global wetland CH_4 emissions. This pattern in NPP response has been reported previously (for the LPJ model) (Hickler et al., 2008; Poulter et al., 2010). CLM4Me has the opposite pattern with a three-times stronger response from the extratropics. This model response comes from a combination of factors: (1) a stronger NPP enhancement in the extratropics than the tropics, (2) a strong increase in the ratio of emitted to produced CH_4 in the extratropics, and (3) an increase in soil temperature of up to 2.5 °C in the extratropics with a decrease in the tropics. The increase and decrease in soil temperature in the extratropics and tropics, respectively, occurred because of the impacts of $[CO_2]$ on stomatal conductance, leading to a changed surface energy balance, soil evaporation, and transpiration. These complexities are discussed in more detail in Subin et al. (2012).

The general increase in methane emissions from CO_2 enrichment, as simulated by the models, is supported by empirical evidence. Wetland ecosystems and mesocosms exposed to elevated atmospheric $[CO_2]$ have generally shown an increase in CH_4 fluxes across many studies (Hutchin et al., 1995; Megonigal and Schlesinger, 1997; Saarnio and Silvola, 1999; Saarnio et al., 2003), with some notable exceptions of no significant change (Kang et al., 2001), or even a decline in emissions (Silvola et al., 2003). There is also recent evidence that different wetland types, such as bogs vs. fens, respond differently to CO_2 enrichment (Boardman et al., 2011), and other influences such as nitrogen (N) deposition could counteract the effect of the CO_2 enrichment (Saarnio and Silvola, 1999) or affect litter quality, decreasing CH_4 fluxes (Pancotto et al., 2010). van Groenigen et al. (2011) performed a meta-analysis of studies investigating the effect of increased atmospheric $[CO_2]$ to projected future increases in emissions of CH_4 and N_2O in soils. They anticipate an increase from natural wetlands of 13.2 % (95 % bootstrapping confidence interval of −4.8 % to 35.7 %, $n = 24$) for an atmospheric $[CO_2]$ of between 473–780 ppm. Our models' average is much higher than this, but we performed our tests with a higher $[CO_2]$ (857 ppm) than the upper bound of their range. Additionally, it is difficult to tell if the results are appropriate to compare due to differing rates of perturbation, and that our simulations were run until equilibrium was re-established.

While the models' results are generally consistent with the majority of empirical CO_2 enrichment studies, the models are likely too simplistic in the limits they place on the conversion of substrate to CH_4. No participating model distinguishes different wetland types, such as bogs vs. fens, explicitly. This lack of distinction limits the models' ability to simulate divergent responses to CO_2 enrichment, such as that observed by Boardman et al. (2011). Nutrient limitations to future increases in NPP are projected to be important (Hungate et al., 2003), but only a few of our models presently incorporate explicit accounting of the N cycle (SDGVM and CLM4Me). The lack of incorporation of nutrient cycles introduces uncertainty as studies explicitly accounting for N (Zaehle et al., 2010) and N and phosphorus (Goll et al., 2012) show a more muted NPP response to CO_2 fertilization.

3.3.2 Sensitivity of CH_4 emissions and wetland area to increased air temperature

Wetland area and CH_4 flux anomalies due to increased surface air temperature (SAT) are presented in Fig. 9 and Table 5. Wetland area experiences a moderate decline in all models with a mean drop of 7.9 ± 6.0 % under elevated SAT. CH_4 emissions have a general slight, non-significant, decline under warmer SAT (-4.5 ± 20.9 %). IAP-RAS is the only model to simulate a large increase in CH_4 emissions. This response is a result of the IAP-RAS prescribed soil hydrology and wetland extent that does not allow increased evaporation under warmer SAT and no change in wetland area. Methane production in IAP-RAS is then augmented by the increased SAT with an additional boost in the high latitudes due to shorter periods with snow cover, allowing summer warmth to penetrate deeper into the soil column. Excluding the result of IAP-RAS gives a small significant decrease in estimated global CH_4 emissions of -11.5 ± 11.2 %.

The decrease in CH_4 flux is not uniform across latitudes. On average, the tropics decrease in CH_4 flux while the extratropics increase, with both latitude bands showing large differences between models (Table 5). Excluding the results of IAP-RAS gives the tropics a larger mean decrease in CH_4 flux (-18.0 ± 13.0 %), while the extratropics mean response becomes neutral (3.2 ± 25.4 %). It is difficult to determine if the tropical decrease is a realistic response. Increased SAT can cause water stress/drought for the vegetation; however this water stress should not necessarily have an impact upon the vegetation growing in wetland areas (as they could still have standing water conditions), but the models are not able to distinguish this effect. Presently, most of the models that simulate tropical wetlands do not separately treat wetland vs. terrestrial hydrology. A separate treatment of wetland vs. terrestrial hydrology would also improve CH_4 flux simulation because processes such as inhibition of soil respiration under saturated conditions could be better captured (Sulman et al., 2012). Interestingly, DLEM, the only WETCHIMP model that does separate wetland vs. terrestrial hydrology, simulates the largest negative tropical CH_4 flux anomaly of all the models. The same reasoning could also apply for sub-grid treatment of methanogenesis substrate. For example, ORCHIDEE partially allows for sub-grid treatment of hydrology through its coupling to TOPMODEL concepts. However,

Table 5. Percent change between the sensitivity tests (CO_2 increase – Experiment 4; air temperature increase – Experiment 5; and precipitation increase – Experiment 6) and the equilibrium model state (Experiment 1 – Equilibrium). "n.a." indicates the model does not produce output for that region or variable.

	Percent change ([CO_2] Exp. 4–Exp. 1)				Percent change (Temperature Exp. 5–Exp. 1)				Percent change (Precipitation Exp. 6–Exp. 1)			
	Wetland	CH_4			Wetland	CH_4			Wetland	CH_4		
Model	area	Global	Tropics[a]	Extratropics[b]	area	Global	Tropics[a]	Extratropics[b]	area	Global	Tropics[a]	Extratropics[b]
LPJ-Bern	9.5	54.0	61.1	39.0	−1.9	−0.7	−11.5	21.1	1.3	1.3	1.1	1.4
CLM4Me	8.5	84.2	54.1	147.3	−8.9	−25.3	−19.9	−37.0	2.6	6.8	5.8	8.8
DLEM	2.2	22.4	29.1	14.0	−2.8	−15.1	−40.9	24.5	1.4	2.2	1.3	4.3
IAP-RAS[c]	n.a.	n.a.	n.a.	n.a.	n.a.	36.9	32.9	47.8	n.a.	0.0	0.0	0.1
LPJ-WHyMe	n.a.	n.a.	n.a.	40.1	n.a.	n.a.	n.a.	24.1	n.a.	n.a.	n.a.	6.9
LPJ-WSL[d]	n.a.	76.3	87.8	44.1	n.a.	−8.1	−11.1	−0.5	n.a.	0.6	0.5	1.2
ORCHIDEE	8.6	162.0	176.6	118.2	−18.7	−21.8	−21.5	−26.1	5.0	13.7	14.6	10.4
SDGVM	0.3	40.1	46.2	26.7	−7.4	2.3	−3.3	16.6	2.0	7.6	9.4	3.2
UVic-ESCM[e]	12.7	n.a.	n.a.	n.a.	−7.4	n.a.	n.a.	n.a.	2.3	n.a.	n.a.	n.a.
Mean $\pm 1\sigma$	7.0 ± 4.7	73.2 ± 49.1	75.8 ± 53.0	61.3 ± 50.5	-7.9 ± 6.0	-4.5 ± 20.9	-10.8 ± 22.6	8.8 ± 28.3	2.4 ± 1.4	4.6 ± 5.0	4.5 ± 3.8	4.7 ± 5.6
(n)	(6)	(6)	(6)	(7)	(6)	(7)	(7)	(8)	(6)	(7)	(7)	(8)

[a] The tropics are defined here as 30° S to 30° N.
[b] Extratropical region low latitude limit (> 35° N) chosen to coincide with the low latitude limit of peatland distribution in Tarnocai et al. (2009) used by the LPJ-WHyMe model.
[c] IAP-RAS is not sensitive to [CO_2], so we did not perform this experiment (see Eliseev et al., 2008; Wania et al., 2012). Additionally, IAP-RAS has fixed wetland extents.
[d] LPJ-WSL has prescribed wetland extents from the GIEMS inundation dataset and are thus unchanging across the experiments.
[e] UVic-ESCM does not presently simulate CH_4 emissions.

there is no ORCHIDEE PFT functioning as a true wetland PFT whose extent is linked to the diagnosed wetland fraction. Instead of this, the mean grid-cell soil labile carbon content is used to estimate the methanogenesis substrate, which makes the substrate overly sensitive to soil water modification.

ORCHIDEE simulated the greatest drop in wetland extent with an almost 20 % decline. A similar response was noted for ORCHIDEE under a SRES A2 scenario by Ringeval et al. (2011). The largest areas of wetland loss for ORCHIDEE were in the high northern latitudes where there is a large increase during boreal summer in potential evaporation driving changes in the region's hydrologic regime.

Reduced CH_4 emissions in the tropics could also be due to increased temperatures, in already very warm regions, resulting in a down-regulation of photosynthesis, decreasing NPP and reducing substrate available for CH_4 production. This effect is likely to be important in relatively few regions and thus the broad tropical response is more likely due to water stress/drought as the dominant driver. Outside of areas with increased water stress/drought, the effect of increasing SAT should be to increase CH_4 flux due to a direct enhancement of methanogenesis and an indirect effect via NPP. This effect is visible in parts of the high latitudes for many of the models (Fig. 9) (see also Koven et al., 2011). Across the extratropical region as a whole, while the models have no significant trend with a large range of up to ~ 40 % increase or decrease dependent upon the model, most models have enhanced CH_4 emissions above $\sim 50°$ N in parts of Canada and Eurasia. The effect of model treatment of processes such as permafrost dynamics, snow pack, and surface runoff influence the results in these regions heavily. Areas that lose underlying permafrost have enhanced drainage resulting in drier soils less conducive to CH_4 production. This effect is primarily responsible for the CH_4 flux patterns simulated by CLM4Me, while this effect is not captured by LPJ-Bern whose wet mineral soils expand due to thaw activation of soil processes. As IAP-RAS does not allow changes to its hydrology due to increased SAT, the response of IAP-RAS in the higher latitudes is demonstrating the influence of temperature solely.

Attributing differences in the model CH_4 flux anomalies to particular model parameters, such as CH_4 production Q_{10} values, is difficult due to confounding effects of simultaneous changes to wetland extents, land surface characteristics (such as permafrost, snow cover, and vegetation dynamics), NPP, and CH_4 production and oxidation rates.

3.3.3 Sensitivity of CH_4 emissions and wetland area to increased precipitation

The models' response to the precipitation increase sensitivity test is uniformly low with global wetland areal extent increasing modestly (2.4±1.4 %) (Table 5). This increase is the smallest of the sensitivity tests, and all models show a smaller percent change in wetland area than the step increase in precipitation (+3.9 %) except for ORCHIDEE. While the globally uniform spatial pattern of increase in precipitation is not realistic, this demonstrates that there is not a simple 1 : 1 relationship between precipitation and predicted global wetland extent.

The global mean simulated change in CH_4 emissions is an increase that, while not significant, is observed in all of the models (Table 5). This increase is also evident in the tropics and boreal regions. The least and most sensitive models are again IAP-RAS and ORCHIDEE, respectively. IAP-RAS, due to its prescribed hydrology, shows no response to precipitation changes, as would be expected. The general pattern of increased CH_4 emissions with increased precipitation is related directly to two main processes. The first is a simple

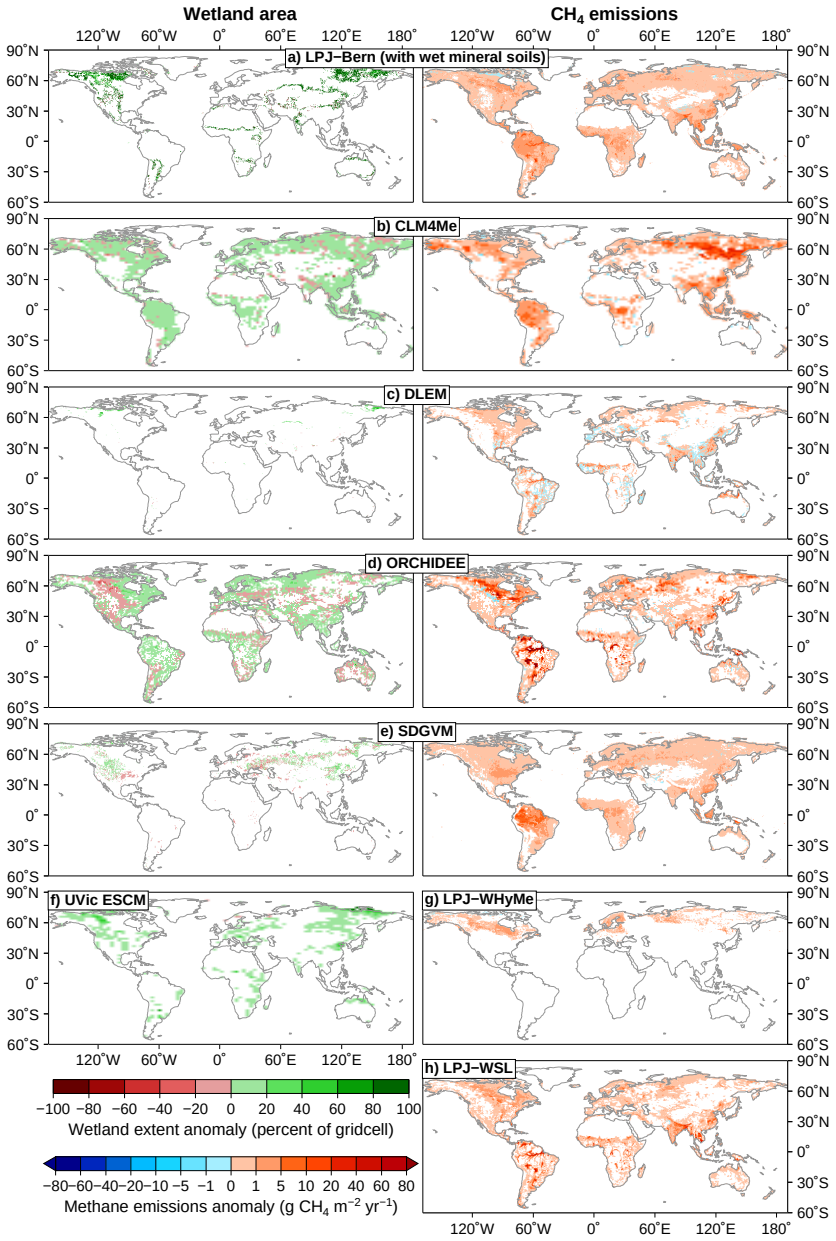

Fig. 8. Model wetland areas and CH_4 flux anomalies from the model state with elevated atmospheric [CO_2] (Experiment 4) compared to the equilibrium simulation (Experiment 1). Methane flux anomalies are referenced to grid cell m^2.

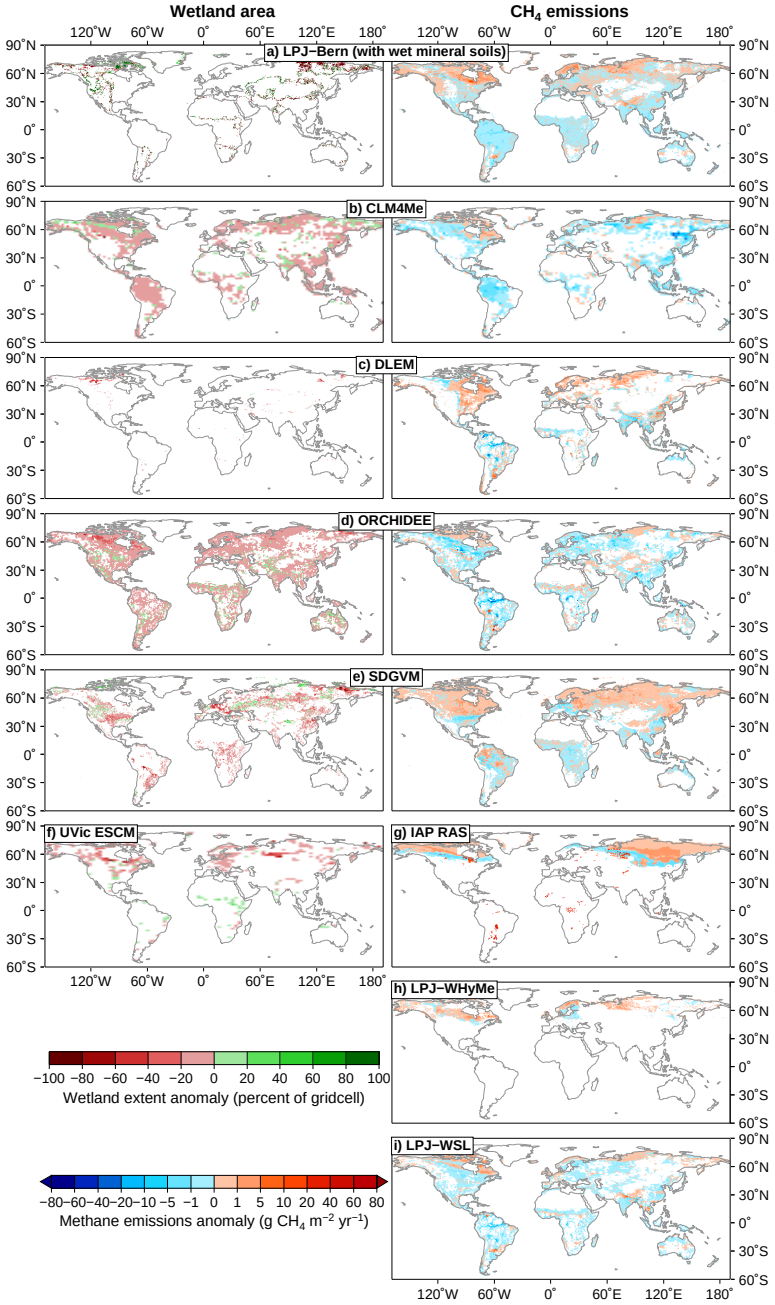

Fig. 9. Model wetland areas and CH_4 flux anomalies from the model state with a uniform 3.4 °C increase in air temperature (Experiment 5) compared to the equilibrium simulation (Experiment 1 – Equilibrium) Methane flux intensities are referenced to grid cell m^2.

increase in wetland extent due to higher water table position (WTP). The second is due to higher WTP reducing the oxic portion of the soil column, thus decreasing oxidative loss of CH_4 during transport from the site of methanogenesis to the atmosphere. In areas that are water-limited, the increased precipitation could increase NPP of the vegetation because of reduced water stress. This process is minor and mostly related to unrealistic modelling of terrestrial hydrology for wetland locations (discussed in Sect. 3.3.2).

3.3.4 Combined impacts of [CO_2], SAT, and precipitation change

In WETCHIMP, we did not perform tests for the combined effect of [CO_2], SAT, and precipitation change; however we can compare the relative contributions of these three drivers. The strongest response in modelled CH_4 emission is due to CO_2 fertilization. If the increase in CH_4 due to CO_2 fertilization is of similar magnitude to our models' mean, this represents a very strong feedback to rising levels of atmospheric CO_2. Because of this strong feedback, the relative importance of CH_4 in global climate forcing may increase. The response of the wetland systems will, however, likely be tempered by increasing SAT, which generally causes a reduction in global methane production. Precipitation has a smaller influence, but our test is likely poorly representative of how global wetlands will respond to a more spatially heterogeneous change in global precipitation.

Our transient simulation does allow some insight into simulated wetlands' response to relatively small changes in SAT and precipitation. The models' mean CH_4 emissions increase of $\sim 5\,\%$ (relative to 1997) in record-breaking hot, and wet, 1998 but little response to other similarly hot, but dry, years (2002 and 2003) demonstrates the effect of the climate drivers working in tandem. The possibility of non-linear effects, as all three of these drivers ([CO_2], SAT, and precipitation) change into the future, greatly increases uncertainty of any projections based on the sensitivity tests presented here.

Other sources of uncertainty include processes in the models that are poorly represented, missing, or even incorrectly represented. For example, Sulman et al. (2012) demonstrated that observed gross ecosystem productivity (GEP) and ecosystem respiration (ER) for fens were higher during dry periods than wet periods. A suite of wetland models run for the three sites studied predicted either the opposite relationship or no significant difference. The incorrect response of the models was suggested to be due to model treatment of hydrology (not wetland-specific) and a lack of inhibition of GEP and ER under saturated conditions.

While not especially apparent in earlier simulations, the differences in model complexity are more apparent in our sensitivity tests. The response of the models to increased SAT in the boreal regions especially demonstrates the marked difference between models that resolve permafrost dynamics (CLM4Me, UVic-ESCM, LPJ-Bern, LPJ-WHyMe, ORCHIDEE) against those that do not (SDGVM, DLEM, IAP-RAS, LPJ-WSL). This is also evident in the CH_4 flux response of IAP-RAS, the most simplistic model, to increased SAT, as the model hydrology can not adapt to the increased water demand and thereby simulates an erroneously high CH_4 flux increase. Gaining complexity in a model does come with risk. Models that attempt to represent mechanistic detail require more parameters, more representation of related processes (such as O_2 concentrations), and a more detailed representation of spatial heterogeneity. However, for many parameters used in these models (e.g. $V_{\max}$ and K_{m} for oxidation, aerenchyma area, diffusivity, seasonal dynamics), there simply is not enough data to properly constrain them across the globe (Riley et al., 2011). Therefore, increased model complexity can result in problems associated with equifinality of parameterizations (Tang and Zhuang, 2008), raising legitimate questions about the value of increased model complexity and stressing the importance of a balance between capturing the important processes, but as simply as possible.

4 Conclusions

Ten large-scale wetland and wetland CH_4 models participated in the WETCHIMP. The models cover a wide-range of complexity in their parameterizations to mechanistically determine wetland extent and associated CH_4 fluxes. Model results presented here include a transient simulation, forced with observed climate and [CO_2] through 1993 to 2004, as well as three sensitivity tests run as equilibrium simulations for increased [CO_2], surface air temperature (SAT), and precipitation.

The participating models adopted three distinct approaches to estimating wetland location and extent: prescribed extents, parameterization/forcing with a remotely sensed inundation dataset, or independent wetland location determination via a hydrological model. The models' simulated wetland extents have an almost four-fold difference between the lower and upper estimates (8.6 to $26.9 \times 10^6\,\mathrm{km}^2$, excluding the models with prescribed extents and the wet mineral soils of LPJ-Bern). This degree of uncertainty is only slightly worse than literature estimates from inundation and wetland mapping sources, which vary three-fold (4.3 to $12.9 \times 10^6\,\mathrm{km}^2$). The models independently determining wetland location via their hydrologic model simulated larger wetland extents than those informed by inundation datasets. The latter models were also more in line with observational estimates of global wetland extents, but those observational datasets have several discrepancies that make their use problematic. Given the disagreements between inundation and wetland mapping datasets, it appears that model reliance upon inundation datasets does not ensure accurate wetland location determination, and underlines a need for improved accuracy in observational datasets.

The participating models' wetland zonal extents have best agreement amongst themselves in the high northern latitudes above 45° N, but poor agreement in the equatorial band. The seasonal dynamics of wetland extent also show wide-spread disagreement between the models, save a general pattern of higher global wetland extent in the boreal summer. The simulated months, and peak magnitudes, of global wetland extent also vary greatly between the models. Across the transient simulation (1993–2004), the models simulate no trend in global wetland extent, at odds with a reported decrease in global remotely sensed inundation (Papa et al., 2010).

Simulated global CH_4 flux estimates by the participating models (141 to 264 $Tg\,CH_4\,yr^{-1}$ with a mean value of 190 $Tg\,CH_4\,yr^{-1}$) are in-line with literature forward and inverse model values. Given the large range encompassed by the WETCHIMP model estimates ($\sim \pm 40$ % of the models' mean), we are not able to greatly reduce the uncertainty of global wetland CH_4 estimates.

To further evaluate our simulation results, we require observation datasets at appropriate spatial and temporal scales for the coarse resolution of global-scale models. The common use of intermittent and spatially non-representative chamber-based observations, without ancillary ecosystem measurements (see, e.g. Bartlett and Harriss , 1993), is insufficient to test the mechanistically complex models used for global CH_4 emission estimates. As pointed out by Riley et al. (2011), it is possible to simulate the fluxes well for a given location, but with incorrect contributing processes, such as production, oxidation, or transport. Therefore, there is a need for site-level observations of both CH_4 fluxes and the physical and biogeochemical state variables associated with the large range of mechanisms represented in these types of models (e.g. NPP, labile carbon production, soil temperature, water content, water table position, soil depth, plant species present, CH_4 and O_2 content in soil, soil pH, etc.). The observations need to occur at sufficient frequency to resolve rapid, random events (i.e. ebullition); occur over a long enough time to capture seasonal dynamics in substrate production, aerenchyma changes, etc.; and accurately capture the impacts of spatial heterogeneity. Studies with site-level observations are well suited for evaluating model components and ensuring that the model simulations of processes such as CH_4 production and oxidation are appropriate. Inclusion of modellers in designing measurement protocols for a sampling campaign could be of great value. Areas of priority could include the equatorial band and parts of South America extending down into the Pampas region. Recent work in this region by Beck et al. (2012) is encouraging. The climate space of global wetlands could also provide guidance for effectively filling data and knowledge gaps, by collecting data from wetlands across the full spectrum of wetland temperature and precipitation regimes. Expanding beyond large-scale observational datasets, an inter-comparison of inverse CH_4 models could be useful for information about the latitudinal gradient of CH_4 emissions. Further WETCHIMPs could also be used for more in-depth comparison of the underlying processes of wetland determination and CH_4 emission, given careful planning of project experiments.

The current paucity of appropriate observational datasets presents a large obstacle to improving our understanding and ability to model global wetlands. For one of the few well-studied large regions, the Hudson Bay Lowlands, many of the WETCHIMP models appear to overestimate CH_4 emissions, sometimes several-fold over observationally based estimates.

As expected, given the wetland extent modelling results, the models disagree in the relative timing of CH_4 fluxes throughout the year, as they do for wetland extent. The demonstrated close correlation between wetland extent and CH_4 emissions (models' mean global ρ value of 0.898) makes it evident that errors in the wetland extent propagate to the CH_4 emissions simulated. Indeed, as the wetland CH_4 models themselves are integrated into vegetation models, they are susceptible to the biases in the vegetation models for variables such as net primary productivity, soil physics and hydrology, and vegetation dynamics.

The three sensitivity tests show a strong sensitivity of the models to increased [CO_2] (increase in CH_4 and wetland area), a more mixed and moderate response to increased SAT (decrease in global wetland area and decrease in tropical CH_4 emissions), and a weak response to increased precipitation (increase in global wetland extent and CH_4 emissions). It is worth noting that all models responded with an increase in wetland area and CH_4 emissions under elevated [CO_2], while the other two sensitivity tests yielded more divergent model responses. It is likely the magnitude of the model response to [CO_2] is overestimated due to missing models processes (such as NPP nutrient limitations, wetland specific hydrology and vegetation, etc.), but the direction of change appears robust.

This study clearly demonstrates that to reduce the large uncertainties in wetland response to projected climate change further work is needed to better parameterize and evaluate the models. The large range in predicted CH_4 emission rates leads to the conclusion that there is substantial parameter and structural uncertainty in large-scale CH_4 emission models, even after uncertainties in wetland areas are accounted for. Of paramount importance for improving the models is increases in availability of accurate and suitable observational datasets of both wetland extent and CH_4 emissions at large spatial scales. Further inter-comparisons of the models will aid our understanding of which natural processes are key to making large improvements in model accuracy. The results of this first iteration of WETCHIMP are designed to be a baseline, on which further improvements can be gauged and priorities identified.

Appendix A

A1 Wetland variability by model

CLM4Me shows substantial intra- but little inter-annual variability with a peak global wetland extent starting in June and continuing into August/September (Fig. 2a). Here CLM4Me is responding only to climate changes across this period as the [CO_2] was held constant (this is the only model with constant [CO_2]). For CLM4Me, the boreal summer is an important control of global wetland area, with their simulated wetland extent dropping off quickly after September. The lowest simulated global wetland extent in the boreal winter months across all models is simulated by CLM4Me with an average value under 2×10^6 km^2 in December/January. This pattern is likely an artefact of the modelling scheme as the modelled inundated areas are set to zero when the ground freezes (Riley et al., 2011). CLM4Me also has the fastest relative rate of increase in global wetland area during the boreal spring (Fig. 2g). The general pattern of rapid boreal spring wetland expansion and boreal autumn wetland contraction is also seen in SDGVM (Fig. 2e).

DLEM fixes the annual maximal wetland extent of each year to that from the GIEMS dataset; thus, the annual maximal values are not independent of this dataset. However, the intra-annual variability is calculated within the model and shows low variability with a broad peak in maximum wetland extent consistently around July and with a minimum in February (Fig. 2b). The duration of elevated global wetland extent is the longest of all models with a consistent six month period of relatively high wetland extents spanning May to October.

The largest maximal wetland areal extent of all models is simulated by LPJ-Bern with a peak extent of $\sim 25 \times 10^6$ km^2, although this does include their wet mineral soils parameterization (Fig. 2c). The LPJ-Bern timing of minimum global wetland/wet soils area occurs in May, which is in contrast to the other models that generally show a boreal winter minimum, with the exception of UVic-ESCM (boreal autumn minimum). The intra-annual wetland extent dynamics of LPJ-Bern are evidently heavily controlled by the wet mineral soils parameterization as the inundated wetlands and peatlands, which are also considered by LPJ-Bern, follow the GIEMS dataset or are static, respectively. The wet mineral soils parameterization appears to almost have a bimodal distribution for monthly maximal wetland extent with a peak in August/September and a smaller peak in February/March. This unique seasonal pattern highlights the fundamental differences between the parameterization of "wetland/inundated" areas and wet mineral soils as determined by LPJ-Bern.

ORCHIDEE consistently has a small annual peak in wetland extent with a maximum extent of only $\sim 5 \times 10^6$ km^2 (Fig. 2d), only slightly smaller than CLM4Me. The pattern of ORCHIDEE simulated wetland extent is generally consistent with CLM4Me and SDGVM, giving a maximal wetland extent around July and a minimum around December. The relative difference between maximum and minimum wetland extents is, however, lower for ORCHIDEE than CLM4Me, SDGVM and GIEMS (Fig. 2g).

SDGVM has more variability in months of maximal and minimum wetland extents compared to most of the other models with the maximal extent occurring between June and August and the minimum extent in either February or November (Fig. 2e). The variability is a reflection of the binary nature of the model parameterization where the grid cell has either total or no wetland extent. That simple parameterization does not preclude SDGVM from fairly closely following the annual pattern of the GIEMS inundation dataset (Fig. 2g), although the inundation dataset peak occurs principally in August while the SDGVM peak occurs on average between June and August. SDGVM likely can have peak wetland extent earlier due to its lack of freezing soils.

UVic-ESCM has an annual pattern strongly contrasting to that of the SDGVM and the GIEMS datasets, and almost antiphase to LPJ-Bern. The annual global peak in wetland area is simulated to occur in May to June, but wetland extents are elevated generally from January through July. UVic-ESCM is similar to SDGVM with relatively higher variability in timing of the month of minimum/maximum wetland extents. UVic-ESCM and LPJ-Bern are the lone models to show elevated wetland extents in the boreal winter though the reasons behind this pattern differ. A large portion of the UVic-ESCM wetland extent comes from the tropical regions, where the model results are likely questionable for reasons discussed earlier. However, as LPJ-Bern's global wetland extent pattern is principally driven by its wet soils parameterization, the similarity between the two models demonstrates that the UVic-ESCM parameterization functions similarly to the wet mineral soils of LPJ-Bern, but UVic-ESCM does include a topographic criteria that is not part of the LPJ-Bern parameterization. The timing of changes in UVic-ESCM wetland extent in the boreal regions follows those of the other models and the GIEMS dataset much more closely (see discussion in Sect. 3.1.2).

Monthly zonally averaged wetland area plots for 1993 to 2004 are shown in Fig. A2. CLM4Me has a pattern of extensive boreal summer wetlands above 60° N with no wetlands evident outside of the summer months (Fig. A2a), similar to the pattern simulated by SDGVM (Fig. A2e) and UVic-ESCM (Fig. A2f). This pattern is also observed by the GIEMS dataset (Fig. A2g), although this could be influenced by the snow cover mask used in generating the dataset.

The lack of wetlands outside of summer months for CLM4Me is related to the parameterization of no wetlands: (1) if there is snow on the ground, or (2) if the soil temperature is below freezing. Outside of the boreal regions, CLM4Me shows relatively little variation inter- and intra-annually for latitudinal bands centred around 30° N and the equator. An equatorial band with little variation in wetland

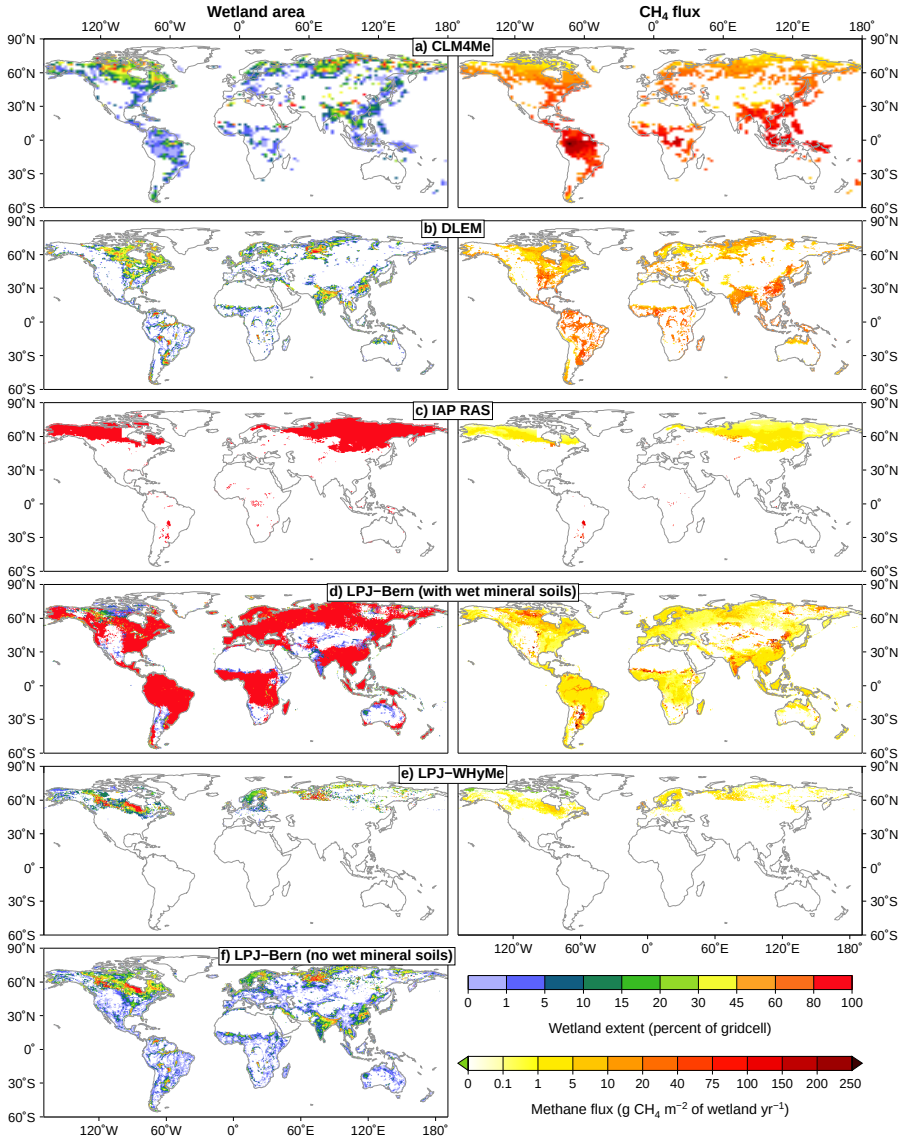

Fig. A1. Maximal wetland extent and mean annual CH_4 flux densities for Experiment 1 for all models.

extent is a characteristic shared with DLEM (Fig. A2b). DLEM, however, does simulate a much stronger seasonal cycle in the 10° N–30° N latitudinal band and also has a weaker seasonal cycle in the Northern Hemisphere boreal regions. DLEM and ORCHIDEE (Fig. A2d) overall share many similarities in their wetland extent patterns, with only slight differences such as a broader boreal summer wetland extent peak in DLEM and a more seasonally varying equatorial wetland extent simulated by ORCHIDEE.

LPJ-Bern has wetland areas at all latitudes during all periods of the year. The high latitude winter wetland areas in Fig. A2c are prescribed peatlands. The variability

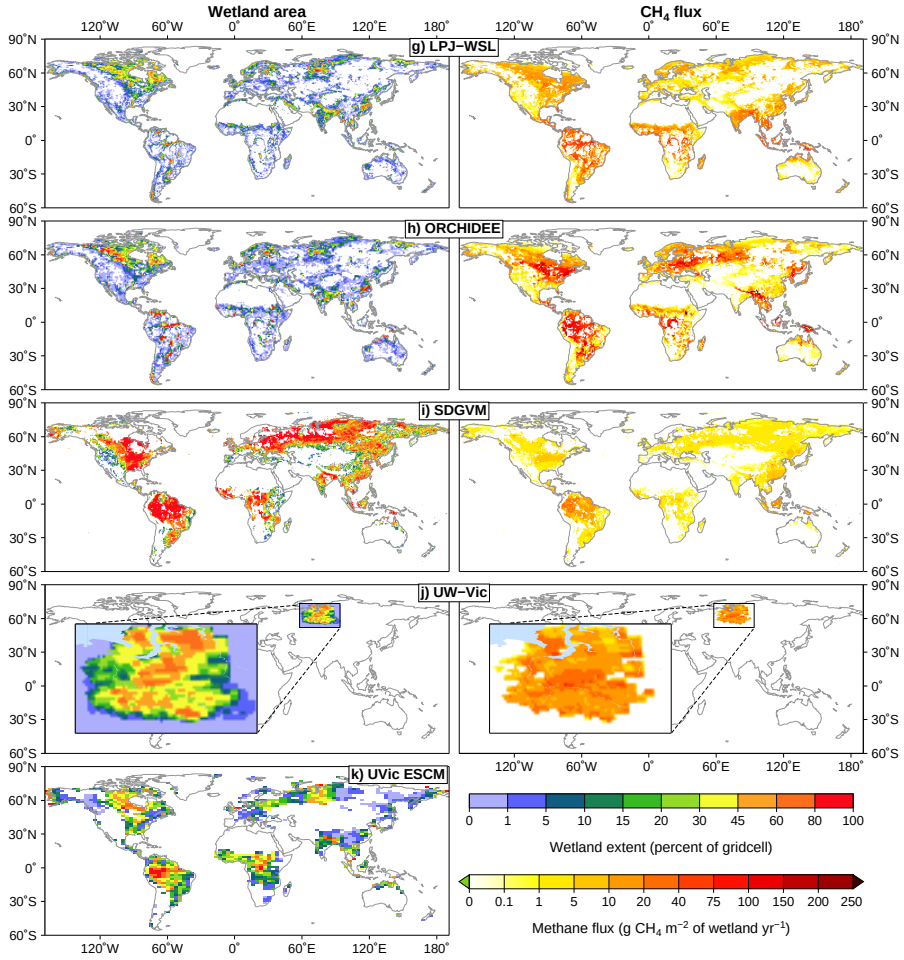

Fig. A1. Continued.

in "wetland" extent for LPJ-Bern was determined based upon CH_4 emissions. This was to allow a consistent definition of "wetland" for comparison as the model also simulates wet mineral soils, inundated wetlands, and peatlands. The peatland area in reality is constant, but the area of methane emissions in peatlands is varying. During the winter, some small CH_4 emissions could occur (on the order of $0.01\,\mathrm{g\,CH_4\,m^{-2}\,month^{-1}}$) making these grid cells appear as wetlands. The LPJ-Bern wetland/wet soils peak extent traces a rapid rise at the start of the boreal summer with a more gradual decline with latitude as the boreal summer ends. In the tropical regions, LPJ-Bern has a strong seasonal cycle of wetland/wet soils area with high extents in the southern tropics during the austral summer and high extents in the northern tropics during the boreal summer. The seasonal pattern simulated by LPJ-Bern shares some characteristics with SDGVM and UVic-ESCM. Both SDGVM and UVic-ESCM show strong seasonality in the tropics and subtropics, with both models following the patterns of precipitation in those regions. Interestingly, the GIEMS dataset does not show a strong seasonal cycle following precipitation patterns as evident in LPJ-Bern, SDGVM and UVic-ESCM. Both SDGVM and UVic-ESCM additionally have strong peaks in the boreal summer with little to no wetlands during the winter at latitudes as low as 40° N. Given the close resemblance between UVic-ESCM and the GIEMS dataset for the boreal

regions, it appears correct to assume that the dominant driver of the global pattern of wetland extent for UVic-ESCM in Fig. 2f is the model's tropical regions. Interestingly, while SDGVM does not have freezing soils, it has a similar temporal pattern to UVic-ESCM, but has generally higher percent wetlands at the same latitudes. SDGVM could be simply responding to the general summer peak in precipitation at these latitudes, particularly as the wetland area was constrained under two conditions: (1) the monthly air temperature must be above 5 °C, and (2) if the temperature in a given grid cell during the current year is always greater than 0 °C, then in a given month the evapotranspiration must not exceed precipitation.

A2 Methane fluxes by model

CLM4Me has high CH_4 flux intensity in the tropics, primarily the Amazon, Congo, and Indonesia, and in the boreal regions near the eastern Russia–China border, and the West and Central Siberian lowlands (Fig. 4a). These hotspots of CH_4 emissions are visible in the meridional and zonal emission sums (which account for the actual wetland extent per latitude/longitude band). The peak around latitudes 20°–30° N is an area of intense rice agriculture. These rice paddies have not been masked from the CLM4Me outputs. The intense tropical CH_4 fluxes, in part, result from a well-known tropical NPP bias in CLM4Me (Bonan et al., 2012) providing large amounts of substrate for methanogenesis. These emissions from CLM4Me could be biased low due to the model seeing a constant [CO_2] of 303 ppm (it is the only model without an evolving [CO_2] in this experiment).

The DLEM model has a more diffuse pattern of methane emissions than CLM4Me with a lower CH_4 flux intensity (Fig. 4b). The CH_4 flux intensity map shows a large number of individual grid cells with high emissions intensity and little consistent pattern of high emission regions. China shows strong emissions in the extratropics, as well as the central Eastern US.

IAP-RAS has a meridional and zonal emissions pattern primarily influenced by its wetland distribution dataset (Fig. 4c). CH_4 emissions intensity is generally low and not highly variable across much of the boreal region, with some notable exceptions in the HBL and areas of the southern West Siberian Lowlands where CH_4 emissions intensity is almost an order of magnitude larger than the rest of the boreal region. This pattern relates to the differences in soil depth between peat and mineral soils in the model input datasets. IAP-RAS active layer thickness is heavily influenced by the thermophysical parameters of the peat or mineral soil, impacting upon the soil temperature and hydrology. IAP-RAS's CH_4 emissions from the small amount of tropical and subtropical wetlands are of relatively high intensity and, since they are 100 % wetland cover, have strong peaks in the zonal and meridional sum plots.

The wet mineral soils parameterization of LPJ-Bern gives zonal and meridional CH_4 sum plots with broad peaks more similar to the results of DLEM than either IAP-RAS or CLM4Me (Fig. 4d). LPJ-Bern also accounts for rice agriculture, reducing the natural wetland emissions in these regions similar to DLEM. The wet mineral soils of LPJ-Bern do not contribute a large amount of CH_4 as the areas of highest CH_4 fluxes are those that were part of either the inundation, or peatland, datasets (see Fig. A1f). The LPJ-Bern areas of highest annual CH_4 emissions intensity are the Pantanal, India, and eastern China. There are also areas of high CH_4 emitting wetlands in north-central Africa that are part of the GIEMS inundation dataset. LPJ-Bern has strong boreal CH_4 emissions in Northern Canada and Eastern Siberia. This intensity of CH_4 emissions comes from inundated regions, as these areas are not prescribed as peatlands.

LPJ-WHyMe simulates a pattern of CH_4 emissions unique from the global-scale models (Fig. 4e). High CH_4 flux intensity is simulated for the British Isles by LPJ-WHyMe, a result not found by the other models. The climate of this region, as well as the Pacific coast of North America and the Atlantic coast of Europe, has mild winters that allow CH_4 emissions to continue year-round, yielding high annual emissions intensity for LPJ-WHyMe.

LPJ-WSL shows a strong gradient between latitudes with tropical regions generally simulated with higher CH_4 fluxes then decreasing relatively steadily poleward (Fig. 4f). This pattern is due to the model parameterization of CH_4 flux as an exponential function of respiration that is sensitive to surface temperatures. Some zones of exception exist to this trend, primarily in the HBL and West Siberian lowland regions. The overall meridional and zonal patterns of CH_4 fluxes of LPJ-WSL are most similar to ORCHIDEE. Spatially, ORCHIDEE CH_4 flux density is more evenly distributed across wetland areas (Fig. 4g). ORCHIDEE simulates broad areas of strong CH_4 emissions across the tropics, as well as the Ganges delta and eastern China. Boreal emissions are strongest across broad areas of the Northern US and Eastern Europe into Western Siberia. The use of an inundation dataset for model parameterization is also visible, giving a patchy appearance to areas such as the Amazon (see Fig. 1).

SDGVM has a much lower overall CH_4 flux density, with the strongest CH_4 emissions simulated in the Amazon region. This low CH_4 flux density compensates for the high wetland extent simulated by the model. SDGVM has the smoothest pattern of meridional and zonal CH_4 sums across all models (CLM4Me's predictions appear relatively smooth due to the coarse resolution of its grid cells), with its largest zonal peak in emissions at the equator and smaller secondary peaks for the Ganges delta and southern China, as well as a broad peak between about 40°–60° N. The meridional CH_4 sum plot is dominated by a large peak representing the contribution from the Amazon River catchment.

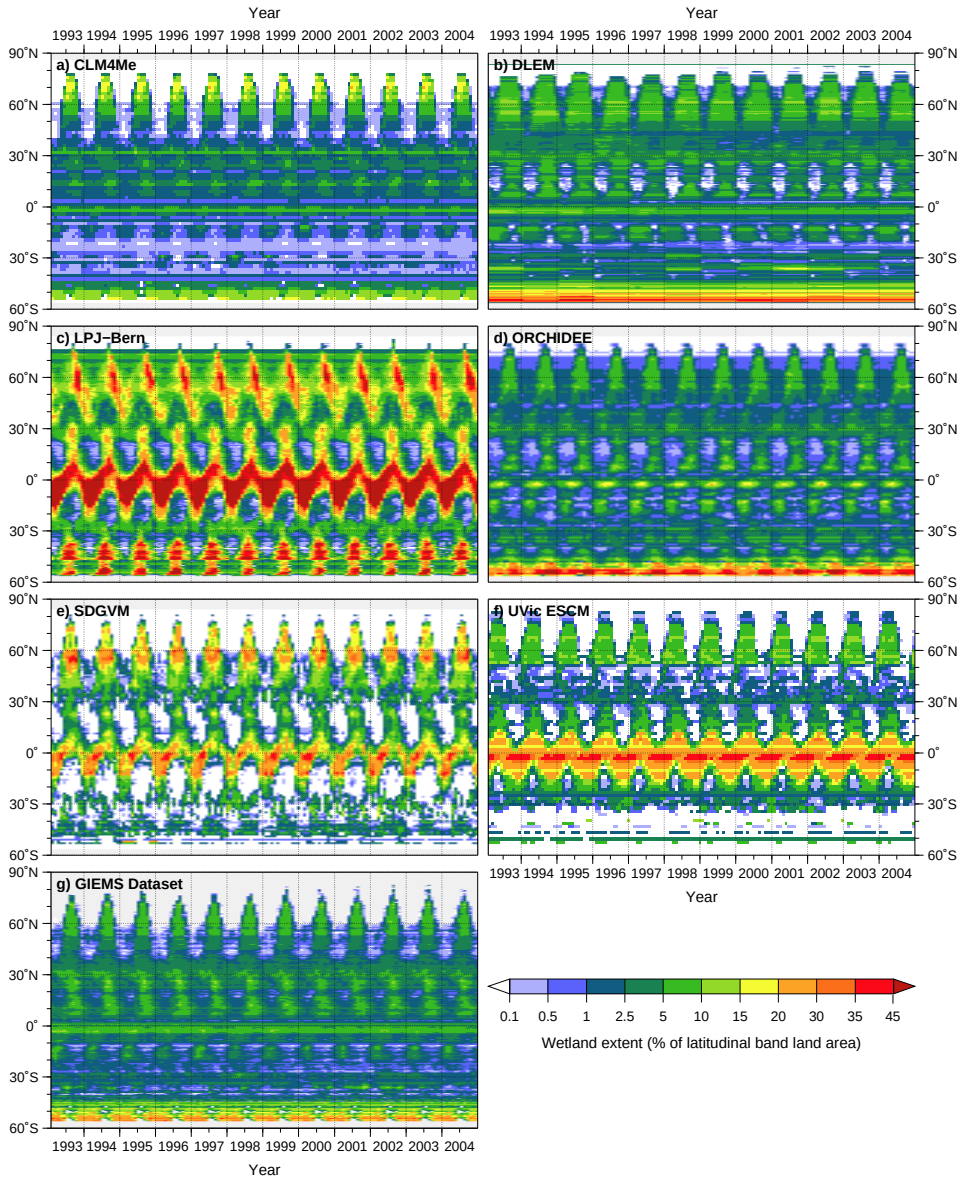

Fig. A2. Monthly zonally averaged wetland area for 1993–2004 for all models that have independent calculation of intra-annual variability. The inundation dataset, GIEMS, is included as an approximate observed wetland area.

When the wetland methane emissions are looked at dynamically, the seasonal timing and relative contributions from latitudinal bands to CH_4 fluxes are highly variable between the models (Fig. 6). CLM4Me has an early global peak in CH_4 emissions driven by the boreal band (40°–90° N), appearing in June (Fig. 6a) and corresponding to their simulated

Table A1. Listing of masks used to correct simulated wetland areas for non-natural wetland waterbodies per model. GICEW is the global land, ice and water mask from Hurtt et al. (2006).

Model	Masking Applied		
	Major rivers	Large lakes	Rice agriculture
LPJ-Bern	GICEW	GICEW	Leff et al. (2004)
CLM4Me			
DLEM			
IAP-RAS	n.a.	n.a.	n.a.
LPJ-WHyMe	n.a.	n.a.	n.a.
LPJ-WSL			Leff et al. (2004)
ORCHIDEE			Leff et al. (2004)
SDGVM			
UVic-ESCM			
UW-VIC			

maximal global wetland extent (Fig. 2a). CLM4Me simulates relatively small seasonality in the tropics (30° S–30° N), with an intra-annual change on the order of $5\,\mathrm{Tg\,CH_4\,yr^{-1}}$, consistent with the simulated relatively small change in wetland area (Fig. A2a). The much smaller maximum in northern subtropical (20°–40° N) CH_4 fluxes peaks later than boreal emissions (in July), although the entire annual range for this latitudinal band is also only about $5\,\mathrm{Tg\,CH_4\,yr^{-1}}$.

DLEM has a distinctly different global CH_4 flux pattern with peak emissions occurring in August (Fig. 6b), two months after CLM4Me, but again relatively consistent to the pattern of DLEM simulated wetland extent (Fig. 2b). As well, the main source of variation in the DLEM emissions peak is primarily driven by the tropical, boreal, and northern subtropical bands. The DLEM tropical band has a CH_4 emissions peak in August, again two months after CLM4Me, but this peak is not obviously dependent upon wetland extent (Fig. A2b). LPJ-Bern simulates a global CH_4 emissions peak in August, with a strong contribution from the boreal region in that month, but also strongly emitting from July into September (Fig. 6c). The LPJ-Bern tropical band also contributes with a broad boreal summer peak in emissions. This timing slightly leads the usual month of greatest wetland/wet soils extent, simulated by LPJ-Bern to be September (Fig. 2c). Given the pattern of LPJ-Bern CH_4 emissions, it appears that the wet mineral soils are contributing small CH_4 flux densities (but large areas) for much of the year (compare Fig. 6c to Fig. 2c), but with a roughly equal flux contributed by the inundated and peatland fractions.

LPJ-WSL shows an intermediate time for peak global CH_4 emissions, peaking in July, with contributions fairly equally from the entire Northern Hemisphere (Fig. 6d). This pattern is due to the model parameterization responding to the gradient in surface temperature poleward. The model CH_4 parameterization scales heterotrophic respiration by surface temperature and two latitudinal scaling factors to calculate CH_4 flux densities (see description in Hodson et al., 2011; Wania et al., 2012). Like most models, LPJ-WSL shows a reasonably strong anticorrelation between the northern and southern tropical region CH_4 fluxes, with the northern region's peak emissions occurring in the northern summer. This tropical CH_4 flux anticorrelation pattern is also present in the results of CLM4Me, but it is the weakest of all the models. ORCHIDEE has a similar timing of peak global CH_4 emissions, occurring in July, to LPJ-WSL (Fig. 6e). The ORCHIDEE global CH_4 emissions peak is strongly driven by the northern boreal region. ORCHIDEE also has a strong CH_4 flux cycle in the southern tropics, much stronger than that of the northern counterpart. SDGVM simulates a strong seasonal cycle of CH_4 emissions in the southern tropical region (Fig. 6f), while the largest driver of peak global emissions for SDGVM is the northern boreal region. SDGVM shares some similarity with ORCHIDEE in its CH_4 flux pattern for the southern tropical band with a strong seasonal cycle of higher fluxes around March and lower fluxes around August to September.

Acknowledgements. The authors are grateful to the COST Action ES0805 TERRABITES for providing support for the WETCHIMP workshop. We thank Sylvia Houston and Olga Petrikova for assistance with organizing the project meeting and Kristen Krumhardt for assistance producing the figures. J. R. M. was supported by the Swiss Ministry for Research and Education (grant C09.0054). J. O. K. acknowledges support from the Swiss National Science Foundation (grant PP0022_119049 and PP00P2_39193). The contributions of W. J. R. and Z. M. S. were supported by the Director, Office of Science, Office of Biological and Environmental Research, Climate and Environmental Science Division, of the US Department of Energy under Contract No. DE-AC02-05CH11231 to Berkeley Lab (IMPACTS and C-Climate Uncertainties projects). The contributions of T. J. B. and D. P. L. were supported by NASA's ROSES program, grant NNX08AH97G. The contribution of Z. C. Y. was supported by a US NSF grant (ARC-1107981) and a grant from The Max Planck Society (Germany). A. V. E. and S. N. D. were supported by the the President of Russia grant 5467.2012.5, by the Russian Foundation for Basic Research, and by the programs of the Russian Academy of Sciences. The contributions of R. S. and S. Z. were supported by the Swiss National Science Foundation and by the European Research Council advanced grant MATRICs (ERC grant agreement no. 226172) under the European Community's Seventh Framework Programme. P. O. H. is supported by a NERC UK grant NE/I010912/1 and previously through NERC UK/INSU France QUEST-DESIRE project. E. L. H. was supported by ETH Competence Center Environment and Sustainability's grant MAIOLICA. H. T. and G. C. wish to thank Xiaofeng Xu for assistance with formatting inputs and setting up earlier DLEM model simulations. We thank two anonymous referees for their comments that improved this manuscript.

Edited by: A. Arneth

References

Avis, C., Weaver, A. J., and Meissner, K. J.: Reduction in areal extent of high-latitude wetlands in response to permafrost thaw, Nat. Geosci., 4, 444–448, doi:10.1038/ngeo1160, 2011.

Bartlett, K. and Harriss, R.:Review and assessment of methane emissions from wetlands, Chemosphere, 26, 261–320, doi:10.1016/0045-6535(93)90427-7, 1993.

Bartlett, K. Bartlett, D., Harriss, R., and Sebacher, D.:Methane emissions along a salt marsh salinity gradient, Biogeochemistry, 3,183–202, doi:10.1007/BF02187365, 1987.

Beck, V., Chen, H., Gerbig, C., Bergamaschi, P., Bruhwiler, L., Houweling, S., Röckmann, T., Kolle, O., Steinbach, J., Koch, T., Sapart, C. J., van der Veen, C., Frankenberg, C., Andreae, M. O., Artaxo, P., Longo, K., M., and Wofsy, S. C.:Methane airborne measurements and comparison to global models during BARCA, J. Geophys. Res., 171, D15310, doi:10.1029/2011JD017345, 2012.

Beerling, D. J., Fox, A., Stevenson, D. S., and Valdes, P. J.: Enhanced chemistry-climate feedbacks in past greenhouse worlds, Proc. Natl. Acad. Sci., 108, 9770–9775, doi:10.1073/pnas.1102409108, 2011.

Bellisario, L. M., Bubier, J. L., Moore, T., and Chanton, J. P.: Controls on CH_4 emissions from a northern peatland, Global Biogeochem. Cy., 13, 81–91, 1999.

Bergamaschi, P., Frankenberg, C., Meirink, J. F., Krol, M., Dentener, F. J., Wagner, T., Platt, U., Kaplan, J. O., Körner, S., Heimann, M., Dlugokencky, E. J., and Goede, A.: Satellite chartography of atmospheric methane from SCIAMACHY on board ENVISAT: 2. Evaluation based on inverse model simulations, J. Geophys. Res., 112, 1–26, doi:10.1029/2006JD007268, 2007.

Beven, K. J. and Kirkby, M. J.: A physically based, variable contributing area model of basin hydrology / Un modèle à base physique de zone d'appel variable de l'hydrologie du bassin versant, Hydrol. Sci. Bull., 24, 43–69, 1979.

Bloom, A., Palmer, P., Fraser, A., and Reay, D.: Large-scale controls of methanogenesis inferred from methane and gravity spaceborne data, Science, 327, 322–325, doi:10.1126/science.1175176, 2010.

Boardman, C. P., Gauci, V., Watson, J. S., Blake, S., and Beerling, D. J.: Contrasting wetland CH_4 emission responses to simulated glacial atmospheric CO_2 in temperate bogs and fens., New Phytol., 192, 1–14, doi:10.1111/j.1469-8137.2011.03849.x, 2011.

Bohn, T. J. and Lettenmaier, D. P.: Systematic biases in large-scale estimates of wetland methane emissions arising from water table formulations, Geophys. Res. Lett., 37, 1–6, doi:10.1029/2010GL045450, 2010.

Bohn, T. J., Lettenmaier, D. P., Sathulur, K., Bowling, L. C., Podest, E., McDonald, K. C., and Friborg, T.: Methane emissions from Western Siberian wetlands: heterogeneity and sensitivity to climate change, Environ. Res. Lett., 2, 045015, doi:10.1088/1748-9326/2/4/045015, 2007.

Bonan, G. B., Oleson, K. W., Fisher, R. A., Lasslop, G., and Reichstein, M.: Reconciling leaf physiological traits and canopy flux data: use of the TRY and FLUXNET databases in the community land model version 4, J. Geophys. Res., 117, 1–19, doi:10.1029/2011JG001913, 2012.

Bousquet, P., Ciais, P., Miller, J. B., Dlugokencky, E. J., Hauglustaine, D. A., Prigent, C., van der Werf, G. R., Peylin, P., Brunke, E.-G. G., Carouge, C., Langenfelds, R. L., Lathière, J., Papa, F., Ramonet, M., Schmidt, M., Steele, L. P., Tyler, S. C., White, J. W. C., Werf, G. R. V. D., and Lathiere, J.: Contribution of anthropogenic and natural sources to atmospheric methane variability, Nature, 443, 439–443, doi:10.1038/nature05132, 2006.

Bousquet, P., Ringeval, B., Pison, I., Dlugokencky, E. J., Brunke, E.-G., Carouge, C., Chevallier, F., Fortems-Cheiney, A., Frankenberg, C., Hauglustaine, D. A., Krummel, P. B., Langenfelds, R. L., Ramonet, M., Schmidt, M., Steele, L. P., Szopa, S., Yver, C., Viovy, N., and Ciais, P.: Source attribution of the changes in atmospheric methane for 2006–2008, Atmos. Chem. Phys., 11, 3689–3700, doi:10.5194/acp-11-3689-2011, 2011.

Brook, E. J., Harder, S., Severinghaus, J. P., Steig, E. J., and Sucher, C. M.: On the origin and timing of rapid changes in atmospheric methane during the last glacial period, Global Biogeochem. Cy., 14, 559–572, 2000.

Bullock, A. and Acreman, M.: The role of wetlands in the hydrological cycle, Hydrol. Earth Syst. Sci., 7, 358–389, doi:10.5194/hess-7-358-2003, 2003.

Cao, M., Marshall, S., and Gregson, K.: Global carbon exchange and methane emissions from natural wetlands: application of a process-based model, J. Geophys. Res., 101, 14399–14414, 1996.

CCSP, Clark, P. U., Weaver, A. J., Brook, E., Cook, E. R., Delworth, T. L., and Steffen, K.: Abrupt Climate Change, a report by the US Climate Change Science Program and the Subcommittee on Global Change Research, Tech. rep., US Geological Survey, Reston, VA, 2008.

Chanton, J. P., Bauer, L. J. E., Glaser, I. P. A., Siegel, D. I., Kelley, C. A., Tyler, S. C., Romanowicz, E. H., Lazrus, A., Bauer, J. E., and Glaser, P. A.: Radiocarbon evidence for the substrates supporting methane formation within Northern Minnesota peatlands, Geochim. Cosmochim. Acta, 59, 3663–3668, doi:10.1016/0016-7037(95)00240-Z, 1995.

Chappellaz, J., Blunier, T., Kints, S., Dällenbach, A., Barnola, J.-M. J., Schwander, J., Raynaud, D., and Stauffer, B.: Changes in the atmospheric CH_4 gradient between Greenland and Antarctica during the Holocene, J. Geophys. Res., 102, 15987–15997, 1997.

Chasar, L. S., Chanton, J. P., Glaser, P. H., and Siegel, D. I.: Methane concentration and stable isotope distribution as evidence of rhizospheric processes: comparison of a fen and bog in the glacial Lake Agassiz peatland complex, Ann. Bot., 86, 655–663, doi:10.1006/anbo.2000.1172, 2000.

Chen, Y.-H. and Prinn, R. G.: Estimation of atmospheric methane emissions between 1996 and 2001 using a three-dimensional global chemical transport model, J. Geophys. Res., 111, 1–38, doi:10.1029/2005JD006058, 2006.

Christensen, T. R. and Cox. P.:Response of methane emission from arctic tundra to climatic change: results from a model simulation, Tellus B, 47, 301–309, 1995.

Christensen. T. R. Prentice, I. C., Kaplan, J. O., Haxeltine, A., and Sitch, S.: Methane flux from northern wetlands and tundra - An ecosystem source modelling approach, Tellus B, 48, 652–661, 1996.

Cogley, J.: GGHYDRO: global hydrographic data, Peterborough, Ontario, Canada, 1994.

Denman, K. L., Brasseur, G., Chidthaisong, A., Ciais, P., Cox, P. M., Dickinson, R. E., Hauglustaine, D. A., Heinze, C., Holland, E.,

Jacob, D., Lohmann, U., Ramachandran, S., da Silva Dias, P., Wofsy, S., and Zhang, X.: Couplings between changes in the climate system and biogeochemistry, in: Climate Change 2007: The Physical Science Basis, Contribution of Working Group I to the Fourth Assessment Report of the Intergovernmental Panel on Climate Change, edited by: Solomon, S., Qin, D., Manning, M. R., Chen, Z., Marquis, M., Averyt, K., Tignor, M., and Miller, H. L., Cambridge University Press, Cambridge UK and New York, NY, USA, chap. 7, 1–90, 2007.

Dlugokencky, E. J., Walter, B. P., Masarie, K., Lang, P., and Kasischke, E. S.: Measurements of an anomalous global methane increase during 1998, Geophys. Res. Lett., 28, 499–502, 2001.

Dugan, P.: Wetlands in Danger: A World Conservation Atlas, Oxford University Press, New York, NY, 1993.

Eliseev, A. V., Mokhov, I. I., Arzhanov, M. M., Demchenko, P. F., and Denisov, S. N.: Interaction of the methane cycle and processes in wetland ecosystems in a climate model of intermediate complexity, Izvestiya, Atmos. Ocean. Phys., 44, 139–152, doi:10.1134/S0001433808020011, 2008.

Ferretti, D. F., Miller, J. B., White, J. W. C., Lassey, K. R., Lowe, D. C., and Etheridge, D. M.: Stable isotopes provide revised global limits of aerobic methane emissions from plants, Atmos. Chem. Phys., 7, 237–241, doi:10.5194/acp-7-237-2007, 2007.

Finlayson, C., Davidson, N. C., Spiers, A., and Stevenson, N.: Global wetland inventory – current status and future priorities, Mar. Freshwater Res., 50, 717–727, 1999.

Frankenberg, C., Bergamaschi, P., Butz, A., Houweling, S., Meirink, J. F., Notholt, J., Petersen, A. K., Schrijver, H., Warneke, T., and Aben, I.: Tropical methane emissions: a revised view from SCIAMACHY onboard ENVISAT, Geophys. Res. Lett., 35, 1–5, L15811, doi:10.1029/2008GL034300, 2008.

Frey, K. E. and Smith, L. C.: How well do we know northern land cover? Comparison of four global vegetation and wetland products with a new ground-truth database for West Siberia, Global Biogeochem. Cy., 21, 1–15, GB1016, doi:10.1029/2006GB002706, 2007.

Friedlingstein, P., Cox, P. M., Betts, R., Bopp, L., von Bloh, W., Brovkin, V., Cadule, P., Doney, S., Eby, M., Fung, I., Bala, G., John, J., Jones, C., Joos, F., Kato, T., Kawamiya, M., Knorr, W., Lindsay, K., Matthews, H. D., Raddatz, T., Rayner, P. J., Reick, C. H., Roeckner, E., Schnitzler, K.-G., Schnur, R., Strassman, K., Weaver, A. J., Yoshikawa, C., and Zeng, N.: Climate-carbon cycle feedback analysis: results from the C4MIP model intercomparison, J. Climate, 19, 3337–3354, 2006.

Fung, I. Y., Prather, M., Fraser, P. J., John, J., Lerner, J., Matthews, E., and Steele, L. P.: Three-dimensional model synthesis of the global methane cycle, J. Geophys. Res., 96, 13033–13065, 1991.

Gedney, N., Cox, P. M., and Huntingford, C.: Climate feedback from wetland methane emissions, Geophys. Res. Lett., 31, 1–4, doi:10.1029/2004GL020919, 2004.

Glagolev, M., Kleptsova, I., Filippov, I., Maksyutov, S., and Machida, T.: Regional methane emission from West Siberia mire landscapes, Environ. Res. Lett., 6, 1–7, 045214, doi:10.1088/1748-9326/6/4/045214, 2011.

Goll, D. S., Brovkin, V., Parida, B. R., Reick, C. H., Kattge, J., Reich, P. B., van Bodegom, P. M., and Niinemets, Ü.: Nutrient limitation reduces land carbon uptake in simulations with a model of combined carbon, nitrogen and phosphorus cycling, Biogeosciences, 9, 3547–3569, doi:10.5194/bg-9-3547-2012, 2012.

Gorham, E.: Northern peatlands: role in the carbon cycle and probable responses to climatic warming, Ecol. Appl., 1, 182–195, 1991.

Guerrero, O. J., Jiménez, R., Lin, J. C., Diskin, G. S., Sachse, G. W., Kort, E. A., and Kaplan, J. O.: Assessing methane fluxes in Colombia from Lagrangian simulation analysis of aircraft-borne measurements during TC4, in: NASA Goddard Space Flight Center Seminar, vol. 108, 1 pp., Greenbelt, MD, 2011.

Hansen, J., Ruedy, R., Sato, M., and Lo, K.: Global surface temperature change, Rev. Geophys., 48, 1–29, RG4004, doi:10.1029/2010RG000345, 2010.

Harriss, R., Wofsy, S., Hoell, J. M. J., Bendura, R., Drewry, J., McNeal, R. J., Pierce, D., Rabine, V., and Snell, R. L.: The Arctic Boundary Layer Expedition (ABLE-3B): July–August 1990, J. Geophys. Res., 99, 1635–1643, 1994.

Hein, R., Crutzen, P. J., and Heimann, M.: An inverse modeling approach to investigate the global atmospheric methane cycle, Global Biogeochem. Cy., 11, 43–76, 1997.

Hickler, T., Smith, B., Prentice, C. I., Mjöfors, K., Miller, P., Arneth, A., and Sykes, M. T.: CO_2 fertilization in temperate FACE experiments not representative of boreal and tropical forests, Glob. Change Biol., 14, 1531–1542, doi:10.1111/j.1365-2486.2008.01598.x, 2008.

Hodson, E. L., Poulter, B., Zimmermann, N. E., Prigent, C., and Kaplan, J. O.: The El Niño–Southern Oscillation and wetland methane interannual variability, Geophys. Res. Lett., 38, 1–4, doi:10.1029/2011GL046861, 2011.

Hopcroft, P. O., Valdes, P. J., and Beerling, D. J.: Simulating idealized Dansgaard-Oeschger events and their potential impacts on the global methane cycle, Quat. Sci. Rev., 30, 3258–3268, doi:10.1016/j.quascirev.2011.08.012, 2011.

Houweling, S., Dentener, F., and Lelieveld, J.: Simulation of preindustrial atmospheric methane to constrain the global source strength of natural wetlands, J. Geophys. Res., 105, 17243–17255, 2000.

Houweling, S., Röckmann, T., Aben, I., Keppler, F., Krol, M., Meirink, J. F., and Dlugokencky, E. J.: Atmospheric constraints on global emissions of methane from plants, Geophys. Res. Lett., 33, 1–5, doi:10.1029/2006GL026162, 2006.

Huber, C., Leuenberger, M., Spahni, R., Flückiger, J., Schwander, J., Stocker, T. F., Johnsen, S., Landais, A., and Jouzel, J.: Isotope calibrated Greenland temperature record over Marine Isotope Stage 3 and its relation to CH_4, Earth Planet. Sc. Lett., 243, 504–519, doi:10.1016/j.epsl.2006.01.002, 2006.

Hungate, B. A., Dukes, J. S., Shaw, M. R., Luo, Y., and Field, C. B.: Nitrogen and climate change, Science, 302, 1512–1513, doi:10.1126/science.1091390, 2003.

Hurtt, G. C., Frolking, S., Fearon, M. G., Moore, B., Shevliakova, E., Malyshev, S., Pacala, S. W., and Houghton, R. A.: The underpinnings of land-use history: three centuries of global gridded land-use transitions, wood-harvest activity, and resulting secondary lands, Glob. Change Biol., 12, 1208–1229, doi:10.1111/j.1365-2486.2006.01150.x, 2006.

Hutchin, P. R., Press, M. C., Lee, J. A., and Ashenden, T. W.: Elevated concentrations of CO_2 may double methane emissions from mires, Glob. Change Biol., 1, 125–128, 1995.

IPCC: Emissions Scenarios, Special Report of the Intergovernmental Panel on Climate Change, Cambridge University Press, Cam-

bridge UK, 2000.

Kang, H., Freeman, C., and Ashendon, T. W.: Effects of elevated CO_2 on fen peat biogeochemistry, Sci. Total Environ., 279, 45–50, 2001.

Kaplan, J. O.: Wetlands at the Last Glacial Maximum: distribution and methane emissions, Geophys. Res. Lett., 29, 3–6, doi:10.1029/2001GL013366, 2002.

Kaplan, J. O., Folberth, G., and Hauglustaine, D. A.: Role of methane and biogenic volatile organic compound sources in late glacial and Holocene fluctuations of atmospheric methane concentrations, Global Biogeochem. Cy., 20, 1–16, doi:10.1029/2005GB002590, 2006.

Kirschbaum, M. U., Bruhn, D., Etheridge, D. M., Evans, J. R., Farquhar, G. D., Gifford, R. M., Paul, K. I., and Winters, A. J.: A comment on the quantitative significance of aerobic methane release by plants, Funct. Plant Biol., 33, 521–530, doi:10.1071/FP06051, 2006.

Koven, C. D., Ringeval, B., Friedlingstein, P., Ciais, P., Cadule, P., Khvorostyanov, D., Krinner, G., and Tarnocai, C.: Permafrost carbon-climate feedbacks accelerate global warming., Proc. Natl. Acad. Sci., 108, 14769–14774, doi:10.1073/pnas.1103910108, 2011.

Leff, B., Ramankutty, N., and Foley, J. A.: Geographic distribution of major crops across the world, Global Biogeochem. Cy., 18, 27, GB1009, doi:10.1029/2003GB002108, 2004.

Lehner, B. and Döll, P.: Development and validation of a global database of lakes, reservoirs and wetlands, J. Hydrol., 296, 1–22, doi:10.1016/j.jhydrol.2004.03.028, 2004.

Loulergue, L., Schilt, A., Spahni, R., Masson-Delmotte, V., Blunier, T., Lemieux, B., Barnola, J.-M., Raynaud, D., Stocker, T. F., and Chappellaz, J.: Orbital and millennial-scale features of atmospheric CH_4 over the past 800,000 years, Nature, 453, 383–386, doi:10.1038/nature06950, 2008.

Loveland, T., Reed, B., and Brown, J.: Development of a global land cover characteristics database and IGBP DISCover from 1 km AVHRR data, Int. J. Remote Sens., 21, 1303–1330, 2000.

Matthews, E. and Fung, I. Y.: Methane emission from natural wetlands: global distribution, area, and environmental characteristics, Global Biogeochem. Cy., 1, 61–86, 1987.

Meehl, G. A., Stocker, T. F., Collins, W. D., Friedlingstein, P., Gaye, A. T., Gregory, J. M., Kitoh, A., Knutti, R., Murphy, J. M., Noda, A., Raper, S. C. B., Watterson, I. G., Weaver, A. J., and Zhao, Z.-C.: Global climate projections, in: Climate Change 2007: The Physical Science Basis, Contribution of Working Group I to the Fourth Assessment Report of the Intergovernmental Panel on Climate Change, edited by: Solomon, S., Qin, D., Manning, M., Chen, Z., Marquis, M., Averyt, K., Tignor, M., and Miller, H., Cambridge University Press, Cambridge, UK and New York, NY, US A., chap. 10, pp. 748–844, 2007.

Megonigal, J. P. and Schlesinger, W.: Enhanced CH_4 emissions from a wetland soil exposed to elevated CO_2, Biogeochemistry, 37, 77–88, 1997.

Melack, J. M., Hess, L. L., Gastil, M., Forsberg, B. R., Hamilton, S. K., Lima, I. B. T., Novo, E. M. E., Barbara, S., Corners, H., and Espaciais, D. P.: Regionalization of methane emissions in the Amazon Basin with microwave remote sensing, Glob. Change Biol., 10, 530–544, doi:10.1111/j.1529-8817.2003.00763.x, 2004.

Mikaloff Fletcher, S. E., Tans, P. P., Bruhwiler, L. M., Miller, J. B., and Heimann, M.: CH_4 sources estimated from atmospheric observations of CH_4 and its $^{13}C/^{12}C$ isotopic ratios: 1. Inverse modeling of source processes, Global Biogeochem. Cy., 18, 1–17, doi:10.1029/2004GB002223, 2004.

Miller, J. B., Gatti, L. V., D'Amelio, M. T. S., Crotwell, A. M., Dlugokencky, E. J., Bakwin, P., Artaxo, P., and Tans, P. P.: Airborne measurements indicate large methane emissions from the Eastern Amazon basin, Geophys. Res. Lett., 34, 1–5, doi:10.1029/2006GL029213, 2007.

Mitsch, W. and Gosselink, J. G.: Wetlands, John Wiley & Sons, New York, 3rd edn., 2000.

Mokhov, I. I., Eliseev, A. V., and Denisov, S. N.: Model diagnostics of variations in methane emissions by wetlands in the second half of the 20th century based on reanalysis data, Doklady Earth Sci., 417, 1293–1297, doi:10.1134/S1028334X07080375, 2007.

Moore, T. and Roulet, N.: Spatial and temporal variations of methane flux from subarctic/northern boreal fens, Global Biogeochem. Cy., 4, 29–46, 1990.

National Wetlands Working Group: Wetlands of Canada, Sustainable Development Branch, Environment Canada, Ottawa, Ontario, and Polyscience Publications Inc., Montreal, Quebec, 1988.

NOAA National Climatic Data Center: State of the Climate: Global Analysis for Annual 2003, available at: http://www.ncdc.noaa.gov/sotc/global/2003/13, 2003.

OECD: Guidelines for aid agencies for improved conservation and sustainable use of tropical and sub-tropical wetlands, Tech. rep., Organization for Economic Co-operation and Development, Paris, France, 1996.

ORNL DAAC: MODIS subsetted land products, available at: http://daac.ornl.gov/MODIS/modis.html, 2000.

Page, S. E., Rieley, J. O., and Banks, C. J.: Global and regional importance of the tropical peatland carbon pool, Glob. Change Biol., 17, 798–818, doi:10.1111/j.1365-2486.2010.02279.x, 2011.

Pancotto, V., Bodegom, P. V., Hal, J. V., van Logtestijn, R., Blokker, P., Toet, S., and Aerts, R.: N deposition and elevated CO_2 on methane emissions: differential responses of indirect effects compared to direct effects through litter chemistry feedbacks, J. Geophys. Res., 115, G02001, doi:10.1029/2009JG001099, 2010.

Papa, F., Prigent, C., Aires, F., Jimenez, C., Rossow, W. B., and Matthews, E.: Interannual variability of surface water extent at the global scale, 1993–2004, J. Geophys. Res., 115, 1–17, doi:10.1029/2009JD012674, 2010.

Peregon, A., Maksyutov, S., Kosykh, N. P., and Mironycheva-Tokareva, N. P.: Map-based inventory of wetland biomass and net primary production in Western Siberia, J. Geophys. Res., 113, 1–12, doi:10.1029/2007JG000441, 2008.

Petrescu, A. M. R., van Huissteden, J., Jackowicz-Korczynski, M., Yurova, A., Christensen, T. R., Crill, P. M., Bäckstrand, K., Maximov, T. C.: Modelling CH_4 emissions from arctic wetlands: effects of hydrological parameterization, Biogeosciences, 5, 111–121, doi:10.5194/bg-5-111-2008, 2008.

Pickett-Heaps, C. A., Jacob, D. J., Wecht, K. J., Kort, E. A., Wofsy, S. C., Diskin, G. S., Worthy, D. E. J., Kaplan, J. O., Bey, I., and Drevet, J.: Magnitude and seasonality of wetland methane emissions from the Hudson Bay Lowlands (Canada),

Atmos. Chem. Phys., 11, 3773–3779, doi:10.5194/acp-11-3773-2011, 2011.

Potter, C.: An ecosystem simulation model for methane production and emission from wetlands, Global Biogeochem. Cy., 11, 495–506, 1997.

Poulter, B., Aragão, L., Heyder, U., Gumpenberger, M., Heinke, J., Langerwisch, F., Rammig, A., Thonicke, K., and Cramer, W.: Net biome production of the Amazon Basin in the 21st century, Glob. Change Biol., 16, 2062–2075, doi:10.1111/j.1365-2486.2009.02064.x, 2010.

Prentice, I., Farquhar, G., Fasham, M., Goulden, M., Heimann, M., Jaramillo, V., Kheshgi, H., Quéré, C. L., Scholes, R., and Wallace, D.: The carbon cycle and atmospheric carbon dioxide, in: IPCC Third Assessment Report: Climate Change 2001 (TAR), edited by: Pitelka, L. and Ramirez Rojas, A., Cambridge University Press, Cambridge UK, chap. 3, 1–56, 2001.

Prigent, C., Papa, F., Aires, F., Rossow, W. B., and Matthews, E.: Global inundation dynamics inferred from multiple satellite observations, 1993–2000, J. Geophys. Res., 112, 1–13, doi:10.1029/2006JD007847, 2007.

Riley, W. J., Subin, Z. M., Lawrence, D. M., Swenson, S. C., Torn, M. S., Meng, L., Mahowald, N. M., and Hess, P.: Barriers to predicting changes in global terrestrial methane fluxes: analyses using CLM4Me, a methane biogeochemistry model integrated in CESM, Biogeosciences, 8, 1925–1953, doi:10.5194/bg-8-1925-2011, 2011.

Ringeval, B.: Interactions entre climat et émissions de méthane par les zones humides à l'échelle globale, PhD thesis, Universite Pierre & Marie Curie, Paris, France, 2011.

Ringeval, B., de Noblet-Ducoudré, N., Ciais, P., Bousquet, P., Prigent, C., Papa, F., and Rossow, W. B.: An attempt to quantify the impact of changes in wetland extent on methane emissions on the seasonal and interannual time scales, Global Biogeochem. Cy., 24, 1–12, doi:10.1029/2008GB003354, 2010.

Ringeval, B., Friedlingstein, P., Koven, C., Ciais, P., de Noblet-Ducoudra, N., Decharme, B., and Cadule, P.: Climate-CH_4 feedback from wetlands and its interaction with the climate-CO_2 feedback, Biogeosciences, 8, 2137–2157, doi:10.5194/bg-8-2137-2011, 2011.

Ringeval, B., Decharme, B., Piao, S. L., Ciais, P., Papa, F., de Noblet-Ducoudré, N., Prigent, C., Friedlingstein, P., Gouttevin, I., Koven, C. D., and Ducharne, A.: Modelling subgrid wetland in the ORCHIDEE global land surface model: evaluation against river discharges and remotely sensed data, Geosci. Model Dev., 5, 683–735, doi:http://dx.doi.org/10.5194/gmdd-5-683-201210.5194/gmdd-5-683-2012, 2012.

Roulet, N., Jano, A., Kelly, C., and Klinger, L.: Role of the Hudson Bay Lowland as a source of atmospheric methane, J. Geophys. Res., 99, 1439–1454, 1994.

Saarnio, S. and Silvola, J.: Effects of increased CO_2 and N on CH_4 efflux from a boreal mire: a growth chamber experiment, Oecologia, 119, 349–356, 1999.

Saarnio, S., Järvio:, S., Saarinen, T., Vasander, H., and Silvola, J.: Minor changes in vegetation and carbon gas balance in a boreal mire under a raised CO_2 or NH_4NO_3 supply, Ecosystems, 6, 46–60, doi:10.1007/s10021-002-0208-3, 2003.

Sanderson, M. G.: Hadley Centre Technical Note 32: Global Distribution of Freshwater Wetlands for use in STOCHEM, UK Met Office, London, UK, 1–10, 2001.

Schroeder, R., Rawlins, M. A., McDonald, K. C., Podest, E., Zimmermann, R., and Kueppers, M.: Satellite microwave remote sensing of North Eurasian inundation dynamics: development of coarse-resolution products and comparison with high-resolution synthetic aperture radar data, Environ. Res. Lett., 5, 015003, doi:10.1088/1748-9326/5/1/015003, 2010.

Segers, R. and Leffelaar, P. A.: Modeling methane fluxes in wetlands with gas-transporting plants, 3. Plot scale, J. Geophys. Res., 106, 3541–3558, doi:10.1029/2000JD900482, 2001.

Shindell, D. T., Walter, B. P., and Faluvegi, G.: Impacts of climate change on methane emissions from wetlands, Geophys. Res. Lett., 31, L21202, doi:10.1029/2004GL021009, 2004.

Silvola, J., Saarnio, S., Foot, J., Sundh, I., Greenup, A., Heijmans, M., Ekberg, A., Mitchell, E., and van Breemen, N.: Effects of elevated CO_2 and N deposition on CH_4 emissions from European mires, Global Biogeochem. Cy., 17, 1068–1080, doi:10.1029/2002GB001886, 2003.

Singarayer, J. S., Valdes, P. J., Friedlingstein, P., Nelson, S., and Beerling, D. J.: Late Holocene methane rise caused by orbitally controlled increase in tropical sources., Nature, 470, 82–85, doi:10.1038/nature09739, 2011.

Smith, L. K., Lewis, W. M., Chanton, J. P., Cronin, G., and Hamilton, S. K.: Methane emissions from the Orinoco River floodplain, Venezuela, Biogeochemistry, 51, 113–140, 2000.

Spahni, R., Wania, R., Neef, L., van Weele, M., Pison, I., Bousquet, P., Frankenberg, C., Foster, P. N., Joos, F., Prentice, I. C., and van Velthoven, P.: Constraining global methane emissions and uptake by ecosystems, Biogeosciences, 8, 1643–1665, doi:10.5194/bg-8-1643-2011, 2011.

Stillwell-Soller, L., Klinger, L., Pollard, D., and Thompson, S. L.: The global distribution of freshwater wetlands, Tech. Rep., September, National Center for Atmospheric Research, Boulder, Colorado, USA, 1995.

Sulman, B. N., Desai, A. R., Schroeder, N. M., Ricciuto, D., Barr, A., Richardson, A. D., Flanagan, L. B., Lafleur, P. M., Tian, H., Chen, G., Grant, R. F., Poulter, B., Verbeeck, H., Ciais, P., Ringeval, B., Baker, I. T., Schaefer, K., Luo, Y., and Weng, E.: Impact of hydrological variations on modeling of peatland CO_2 fluxes: results from the North American carbon program site synthesis, J. Geophys. Res., 117, 1–21, doi:10.1029/2011JG001862, 2012.

Subin, Z. M., Koven, C. D., Riley, W. J., Torn, M. S., Lawrence, D. M., and Swenson, S. C.:Effects of soil moisture on the responses of soil temperatures to climate change in cold regions, Journal of Climate, in press, 2012.

Tang, J. and Zhuang, Q.: Equifinality in parameterization of process-based biogeochemistry models: a significant uncertainty source to the estimation of regional carbon dynamics, J. Geophys. Res., 113, 1–13, doi:10.1029/2008JG000757, 2008.

Tarnocai, C., Canadell, J. G., Schuur, E. A. G., Kuhry, P., Mazhitova, G., and Zimov, S. A.: Soil organic carbon pools in the northern circumpolar permafrost region, Global Biogeochem. Cy., 23, 1–11, doi:10.1029/2008GB003327, 2009.

Tian, H., Xu, X., Liu, M., Ren, W., Zhang, C., Chen, G., and Lu, C.: Spatial and temporal patterns of CH_4 and N_2O fluxes in terrestrial ecosystems of North America during 1979–2008: application of a global biogeochemistry model, Biogeosciences, 7, 2673–2694, doi:10.5194/bg-7-2673-2010, 2010.

Tian, H., Xu, X., Lu, C., Liu, M., Ren, W., Chen, G., Melillo, J. M., and Liu, J.: Net exchanges of CO_2, CH_4, and N_2O between China's terrestrial ecosystems and the atmosphere and their contributions to global climate warming, J. Geophys. Res., 116, 1–13, doi:10.1029/2010JG001393, 2011.

Turunen, J., Tomppo, E., Tolonen, K., and Reinikainen, A.: Estimating carbon accumulation rates of undrained mires in Finland – application to boreal and subarctic regions, The Holocene, 12, 69–80, doi:10.1191/0959683602hl522rp, 2002.

Valdes, P. J., Beerling, D. J., and Johnson, C. E.: The ice age methane budget, Geophys. Res. Lett., 32, 1–4, doi:10.1029/2004GL021004, 2005.

van Bodegom, P. and Goudriaan, J.: A mechanistic model on methane oxidation in a rice rhizosphere, Biogeochemistry, 55, 145–177, 2001.

van Bodegom, P., Wassmann, R., and Metra-Corton, T.: A process-based model for methane emission predictions from flooded rice paddies, Global Biogeochem. Cy., 15, 247–263, 2001.

van Bodegom, P., Verburg, P. H., and Denier van der Gon, H. A. C.: Upscaling methane emissions from rice paddies: problems and possibilities, Global Biogeochem. Cy., 16, 1014, doi:10.1029/2000GB001381, 2002.

van Groenigen, K. J., Osenberg, C. W., and Hungate, B. A.: Increased soil emissions of potent greenhouse gases under increased atmospheric CO_2, Nature, 475, 214–216, doi:10.1038/nature10176, 2011.

van Huissteden, J.: Methane emission from northern wetlands in Europe during Oxygen Isotope Stage 3, Quat. Sci. Rev., 23, 1989–2005, doi:10.1016/j.quascirev.2004.02.015, 2004.

van Huissteden, J., Berrittella, C., Parmentier, F. J. W., Mi, Y., Maximov, T. C., and Dolman, A. J.: Methane emissions from permafrost thaw lakes limited by lake drainage, Nat. Clim. Change, 1, 119–123, doi:10.1038/nclimate1101, 2011.

van Huissteden, J., Berrittella, C.,Parmentier, F. J. W., Mi, Y., Maximov, T. C., and Dolman, A. J.:Methane emissions from permafrost thaw lakes limited by lake drainage, Nature Climate Change, 1, 119–123, doi:10.1038/nclimate1101, 2011.

Vann, C. D. and Megonigal, J. P.: Elevated CO_2 and water depth regulation of methane emissions: comparison of woody and nonwoody wetland plant species, Global Biogeochem. Cy., 63, 117–134, 2003.

Walker, D. A., Raynolds, M. K., Daniëls, F. J., Einarsson, E., Elvebakk, A., Gould, W. A., Katenin, A. E., Kholod, S. S., Markon, C. J., Melnikov, E. S., Moskalenko, N. G., Talbot, S. S., Yurtsev, B. A., and CAVM: The circumpolar arctic vegetation map, J. Veg. Sci., 16, 267–282, doi:10.1111/j.1654-1103.2005.tb02365.x, 2005.

Walter, B. P.: Development of a process-based model to derive methane emissions from natural wetlands for climate studies, Ph.D. thesis, Max-Planck-Institut Für Meteorologie, Hamburg, Germany, 1998.

Walter, B. P. and Heimann, M.: A process-based, climate-sensitive model to derive methane emissions from natural wetlands: application to five wetland sites, sensitivity to model parameters, and climate, Global Biogeochem. Cy., 14, 745–765, 2000.

Walter, B. P., Heimann, M., Shannon, R. D., and White, J.: A process-based model to derive methane emissions from natural wetlands, Geophys. Res. Lett., 23, 3731–3734, 1996.

Walter, B. P., Heimann, M., and Matthews, E.: Modeling modern methane emissions from natural wetlands, 1: Model description and results, J. Geophys. Res., 106, 34189–34206, 2001.

Walter Anthony, K. M., Chanton, J. P., Chapin, S. F. I., Schuur, E. I. G., Zimov, S. A., and Iii, F. S. C.: Methane production and bubble emissions from arctic lakes: isotopic implications for source pathways and ages, J. Geophys. Res., 113, G00A08, doi:10.1029/2007JG000569, 2008.

Wang, J. S., Logan, J. A., McElroy, M. B., Duncan, B. N., Megretskaia, I. A., and Yantosca, R. M.: A 3-D model analysis of the slowdown and interannual variability in the methane growth rate from 1988 to 1997, Global Biogeochem. Cy., 18, 1–31, doi:10.1029/2003GB002180, 2004.

Wania, R., Ross, I., and Prentice, C. I.: Integrating peatlands and permafrost into a dynamic global vegetation model: 1. Evaluation and sensitivity of physical land surface processes, Global Biogeochem. Cy., 23, 1–19, doi:10.1029/2008GB003412, 2009a.

Wania, R., Ross, I., and Prentice, C. I.: Integrating peatlands and permafrost into a dynamic global vegetation model: 2. Evaluation and sensitivity of vegetation and carbon cycle processes, Global Biogeochem. Cy., 23, 1–15, doi:10.1029/2008GB003413, 2009b.

Wania, R., Ross, I., and Prentice, I. C.: Implementation and evaluation of a new methane model within a dynamic global vegetation model: LPJ-WHyMe v1.3.1, Geosci. Model Dev., 3, 565–584, doi:10.5194/gmd-3-565-2010, 2010.

Wania, R., Melton, J. R., Hodson, E. L., Poulter, B., Ringeval, B., Spahni, R., Bohn, T. J., Avis, C. A., Chen, G., Eliseev, A. V., Hopcroft, P. O., Riley, W. J., Subin, Z. M., Tian, H., van Bodegom, P., Kleinen, T., Yu, Z., Singarayer, J. S., Zürcher, S., Lettenmaier, D. P., Beerling, D. J., Denisov, S. N., Prigent, C., Papa, F., and Kaplan, J. O.: Present state of global wetland extent and wetland methane modelling: methodology of a model intercomparison project (WETCHIMP), Geosci. Model Dev. Discuss., 5, 4071–4136, doi:10.5194/gmdd-5-4071-2012, 2012.

Wetlands International: Ramsar Database, Wetlands International, Wageningen, The Netherlands, 2002.

Whiticar, M. J.: Carbon and hydrogen isotope systematics of bacterial formation and oxidation of methane, Chem. Geol., 161, 291–314, doi:10.1016/S0009-2541(99)00092-3, 1999.

Whiting, G. J. and Chanton, J. P.: Primary production control of methane emission from wetlands, Nature, 364, 794–795, 1993.

Williams, M.: Wetlands: A Threatened Landscape, Blackwell Publishing Ltd, Cambridge Massachusetts, USA, 1991.

Winderlich, J., Chen, H., Gerbig, C., Seifert, T., Kolle, O., Lavrič, J. V., Kaiser, C., Höfer, A., and Heimann, M.: Continuous low-maintenance $CO_2/CH_4/H_2O$ measurements at the Zotino Tall Tower Observatory (ZOTTO) in Central Siberia, Atmos. Meas. Tech., 3, 1113–1128, doi:10.5194/amt-3-1113-2010, 2010.

Woo, M.-K. and Winter, T. C.: The role of permafrost and seasonal frost in the hydrology of northern wetlands in North America, J. Hydrol., 141, 5–31, 1993.

Woo, M.-K. and Young, K. L.: High Arctic wetlands: their occurrence, hydrological characteristics and sustainability, J. Hydrol., 320, 432–450, doi:10.1016/j.jhydrol.2005.07.025, 2006.

Worthy, D. E. J., Levin, I., Hopper, F., Ernst, M. K., and Trivett, N. B. A.: Evidence for a link between climate and northern

wetland methane emissions, J. Geophys. Res., 105, 4031–4038, doi:10.1029/1999JD901100, 2000.

Xu, X. and Tian, H.: Methane exchange between marshland and the atmosphere over China during 1949–2008, Global Biogeochem. Cy., 26, 1–14, doi:10.1029/2010GB003946, 2012.

Yu, Z.: Northern peatland carbon stocks and dynamics: a review, Biogeosciences, 9, 4071–4085, doi:10.5194/bg-9-4071-2012, 2012.

Yu, Z., Loisel, J., Brosseau, D. P., Beilman, D. W., and Hunt, S. J.: Global peatland dynamics since the Last Glacial Maximum, Geophys. Res. Lett., 37, 1–5, doi:10.1029/2010GL043584, 2010.

Zaehle, S., Friedlingstein, P., and Friend, A. D.: Terrestrial nitrogen feedbacks may accelerate future climate change, Geophys. Res. Lett., 37, 1–5, doi:10.1029/2009GL041345, 2010.

Zhuang, Q., Melillo, J. M., Sarofim, M. C., Kicklighter, D. W., McGuire, A. D., Felzer, B. S., Sokolov, A., Prinn, R. G., Steudler, P. A., and Hu, S.: CO_2 and CH_4 exchanges between land ecosystems and the atmosphere in northern high latitudes over the 21st century, Geophys. Res. Lett., 33, 1–5, doi:10.1029/2006GL026972, 2006.

4.2 Present state of global wetland extent and wetland methane modelling: Methodology of a model intercomparison project (WETCHIMP)

R. Wania, J. R. Melton, E. L. Hodson, B. Poulter, B. Ringeval, R. Spahni, T. Bohn, C. A. Avis, D. J. Beerling, G. Chen, A. V. Eliseev, S. N. Denisov, P. O. Hopcroft, D. P. Lettenmaier, W. J. Riley, J. S. Singarayer, Z. M. Subin, H. Tian, S. Zürcher, V. Brovkin, P. M. van Bodegom, T. Kleinen, Z. C. Yu, and J. O. Kaplan

Published in Geoscientific Model Development, 6, 617-641 , 2013

doi:10.5194/gmd-6-617-2013

Present state of global wetland extent and wetland methane modelling: methodology of a model inter-comparison project (WETCHIMP)

R. Wania[1,*], J. R. Melton[2,], E. L. Hodson[3,***], B. Poulter[4], B. Ringeval[4,5,6], R. Spahni[7], T. Bohn[8], C. A. Avis[9,****], G. Chen[10], A. V. Eliseev[11,12], P. O. Hopcroft[5], W. J. Riley[13], Z. M. Subin[13,*****], H. Tian[10], P. M. van Bodegom[15], T. Kleinen[14], Z. C. Yu[16], J. S. Singarayer[5], S. Zürcher[7], D. P. Lettenmaier[8], D. J. Beerling[17], S. N. Denisov[11], C. Prigent[18], F. Papa[19], and J. O. Kaplan[2]**

[1]Institut des Sciences de l'Evolution, UMR5554, CNRS – Université Montpellier 2, Place Eugène Bataillon, 34090 Montpellier, France
[2]ARVE Group, École Polytechnique Fédérale de Lausanne, Switzerland
[3]Swiss Federal Research Institute WSL, Switzerland
[4]Laboratoire des Sciences du Climat et de L'Environment, CNRS–CEA, UVSQ, Gif-sur Yvette, France
[5]BRIDGE, School of Geographical Sciences, University of Bristol, UK
[6]Department of Earth Sciences, VU University, Amsterdam, the Netherlands
[7]Climate and Environmental Physics, Physics Institute & Oeschger Centre for Climate Change Research, University of Bern, Switzerland
[8]Dept. of Civil and Environmental Engineering, University of Washington, USA
[9]School of Earth and Ocean Sciences, University of Victoria, Canada
[10]International Center for Climate and Global Change Research and School of Forestry and Wildlife Sciences, Auburn University, Auburn, AL 36849, USA
[11]A.M. Obukhov Institute of Atmospheric Physics, Russian Academy of Sciences, Russia
[12]Kazan (Volga region) Federal University, Russia
[13]Earth Sciences Division (ESD), Lawrence Berkeley National Lab, USA
[14]Max Planck Institute für Meteorologie, Hamburg, Germany
[15]Department of Ecological Sciences, VU University, Amsterdam, the Netherlands
[16]Department of Earth and Environmental Sciences, Lehigh University, USA
[17]Dept. of Animal and Plant Sciences, University of Sheffield, Sheffield S10 2TN, UK
[18]CNRS/LERMA, Observatoire de Paris, 61 Ave. de l'Observatoire, 75014 Paris, France
[19]LEGOS, IRD, 18 Ave. Edouard Belin, 31400 Toulouse, France
[*]now at: Lanser Strasse 30, 6080 Igls, Austria
[**]now at: Canadian Centre for Climate Modelling and Analysis, Environment Canada, Victoria, BC, V8W 2Y2, Canada
[***]now at: AAAS Science and Technology Policy Fellow, Office of Climate Change Policy and Technology, US Department of Energy, USA
[****]now at: Physics and Astronomy department, Camosun College, Victoria, BC, Canada
[*****]now at: Princeton Environmental Institute, Princeton University, Princeton, New Jersey, USA

Correspondence to: J. R. Melton (joe.melton.sci@gmail.com)

Received: 30 October 2012 – Published in Geosci. Model Dev. Discuss.: 10 December 2012
Revised: 12 April 2013 – Accepted: 19 April 2013 – Published: 15 May 2013

Abstract. The Wetland and Wetland CH_4 Intercomparison of Models Project (WETCHIMP) was created to evaluate our present ability to simulate large-scale wetland characteristics and corresponding methane (CH_4) emissions. A multi-model comparison is essential to evaluate the key uncertainties in the mechanisms and parameters leading to methane emissions. Ten modelling groups joined WETCHIMP to run eight global and two regional models with a common experimental protocol using the same climate and atmospheric carbon dioxide (CO_2) forcing datasets. We reported the main conclusions from the intercomparison effort in a companion paper (Melton et al., 2013). Here we provide technical details for the six experiments, which included an equilibrium, a transient, and an optimized run plus three sensitivity experiments (temperature, precipitation, and atmospheric CO_2 concentration). The diversity of approaches used by the models is summarized through a series of conceptual figures, and is used to evaluate the wide range of wetland extent and CH_4 fluxes predicted by the models in the equilibrium run. We discuss relationships among the various approaches and patterns in consistencies of these model predictions. Within this group of models, there are three broad classes of methods used to estimate wetland extent: prescribed based on wetland distribution maps, prognostic relationships between hydrological states based on satellite observations, and explicit hydrological mass balances. A larger variety of approaches was used to estimate the net CH_4 fluxes from wetland systems. Even though modelling of wetland extent and CH_4 emissions has progressed significantly over recent decades, large uncertainties still exist when estimating CH_4 emissions: there is little consensus on model structure or complexity due to knowledge gaps, different aims of the models, and the range of temporal and spatial resolutions of the models.

1 Introduction

In order to study the importance of wetlands in the global water and carbon cycle a variety of hydrological and biogeochemical models have been developed over the last three decades. The first studies of global-scale wetland CH_4 modelling appeared twenty-five years ago (Matthews and Fung, 1987). Matthews and Fung (1987) combined vegetation, soil and fractional inundation maps along with estimates of CH_4 flux intensity to generate a map of global wetland distribution and an annual wetland emissions estimate of $\sim 100\,\mathrm{Tg\,CH_4\,yr^{-1}}$. Aselman and Crutzen (1989) soon followed developing their own wetland distribution datasets, and assumed CH_4 emission flux rates, yielding a wetland emissions estimated range of 40–160 $\mathrm{Tg\,CH_4\,yr^{-1}}$. These early approaches are limited by uncertainties inherent in upscaling point measurements to large regions, and an inability to predict changes to wetland systems due to changes in climate and hydrology because of the use of static wetland extent and simple scaling-based estimates of CH_4 emissions.

As an attempt to circumvent these limitations, process-based modelling of global CH_4 emissions from wetland systems was first pioneered by Fung et al. (1991) followed by Christensen and Cox (1995), Christensen et al. (1996), and Cao et al. (1996). While those early global studies used the static wetland maps of Matthews and Fung (1987), they differed in their approach to simulate the CH_4 emissions. Christensen and Cox (1995) was the first study to introduce a formulation for oxidation and a soil vertical discretization in a one-dimensional, single-column model. The simple approach of Christensen et al. (1996) estimates net CH_4 emissions as a fraction of heterotrophic respiration calculated by an equilibrium vegetation model (BIOME2) giving a climate sensitive, but perhaps simplistic CH_4 emissions estimate. A more mechanistic approach was adopted by Cao et al. (1996) whose CH_4 emission model assumes substrate supply to methanogens is controlled by plant primary productivity and soil organic matter decomposition. Methane production is then modelled as a function of soil temperature, soil organic matter decomposition, water table position, and a fixed ratio of CH_4 production to decomposed organic carbon. Oxidation of produced CH_4 is assumed to scale with gross primary productivity (GPP) and to increase to a fixed fraction under non-inundated conditions (Cao et al., 1996).

None of these initial modelling studies performed transient simulations and the models originally accounted for hydrologic variability only in the vertical dimension, not spatially within model grid cells. Other process-based models soon followed but were not applied on a global scale, at least initially (Walter et al., 1996; Potter, 1997; Walter and Heimann, 2000). These initial papers included mechanistic modelling of such processes as diffusive, aerenchymal, and ebullition gas and oxygen transport. More recent work has devoted much effort to improving modelling of these processes (Segers and Leffelaar, 2001; van Bodegom et al., 2001a,b; Zhuang et al., 2006) and other controls on CH_4 production such as pH (Zhuang et al., 2004). Oxidation in the oxic portion of the soil, water column, and rhizosphere has also been parameterized (Ridgwell et al., 1999; Segers and Leffelaar, 2001; Zhuang et al., 2006; Curry, 2007, 2009). Model simulations have also moved on from equilibrium-only simulations to transient simulations (Walter et al., 2001a,b; Shindell et al., 2004; Gedney et al., 2004; Zhuang et al., 2006). Regional- to global-scale models have now been applied for the recent past (Ringeval et al., 2010; Hodson et al., 2011; Spahni et al., 2011; Riley et al., 2011), more distant past climates (Kaplan, 2002; Valdes et al., 2005; Hopcroft et al., 2011; Singarayer et al., 2011; Beerling et al., 2011), and to project responses to future climate change (Shindell et al., 2004; Gedney et al., 2004; Bohn et al., 2007; Bohn and Lettenmaier, 2010; Ringeval, 2011). Wetland and wetland CH_4 models are now becoming included in intermediate complexity (Shindell et al., 2004; Gedney et al., 2004; Avis et al., 2011) and comprehensive (Riley et al., 2011) global climate and earth system models.

Table 1. Description of the WETCHIMP modelling protocol.

Name	Experiment	Climate years	Description
Experiment 1-equil	Equilibrium	1901–1931	Spin-up of models with 1901–1931 climate until equilibrium.
Experiment 2-trans	Transient	1932–2009	Continuing from equilibrium, models are run transiently. Comparison phase is 1993–2004.
Experiment 3-opt	Optimized	User-defined	Model run with user selected "optimal" configuration. Comparison phase is 1993–2004.
Experiment 4-CO_2	Atmospheric [CO_2] sensitivity	1901–1931	From the model state at end of Experiment 1-equil simulation, apply a globally uniform step increase in [CO_2] to reach SRES A2 2100 levels (857 ppmv). Run model until equilibrium[a] is re-established.
Experiment 5-T	Temperature sensitivity	1901–1931	From the model state at end of equilibrium run, apply a step increase in air temperature reflecting mean SRES A2 2100 increase (multi-model mean SAT warming for 2090 to 2099 relative to 1980 to 1999: $\approx +3.4\,^{\circ}$C). Run model until equilibrium[a] re-established.
Experiment 6-P	Moisture sensitivity	1901–1931	From the model state at end of transient equilibrium run, a step increase in precipitation to reflecting mean SRES A2 2100 increase (30 yr average 2071 to 2100 relative to 1961 to 1990: $\approx +3.9\,\%$[b]). Run model until equilibrium[a] re-established.

[a] Each modelling group used their own criteria for what equilibrium meant: LPJ-WHyMe, LPJ-Bern, SDGVM used the stability of the soil C pool; UVic-ESCM used soil moisture and temperature variables; DLEM specified an upper limit for inter-annual changes in total ecosystem C storage ($< 0.1\,\mathrm{g\,C\,m^{-2}}$), soil moisture ($< 0.1$), and nitrogen storage ($< 0.1\,\mathrm{g\,N\,m^{-2}}$). LPJ-WSL used soil and vegetation carbon. IAP-RAS is an equilibrium model and thus does not require spin-up. [b] As the IPCC AR4 report does not contain a globally averaged number for the mean precipitation change, this value is from the IPCC TAR Report of 2001.

A number of models have also integrated approaches allowing for dynamic wetland response to climate changes. Approaches to simulate wetland distribution in order to study the interaction between climate and free water bodies were developed by Coe (1997, 1998) and Krinner (2003). The earliest attempt at wetland modelling for the purpose of estimating wetland CH_4 emissions was designed to estimate wetland emissions during the Last Glacial Maximum (LGM, ~ 21 ka; Kaplan, 2002). The simple scheme of Kaplan (2002) used threshold values of slope and soil moisture content to define wetland areas, with the soil moisture calculated by an equilibrium vegetation model (BIOME4); an approach adopted by other models (Shindell et al., 2004; Weber et al., 2010; Avis et al., 2011). Later schemes used land cover datasets to outline peatland regions (Wania et al., 2009a, 2010; Spahni et al., 2011), and/or satellite-derived inundation datasets to prescribe wetlands either directly (Hodson et al., 2011; Ringeval et al., 2010), or indirectly (Ringeval et al., 2011; Riley et al., 2011). Other wetland distribution schemes use internally calculated water table positions or soil moisture thresholds to locate wetlands (Chen et al., 2012).

In this context, the Wetland and Wetland CH_4 Intercomparison of Models Project (WETCHIMP) was designed to offer the first multi-model comparison highlighting similarities and differences between modelling approaches and results. The advantage of using a multi-model comparison is that the range of the current state-of-the-art model estimates for wetland extent and CH_4 emissions can be studied in parallel. This approach allows us to study the sources of uncertainties and spatial and temporal differences in model behaviour. The results of this multi-model comparison are presented in Melton et al. (2013). In this paper, we provide the technical background for WETCHIMP, presenting details of the modelling protocol (Sect. 2), descriptions of the models as used for WETCHIMP (Sect. 3), conceptual comparisons of the models involved and results from the model default simulation to illustrate the differences between models are presented in Sect. 4. Following the definitions set out in Melton et al. (2013), we define wetlands for the purpose of large-scale modelling as grid cells, or fractions thereof, where the land surface has inundated, or saturated, conditions. Peatlands are a form of wetlands characterized by fixed extent, at least on timescales of decades, and contrasting hydrologic and nutrient regimes between dry nutrient-poor bogs and wet nutrient-rich fens (Melton et al., 2013). Inundated areas are assumed to be wetlands (unless masked out with a rice agriculture or lake dataset) with the water table above, or at the soil surface, but do not include areas that are unsaturated at the soil surface but saturated at depth.

2 Modelling protocol

The models participating in WETCHIMP followed a common modelling protocol outlined in Table 1 and adhered to it as closely as possible; divergences from the modelling protocol are described in the individual model description section.

Table 2. List of experiments (described in Table 1) performed by each of the participating modelling groups. "Prognostic" indicates that a model located at least part of its wetlands based either on an inversion to GIEMS and modelled hydrological state or used GIEMS as a spatial or temporal constraint. "Prescribed" means that the model used a distribution map for wetlands and "simulated" means that the model did not input any kind of wetland observational data to locate wetlands (see Sect. 4.1).

Model	Areal extent	Wetlands	CH_4 fluxes	Experiments performed	Contact
CLM4Me	global	prognostic	simulated	1, 2, 3, 4, 5, 6	W. J. Riley
DLEM	global	prognostic	simulated	1, 2, 3, 4, 5, 6	H. Tian
IAP-RAS	global	prescribed	simulated	1, 2, 3, , 5, 6	A. V. Eliseev
LPJ-Bern	global	prognostic	simulated	1, 2, 3, 4, 5, 6	R. Spahni
LPJ-WHyMe	35–90° N	prescribed	simulated	1, 2, , 4, 5, 6	R. Wania
LPJ-WSL*	global	prescribed	simulated	1, 2, 3, 4, 5, 6	E. L. Hodson
ORCHIDEE	global	prognostic	simulated	1, 2, 3, 4, 5, 6	B. Ringeval
SDGVM	global	simulated	simulated	1, 2, , 4, 5, 6	P. O. Hopcroft
UVic-ESCM	global	simulated	n/a	1, 2, 3, 4, 5, 6	C. A. Avis
UW-VIC	W-Siberia	prognostic	simulated	1, 2, 3, , ,	T. Bohn

* LPJ-WSL uses the "prognostic" approach for Experiment 3-opt, using GIEMS as guidance for the wetland distribution.

As briefly described in Melton et al. (2013), WETCHIMP consisted of six experiments, including both a transient simulation and several equilibrium state simulations with step-changes to climate forcing. The first experiment ("Experiment 1-equil") was an equilibrium simulation under repeating 1901–1931 climate and a carbon dioxide concentration ($[CO_2]$) of 303 ppmv. The second experiment ("Experiment 2-trans") was a transient historical simulation from 1901–2009, using observed climate and atmospheric CO_2 concentration ($[CO_2]$), with the final (equilibrium) state of Experiment 1-equil as its initial state. Some models require observed fractional inundation values as an input; these were provided and cover the period 1993–2004 by the Global Inundation Extent from Multi-Satellites (GIEMS) dataset (Prigent et al., 2007; Papa et al., 2010). Thus, the period 1993–2004 was selected from Experiment 2-trans for comparison of model results. A third experiment ("Experiment 3-opt") was run for the same time period as Experiment 2-trans, but allowed the models to run under user-defined optimal configurations (e.g. running coupled into an earth system model or using different meteorological forcing or remotely sensed inundation datasets than those common to Experiment 2-trans).

The remaining three experiments applied step-changes to each model's equilibrium state from Experiment 1-equil. The fourth experiment ("Experiment 4-CO_2") applied an instantaneous increase in atmospheric $[CO_2]$ to 857 ppmv (SRES A2 year 2100 levels from IPCC, 2000) while holding the other meteorological inputs identical to Experiment 1-equil; this perturbed simulation was then run until each model had reached a new equilibrium state. Experiment 5 ("Experiment 5-T") investigated the effect of an instantaneous increase of +3.4 °C in surface air temperature (SAT). The magnitude of this increase was chosen from the SRES A2 year 2100 multi-model mean SAT warming for the period 2080–2099 relative to 1980–1999 (Meehl et al., 2007). The final experiment ("Experiment 6-P") examined model responses to changes in precipitation with an instantaneous increase of +3.9 % (SRES A2 2100 level; 30 yr global average for 2071–2100 relative to 1961–1990) (Prentice et al., 2001). In all cases, the step increases were applied to all months and grid cells uniformly. While actual changes in climate are projected to vary in both space and time, these uniform changes are suitable for the purpose of sensitivity tests (Melton et al., 2013). An overview of which groups conducted which simulations is shown in Table 2.

All data are freely available for download on http://arve.epfl.ch/pub/wetchimp, please send request for a username and password to joe.melton.sci@gmail.com.

2.1 Datasets

2.1.1 Climate data

The CRU (Climate Research Unit) TS3.1 time series (Mitchell and Jones, 2005; Jones and Harris, 2008) was used for monthly climate forcing data and – dependent on the model – precipitation, 2 m air temperature, percentage cloud cover, number of wet days, and vapour pressure were used from this dataset. Models that required data with a higher temporal resolution used the CRUNCEP (CRU and National Centre for Environmental Prediction) data, which is the correction of the 6 hourly NCEP reanalysis by the CRU TS3.1 data (Viovy and Ciais, 2011). CRUNCEP provides incoming long- and short-wave radiation, air specific humidity (used to compute the relative humidity), pressure, total precipitation, temperature, and the zonal and meridional components of the wind. UVic-ESCM (University of Victoria – Earth System Climate Model) used surface winds and diurnal temperature range from the NCEP reanalysis directly.

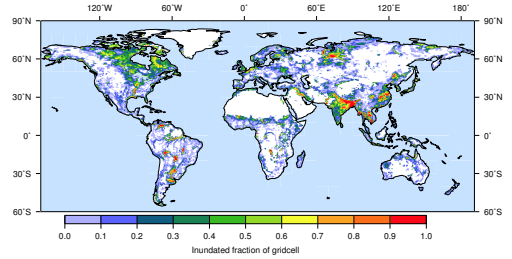

Fig. 1. Mean annual maximum fraction of inundated land between 1993 and 2004 identified by a multi-satellite approach (Papa et al., 2010). White areas indicate areas of no inundation.

2.1.2 Soil and wetland distribution data

The soil data used in WETCHIMP are given in Table 3 and are allocated to each model in Table 4. The model requirements for soil data are too broad to accommodate a uniform soil dataset easily. Soil datasets used, and model treatment of soil textural information, are thus considered part of the wetland model itself.

There are several wetland distribution maps that were used for our simulations: (i) remotely sensed inundation area from GIEMS (Prigent et al., 2007; Papa et al., 2010) (Fig. 1), (ii) northern peatland distribution from NCSCD (Northern Circumpolar Soil Carbon Database; Tarnocai et al., 2007, 2009) (Fig. 2), and (iii) peatland distribution for the West Siberian Lowlands (Sheng et al., 2004) (Fig. 3). In addition, some groups made use of the rice distribution dataset by Leff et al. (2004) (Fig. 4) and the GICEW water bodies and land ice dataset (Fig. 5) to exclude areas from their wetland distribution map.

2.1.3 Global Inundation Extent from Multi-Satellites (GIEMS)

As the GIEMS dataset is used extensively by several models, and forms a comparison for the model outputs in Melton et al. (2013), it will be described in more detail here. The GIEMS dataset (Fig. 1) is a global, multi-year product quantifying the monthly variations of the distribution and extent of episodic and seasonal inundations, wetlands, rivers, lakes and irrigated agriculture at 0.25° resolution at the equator. GIEMS is derived from a complementary suite of satellite observations including passive microwave observations (SSM/I (special sensor microwave/imager) emissivities), active microwave observations (ERS scatterometer), along with AVHRR-NDVI (Advanced Very High Resolution Radiometer-normalized difference vegetation index). The complete methodology is described in detail in Prigent et al. (2007) and Papa et al. (2010) and is briefly summarized here. First, an unsupervised classification of the three sources

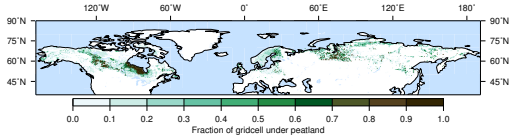

Fig. 2. Fraction of land covered by northern peatlands at present (Tarnocai et al., 2007, 2009).

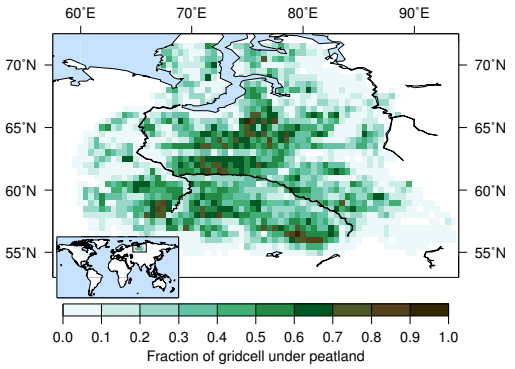

Fig. 3. Fraction of land covered by peatlands at present in the West Siberian Lowlands. Data were taken from Sheng et al. (2004) and aggregated to a $0.5° \times 0.5°$ grid by T. Bohn.

of satellite data is performed, and pixels with satellite signatures likely related to inundation are retained. For each inundated pixel, the monthly fractional coverage by open water is obtained using the passive microwave signal and a linear mixture model with end-members calibrated with scatterometer observations to account for the effects of vegetation cover. We use here the dataset available at a monthly timescale for the period 1993–2004. More detailed information concerning the seasonal and inter-annual behaviour of GIEMS dataset can be found in Prigent et al. (2012) for the global-scale analysis and in Papa et al. (2006) and Papa et al. (2008) for for the tropical and boreal regions, respectively.

3 Participating models

In this section, we describe each model briefly and refer to published papers where more detailed information can be found. Modifications to models that were made after recent publications or specifically for WETCHIMP are described in the respective model section. An overview of which models performed which experiments is given in Table 2 and a list of forcing data for each model is provided in Table 4. The models follow the prescribed modelling protocol listed in Table 1 unless otherwise stated in the respective model description.

Table 3. Names and types of input datasets together with references and a list of models that used the data.

Name of dataset	Description	Used by	Reference
CRU TS3.1	Climate	All models[a]	Mitchell and Jones (2005); Jones and Harris (2008)
CRUNCEP	Climate	All models[a]	Viovy and Ciais (2011)
Law Dome Composite	CO_2	All models	http://grkapweb1.epfl.ch/pub/ARVE_tech_report2_co2spline.pdf
Dentener et al. (2006)	Nitrogen deposition	DLEM	Dentener et al. (2006)
FAO	Soil texture classes	ORCHIDEE	Batjes (1997)
HWSD	Soil texture classes	LPJ-Bern	FAO/IIASA/ISRIC/ISSCAS/JRC (2009)
IGBP-DIS	Soil texture classes	CLM4Me, DLEM	Global Soil Data Task Group (2000)
ISLSCP I	Soil texture classes	SDGVM	Sellers et al. (1996)
ISLSCP II	Soil texture classes, soil carbon density	UVic-ESCM	ISLSCP-II (2009)
MODIS	Distribution of plant functional types (PFTs)	UW-VIC	Bartalev et al. (2003)
ETOPO 2v2	Topography	SDGVM, UVic-ESCM	ETOPO (2006)
HYDRO1k	Topography	ORCHIDEE	http://webgis.wr.usgs.gov/globalgis/metadata_qr/metadata/hydro1k.htm
CLM soil colours	Soil colours	CLM4Me	Lawrence and Chase (2007)
GIEMS	Monthly inundated wetland area 1993–2004 (Fig. 1)	CLM4Me, DLEM, LPJ-Bern, LPJ-WSL, ORCHIDEE, UW-VIC[b]	Prigent et al. (2007); Papa et al. (2010)
Schroeder et al. (2010)	Remotely sensed inundation dataset	UW-VIC[c]	Schroeder et al. (2010)
CDIAC NDP017	Wetland area	IAP-RAS	http://cdiac.esd.ornl.gov/ndps/ndp017.html
GLWD	Global land cover	DLEM	Lehner and Döll (2004)
NCSCD	Annual fractional cover of northern peatlands (Fig. 2)	LPJ-Bern, LPJ-WHyMe	Tarnocai et al. (2007, 2009)
Sheng	Peatland fraction (Fig. 3) and peat depths	UW-VIC	Sheng et al. (2004)
Leff	Annual fractional cover of rice fields scaled by monthly inundation (Fig. 4)	DLEM, LPJ-Bern, LPJ-WSL	Leff et al. (2004), Spahni et al. (2011)
Fries et al. (1998)	Global land cover	DLEM	Fries et al. (1998)
GICEW	Waterbodies and land ice excluding ice sheets (Fig. 5)	LPJ-Bern	http://luh.sr.unh.edu/

[a] These datasets were required for use in Experiments 1, 2, 4, 5, and 6. [b] Used in experiments 1 and 2. [c] Used in experiment 3.

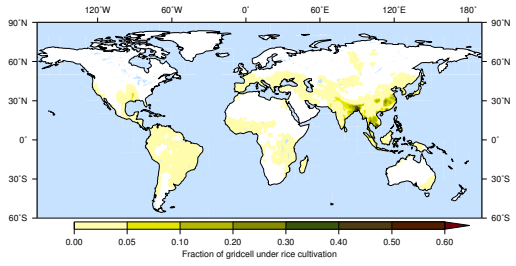

Fig. 4. Annual maximum fraction of land covered by rice fields (Leff et al., 2004).

3.1 CLM4Me

The version of CLM4Me used for this project is described in Riley et al. (2011), and is incorporated into the Community Land Model 4 (CLM4; Lawrence et al., 2011), the land-surface component of CESM1 (Community Earth System Model 1). Using the hydrology, soil carbon cycling, and soil thermal physics predicted in CLM4, net CH_4 fluxes are computed separately in inundated and non-inundated areas in each grid cell, including uptake of atmospheric CH_4. The reaction and transport equations for CH_4 and oxygen (where applicable) include production, consumption, aerenchyma transport, ebullition, and diffusion.

3.1.1 WETCHIMP set-up

The CH_4 model code deviates slightly from that described in Riley et al. (2011); these changes resulted in less than a 5 % difference from the global budget presented in Riley et al. (2011). The changes in the code include: (i) the calculation of below-ground root mass for determining aerenchyma area now uses the time-lagged (1 yr decay time) belowground-to-aboveground NPP (net primary productivity) ratio, instead of the instantaneous one, and (ii) in calculating the water availability for permafrost vegetation, root fraction is weighted over all soil layers down to last year's maximum active layer depth, rather than the instantaneous active layer depth, thereby causing a slight delay in growth in the spring.

Table 4. A list of the models that contributed simulations to WETCHIMP. The "Wetland types" gives a quick overview of what kind of wetlands are used or simulated by each model. The explanations for the wetland types and soil datasets, as well as the full references are given in Table 3.

Model	Resolution (lon × lat)	Wetland types	Climate forcing	Soil data
CLM4Me	2.5° × 1.9°	Simulated inundated area based on predicted water table and runoff and an inversion to GIEMS	CRUNCEP	IGBP-DIS
DLEM	0.5° × 0.5°	Mixture between prescribed and simulated, rice mask by Leff	CRUNCEP	IGBP-DIS
IAP-RAS	0.5° × 0.5°	Olson data for wetlands (bogs/mires, swamps, heaths/ moorlands, tundra)	CRU3.1	Peat in peatlands, loam elsewhere
LPJ-Bern	0.5° × 0.5°	Peatlands from NCSCD, inundated wetlands from GIEMS, rice mask by Leff, permanent water or ice from GICEW, simulated wet soils	CRU3.1	HWSD
LPJ-WHyMe	0.5° × 0.5°	Peatlands from NCSCD	CRU3.1	n/a[a]
LPJ-WSL	0.5° × 0.5°	Inundated area from GIEMS, rice mask by Leff for all experiments except 3[b]	CRU3.1	FAO
ORCHIDEE	1° × 1°	Simulated, but annual mean over 1993–2004 adjusted to mean of GIEMS	CRUNCEP	FAO for mineral
SDGVM	0.5° × 0.5°	All simulated	CRU3.1	ISLSCP I
UVic-ESCM	3.6° × 1.8°	All simulated	CRU3.1+NCEP[c]	ISLSCP II
UW-VIC	100 km[d]	Simulated lakes and peatlands	CRUNCEP	FAO for mineral soils, Sheng for peatland fraction

[a] LPJ-WHyMe is a peatland only model, thus no "soil" data is required. [b] LPJ-WSL Exp. 3 is a mix between prescribed (GIEMS) and simulated inundation area based upon an empirical relationship between simulated water runoff and GIEMS. [c] Surface winds and diurnal temperature are taken from the NCEP reanalysis. [d] 100 km polar azimuthal equal area grid (EASE grid), resampled to 0.5° × 0.5°.

The CLM model requires a number of forcings in addition to the lower atmospheric boundary conditions and fluxes specified in the CRUNCEP forcing. For all the experiments except Experiment 3-opt, the standard CLM4 year 2000 conditions are used for atmospheric [CO_2] experienced by plant stomata (except Experiment 4-CO_2), atmospheric nitrogen deposition, atmospheric aerosol deposition, and vegetation distributions. For Experiment 3-opt, the same configuration as in Riley et al. (2011) is used, namely a spin-up to "1850" conditions using the 1850 [CO_2], nitrogen, aerosols, and vegetation distributions, and then repeated 1948–1972 (Qian et al., 2006) corrected-NCEP forcing. A transient simulation from 1850–2004 is run using transient data for [CO_2], nitrogen, aerosols, and vegetation, using repeated 1948–1972 forcing through 1972, at which point the model is switched to actual-year forcing through 2004.

The model is run at 1.9° × 2.5° resolution and the standard CLM4 datasets are used, except that the default CLM4 1×10^6 km^2 of inland non-vegetated wetland area that were used in Riley et al. (2011), were eliminated. As described in that paper, the CLM4Me model requires three parameters at each grid cell to calculate the inundated fraction as a function of the modelled water table and lagged surface runoff, based on an inversion to Prigent et al. (2007) satellite observations for 1994–1998. For WETCHIMP, the parameters generated in a previous model described in Riley et al. (2011) were used (similar to Experiment 3-opt); however, the parameters were not re-optimised with the CRUNCEP forcing, hence the CRUNCEP 1990s inundated area (e.g. Experiment 2-trans) may differ from that simulated in Experiment 3-opt.

3.2 DLEM

The Dynamic Land Ecosystem Model (DLEM) is a process-based model that simulates daily carbon, water and nitrogen fluxes and pool sizes for land and riverine ecosystems. These pools and fluxes are influenced by changes in atmospheric chemistry (CO_2, ozone concentration and nitrogen deposition), climate, land cover and land use change, management practices (e.g. irrigation, fertilization, rotation, and technology improvement), and other disturbances (e.g. fire, hurricane, insects, disease, and forest harvest) (Tian et al., 2010, 2011a,b, 2012). For WETCHIMP, the disturbance submodel

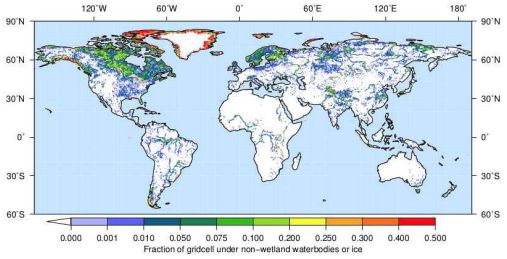

Fig. 5. Fractional grid cells covered by permanent water bodies or ice are not considered to be wetlands (GICEW, http://luh.sr.unh.edu/). The Greenland ice sheet is masked out.

and the influence of ozone chemistry were not used due to a lack of spatially explicit driving data.

The soil biogeochemistry module simulates CH_4 uptake in upland ecosystems and emissions in wetland ecosystems. The mechanisms and algorithms for simulating CH_4 fluxes have been described in Tian et al. (2010, 2011b); Xu et al. (2010). DLEM requires input datasets for daily climate (average, maximum, and minimum air temperature, precipitation, gross radiation, and relative air humidity), atmospheric composition ([CO_2], nitrogen deposition and ozone), annual land use information, soil condition information (soil texture, pH, and soil depth), and topographic data (elevation, slope, and aspect).

Wetlands are defined as those areas that are inundated or saturated by surface water at a frequency and duration sufficient to support vegetation growth, which leads to five wetland types: (i) rice paddy, (ii) permanent herbaceous wetland, (iii) permanent woody wetland, (iv) seasonal herbaceous wetland and (v) seasonal woody wetland. The distribution map for different wetland types are determined based on the data from Stillwell-Soller et al. (1995); Aselman and Crutzen (1989) and Lehner and Döll (2004). DLEM simulates water transport to rivers based upon catchments, but does not explicitly move water through grid cells and thereby does not influence conditions in neighbouring grid cells. The version of DLEM used to simulate CH_4 fluxes for WETCHIMP has been described by Tian et al. (2010, 2011a); Xu et al. (2010). The CH_4 exchanges between ecosystems and the atmosphere are a combination of CH_4 production, oxidation, and transport from soil/water to the atmosphere. DLEM only considers CH_4 production from dissolved organic carbon (DOC), which is indirectly controlled by environmental factors including soil pH, temperature, soil texture and soil moisture content.

3.2.1 WETCHIMP set-up

The input data except those specifically mentioned in the experimental designs were kept constant at 1993 levels during

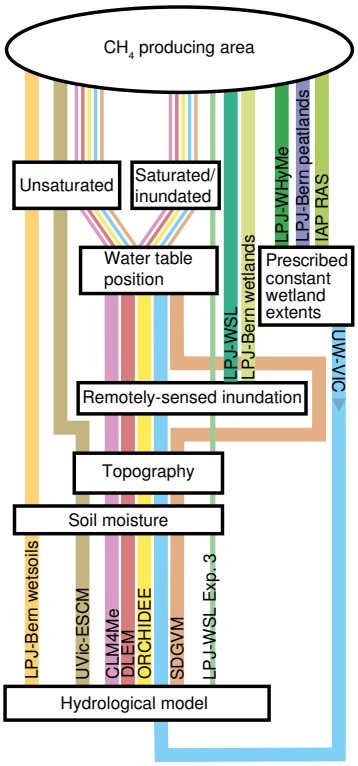

Fig. 6. Conceptual overview of how the participating models derive their "CH_4 producing area" (MPA). Each model (and in some cases, version) is represented by a different colour. The flow of a particular model starts with the model's name and ends at the "CH_4 producing area". The simplest models rely on "Prescribed constant wetland extents" to define their MPAs (LPJ-WHyMe, LPJ-Bern peatlands, IAP-RAS), whereas UW-VIC uses "Prescribed constant wetland extents" only as maximal boundaries. LPJ-WSL and LPJ-Bern wetlands use remotely sensed inundation directly. "Soil moisture" is exclusively simulated by a "Hydrological model" and is used to either derive "Unsaturated" MPAs directly (LPJ-Bern wetsoils) or in combination with "Topography" (UVic-ESCM). Of the remaining models that use "Topography", all but SDGVM depend on "Remotely-sensed inundation" data to arrive at the "Water table position", which CLM4Me, DLEM, ORCHIDEE, UW-VIC and SDGVM use in combination with the other factors (e.g. CLM4Me also uses runoff) to determine "Unsaturated" and "Saturated/inundated" MPAs. LPJ-WSL (Exp. 3) uses "Water table position" to obtain only the "Saturated/inundated" MPA. The order in which processes are calculated do not always strictly follow the path used in this schematic representation.

the WETCHIMP simulations. DLEM was run at a daily time step and a $0.5^\circ \times 0.5^\circ$ spatial resolution. For experiments 1, 4, 5, and 6, DLEM used wetland extent data in 1993 as input, while for experiments 2 and 3, transient wetland extent data was used. Before running it at the global scale, DLEM was first calibrated against field experimental and observational data. The parameters and their values were described in Tian et al. (2010) and Xu et al. (2010). The water cycle module in DLEM used for the WETCHIMP simulations differs from the previous version used in DLEM publications (e.g. Tian et al., 2012). The main difference can be found in the water cycle module, which simulates the dynamics of inundated surface water extent and water table position Liu et al., 2012. The new water cycle module uses components of previously published models, TOPMODEL (Topography based hydrological model; Beven and Kirkby, 1979), SIMTOP (Simple TOPMODEL; Niu et al., 2005) and CLM (Oleson et al., 2008), to improve its soil and surface water dynamics (Liu et al., 2012).

To integrate the GIEMS inundation fraction and rice paddy (Leff et al., 2004) datasets with the DLEM-simulated wetland distribution, some of the DLEM parameterizations were adapted for a semi-prognostic approach to determine wetland area. DLEM separately simulated the extent of two major natural wetland types: permanent and seasonal wetlands. For the permanent natural wetland distribution, areas of the GIEMS dataset that were continually inundated during the growing season (May to August) of 1993–2004 were regarded as permanent wetlands. In these areas, the soil moisture was prescribed at saturation. Excluding areas of permanent wetlands, seasonal wetlands were determined using the DLEM prognostic parameterizations as discussed previously. Thus minimum annual wetland area is controlled by the GIEMS dataset, but daily and seasonal wetland area dynamics above this were determined by internal DLEM model dynamics and controlled by the maximum wetland extent data. The maximum (or potential) wetland extent data was generated based on GIEMS data by taking the largest inundated percentage in each grid cell during 1993–2004. DLEM did not specifically separate peatland from other wetland types. Instead, we separated the five wetland types (listed above) – based on the soil moisture condition and land cover types – for which the CH_4 module is run. The remaining non-inundated fraction in each grid cell was treated as upland land cover. We separately ran each fraction of the grid cells. Before simulations lakes and rivers were masked out using the GWLD (Global Wetland and Lakes Database) dataset (Lehner and Döll, 2004) and rice with the Leff datset (Leff et al., 2004).

3.3 IAP-RAS model

The present version of the IAP-RAS (Institute of Applied Physics – Russian Academy of Sciences) wetland CH_4 emission module is described by Mokhov et al. (2007). The module consists of two parts; one for soil temperature calculations, and a second for calculations of CH_4 emissions. Soil temperature is calculated based on the model by Kudryavtsev et al. (1977). This model represents a generalized solution of Stephan's problem with annual temperature variations at the lower boundary of the atmosphere, while accounting for the influence of snow and moss cover. Moss cover is prescribed as a layer of 10 cm thickness in presence of boreal and tundra vegetation. The depth of seasonal thaw/freeze depends on the annual variation of the near-surface temperature and precipitation. The influence of the effect of snow metamorphism is ignored. The seasonal thaw depth was assessed based on the thickness of the active layer and temperature of the soil surface. Only soil layers to a certain limit depth were included in the calculations. In the standard version, the depths of 15 and 60 cm were used for tropical and extratropical zones, respectively. Similar depth values are obtained for the organic carbon content in soil at the characteristic peat density of 200 $\mathrm{kg\,m^{-3}}$ based on data from http://soils.usda.gov/use/worldsoils/mapindex/soc.html. Deeper layers were ignored in calculations of CH_4 emissions by wetlands. The amount of water in wetlands is considered to be always sufficient for inundation. Methane emissions are calculated based on the empirical model of Christensen and Cox (1995).

3.3.1 WETCHIMP set-up

For WETCHIMP simulations, the model was run at $0.5^\circ \times 0.5^\circ$ resolution using CRU TS3.1 dataset as climate forcing (Mitchell and Jones, 2005). Wetland areal extent was prescribed according to the CDIAC (Carbon Dioxide Information Analysis Center) NDP017 dataset, also known as the Olson database (http://cdiac.esd.ornl.gov/ndps/ndp017.html). In this dataset, only areas with ecosystem codes 44 ("bog/mire of cool or cold climates"), 45+72 ("warm and hot wetlands"), 64 ("heath and moorland"), and 53 ("tundra") are considered as wetlands. The inclusion of tundra regions as methane–producing area was specifically for WETCHIMP; earlier applications of IAP-RAS model neglected their contribution. Outside of wetlands, soil thermophysical parameters are homogeneously prescribed as loam everywhere.

3.4 LPJ-Bern

LPJ-Bern is a subsequent development of the Lund-Potsdam-Jena dynamic global vegetation model (Sitch et al., 2003; Joos et al., 2004; Gerber et al., 2003) that combines process-based, large-scale representations of terrestrial vegetation dynamics, soil hydrology (Gerten et al., 2004; Wania et al., 2009a), human induced land use changes (Strassmann et al., 2008; Stocker et al., 2011), permafrost and peatland establishment (Wania et al., 2009a,b) and simulation of biogeochemical trace gas emissions, such as CH_4 (Wania et al., 2010; Spahni et al., 2011; Zürcher et al., 2013).

3.4.1 WETCHIMP set-up

The CH_4 model within the LPJ-Bern version differs slightly from the LPJ-WHyMe (LPJ Wetland Hydrology and Methane) CH_4 model that was used in Wania et al. (2010) and Spahni et al. (2011). The main differences with respect to CH_4 emissions concern peatland modelling, global carbon cycle parameters and input data. The differences between the model as used in this study and Spahni et al. (2011) (and thus to LPJ-WHyMe version 1.3.1, Wania et al., 2010) are described below ordered by CH_4 source and sink category.

LPJ-Bern uses a different ebullition mechanism for CH_4 emissions from peatlands, which includes variations in partial pressure of CO_2 (Zürcher et al., 2013). The carbon balance over all layers is now preserved after every gas diffusion time step, whereas in LPJ-WHyMe a correction factor for carbon balance is applied at the end of the year. The possible plant functional types in peatlands are limited to flood-tolerant graminoids and *Sphagnum* mosses. Additionally, the prescribed fractional peatland cover per grid cell is taken from NCSCD (Tarnocai et al., 2007, 2009). NCSCD covers histels and histosols in the northern high-latitudes with a total area of 2.7×10^6 km^2, which is larger than the extent (2.06×10^6 km^2) used in Spahni et al. (2011). The global scaling factor used by Wania et al. (2010) to account for the lack of microtopography in the model is thus reduced from 75 to 26 % to constrain CH_4 emissions from peatlands in 2004 to 28.2 Tg CH_4 yr^{-1} (Spahni et al., 2011).

For CH_4 emissions in inundated areas the GIEMS monthly fractional inundation dataset for 1993–2004 was averaged by month (e.g. mean January, mean February, etc.). The fractional area of inundation per grid cell is further limited by the fraction of land available, i.e. land not covered by permanent water or ice (GICEW, http://luh.sr.unh.edu/). In grid cells containing peatlands (35–90° N), the inundated fraction was assumed to include peatlands. If the inundated fraction exceeds the constant peatland fraction, the difference is interpreted as the inundated fraction of mineral soils. This is different to the treatment in Spahni et al. (2011), where the inundated fraction was explicitly set to zero north of 45° N. The fraction of inundated areas was further divided into natural wetlands and rice agriculture using the scheme as described in Spahni et al. (2011). For these two categories the CH_4 to CO_2 conversion tuning parameter was adjusted to obtain total CH_4 emissions in 2004 of 81.3 Tg CH_4 yr^{-1} for natural wetlands and of 43.1 Tg CH_4 yr^{-1} for rice agriculture (Spahni et al., 2011).

For CH_4 emissions in wet mineral soils, the above changes were included and the remaining non-inundated and non-peatland land cover was taken as fractional area of mineral soils. These mineral soils can either function as a CH_4 source or sink, depending on their soil moisture (Spahni et al., 2011). For this study the CH_4 to CO_2 conversion factor – a global scaling factor – for CH_4 emissions from wet mineral soils was scaled to obtain emissions of 63.1 Tg CH_4 yr^{-1} for 2004. For the CH_4 uptake the concentration-to-flux tuning factor was reduced to reach a global consumption of 25.8 Tg CH_4 yr^{-1} (Spahni et al., 2011).

While the peatland fraction is a separate tile in each grid cell with its own carbon and soil water pools, the other three CH_4 source types and the sink share the same tile. So, for the non-peatland areas, there is no interaction between water table position and vegetation growth. Compared to Spahni et al. (2011), an updated soil type map based on the World Harmonized Soil Database (FAO/IIASA/ISRIC/ISSCAS/JRC, 2009) was used by selecting the dominant soil type in each $0.5° \times 0.5°$ grid cell. However, soil properties for the corresponding 9 soil types were not changed to previous simulations (Spahni et al., 2011).

When model results were compared to other WETCHIMP models a unique feature was observed in CH_4 emissions from northern peatlands as simulated by LPJ-Bern. Emissions for the years 1998, 1999 and 2001 are extremely high for some sites compared to average peatland emissions (Melton et al., 2013). Investigating the model output showed the high emission peaks in those years originates from CH_4 gas reservoirs within and below frozen peat layers. Two processes are responsible for the establishment of these CH_4 gas reservoirs. First, in LPJ-Bern, frozen peat layers act as a barrier for gas diffusion thus allowing CH_4 to accumulate beneath. Second, if environmental conditions are suitable methanogenesis can occur in unfrozen layers, regardless whether layers above are frozen. Normally, CH_4 production in deeper layers is negligible, but for the WETCHIMP simulations a considerable amount of CH_4 gas accumulated beneath a frozen layer during the model spin-up procedure (1000 yr). This stored CH_4 could not escape to the atmosphere until the year 1998 in the transient run, the first year showing an exceptional boreal warming that led to thawing of peat layers and burst emissions of CH_4. While the process as such could be questioned, the magnitude of CH_4 emissions is certainly too large, as can be concluded from the model–data comparison in the Hudson Bay lowlands (Melton et al., 2013).

3.5 LPJ-WHyMe

Methane emissions for peatlands north of 35° N were simulated using LPJ-WHyMe (Wania et al., 2009a,b, 2010; Spahni et al., 2011). Location and fractional cover of peatlands are taken from NCSCD (Tarnocai et al., 2007, 2009). Monthly air temperature, precipitation, percentage cloud cover and number of wet days are taken from CRU TS3.1 to force all simulations. The data from 1901–1930 are used repeatedly to spin-up the model for 1000 yr before running it transiently, either for 1901–1930 or 1901–2009.

3.5.1 WETCHIMP set-up

Instead of running LPJ-WHyMe only once for an average topographical microform, two parallel runs were executed for

each experiment. One run represents the wetter microform, lawns, which emit more CH_4, and the other one represents the drier microform, hummocks. The model modifications to approximate these two microforms include setting the daily drainage rate to 0.2 mm (lawns) and to 0.6 mm (hummocks), whereas it was 0 mm in Wania et al. (2010). These modifications lower the water table position in hummocks compared to lawns. The vegetation for hummocks is restricted to *Sphagnum* mosses, whereas lawns are able to grow any plant functional type depending on the water table position (Wania et al., 2009b). Methane emissions from the two parallel runs are averaged under the assumption that hummocks and hollows cover approximately the same surface area.

3.6 LPJ-WSL

The LPJ-WSL CH_4 model used in this analysis is the same as presented in Hodson et al. (2011), but has been recalibrated to a new set of regional CH_4 fluxes as noted below. The wetland CH_4 flux (E) at each $0.5^\circ \times 0.5^\circ$ grid cell (x) and monthly time step (t) is calculated as a linear function of two scaling factors ($r_{\mathrm{CH4:C}}$ and f_{ecosys}), wetland extent (A) and heterotrophic respiration (R_{hetr}) according to the following equation:

$$E(x,t) = r_{\mathrm{CH4:C}} \cdot f_{\mathrm{ecosys}}(x) \cdot A(x,t) \cdot R_{\mathrm{h}}(x,t). \quad (1)$$

The notation in Eq. (1) has been modified from Hodson et al. (2011) to follow Table 5 (to convert between the notation in Eq. (1) and Hodson et al. (2011): $r_{\mathrm{CH4:C}} = \beta$; $f_{\mathrm{ecosys}} = F$; $A = S$).

Together, $r_{\mathrm{CH4:C}}$ and $f_{\mathrm{ecosys}}(x)$ comprise the scaling ratio $F(x)$, which converts C to CH_4 fluxes and is a function of two weighted-regional scaling factors, one representing tropical (T) and another representing boreal (B) wetland climates (with temperate conditions represented as a combination of tropical and boreal). This approach allows the model to account for broad ecosystem differences in CH_4-emitting capacity between wetland types (Eq. 2). The weighting of wetland type (i.e. tropical vs boreal) in each grid cell is calculated based on surface temperature (Eq. 3).

$$F(x) = r_{\mathrm{CH4:C}} \cdot f_{\mathrm{ecosys}}(x) = \sigma(x) F_{\mathrm{T}} + (1 - \sigma(x)) F_{\mathrm{B}} \quad (2)$$

$$\sigma(x) = \exp((T(x) - T_{\max})/8), \quad (3)$$

where $T(x)$ is the mean near-surface temperature between 1960 and 1990, and $T_{\max} = 303.35\,^\circ\mathrm{K}$. $\sigma(x)$ cannot exceed 1. Equations 2 and 3 correct unintentional omissions in both equations as written in Hodson et al. (2011).

3.6.1 WETCHIMP set-up

For WETCHIMP, we constrained the scaling ratios, F_{T} and F_{B}, by minimizing the error between our model fit, inverse modelling results (Spahni et al., 2011) and a regional flux estimate from the Hudson Bay Lowlands (Pickett-Heaps et al., 2011), yielding $F_{\mathrm{T}} = 0.152$ and $F_{\mathrm{B}} = 0.049$. Total global wetland and rice fluxes were constrained at 215.8 Tg CH_4 yr^{-1}, wetland and rice fluxes north of 45° N at 39.6 Tg CH_4 yr^{-1} (Spahni et al., 2011), and wetland and rice fluxes from 50–60° N and 75–96° W at 2.3 Tg CH_4 yr^{-1} (Pickett-Heaps et al., 2011). These are different constraints than were used in Hodson et al. (2011).

R_{hetr} was calculated using the LPJ-WSL dynamic global vegetation model (DGVM), based on the LPJv3.1 DGVM (Sitch et al., 2003; Gerten et al., 2004). The monthly climatology inputs (precipitation, mean temperature, cloud cover, wet days) were taken from CRU TS3.1 and the non-gridded annual CO_2 concentration inputs to LPJ-WSL are described in Hodson et al. (2011). In addition, as in Hodson et al. (2011), soil texture was prescribed from the Food and Agriculture Organization (Zobler, 1986), using a 2-soil layer hydrological model with a total soil depth of 1.5 m. For scenarios 2 and 3, a 1000 yr spin-up was implemented by recycling the first 30 yr of climate data (1901–1930) with preindustrial CO_2 concentrations to equilibrate soil and vegetation carbon pools, followed by a transient climate and CO_2 simulation running from 1901–2005. For scenarios 1, 4, 5, and 6, instead of using a repeating 1901–1930 climate, first a 12 monthly mean annual dataset was created and repeated until equilibrium is reached. The default soil respiration equation in LPJ was used for all scenarios except experiment 3.

We used the same temperature and moisture dependent equation as in Hodson et al. (2011), which allows the soil respiration to drop to zero when soil moisture is zero. For experiment 3, we used the soil moisture–respiration equation from Sitch et al. (2003) that fixes the soil respiration to a minimum of 0.25 in the upper one meter of soil, even when soil moisture drops to values below 0.25.

For all experiments except experiment 3, wetland extent (A) represents natural wetlands and lakes and is the original, monthly varying GIEMS inundation dataset processed to $0.5^\circ \times 0.5^\circ$ spatial resolution with rice growing regions removed (Leff et al., 2004). For experiments 1, 4, 5, and 6, this wetland area satellite product was averaged across all years from 1993–2004 to create a 12 month mean wetland area product. For experiment 3, a combined satellite and model product was used, which is described in Hodson et al. (2011).

3.7 ORCHIDEE

The ORCHIDEE (Organising Carbon and Hydrology in Dynamic Ecosystems) model (Krinner et al., 2005) has been implemented with a wetland CH_4 emissions scheme. This version of ORCHIDEE has been previously used to simulate the evolution of wetland CH_4 emissions under future climate change (Koven et al., 2011) and to study the feedback between climate, atmospheric CH_4, and CO_2 (Ringeval et al., 2011). Simulations of ORCHIDEE for the current time period have also been performed and evaluated against top–down simulations to investigate the role of wetlands in the

Table 5. A general description of the dependencies of CH_4 production, CH_4 oxidation (does not include atmospheric CH_4 oxidation) and CH_4 flux. All of the fluxes are modulated by a CH_4-producing area (see Fig. 6). Parameters and variables used in the models were harmonized where possible, but identical names do not indicate identical values in the different models.

Model	CH_4 production (P)	CH_4 oxidation (O)	Atmospheric CH_4 oxidation (O_{atm})	Net CH_4 flux (F)
CLM4Me	$P = R_{het} r_{CH4:C} f_{pH} f_{pE} Q_{10}$	$O = O_{max} f_{[O_2]} f_{[CH_4]} f_\Theta Q_{10}$	$O_{atm} = R_{o,max} f_{[O_2]} f_{atm[CH_4]} f_{[CH_4]} f_\Theta Q_{10}$	$F = (P - O) f_{transport} - O_{atm}$
DLEM	$P = P_{max} C_{labile} f_T f_{pH} f_\Theta$	$O_{trans} = O_{trans,max} f_{planttrans} f_T$ $O_{soil} = O_{soil,max} f_{[CH_4]} f_{T_{soil}} f_{pH} f_{oxid,\Theta}$	$O_{atm} = O_{atm,max} f_{atm[CH_4]} f_{T_{air}} f_{pH} f_{oxid,\Theta}$	$F = (P - O_{trans} - O_{soil}) f_{transport} - O_{atm}$
IAP-RAS	$P = f_T$	–	–	$F = P f_\Theta Q_{10}$
LPJ-Bern peat	$P = R_{het} r_{CH4:C} f_{root} f_{WTP}$	$O = f_{[O_2]} f_{[CH_4]} r_{O_2}$	–	$F = (P - O) f_{transport}$
LPJ-Bern wetlands	$P = R_{het} r_{CH4:C}$	–	–	$F = P$
LPJ-Bern rice	$P = R_{het} r_{CH4:C}$	–	–	$F = P$
LPJ-Bern wetsoils	$P = R_{het} r_{CH4:C} f_\Theta$	–	$O_{atm} = f_{atm[CH_4]} f_T f_\Theta f_{soil}$	$F = P - O_{atm}$
LPJ-WHyMe	$P = R_{het} r_{CH4:C} f_{root} f_{WTP}$	$O = f_{[O_2]} f_{[CH_4]} r_{O_2}$	–	$F = (P - O) f_{transport}$
LPJ-WSL	$P = R_{het} r_{CH4:C} f_{ecosys}$	–	–	$F = P$
ORCHIDEE	$P = R_0 C_{labile} f_{WTP} f_T Q_{10}$	$O = f_{WTP} f_{[CH_4]} Q_{10}$	–	$F = (P - O) f_{transport}$
SDGVM	$P = R_{het} r_{CH4:C} f_{WTP} f_T Q_{10}$	$O = 0.9P$	–	$F = P - O$
UW-VIC	$P = R_0 f_{NPP} f_{root} f_T Q_{10}$	$O = f_{[CH_4]} Q_{10}$	–	$F = (P - O) f_{transport}$

current atmospheric CH_4 concentration growth rate (Pison et al., 2013).

The wetland CH_4 emissions, $E_{CH_4}(g,t)$, are computed for each grid cell, g, and for each time step, t, through the following equation:

$$E_{CH_4}(g,t) = \sum_{WTP_i} S_{WTP_i}(g,t) D_{WTP_i}(g,t), \quad (4)$$

where S_{WTP_i} is the fraction of g covered by a wetland whose water table position (WTP) is equal to WTP_i. D_{WTP_i} is the CH_4 flux (i.e. g CH_4 (m^{-2} ofwetland) $time^{-1}$) for a wetland whose water table position is equal to WTP_i. S_{WTP_i} and D_{WTP_i} are, respectively, computed by (i) the coupling between a TOPMODEL (Beven and Kirkby, 1979) approach and ORCHIDEE, and (ii) the coupling between a (slightly modified) version of the Walter et al. (2001a) model and ORCHIDEE.

The main modification to the Walter et al. (2001a) model, as described in Ringeval et al. (2010), concerns the methanogenesis substrate. A fraction, α, of the natural labile carbon pool computed by ORCHIDEE is used to estimate the methanogenesis substrate. The α parameter also encompasses the methanogenesis base rate at the reference temperature (see Ringeval et al., 2013). α has been optimized against three sites then extrapolated on all grid cells sharing the same vegetation type (boreal, temperate or tropical).

In contrast to LPJ-WHyMe and its derivatives, ORCHIDEE did not implement wetland-specific PFTs (plant functional types). Instead, a fraction of the mean natural labile carbon pool over the grid cell is used to estimate the substrate supply.

For the computation of S_{WTP_i} in each grid cell, TOPMODEL allows distribution of the mean water deficit computed by ORCHIDEE according to the sub-grid topographic index distribution. This leads to the diagnostic of the grid-cell fraction with a null deficit. The mean deficit over the grid cell is computed from a gap to the field capacity (and not to the saturation, which cannot be reached in ORCHIDEE). The saturated wetland extent is computed from these "field capacity extents" using a shift of the topographic index distribution into each grid cell. The value of this shift is the same for all grid cells and has been chosen to obtain a global coverage by wetlands close to 4 %. The simulated wetland extent has been evaluated both through the induced modification on the simulated river flows and against the GIEMS data (Ringeval et al., 2012). The TOPMODEL approach is used to simulate not only the saturated wetland extent but also the wetland extent with a WTP below the soil surface.

3.7.1 WETCHIMP set-up

In the simulations performed for the WETCHIMP intercomparison, the WTP_i values chosen for each grid cell are: 0, −3 and −9 cm. A value of water table position equal to 0 means that the water is at the soil surface while negative values corresponds to water table position below the soil surface. Thus, for each time step, three fractions of each grid cell are given: (i) a fraction covered by a saturated wetland, (ii) a fraction covered by a wetland with a mean WTP equal to −3 cm (i.e. where the deficit is between 0 and −6 cm) and (iii) a fraction covered by a wetland with a mean WTP equal to −9 cm (i.e. where the deficit is between −6 and −12 cm).

As in Ringeval et al. (2011) the wetland extent is corrected to subtract the systematic biases of the model by normalizing the mean yearly wetland extent to the GIEMS data (i.e. both the seasonal and year to year variability come from TOPMODEL). In the WETCHIMP simulations, a Q_{10} equal to 3 (close to the mean value in Ringeval et al., 2010) has been chosen for all grid cells. As in Ringeval et al. (2013), the reference temperature for methanogenesis is defined as the mean surface temperature computed by ORCHIDEE when forced by the 1960–1991 CRUNCEP climatology.

3.8 SDGVM

The SDGVM (Sheffield Dynamic Global Vegetation Model; Woodward et al., 1995; Beerling and Woodward, 2001) was used in conjunction with a modified version of the Cao et al. (1996) wetland emissions model to perform the WETCHIMP simulations. The modelling set-up follows the approach of Singarayer et al. (2011), however in that study an equilibrium approach was taken wherein the vegetation and CH_4 models were forced with averaged (30 yr) climatologies from a series of general circulation model simulations. For WETCHIMP, a transient approach was required whereby the models were forced sequentially with monthly climatic inputs. The SDGVM and CH_4 models were therefore run in a similar manner as described by Hopcroft et al. (2011), in which a transient set-up of the model is described.

SDGVM requires monthly mean inputs of surface air temperature, precipitation and relative humidity, as well as a map of soil texture and global annual mean atmospheric CO_2 concentrations. The CRU vapour pressure was converted to relative humidity using standard formulae, whilst the temperatures and precipitation were used without modification.

In the CH_4 model, the supply of carbon substrate for methanogenesis is taken to scale with 1 m soil heterotrophic respiration as simulated in SDGVM. 1 m is the model's soil depth. CH_4 production, M_{prod}, is then given by

$$M_{\mathrm{prod}} = R_{\mathrm{hetr}} P_0 f_{\mathrm{w}}(\mathrm{WTP}) f_T(T), \tag{5}$$

where R_{hetr} is the soil heterotrophic respiration rate (g C m^{-2} month^{-1}) from SDGVM, P_0 represents the fraction of decomposed matter converted to CH_4 under optimal conditions (0.47, see Cao et al., 1996). f_{w} and f_T are dimensionless scaling functions, which parameterize the effects of water table position (WTP, in cm, positive up from the soil surface) and temperature (T in °C) on emission rates. These are given by

$$f_{\mathrm{w}}(\mathrm{WTP}) = 0.383 e^{0.096 \times \mathrm{WTP}}, \quad \mathrm{WTP} \leq 10\,\mathrm{cm}; \tag{6}$$

$$f_T(T) = \frac{e^{0.0405 \times T}}{3.375}, \quad 5\,^{\circ}\mathrm{C} < T \leq 30\,^{\circ}\mathrm{C}, \tag{7}$$

where f_{w} is 1.0 for WTP > 10 cm and f_T is 1.0 for $T >$ 30 °C and 0.0 for $T \leq 5.0$ °C. Emissions thus increase with increasing water table depth (up to 10 cm). f_{w} follows observations from Roulet et al. (1992) and Eq. (7) implies a Q_{10} value of 1.5. 90 % of CH_4 produced is assumed to be oxidised. The water table position in each grid cell is calculated from the SDGVM simulated 1 m total soil moisture content using the relations from Cao et al. (1996) for tundra (their Eqs. 15, 16) and a constant global soil porosity.

SDGVM also includes the biogeochemical coupling between the above- and below-ground carbon and nitrogen cycles. This is an important feature of modelling realistic changes in land surface primary production, which depends on, and should be in line with, realistic biological and anthropogenic nitrogen fixation rates (Hungate et al., 2003). In SDGVM, litter production influences soil carbon and nitrogen pools via the Century soil nutrient cycling model (Parton et al., 1993), which in turn feedback to influence the primary production of vegetation; details are provided elsewhere (Beerling and Woodward, 2001).

3.8.1 WETCHIMP set-up

The model output saved from SDGVM simulations includes annual NPP, soil carbon content, monthly heterotrophic respiration, soil moisture content, and GPP. The monthly outputs of CH_4 emissions and water table position were saved from the CH_4 model. The experiment protocol called for monthly and annual maximum wetland area (mmax_weta, amax_weta). Wetland area in this model is not used by the emissions model, which is instead a function of water table position (see Eq. 5). CH_4 emitting area could be used as a proxy for wetland area, but this would include grid cells with a water table far from the surface and with very small CH_4 fluxes. Since most of the other models in the intercomparison were parameterized using inundated area from satellite observations, the SDGVM output was tailored to be somewhat comparable. The wetland area was here taken as simulated inundated area. Since there is no sub-grid hydrology in the model, in each grid cell this area will either be 0 or the area of the grid cell. However, the model includes a correction for sub-grid orography based on the ETOPO5 dataset, which is applied to CH_4 emissions. The orographic correction, F_{corr} is computed as:

$$F_{\mathrm{corr}} = \frac{0.01 - S_{\mathrm{max}}}{0.01}, \tag{8}$$

where S_{max} is the maximum gradient between a grid cell and its 8 nearest neighbours.This correction was also applied to the calculated inundation area. Two climate-dependent conditions on CH_4 emissions are also currently used within the model: (i) the monthly air temperature must be above 5 °C, and (ii) if the temperature in a given grid cell during the current year is always > 0 °C, then in a given month, the evapotranspiration must not exceed precipitation. These two conditions were both also used to correct the simulated inundated area, so that it is more directly relevant to the simulated CH_4 emissions.

3.9 UVic-ESCM

The UVic Earth System Climate Model (Weaver et al., 2001; Meissner et al., 2003) is an intermediate complexity climate model consisting of several coupled components: an energy–moisture balance atmospheric model, a three-dimensional ocean general circulation model, a dynamic–thermodynamic sea ice model and a land surface scheme, which includes a representation of vegetation dynamics. The model was recently modified to include a representation of permafrost and global wetlands (Avis et al., 2011). Wetlands in the UVic model are determined using empirically derived threshold values for unfrozen soil moisture content and terrain slope so that wetlands are present where ground is sufficiently wet and flat (Kaplan, 2002). Wetlands are either "on or off" in a particular grid cell. If they satisfy the soil moisture criterion they are "on" and they occupy the fraction of the grid cell with the requisite terrain slope. Organic and mineral soil properties were specified by using the ISLSCP-II (International Land-Surface Climatology Project II) datasets as the model is presently incapable of generating the observed high soil carbon values in northern high latitudes (none of the participating models is able to couple soil biogeochemical with thermal characteristics yet).

3.9.1 WETCHIMP set-up

The UVic model is nominally run in a fully coupled configuration with coupling between atmospheric, ocean, land surface and other model components. For the purpose of participating in WETCHIMP, the land surface scheme was decoupled from the other model components and run in an offline configuration. This offline configuration uses the monthly CRU data to drive the land surface scheme. The model smoothly interpolates between these CRU fields to obtain data for a particular time step. Some of the atmospheric code from the coupled model's energy–moisture balance model (Weaver et al., 2001) was retained to calculate factors such as incoming solar radiation, which needs to be specified to the land surface scheme and was not specified in the monthly CRU datasets.

Surface air temperature, precipitation and relative humidity were specified from the CRU data, while surface winds and the diurnal temperature range were drawn from the NCEP reanalysis. Incoming long- and short-wave radiation are calculated within the model's atmospheric module.

The land surface scheme also has the capacity to simulate vegetation dynamics using the TRIFFID (Top-down Representation of Interactive Foliage and Flora Including Dynamics) dynamic vegetation model (Cox, 2001). As vegetation parameters were derived based on the coupled model climate, for the purposes of the WETCHIMP simulations, the vegetation distribution and characteristics were fixed and set equal to their mean year-1900 values from an equilibrated version of the coupled model, rather than adjusting vegetation parameters to fit the CRU climate data. Monthly mean fields of vegetation fraction, leaf area index (LAI), vegetation height and litterfall are then obtained from the mean year-1900 model output. The vegetation dynamics are consequently switched off for the offline run, and vegetation parameters for a given model time step are specified by smoothly interpolating between these monthly fields. Non-plant competition based vegetation parameters do remain interactive in the model. For example, plant stomata still open and close in response to factors like changing soil moisture or atmospheric CO_2 concentration.

For the equilibrium run, the model was forced repeatedly with 1901–1931 data for 2000 yr. This time period was found to be sufficient to allow for equilibration of soil moisture and temperature variables. When applying the CO_2, temperature and moisture runs, the 1901–1931 spin-up period was repeated for an additional 2000 yr to allow a new equilibrium to be established.

3.10 UW-VIC

The University of Washington team used the Variable Infiltration Capacity (VIC) model, version 4.1.2, with some extensions specifically tailored for the modelling of boreal peatlands described in Bohn et al. (2007) and Bohn and Lettenmaier (2010). UW-VIC is a large-scale hydrologic model that balances the water and energy budgets of the land surface at an hourly time step and spatial resolutions ranging from 1° to 5 km. Most of the model physics are described in Liang et al. (1994). Land cover is represented as a collection of "tiles", each containing a different plant functional type, overlaying a single soil column divided into 3 hydrologic layers, down to varying depths, but generally no deeper than 3 m. While UW-VIC does not track the storage of carbon in biomass, it computes NPP via a scheme taken from the BETHY (Biosphere Energy-Transfer and Hydrology) model (Knorr, 2000). The seasonal cycle of LAI is prescribed at each grid cell based on the MODIS (Moderate Resolution Imaging Spectroradiometer) LAI product (Myneni et al., 2002). Stomatal resistance is a function of day length, temperature, soil moisture, and vapor pressure deficit. UW-VIC models permafrost and the soil temperature profile via the finite difference scheme of Cherkauer and Lettenmaier (1999) with an exponential node distribution down to 50 m depth and a no-flux bottom boundary condition. Thermal properties of organic soil are also taken into account (Farouki, 1981). To account for dynamic surface water storage (lakes and seasonally flooded wetlands) UW-VIC's lake/wetland model was employed (Bowling and Lettenmaier, 2010). This feature allocates one land cover tile to contain a combination of a lake (representing all lakes in the grid cell) and its surrounding catchment. Within the tile, the inundated area fraction is dynamic, changing as a function of storage and bathymetry. The extent of permanent lakes were assumed equal to the minimum annual observed inundation

extent from the remotely observed inundation datasets (either Schroeder et al. (2010) or GIEMS, see Table 3). Thus, while the minimum and maximum possible extent of inundation within a grid cell are prescribed, the actual inundated extent is a dynamic function of environmental conditions. In the exposed portion of the tile, the water table position is assumed to have a distribution based on peatland microtopography: the peatland consists of a mix of hummocks (or ridges) and hollows (or pools), with the peat underneath hummocks up to 70 cm thicker than under the deepest points of the hollows. The fraction of peatland covered by hummocks is a calibrated parameter. Local water table position under any given point is computed as a function of soil moisture via the formulation described in Frolking et al. (2002). Methane emissions were computed for the lakes, inundated wetlands, and each point in the water table position distribution in the exposed wetlands as a function of water table position, soil temperature, and NPP via the model of Walter and Heimann (2000). A lake emission rate of 375 mg CH_4 m^{-2} d^{-1} was originally assumed during the ice-free season and half that rate during ice-covered season. This rate was found to be in error due to an artefact in the satellite data used to parameterize the lake emission rates. A value of 0 mg CH_4 m^{-2} d^{-1} is now used. The new lake emission rate results in lake CH_4 emissions that more closely resemble observations from the area. The influence of the new value can be observed by comparing from Melton et al. (2013) Fig. A1j (375 mg CH_4 m^{-2} d^{-1}) and Fig. 8j (0 mg CH_4 m^{-2} d^{-1}).

3.10.1 WETCHIMP set-up

For these simulations, each grid cell was separated into two parts: an upland fraction, underlain by mineral soils, with soil textures supplied by the FAO Digital Soil Map of the World (Batjes, 1997); and a lake/wetland fraction, underlain by peat soils, with peat depths given by the database of Sheng et al. (2004) and other characteristics taken from Letts et al. (2000). Simulations were run separately for each portion of the grid cell. The lake/wetland portion of each grid cell was determined as the superset of the Sheng et al. (2004) peatland map; wetlands, wet tundra, and croplands (so that nearby lakes could have a surrounding catchment) given by the Bartalev et al. (2003) land cover classification; and lakes given by the Global Lake and Wetland Database (GLWD; Lehner and Döll, 2004). Bathymetries for the lake/wetlands were estimated by combining lake size distributions from the GLWD; average lake depths from literature for bog pools, Arctic thaw lakes, and other boreal lakes; and topography of surrounding wetlands from the ASTER (Advanced Spaceborne Thermal Emission and Reflection Radiometer) (Hayakawa et al., 2008) and STRM (Shuttle Topography Radar Mission; Digital Elevation Model) (Farr and Kobrick, 2000) DEMs. When lake storage increased beyond the bounds of the "permanent" lake, it was allowed to flood the surrounding wetlands, with drainage rate controlled by a calibrated parameter. Both this parameter and the area fraction of hummocks within the peatland were calibrated to optimize the match with global inundation datasets. For the optimized runs (Experiment 3), the global daily AMSR-E/QuickSCAT-based dataset of Schroeder et al. (2010) was used; for all other runs, the GIEMS dataset was used (Prigent et al., 2007; Papa et al., 2010). Parameters for the CH_4 emissions model were calibrated to optimize the in situ observations of Glagolev et al. (2010) across West Siberia. For experiments other than experiment 3, UW-VIC's parameters were calibrated to match the June/July/August average inundation given by the GIEMS dataset over the period 1993–2004 and used for years outside of that range.

4 Results and discussion

We provide two conceptual overviews of the participating models highlighting similarities as well as differences between the chosen approaches. These overviews are designed to assist discussions of the differences in modelling results (Melton et al., 2013), but they also represent the first attempt at conceptually describing the state-of-the-art approaches used in wetland extent and wetland CH_4 modelling. For the conceptual figures describing the modelling approaches, we defined two variables of interest: the CH_4 *producing area* (Fig. 6) and CH_4 *flux* (Fig. 7). We used these metrics to explore the dominant processes responsible for differences between the models.

4.1 CH_4 producing area

We use the term "CH_4 producing areas" (MPAs) to include all terrestrial areas that may produce CH_4 biogenically. We include wet mineral soils, presently only simulated by LPJ-Bern, that are proposed to function as a CH_4 source or sink depending on the soil moisture level. The participating models use a large diversity of methods to determine MPAs (Fig. 6). We identified the features of the models that we found most strongly controlled the MPAs and visualized the concepts of the models.

The starting points to locate MPAs are either "Prescribed constant wetland extents", "Remotely-sensed inundation" or a "Hydrological model" (Fig. 6). The simplest case of estimating MPAs is where "Prescribed constant wetland extents" are taken from annually, non-varying distribution maps, and are used without modifications. This approach is applied by LPJ-WHyMe and LPJ-Bern (peatlands), which use the northern peatland map from NCSCD (Tarnocai et al., 2007, 2009), and IAP-RAS, which uses the Olson dataset for global MPA location. A similar approach takes seasonally varying "Remotely-sensed inundation" to prescribe MPAs. LPJ-Bern wetlands uses an averaged monthly mean extent from GIEMS, while LPJ-WSL (all experiments except 3) uses the GIEMS dataset without modification. A further step up the

complexity ladder is LPJ-Bern wetsoils, the most basic wetland extent that uses model output. LPJ-Bern wetsoils uses a "Hydrological model" to derive "Soil moisture" and "Unsaturated" MPAs. "Unsaturated" means that the pore-space in the soil is not completely filled with water. This could be the case when – even though a water table position is calculated – it is below the surface or when the soil moisture is estimated as a homogeneous average over the soil depth and its values do not reach saturation. Next, we include approaches that comprise of "Topography" in addition to "Hydrological model" as an additional factor to locate "Unsaturated" areas (UVic-ESCM). SDGVM uses a similar approach to UVic-ESCM but simulates "Water table position" before determining "Unsaturated" as well as "Saturated/inundated" MPAs. CLM4Me, DLEM, ORCHIDEE, UW-VIC and LPJ-WSL (Exp. 3) all use "Remotely sensed inundation" (GIEMS) data in their approaches, but they use these data in different ways: e.g. ORCHIDEE guides the mean simulated wetland extent over the 1993–2004 period and CLM4Me uses the GIEMS dataset to invert for parameters that allow the hydrological state (i.e. water table depth and runoff) to be used to determine wetland extent. More details on the use of GIEMS can be found in the description of each model (Sect. 3). Once the "Water table position" is determined, CLM4Me, DLEM, ORCHIDEE, and UW-VIC identify the MPAs that are either "Unsaturated" or "Saturated/inundated" while LPJ-WSL (Experiment 3-opt) determines MPAs which are "Saturated/inundated" only. The UW-VIC model is the most complex model and takes advantage of all of the features included in Fig. 6, using the fractional peatland cover by Sheng et al. (2004) only as maximal boundaries, rather than as a fixed map.

From the conceptual overview (Fig. 6) one can see that the only two models that simulate MPAs without the guidance of other wetland-relevant observations are the UVic-ESCM and the SDGVM. The difference between these two models is that the UVic-ESCM uses only soil moisture (as well as topography) to find "Unsaturated" areas, whereas the SDGVM also calculates the water table position to find "Unsaturated" as well as "Saturated/inundated" areas. As the UVic-ESCM model was designed to identify wetland areas, not specifically MPAs (it presently has no CH_4 model), the model uses grid-cell mean *unsaturated* soil moisture values and terrain slope as a mean of approximating *saturated* areas.

An additional area of uncertainty that should be noted is the influence of anthropogenic changes to the land surface. Models that explicitly use the GIEMS dataset account for rice agriculture by masking out those regions (Table 3) while also implicitly including areas of human alteration such as wetland drainage, conversion to farmland, etc. Models that independently simulate wetland extent will not be sensitive to these alterations and this could lead to an overestimate of wetland area in these regions. Small lakes could also contribute to an overestimated wetland area for some models. Presently only LPJ-Bern and UW-VIC masks these lakes (Table 3).

4.2 CH_4 flux

The second variable we analyse in detail is the "CH_4 flux" calculation by nine out of the ten participating models – the UVic-ESCM does not yet include CH_4 fluxes. Figure 7 shows which pools and processes models consider to determine CH_4 flux. All models but IAP-RAS base their CH_4 production on some kind of carbon flux, where two groups can be distinguished – one that uses "Wetland PFTs" and one that uses "Upland PFTs" to simulate vegetation net primary production (NPP); only DLEM utilizes NPP (and also GPP) simulated by both types of PFTs for CH_4 production. The UW-VIC model uses NPP in the algorithm for CH_4 production, ORCHIDEE uses a fraction of the most labile of the "Litter + soil C" pool and all remaining models use "Heterotrophic respiration" as the basis for their "CH_4 production" (see also Table 5). LPJ-Bern, LPJ-WHyMe and DLEM add "Exudates"-derived carbon to the "Heterotrophic respiration" calculation.

All models calculate CH_4 production and half of the models consider "Transport" mechanisms such as ebullition, plant-mediated transport, and diffusion to derive "CH_4 fluxes" (Fig. 7, Table 5). This table also gives insight into which models include oxidation of soil-derived CH_4 and how they combine production and oxidation rates to simulate the final net CH_4 flux. Only three of the models include atmospheric CH_4 oxidation (CLM4Me, DLEM, LPJ-Bern wet soils). Thus, we include soil oxidation of atmospheric methane in Table 5 for completeness, but we excluded soil oxidation of atmospheric methane from model results as far as possible in order to compare gross CH_4 fluxes. The separation of gross CH_4 fluxes and atmospheric CH_4 uptake fluxes was not completely feasible in CLM4Me as the CH_4 uptake occurs implicitly in the reaction-transport solution, although for Melton et al. (2013) an estimate was determined to allow better comparison between models. Across the models, the complexity of equations for CH_4 production covers a wide range. The IAP-RAS model is the simplest model relating CH_4 production only to temperature, whereas all other models use some estimate of the available carbon flux rate. All but two models (IAP-RAS and LPJ-WSL) include some kind of soil-derived CH_4 oxidation, which can be as simple as reducing production by a fixed fraction (SDGVM) or by including up to five different terms in the equation (Table 5).

4.3 Methane producing area and methane flux

Mean annual maximum extent of wetland area and mean annual CH_4 fluxes for Experiment 1-equil are shown in Fig. 8. Total MPAs and CH_4 emissions for each model are listed in the bottom left corner of each sub-figure. Two of the models are regional models (LPJ-WHyMe and UW-VIC), the rest

are global models in which the UVic-ESCM does not simulate CH_4 fluxes. CLM4Me, DLEM, LPJ-Bern (without mineral soils), LPJ-WSL, and ORCHIDEE share similar wetland distributions due to their varying degrees of reliance on remotely sensed inundation data (see Fig. 6). The similarity of approaches is also reflected in the total MPA of these models (CLM4Me: 6.8×10^6, DLEM: 7.9×10^6, LPJ-Bern without mineral soils: 7.9×10^6, LPJ-WSL: 7.4×10^6, and ORCHIDEE: 9.2×10^6 km^2). Two models (IAP-RAS and LPJ-Bern with wet mineral soils) stand out visually because of their large areas of 80–100 % MPA per grid cell. The IAP-RAS model uses a binary approach – either a grid cell is a wetland or it is not – resulting in a total MPA of 20.3×10^6 km^2, which is an entirely prescribed amount. Given the definition of the wet mineral soils as CH_4 source, the LPJ-Bern wet mineral soils map should be interpreted as a map of "potential CH_4 emissions in at least one month per year". Since LPJ-Bern does not use a sub-grid-cell hydrology for wet mineral soils to estimate the CH_4 production capacity, the wet mineral soils component of LPJ-Bern is also a binary approach. However, the extent of wet mineral soils in a given grid cell can be reduced by peatland area and inundated area so that they jointly sum to 100 %, but as soon as a grid cell qualifies as wet mineral soils, the MPA of that grid cell is 100 %. This approach leads to the largest total MPA of 76.6×10^6 km^2 of the WETCHIMP models.

The only two models that use an explicit water balance scheme to simulate wetland extent without relying on wetland or inundation datasets are the SDGVM and the UVic-ESCM (Fig. 8). They show a similar spatial distribution but differ notably in Eastern Siberia, the western United States and northern Canada. SDGVM uses soil moisture content to first diagnose water table position and then MPAs, whereas UVic-ESCM uses soil moisture directly to derive MPAs. The differences between these two models could be related to parameterization of permafrost (present in UVic-ESCM, but absent in SDGVM) and other soil physics or hydrology parameters, i.e. hydraulic conductivity, porosity, etc. Further, the percentages of grid cells covered by wetlands are generally higher for SDGVM than for the UVic-ESCM leading to a higher overall wetland area of 34.9×10^6 km^2 vs 14.9×10^6 km^2, respectively.

Of the two regional models, LPJ-WHyMe uses a fixed peatland distribution (Fig. 8e) whereas the UW-VIC model uses the most sophisticated method of all participating models to simulate saturated and unsaturated wetland areas in the West Siberian Lowlands (Fig. 8j). A comparison focused on the West Siberian Lowlands is planned to evaluate the differences between a highly regionalized model like the UW-VIC model and the rest of the WETCHIMP models (T. Bohn, personal communication, June 2012).

Simulated CH_4 fluxes of nine of the participating models are shown on the right hand side in Fig. 8. Methane fluxes ranged from 0 to over 250 g CH_4 m^{-2} of wetland yr^{-1} with CLM4Me, DLEM, LPJ-WSL, and ORCHIDEE showing

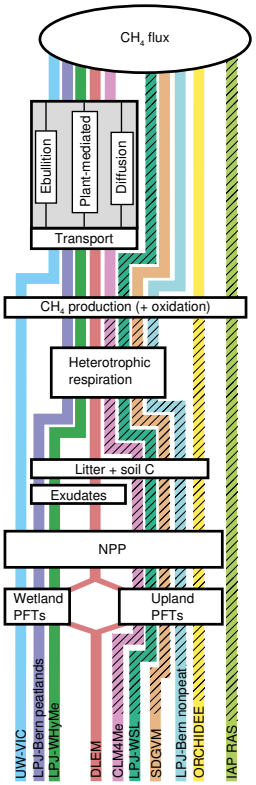

Fig. 7. Conceptual overview of the pathways from the carbon source to "CH_4 flux" (CH_4 flux per m^2 of wetland) in the participating models. Each model (and in some cases, version) is represented by a different colour. The flow of a particular model starts with the model's name. The hatching of the lines indicates that the CH_4 model is *not* influenced by *wetland* hydrology (beyond changes in extent). "Wetland PFTs" means that the model uses wetland-specific PFTs, whereas "Upland PFTs" indicates that the model uses the already existing PFTs used for upland ecosystems. "NPP" stands for net primary production, "Exudates" are root exudates carbon pool. All models but the IAP-RAS model use NPP as a precursor of the carbon used directly in CH_4 production or indirectly in CH_4 production by estimating "Litter and Soil C", "Exudates", and "Heterotrophic respiration". The models then calculate "CH_4 production" and the oxidation based on the equations given in Table 5. Some models include the effect of "Transport" mechanisms explicitly, whereas others include transport only implicitly by either producing less CH_4 or oxidizing it before emitting it to the atmosphere. All models use some sort of temperature dependence when calculating NPP, heterotrophic respiration, and/or CH_4 production. In this figure, "LPJ-Bern nonpeat" includes both wetlands and wetsoils, which also incorporate plant exudates (graphical simplification).

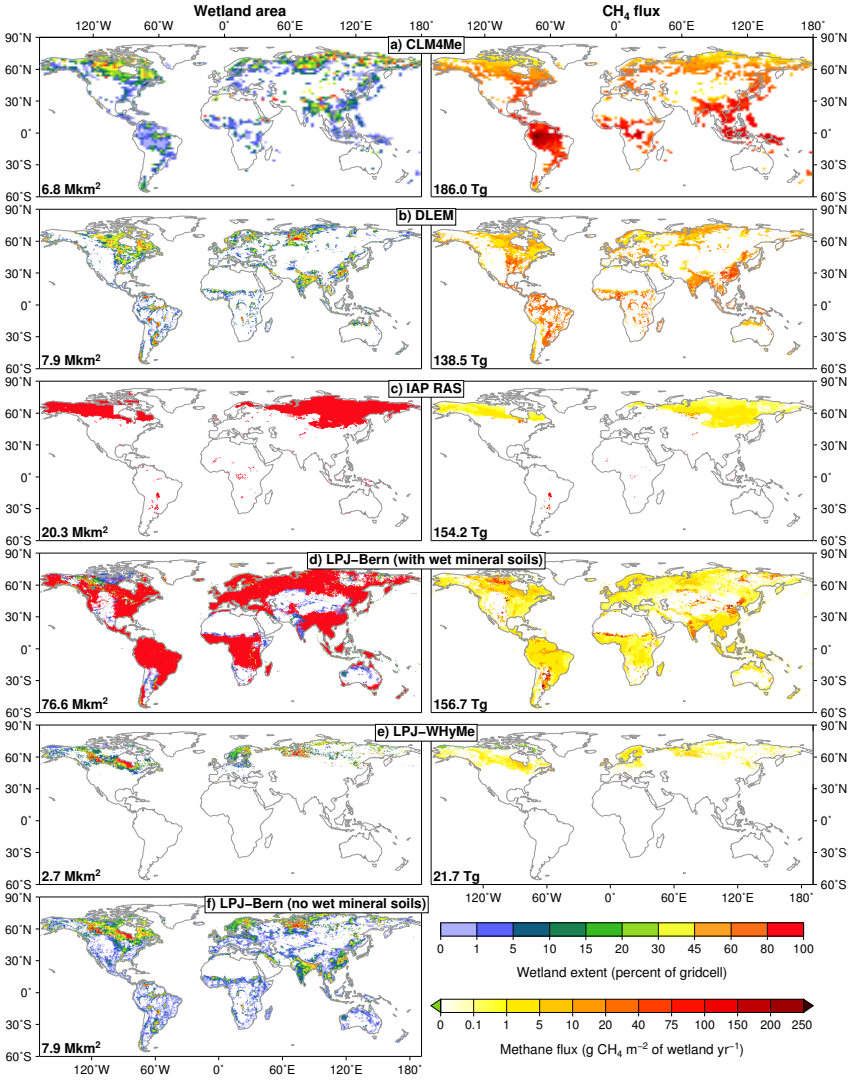

Fig. 8. Mean annual maximum extent of prescribed or simulated wetland area and mean annual CH_4 flux for Experiment 1-equil over the 1901–1931 period. Global total wetland area (Mkm^2 = Million km^2) and CH_4 emissions (Tg = Tg CH_4 per year) have been added to each plot.

widespread high fluxes (Fig. 8a, b, g, h) and IAP-RAS, LPJ-Bern, LPJ-WHyMe, SDGVM, and UW-VIC showing low fluxes (Fig. 8c, d, e, i, j). Of the five models that show widespread high fluxes, three base their CH_4 flux on upland PFTs (CLM4Me, LPJ-WSL, ORCHIDEE), and one on both wetland and upland PFTs (DLEM) (Fig. 7). Of the four models that show low CH_4 fluxes, three rely on wetland PFTs (LPJ-Bern, LPJ-WHyMe, and UW-VIC), one on upland PFTs (SDGVM) and one does not rely on PFTs at all (IAP-RAS). This could indicate a general tendency to higher CH_4 fluxes when upland PFTs instead of wetland PFTs are used to simulate NPP. Some of the models show higher fluxes

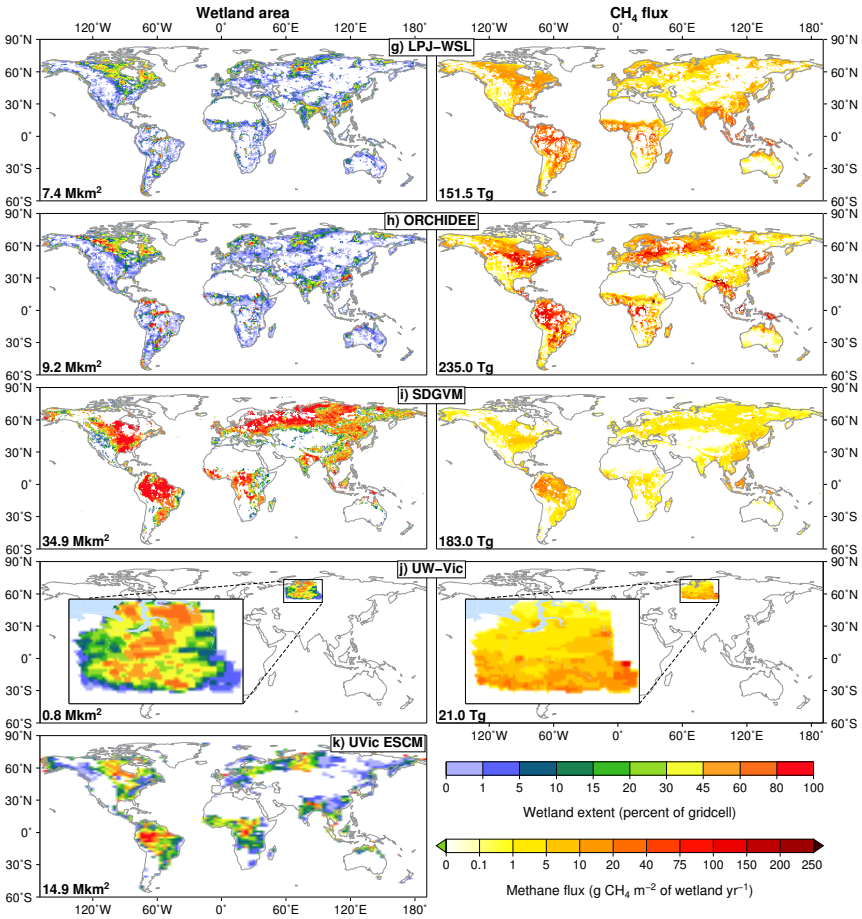

Fig. 8. Continued.

in the tropics than in the extra-tropics (CLM4Me, IAP-RAS, SDGVM), whereas others show equally high fluxes (DLEM, LPJ-Bern, LPJ-WSL, ORCHIDEE), which may be linked to the model-inherent temperature sensitivities of, e.g. NPP, heterotrophic respiration or CH_4 production, but without specific parameter sensitivity studies it is impossible to evaluate where the differences arise from.

The patterns of CH_4 fluxes do not always match the pattern of wetland distribution (e.g. compare wetland area and CH_4 fluxes for the Amazon from CLM4Me). Total CH_4 emissions for a grid cell are calculated as the product of fluxes and wetland area (except for CLM4Me, which also considers production in upland soils). Therefore, models may simulate similar global CH_4 emissions with completely different MPAs and CH_4 fluxes (e.g. CLM4Me: 186 Tg CH_4 yr^{-1} vs SDGVM: 183 Tg CH_4 yr^{-1}, or IAP-RAS: 154.2 Tg CH_4 yr^{-1} vs LPJ-Bern: 156.6 Tg CH_4 yr^{-1} vs LPJ-WSL: 151.5 Tg CH_4 yr^{-1}) (Fig. 8). The comparability of these simulated global CH_4 emissions emphasizes the fact that most models are tuned to some degree towards a global total CH_4 emissions value, which allows the MPAs to vary more between the models than global CH_4 emissions. As highlighted in Melton et al. (2013), the fact that the models agree fairly well on global CH_4 emissions with very different MPAs and CH_4 fluxes underlines the importance of regional-scale observational estimates to constrain this dichotomy.

Table 6. Explanation of variable names used in Table 5.

Variable name	Description
C_{labile}	labile carbon pool
O_{air}	soil oxidation of atmospheric CH_4, i.e. CH_4 uptake
$O_{air,max}$	maximum soil oxidation of atmospheric CH_4 rate
O_{soil}	oxidation in the soil pore water
$O_{soil.max}$	maximum oxidation rate in the soil pore water
O_{trans}	oxidation associated with transport through plants
$O_{trans,max}$	maximum oxidation associated with transport through plants
O_{max}	maximum oxidation rate
P_{max}	maximum CH_4 production
Q_{10}	factor describing dependence on temperature
R_{hetr}	heterotrophic respiration
R_0	CH_4 production rate
$f_{[CH_4]}$	function of pore water CH_4 concentration
$f_{atm[CH_4]}$	function of atmospheric CH_4 concentration
f_{ecosys}	function of ecosystem type
f_{GPP}	function of the ratio of monthly to annual net primary production (NPP)
$f_{[O_2]}$	function of pore water O_2 concentration, determined by rate of O_2 diffusion through soil water and aerenchyma
f_{pE}	function of alternative electron acceptors
f_{pH}	function of pH value
$f_{planttrans}$	function of plant-mediated CH_4 transport
f_{root}	function of vertical root distribution
f_{soil}	function of soil type
f_T	function of temperature
f_Θ	function of soil moisture
$f_{transport}$	function of CH_4 transport
f_{WTP}	function of water table position
$r_{CH4:C}$	fraction of C converted to CH_4
r_{O_2}	fraction of O_2 used for CH_4 oxidation

5 Summary and conclusions

WETCHIMP is the first multi-model comparison of wetland extent and wetland CH_4 emissions. Our analysis demonstrates how diverse modelling approaches, wetland definitions, and wetland extent can be, while still leading to comparable values of global CH_4 emissions. In terms of modelling CH_4 producing areas (MPAs), there are three main approaches: (i) the fixed MPA (IAP-RAS, LPJ-Bern (peatlands and wetlands), LPJ-WHyMe), (ii) the guided MPA (CLM4Me, DLEM, LPJ-WSL, ORCHIDEE, UW-VIC) and (iii) the fully simulated MPA (UVic-ESCM, SDGVM, LPJ-Bern wetsoils). Total MPA can vary significantly between models depending on their definitions, which also influences CH_4 fluxes, but does not have as much impact on the global CH_4 emissions. Achieving similar global CH_4 emissions with very different MPA distributions also means that the CH_4 fluxes between the models differ greatly. A wide range of parameterization complexity is used to simulate CH_4 fluxes in the participating models, which influences not just the present day flux but also its sensitivity to climate factors.

Each individual model's approach needs to be considered carefully when interpreting results, especially past and future climate change experiments or sensitivity experiments such as those that were conducted as part of WETCHIMP (Melton et al., 2013). There are several factors that need to be kept in mind: a fixed wetland distribution as used by some models or a seasonally varying distribution based on presently observed patterns is unlikely to be representative of past or future conditions. Another limitation is the absence of wetland specific PFTs in most models. Models that lack wetland specific PFTs (i.e. CLM4Me, LPJ-WSL, SDGVM, LPJ-Bern non-peatland, ORCHIDEE, IAP-RAS) may overestimate NPP due to an unrealistic lack of plant stress that would be caused by inundation or nutrient limitation. We expect these models to show different responses to changes in temperature, precipitation and CO_2 fertilization than the models that include wetland specific PFTs (i.e. DLEM, LPJ-WHyMe, LPJ-Bern peatlands, UW-VIC). For example, changes in precipitation will affect wetland specific PFTs that grow under inundated conditions differently than upland plants. Also, the effect of CO_2 fertilization on wetland plants is still unclear (Berendse et al., 2001; Heijmans et al., 2001, 2002a,b; Boardman et al.,

2011) and therefore wetland NPP under CO_2 fertilization calculated by models that include wetland specific PFTs remains highly uncertain.

There are features that are still missing, or are crudely represented, in almost all of the models, partially due to the difficulties of simulating small-scale processes in large-scale models. Such features include (i) lateral transport of water and groundwater dynamics within (beyond the assumptions of the TOPMODEL formulation) and between grid cells, and explicit treatments of floodplains and mangroves; (ii) plant nutrients (nitrogen, phosphorus and sulphur) and their interactions (presently only SDGVM, DLEM, and CLM4Me include carbon–nitrogen interactions); (iii) microtopographical features such as lawns, hollows or hummocks and their impacts upon overall CH_4 dynamics; (iv) vertically resolved carbon pools and soil organic matter remineralization modelling; (v) permafrost-preserved carbon; (vi) feedbacks between peat or carbon dynamics and thermal and hydrological processes in soil; (vii) hydrology affected by thawing permafrost; (viii) wetland specific vegetation (improvements for boreal peatlands, introduction of tropical wetland PFTs); and (ix) anthropogenic disturbance (such as wetland drainage) and management (such as dams and reservoirs).

WETCHIMP provides a the first multi-model platform to explore the current knowledge, recent improvements, and necessary future developments of models simulating wetland extent and wetland CH_4 emissions. The design of future iterations of WETCHIMP will be focused on analysing and understanding the different uncertainties and sensitivities of participating models with the goal of greatly improving the performance of the models for both wetland and wetland CH_4 modelling. The simulations conducted in WETCHIMP are available (http://arve.epfl.ch/pub/wetchimp, please contact J. R. Melton for immediate access) and their use is encouraged to advance research in this area.

Acknowledgements. The authors are grateful to the COST Action ES0805 TERRABITES for providing support for the WETCHIMP workshop. We thank Sylvia Houston and Olga Petrikova for assistance with organizing the project meeting and Kristen Krumhardt for assistance producing the figures. J. R. M. was supported by the Swiss Ministry for Research and Education (grant C09.0054). J. O. K. acknowledges support from the Swiss National Science Foundation (grants PP0022_119049 and PP00P2_139193). The contributions of W. J. R. and Z. M. S. were supported by the Director, Office of Science, Office of Biological and Environmental Research, Climate and Environmental Science Division, of the US Department of Energy under Contract No. DE-AC02-05CH11231 to Berkeley Lab (IMPACTS and C-Climate Uncertainties projects). The contributions of T. J. B. and D. P. L. were supported by NASA's ROSES program, grant NNX08AH97G. The contribution of Z. C. Y. was supported by a US NSF grant (ARC-1107981) and a grant from The Max Planck Society (Germany). A. V. E. and S. N. D. were supported by the the President of Russia grant 5467.2012.5, by the Russian Foundation for Basic Research, and by the programs of the Russian Academy of Sciences. The contributions of R. S. and S. Z. were supported by the Swiss National Science Foundation and by the European Research Council advanced grant MATRICs (ERC grant agreement no. 226172) under the European Community's Seventh Framework Programme. P. O. H. is supported by a NERC UK grant NE/I010912/1 and previously through NERC UK/INSU France QUEST-DESIRE project. E. L. H. was supported by ETH Competence Center Environment and Sustainability's grant MAIOLICA. We also thank Steve Frolking and one anonymous reviewer for their comments which have improved our manuscript.

Edited by: D. Roche

References

Aselman, I. and Crutzen, P. J.: Global distribution of natural freshwater wetlands and rice paddies, and their net primary productivity, seasonality and possible methane emissions, J. Atmos. Chem., 8, 307–358, 1989.

Avis, C. A., Weaver, A. J., and Meissner, K. J.: Reduction in areal extent of high-latitude wetlands in response to permafrost thaw, Nat. Geosci., 4, 444–448, 2011.

Bartalev, S. A., Belward, A. S., Erchov, D. V., and Isaev, A. S.: A new SPOT4-VEGETATION derived land cover map of Northern Eurasia, Int. J. Remote Sens., 24, 1977–1982, 2003.

Batjes, N. H.: A world dataset of derived soil properties by FAO-UNESCO soil unit for global modelling, Soil Use Manage., 13, 9–16, 1997.

Beerling, D. J. and Woodward, F. I.: Vegetation and the Terrestrial Carbon Cycle: Modelling the first 400 Million Years, Cambridge University Press, Cambridge, 2001.

Beerling, D. J., Fox, A., Stevenson, D. S., and Valdes, P. J.: Enhanced chemistry-climate feedbacks in past greenhouse worlds, P. Natl. Acad. Sci. USA, 108, 9770–9775, doi:10.1073/pnas.1102409108, 2011.

Berendse, F., Breemen, N. V., Rydin, H., Buttler, A., Heijmans, M., Hoosbeek, M. R., Lee, J. A., Mitchell, E., Saarinen, T., Vasander, H., and Wallen, B.: Raised atmospheric CO_2 levels and increased N deposition cause shifts in plant species composition and production in *Sphagnum* bogs, Glob. Change Biol., 7, 591–598, 2001.

Beven, K. J. and Kirkby, M. J.: A physically based, variable contributing area model of basin hydrology, Hydrol. Sci. J., 24, 43–69, 1979.

Boardman, C. P., Gauci, V., Watson, J. S., Blake, S., and Beerling, D. J.: Contrasting wetland CH_4 emission responses to simulated glacial atmospheric CO_2 in temperate bogs and fens, New Phytol., 192, 898–911, 2011.

Bohn, T. J. and Lettenmaier, D. P.: Systematic biases in large-scale estimates of wetland methane emissions arising from water table formulations, Geophys. Res. Lett., 37, L22401, doi:10.1029/2010GL045450 2010.

Bohn, T. J., Lettenmaier, D. P., Sathulur, K., Bowling, L. C., Podest, E., McDonald, K. C., and Friborg, T.: Methane emissions from western Siberian wetlands: heterogeneity and sensitivity to climate change, Environ. Res. Lett., 2, 259–268, 2007.

Bowling, L. C. and Lettenmaier, D. P.: Modeling the effects of lakes and wetlands on the water balance of Arctic environments, J. Hydrometeorol., 11, 276–295, 2010.

Cao, M. K., Marshall, S., and Gregson, K.: Global carbon exchange and methane emissions from natural wetlands: application of a process-based model, J. Geophys. Res., 101, 14399–14414, 1996.

Chen, G., Tian, H., Zhang, C., Liu, M., Ren, W., Zhu, W., Chappelka, A., Prior, S. A., and Lockaby, G.: Drought in the southern United States over the last century: variability and its impacts on terrestrial ecosystem productivity and carbon storage, Clim. Change, 114, 379–397, doi:10.1007/s10584-012-0410-z, 2012.

Cherkauer, K. A. and Lettenmaier, D. P.: Hydrologic effects of frozen soils in the upper Mississippi River basin, J. Geophys. Res.-Atmos., 104, 19599–19610, 1999.

Christensen, T. R. and Cox, P.: Response of methane emission from arctic tundra to climatic change: results from a model simulation, Tellus B, 47, 301–309, 1995.

Christensen, T. R., Prentice, I. C., Kaplan, J., Haxeltine, A., and Sitch, S.: Methane flux from northern wetlands and tundra – an ecosystem source modelling approach, Tellus B, 48, 652–661, 1996.

Coe, M. T.: Simulating continental surface waters: an application to Holocene northern Africa, J. Clim., 10, 1680–1689, doi:10.1175/1520-0442(1997)010%3C1680:SCSWAA%3E2.0.CO;2, 1997.

Coe, M. T.: A linked global model of terrestrial hydrologic processes: simulation of modern rivers, lakes, and wetlands, J. Geophys. Res., 103, 8885–8899, 1998.

Cox, P.: Description of the TRIFFID dynamic global vegetation model, Hadley Centre, Met Office, Technical Note 24, 2001.

Curry, C. L.: Modelling the soil consumption of atmospheric methane at the global scale, Global Biogeochem. Cy., 21, gB4012, doi:10.1029/2006GB002818, 2007.

Curry, C. L.: The consumption of atmospheric methane by soil in a simulated future climate, Biogeosciences, 6, 2355–2367, doi:10.5194/bg-6-2355-2009, 2009.

Dentener, F., Drevet, J., Lamarque, J., Bey, I., Eickhout, B., Fiore, A., Hauglustaine, D., Horowitz, L., Krol, M., and Kulshrestha, U.: Nitrogen and sulfur deposition on regional and global scales: a multimodel evaluation, Global Biogeochem. Cy., 20, gB4003, doi:10.1029/2005GB002672, 2006.

ETOPO: 2-minute gridded global relief data (ETOPO2v2), US Department of Commerce, National Oceanic and Atmospheric Administration, National Geophysical Data Center, available at: http://www.ngdc.noaa.gov/mgg/fliers/06mgg01.html (last access: 14 August 2012), 2006.

FAO/IIASA/ISRIC/ISSCAS/JRC: Harmonized World Soil Database (version 1.1), Tech. rep., FAO, Rome, Italy and IIASA, Laxenburg, Austria, 2009.

Farouki, O. T.: The thermal-properties of soils in cold regions, Cold Reg. Sci. Technol., 5, 67–75, 1981.

Farr, T. G. and Kobrick, M.: Shuttle radar topography mission produces a wealth of data, EOS Trans. Am. Geophys. Union, 81, 583–585, 2000.

Fries, R. D., Hansen, M., Townshend, J., and Sohlberg, R.: Global land cover classifications at 8 km spatial resolution: the use of training data derived from Landsat imagery in decision tree classifiers, Int. J. Remote Sens., 19, 3141–3168, 1998.

Frolking, S., Roulet, N. T., Moore, T. R., Lafleur, P. M., Bubier, J. L., and Crill, P. M.: Modeling seasonal to annual carbon balance of Mer Bleue Bog, Ontario, Canada, Global Biogeochem. Cy., 16, 4-1–4-21, doi:10.1029/2001GB001457 2002.

Fung, I. Y., John, J., Lerner, J., Matthews, E., Prather, M., Steele, L. P., and Fraser, P. J.: Three-dimensional model synthesis of the global methane cycle, J. Geophys. Res., 96, 13033–13065, 1991.

Gedney, N., Cox, P. M., and Huntingford, C.: Climate feedback from wetland methane emissions, Geophys. Res. Lett., 31, L20503, doi:10.1029/2004GL020919, 2004.

Gerber, S., Joos, F., Brugger, P., Stocker, T., Mann, M., Sitch, S., and Scholze, M.: Constraining temperature variations over the last millennium by comparing simulated and observed atmospheric CO_2, Clim. Dynam., 20, 281–299, doi:10.1007/s00382-002-0270-8, 2003.

Gerten, D., Schaphoff, S., Haberlandt, U., Lucht, W., and Sitch, S.: Terrestrial vegetation and water balance – hydrological evaluation of a dynamic global vegetation model, J. Hydrol., 286, 249–270, 2004.

Glagolev, M. V., Kleptsova, I. E., Filippov, I. V., Kazantsev, V. S., Machida, T., and Maksyutov, S.: Methane emissions from subtaiga mires of Western Siberia: the Standard Model Bc5, Moscow Univ. Soil Sci. Bull., 65, 86–93, 2010.

Global Soil Data Task Group: Global gridded surfaces of selected soil characteristics (IGBP-DIS), Oak Ridge National Laboratory Distributed Active Archive Center, Oak Ridge, Tennessee, USA, available at: http://www.daac.ornl.gov (last access: 14 August 2012), 2000.

Hayakawa, Y. S., Oguchi, T., and Lin, Z.: Comparison of new and existing global digital elevation models: ASTER G-DEM and SRTM-3, Geophys. Res. Lett., 35, 19599–19610, 2008.

Heijmans, M. M. P. D., Arp, W. J., and Berendse, F.: Effects of elevated CO_2 and vascular plants on evapotranspiration in bog vegetation, Glob. Change Biol., 7, 817–827, 2001.

Heijmans, M. M. P. D., Klees, H., and Berendse, F.: Competition between *Sphagnum magellanicum* and *Eriophorum angustifolium* as affected by raised CO_2 and increased N deposition, Oikos, 97, 415–425, 2002a.

Heijmans, M. M. P. D., Klees, H., de Visser, W., and Berendse, F.: Response of a *Sphagnum* bog plant community to elevated CO_2 and N supply, Plant Ecol., 162, 123–134, 2002b.

Hodson, E. L., Poulter, B., Zimmermann, N. E., Prigent, C., and Kaplan, J. O.: The El Niño-Southern Oscillation and wetland methane interannual variability, Geophys. Res. Lett., 38, L08810, doi:10.1029/2011GL046861, 2011.

Hopcroft, P. O., Valdes, P. J., and Beerling, D. J.: Simulating idealized Dansgaard-Oeschger events and their potential impacts on the global methane cycle, Quaternary Sci. Rev., 30, 3258–3268, 2011.

Hungate, B. A., Dukes, J. S., Shaw, M. R., Luo, Y. Q., and Field, C. B.: Nitrogen and climate change, Science, 302, 1512–1513, 2003.

IPCC: Emissions Scenarios, Special Report of the Intergovernmental Panel on Climate Change, Tech. Rep., Cambridge University Press, Cambridge UK, 2000.

ISLSCP-II: Global Gridded Surfaces of Selected Soil Characteristics for the International Satellite Land Surface Climatology Project (ISLSCP) Initiative II Data Collection, Global Soil Data Task Group, Oak Ridge, Tennessee, USA, available at: https://daac.ornl.gov (last access: 14 August 2012), 2009.

Jones, P. D. and Harris, I.: CRU Time Series (TS) high resolution gridded datasets, University of East Anglia Climatic Research Unit (CRU), available at: http://badc.nerc.ac.uk/view/badc.nerc.ac.uk_ATOM_dataent_1256223773328276 (last access: 28 August 2012), 2008.

Joos, F., Gerber, S., Prentice, I. C., Otto-Bliesner, B. L., and Valdes, P. J.: Transient simulations of Holocene atmospheric carbon dioxide and terrestrial carbon since the Last Glacial Maximum, Global Biogeochem. Cy., 18, GB2002, doi:10.1029/2003GB002156, 2004.

Kaplan, J. O.: Wetlands at the Last Glacial Maximum: Distribution and methane emissions, Geophys. Res. Lett., 29, 1079, doi:10.1029/2001GL013366, 2002.

Knorr, W.: Annual and interannual CO_2 exchanges of the terrestrial biosphere: process-based simulations and uncertainties, Global Ecol. Biogeogr., 9, 225–252, 2000.

Koven, C. D., Ringeval, B., Friedlingstein, P., Ciais, P., Cadule, P., Khvorostyanov, D., Krinner, G., and Tarnocai, C.: Permafrost carbon-climate feedbacks accelerate global warming, P. Natl. Acad. Sci., 108, 14769–14774, 2011.

Krinner, G.: Impact of lakes and wetlands on boreal climate, J. Geophys. Res., 108, 4520,doi:10.1029/2002JD002597, 2003.

Krinner, G., Viovy, N., de Noblet-Ducoudre, N., Ogee, J., Polcher, J., Friedlingstein, P., Ciais, P., Sitch, S., and Prentice, I. C.: A dynamic global vegetation model for studies of the coupled atmosphere-biosphere system, Global Biogeochem. Cy., 19, 941–962, 2005.

Kudryavtsev, V. A., Garagula, L. S., Kondratiyeva, K. A., and Melamed, V. E.: Frost Forecasting in Geological Engineering Investigations, CRREL, Hanover, NH, 1977.

Lawrence, D. M., Oleson, K. W., Flanner, M. G., Thornton, P. E., Swenson, S. C., Lawrence, P. J., Zeng, X., Yang, Z.-L., Levis, S., Sakaguchi, K., Bonan, G. B., and Slate, A. G.: Parameterization improvements and functional and structural advances in version 4 of the Community Land Model, J. Adv. Model. Earth. Sys., 3, M03001, doi:10.1029/2011MS000045, 2011.

Lawrence, P. J. and Chase, T. N.: Representing a new MODIS consistent land surface in the Community Land Model (CLM 3.0), J. Geophys. Res., 112, G01023, doi:10.1029/2006JG000168, 2007.

Leff, B., Ramankutty, N., and Foley, J.: Geographic distribution of major crops across the world, Global. Biogeochem. Cy., 18, GB1009, doi:10.1029/2003GB002108, 2004.

Lehner, B. and Döll, P.: Development and validation of a global database of lakes, reservoirs and wetlands, J. Hydrol., 296, 1–22, 2004.

Letts, M. G., Roulet, N. T., Comer, N. T., Skarupa, M. R., and Verseghy, D. L.: Parametrization of peatland hydraulic properties for the Canadian Land Surface Scheme, Atmos. Ocean, 38, 141–160, 2000.

Liang, X., Lettenmaier, D. P., Wood, E. F., and Burges, S. J.: A simple hydrologically based model of land-surface water and energy fluxes for general-circulation models, J. Geophys. Res., 99, 14415–14428, 1994.

Liu, M., Tian, H., Yang, Q., Yang, J., Song, X., Lohrenz, S. E., and Cai, W.: Long-term trends in evapotranspiration and runoff over the drainage basins of the Gulf of Mexico during 1901–2008, Water Resour. Res., 49, 1–25, 10.1002/wrcr.20180, 2013.

Matthews, E. and Fung, I. Y.: Methane emission from natural wetlands: Global distribution, area, and environmental characteristics of sources, Global Biogeochem. Cy., 1, 61–86, 1987.

Meehl, G. A., Stocker, T. F., Collins, W. D., Friedlingstein, P., Gaye, A. T., Gregory, J. M., Kitoh, A., Knutti, R., Murphy, J. M., Noda, A., Raper, S. C. B., Watterson, I. G., Weaver, A. J., and Zhao, Z.-C.: Global climate projections, in: Climate change 2007: The physical science basis. Contribution of Working Group I to the Fourth Assessment Report of the Intergovernmental Panel on Climate Change, edited by: Solomon, S., Qin, D., Manning, M., Chen, Z., Marquis, M., Averyt, K. B., Tignor, M., and Miller, H. L., chap. 10, Cambridge University Press, Cambridge, UK and New York, NY, USA, 747–846, 2007.

Meissner, K. J., Weaver, A. J., Matthews, H. D., and Cox, P. M.: The role of land surface dynamics in glacial inception: a study with the UVic Earth System Model, Clim. Dynam., 21, 515–537, 2003.

Melton, J. R., Wania, R., Hodson, E. L., Poulter, B., Ringeval, B., Spahni, R., Bohn, T., Avis, C. A., Beerling, D. J., Chen, G., Eliseev, A. V., Denisov, S. N., Hopcroft, P. O., Lettenmaier, D. P., Riley, W. J., Singarayer, J. S., Subin, Z. M., Tian, H., Zürcher, S., Brovkin, V., van Bodegom, P. M., Kleinen, T., Yu, Z. C., and Kaplan, J. O.: Present state of global wetland extent and wetland methane modelling: conclusions from a model intercomparison project (WETCHIMP), Biogeosciences, 10, 753–788, doi:10.5194/bg-10-753-2013, 2013.

Mitchell, T. D. and Jones, P. D.: An improved method of constructing a database of monthly climate observations and associated high-resolution grids, Int. J. Climatol., 25, 693–712, 2005.

Mokhov, I. I., Eliseev, A. V., and Denisov, S. N.: Model diagnostics of variations in methane emissions by wetlands in the second half of the 20th century based on reanalysis data, Doklady Earth Sci., 417, 1293–1297, doi:10.1134/S1028334X07080375, 2007.

Myneni, R. B., Hoffman, S., Knyazikhin, Y., Privette, J. L., Glassy, J., Tian, Y., Wang, Y., Song, X., Zhang, Y., Smith, G. R., Lotsch, A., Friedl, M., Morisette, J. T., Votava, P., Nemani, R. R., and Running, S. W.: Global products of vegetation leaf area and fraction absorbed PAR from year one of MODIS data, Remote Sens. Environ., 83, 214–231, 2002.

Niu, G., Yang, Z., Dickinson, R. E., and Gulden, L. E.: A simple TOPMODEL-based runoff parameterization (SIMTOP) for use in global climate models, J. Geophys. Res., 110, D21106, doi:10.1029/2005JD006111, 2005.

Oleson, K. W., Niu, G. -Y., Yang, Z. -L., Lawrence, D. M., Thornton, P. E., Lawrence, P. J., Stöckli, R., Dickinson, R. E., Bonan, G. B., Levis, S., Dai, A., and Qian, T.: Improvements to the Community Land Model and their impact on the hydrological cycle, J. Geophys. Res. Biogeosci., 113, 2156–2202, doi:10.1029/2007JG000563, 2008.

Papa, F., Prigent, C., Durand, F., and Rossow, W. B.: Wetland dynamics using a suite of satellite observations: a case study of application and evaluation for the Indian Subcontinent, Geophys. Res. Lett., 33, L08401, doi:10.1029/2006GL025767, 2006.

Papa, F., Prigent, C., and Rossow, W. B.: Monitoring flood and discharge variations in the large Siberian rivers from a multi-satellite technique, Surv. Geophys., 29, 297–317, doi:10.1007/s10712-008-9036-0, 2008.

Papa, F., Prigent, C., Aires, F., Jimenez, C., Rossow, W. B., and Matthews, E.: Interannual variability of surface water extent at the global scale, 1993–2004, J. Geophys. Res., 115, D12111, doi:10.1029/2009JD012674, 2010.

Parton, W. J., Scurlock, J. M. O., Ojima, D. S., Gilmanov, T. G., Scholes, R. J., Schimel, D. S., Kirchner, T., Menaut, J. C., Seastedt, T., Moya, E. G., Kamnalrut, A., and Kinyamario, J. I.: Observations and modeling of biomass and soil organic-matter dynamics for the grassland biome worldwide, Global Biogeochem. Cy., 7, 785–809, 1993.

Pickett-Heaps, C. A., Jacob, D. J., Wecht, K. J., Kort, E. A., Wofsy, S. C., Diskin, G. S., Worthy, D. E. J., Kaplan, J. O., Bey, I., and Drevet, J.: Magnitude and seasonality of wetland methane emissions from the Hudson Bay Lowlands (Canada), Atmos. Chem. Phys., 11, 3773–3779, doi:10.5194/acp-11-3773-2011, 2011.

Pison, I., Ringeval, B., Bousquet, P., Prigent, C., and Papa, F.: Stable atmospheric methane in the 2000s: key-role of emissions from natural wetlands, Atmos. Chem. Phys. Discuss., 13, 9017–9049, doi:10.5194/acpd-13-9017-2013, 2013.

Potter, C. S.: An ecosystem simulation model for methane production and emission from wetlands, Global Biogeochem. Cy., 11, 495–506, 1997.

Prentice, I. C., Farquhar, G. D., Fasham, M. J. R., Goulden, M., Heimann, M., Jaramillo, V., Kheshgi, H., Quéré, C.-L., Scholes, R., and Wallace, D.: The Carbon Cycle and Atmospheric Carbon Dioxide, in: Climate Change 2001: The scientific basis, Contributions of Working Group I to the Third Assessment Report of the Intergovernmental Panel on Climate Change, edited by: Pitelka, L. F. and Rojas, A. R., Cambridge University Press, Cambridge, 183–237, 2001.

Prigent, C., Papa, F., Aires, F., Rossow, W. B., and Matthews, E.: Global inundation dynamics inferred from multiple satellite observations, 1993–2000, J. Geophys. Res., 112, 305–317, doi:10.1029/2006JD007847, 2007.

Prigent, C., Papa, F., Aires, F., Jimenez, C., Rossow, W. B., and Matthews, E.: Changes in land surface water dynamics since the 1990s and relation to population pressure, Geophys. Res. Lett., 39, L08403, doi:10.1029/2012GL051276, 2012.

Qian, T. T., Dai, A., Trenberth, K. E., and Oleson, K. W.: Simulation of global land surface conditions from 1948 to 2004, part I: forcing data and evaluations, J. Hydrometeorol., 7, 953–975, 2006.

Ridgwell, A., Marshall, S. J., and Gregson, K.: Consumption of atmospheric methane by soils: a process-based model, Global Biogeochem. Cy., 13, 59–70, 1999.

Riley, W. J., Subin, Z. M., Lawrence, D. M., Swenson, S. C., Torn, M. S., Meng, L., Mahowald, N. M., and Hess, P.: Barriers to predicting changes in global terrestrial methane fluxes: analyses using CLM4Me, a methane biogeochemistry model integrated in CESM, Biogeosciences, 8, 1925–1953, doi:10.5194/bg-8-1925-2011, 2011.

Ringeval, B.: Interactions entre climat et émissions de méthane par les zones humides à l'échelle global, Ph. D. thesis, Université Pierre & Marie Curie, Paris, France, 2011.

Ringeval, B., de Noblet-Ducoudre, N., Ciais, P., Bousquet, P., Prigent, C., Papa, F., and Rossow, W. B.: An attempt to quantify the impact of changes in wetland extent on methane emissions on the seasonal and interannual time scales, Global Biogeochem. Cy., 24, 611–617, 2010.

Ringeval, B., Friedlingstein, P., Koven, C., Ciais, P., de Noblet-Ducoudré, N., Decharme, B., and Cadule, P.: Climate-CH_4 feedback from wetlands and its interaction with the climate-CO_2 feedback, Biogeosciences, 8, 2137–2157, doi:10.5194/bg-8-2137-2011, 2011.

Ringeval, B., Decharme, B., Piao, S. L., Ciais, P., Papa, F., de Noblet-Ducoudré, N., Prigent, C., Friedlingstein, P., Gouttevin, I., Koven, C., and Ducharne, A.: Modelling sub-grid wetland in the ORCHIDEE global land surface model: evaluation against river discharges and remotely sensed data, Geosci. Model Dev., 5, 941–962, doi:10.5194/gmd-5-941-2012, 2012.

Ringeval, B., Hopcroft, P. O., Valdes, P. J., Ciais, P., Ramstein, G., Dolman, A. J., and Kageyama, M.: Response of methane emissions from wetlands to the Last Glacial Maximum and an idealized Dansgaard-Oeschger climate event: insights from two models of different complexity, Clim. Past, 9, 149–171, doi:10.5194/cp-9-149-2013, 2013.

Roulet, N. T., Moore, T. R., Bubier, J., and Lafleur, P.: Northern fens: methane flux and climate change, Tellus, 44B, 100–106, 1992.

Schroeder, R., Rawlins, M. A., McDonald, K. C., Podest, E., Zimmermann, R., and Kueppers, M.: Satellite microwave remote sensing of North Eurasian inundation dynamics: development of coarse-resolution products and comparison with high-resolution synthetic aperture radar data, Environ. Res. Lett., 5, 14415–14428, 2010.

Segers, R. and Leffelaar, P. A.: Modeling methane fluxes in wetlands with gas-transporting plants 3, plot scale, J. Geophys. Res., 106, 3541–3558, 2001.

Sellers, P. J., Meeson, B. W., Closs, J., Corprew, F., Dazlich, D., Hall, F. G., Kerr, Y., Koster, R., Los, S., Mitchell, K., McManus, J., Myers, D., Sun, K.-J., and National Aeronautics and Space Administration and Goddard Space Flight Center, P. J. T.: International Satellite Land Surface Climatology Project – Initiative I data collection (ISLSCP I), available at: http://badc.nerc.ac.uk/view/badc.nerc.ac.uk__ATOM__dataent_ISLSCP (last access: 1 September 2012), 1996.

Sheng, Y. W., Smith, L. C., MacDonald, G. M., Kremenetski, K. V., Frey, K. E., elichko, A. A., Lee, M., Beilman, D. W., and Dubinin, P.: A high-resolution GIS-based inventory of the west Siberian peat carbon pool, Global Biogeochem. Cy., 18, 14415–14428, 2004.

Shindell, D. T., Walter, B. P., and Faluvegi, G.: Impacts of climate change on methane emissions from wetlands, Geophys. Res. Lett., 31, L21202, doi:10.1029/2004GL021009, 2004.

Singarayer, J. S., Valdes, P. J., Friedlingstein, P., Nelson, S., and Beerling, D. J.: Late Holocene methane rise caused by orbitally controlled increase in tropical sources, Nature, 470, 82–91, 2011.

Sitch, S., Smith, B., Prentice, I. C., Arneth, A., Bondeau, A., Cramer, W., Kaplan, J. O., Levis, S., Lucht, W., Sykes, M. T., Thonicke, K., and Venevsky, S.: Evaluation of ecosystem dynamics, plant geography and terrestrial carbon cycling in the LPJ dynamic global vegetation model, Glob. Change Biol., 9, 161–185, 2003.

Spahni, R., Wania, R., Neef, L., van Weele, M., Pison, I., Bousquet, P., Frankenberg, C., Foster, P. N., Joos, F., Prentice, I. C., and van Velthoven, P.: Constraining global methane emissions and uptake by ecosystems, Biogeosciences, 8, 1643–1665, doi:10.5194/bg-8-1643-2011, 2011.

Stillwell-Soller, L. M., Klinger, L. F., Pollard, D., and Thompson, S. L.: The Global Distribution of Freshwater Wetlands, Tech. Rep. NCAR/TN-416+STR, NCAR, available

at: http://www.cisl.ucar.edu/ess/services/dbst/wetlands/ (last access: 11 September 2012), 1995.

Stocker, B. D., Strassmann, K., and Joos, F.: Sensitivity of Holocene atmospheric CO_2 and the modern carbon budget to early human land use: analyses with a process-based model, Biogeosciences, 8, 69–88, doi:10.5194/bg-8-69-2011, 2011.

Strassmann, K. M., Joos, F., and Fischer, G.: Simulating effects of land use changes on carbon fluxes: past contributions to atmospheric CO_2 increases and future commitments due to losses of terrestrial sink capacity, Tellus B, 60, 583–603, doi:10.1111/j.1600-0889.2008.00340.x, 2008.

Tarnocai, C., Swanson, D., Kimble, J., and Broll, J.: Northern Circumpolar Soil Carbon Database, Tech. Rep. Version 1, Research Branch, Agriculture and Agri-Food Canada,, available at: http://wms1.agr.gc.ca/NortherCircumpolar/northercircumpolar.zip (last access: 1 October 2012), 2007.

Tarnocai, C., Canadell, J. G., Schuur, E. A. G., Kuhry, P., Mazhitova, G., and Zimov, S.: Soil organic carbon pools in the northern circumpolar permafrost region, Global Biogeochem. Cy., 23, GB2023, doi:10.1029/2008GB003327, 2009.

Tian, H., Xu, X., Liu, M., Ren, W., Zhang, C., Chen, G., and Lu, C.: Spatial and temporal patterns of CH_4 and N_2O fluxes in terrestrial ecosystems of North America during 1979–2008: application of a global biogeochemistry model, Biogeosciences, 7, 2673–2694, doi:10.5194/bg-7-2673-2010, 2010.

Tian, H. Q., Melillo, J., Lu, C. Q., Kicklighter, D., Liu, M. L., Ren, W., Xu, X. F., Chen, G. S., Zhang, C., Pan, S. F., Liu, J. Y., and Running, S.: China's terrestrial carbon balance: contributions from multiple global change factors, Global Biogeochem. Cy., 25, 222–240, 2011a.

Tian, H. Q., Xu, X. F., Lu, C. Q., Liu, M. L., Ren, W., Chen, G. S., Melillo, J., and Liu, J. Y.: Net exchanges of CO_2, CH_4, and N_2O between China's terrestrial ecosystems and the atmosphere and their contributions to global climate warming, J. Geophys. Res., 116, G02011, doi:10.1029/2010JG001393, 2011b.

Tian, H. Q., Lu, G., Chen, G. S., Tao, S., Pan, S. F., Del Grosso, S. J., Xu, X. F., Bruhwiler, L., Wofsy, S. C., Kort, E. A., and Prior, S. A.: Contemporary and projected biogenic fluxes of methane and nitrous oxide in terrestrial ecosystems of North America, Frontiers in Ecology and the Environment, 10, 528–536, doi:10.1890/120057, 2012.

Valdes, P. J., Beerling, D. J., and Johnson, C. E.: The ice age methane budget, Geophys. Res. Lett., 32, 941–962, 2005.

van Bodegom, P., Goudriaan, J., and Leffelaar, P.: A mechanistic model on methane oxidation in a rice rhizosphere, Biogeochem., 55, 145–177, 2001a.

van Bodegom, P., Wassmann, R., and Metra-Corton, T.: A process-based model for methane emission predictions from flooded rice paddies, Global Biogeochem. Cy., 15, 247–263, 2001b.

Viovy, N. and Ciais, P.: CRUNCEP data set for 1901–2008, Tech. Rep. Version 4, Laboratoire des Sciences du Climat et de l'Environnement, available at: http://dods.extra.cea.fr/data/p529viov/cruncep/, last access: 1 September 2011.

Walter, B. P. and Heimann, M.: A process-based, climate-sensitive model to derive methane emissions from natural wetlands: application to five wetland sites, sensitivity to model parameters, and climate, Global Biogeochem. Cy., 14, 745–765, 2000.

Walter, B. P., Heimann, M., Shannon, R. D., and White, J. R.: A process-based model to derive methane emissions from natural wetlands, Geophys. Res. Lett., 23, 3731–3734, 1996.

Walter, B. P., Heimann, M., and Matthews, E.: Modeling modern methane emissions from natural wetlands 1, model description and results, J. Geophys. Res., 106, 34189–34206, 2001a.

Walter, B. P., Heimann, M., and Matthews, E.: Modeling modern methane emissions from natural wetlands 2, interannual variations 1982–1993, J. Geophys. Res., 106, 34207–34219, 2001b.

Wania, R., Ross, I., and Prentice, I. C.: Integrating peatlands and permafrost into a dynamic global vegetation model, I: evaluation and sensitivity of physical land surface processes, Global Biogeochem. Cy., 23, GB3014, doi:10.1029/2008GB003412, 2009a.

Wania, R., Ross, I., and Prentice, I. C.: Integrating peatlands and permafrost into a dynamic global vegetation model, II: evaluation and sensitivity of vegetation and carbon cycle processes, Global Biogeochem. Cy., 23, GB3015, doi:10.1029/2008GB003413, 2009b.

Wania, R., Ross, I., and Prentice, I. C.: Implementation and evaluation of a new methane model within a dynamic global vegetation model: LPJ-WHyMe v1.3.1, Geosci. Model Dev., 3, 565–584, doi:10.5194/gmd-3-565-2010, 2010.

Weaver, A. J., Eby, M., Wiebe, E. C., Bitz, C. M., Duffy, P. B., Ewen, T. L., Fanning, A. F., Holland, M. M., MacFadyen, A., Matthews, H. D., Meissner, K. J., Saenko, O., Schmittner, A., Wang, H. X., and Yoshimori, M.: The UVic Earth System Climate Model: model description, climatology, and applications to past, present and future climates, Atmos. Ocean, 39, 361–428, 2001.

Weber, S. L., Drury, A. J., Toonen, W. H. J., and van Weele, M.: Wetland methane emissions during the Last Glacial Maximum estimated from PMIP2 simulations: Climate, vegetation, and geographic controls, J. Geophys. Res., 115, D06111, doi:10.1029/2009JD012110, 2010.

Woodward, F. I., Smith, T. M., and Emanuel, W. R.: A global land primary productivity and phytogeography model, Global Biogeochem. Cy., 9, 471–490, 1995.

Xu, X. F., Tian, H. Q., Zhang, C., Liu, M. L., Ren, W., Chen, G. S., Lu, C. Q., and Bruhwiler, L.: Attribution of spatial and temporal variations in terrestrial methane flux over North America, Biogeosciences, 7, 3637–3655, doi:10.5194/bg-7-3637-2010, 2010.

Zhuang, Q., Melillo, J. M., Kicklighter, D. W., Prinn, R. G., McGuire, A. D., Steudler, P. A., Felzer, B. S., and Hu, S.: Methane fluxes between terrestrial ecosystems and the atmosphere at northern high latitudes during the past century: A retrospective analysis with a process-based biogeochemistry model, Global Biogeochem. Cy., 18, GB3010, doi:10.1029/2004GB002239, 2004.

Zhuang, Q., Melillo, J. M., Sarofim, M. C., Kicklighter, D. W., McGuire, A. D., Felzer, B. S., Sokolov, A., Prinn, R. G., Steudler, P. A., and Hu, S.: CO_2 and CH_4 exchanges between land ecosystems and the atmosphere in northern high latitudes over the 21st century, Geophys. Res. Lett., 33, L17403, doi:10.1029/2006GL026972, 2006.

Zobler, L.: A world soil file for global climate modelling, Technical Memorandum 87802, 32, NASA, 1986.

Zürcher, S., Spahni, R., Joos, F., Steinacher, M., and Fischer, H.: Impact of an abrupt cooling event on interglacial methane emissions in northern peatlands, Biogeosciences, 10, 1963–1981, doi:10.5194/bg-10-1963-2013, 2013.

Chapter 5

Methane isotopes - model simulations and sensitivity tests

In Chapter 2, the implementation of CH_4 isotopes in LPX was described. Information about the precursor material and the following processes was given. The fractionation during production was parameterized via present day simulations for NH peatlands (see Chap. 2.5.2.1), the different fractionation effects due to oxidation and transport pathway were analysed in site simulations and the simulated soil profiles were compared to recent measurements (see Chap. 2.6.2). In this Chapter, simulations for the NH peatlands are presented in more detail for present day and over the Holocene. The sensitivity of the isotopic signature of methane emissions to the different plant types simulated in the peatland area are investigated. Further, the correlation between the emitted CH_4 signature and input parameters like temperature or precipitation or model parameters like the fraction of one transport pathway to the total transported CH_4 are presented. Finally, the impact of NH peatland CH_4 emissions on the atmospheric signal during the Holocene is studied.

5.1 NH runs for present day

5.1.1 Input data

For the simulations presented in this Chapter, LPX was used as described in Chap. 2.4.2. Peatland fractions for present-day northern peatlands were used from the Northern Circumpolar Soil Carbon Database (NCSCD, Tarnocai et al., 2007) with a total area of $2.71 \cdot 10^6$ km^2 (for more details see (Spahni et al., 2013)). As climatic input (temperature, precipitation, number of wetdays per month and cloud cover; see also Chap. 3 for details on input data needed by LPX), CRU data TS 3.1 from 1901-2008 was taken (Harris & Lister, 2013) with a 1000-year spin-up, which means that the soil pools are in equilibrium. The average temperature and monthly precipitation for 1991-2008 are illustrated in Fig. 5.1c and d.

5.1.2 Results

Global runs were driven with CRU data and with the newly implemented and calibrated fractionation processes (see Chap. 2.5 and with the parametrisation of the production discussed in Sec. 2.5.2.1). Fig. 5.1 shows the total emission flux per year (sum of plant transport, diffusion into the atmosphere and ebullition events) per m^{-2} and the corresponding signature per grid cell averaged from 1991-2008. The simulated range is -101 to -49 permil. To have a better resolution in the areas with the main contribution to the CH_4 emissions, only the range of -80 to -62 permil is shown. Very few grid cells lay beyond this range (compare with Fig. 2.6). The areas with the main contribution to the total NH peatland emissions have an isotopic flux signature around -67 to -74 permil. The total flux weighted average over all peatland

grid cells is about -71 permil. The results are in range with measurements of CH_4 emissions from ombrotrophic bogs that are typically -74.9 ± 9.8 permil and of fens that are -64.8 ± 4.0 permil (Hornibrook, 2009). The range of $\delta^{13}C$ values reported to date for peatland CH_4 emissions starts at about -100 permil for gas transported through aerenchyma of vascular plants (Chanton et al., 2002) and ends at about -42 permil for residual CH_4 after preferential loss of ^{12}C due to methanotrophy or diffusion through plant aerenchyma (Gerard & Chanton, 1993).

Generally, emissions are correlated to the temperature and precipitation: high soil temperatures and sufficient water result in high CH_4 emissions. Therefore the pattern of the total emissions resembles the pattern of the temperature and precipitation. The signature of the emissions shows a pattern that has more negative values for lower emission rates and more positive values for higher emission rates. The signature is not only influenced by the amount of emitted CH_4, but as well depends on the temperature distribution in the soil and the water content in the soil as different transport pathways prevail for different climatic conditions.

For grid cells with moderate to high emissions (20-50 $gC\,m^{-2}yr^{-1}$) the following observations can be made: Grid cells that have higher temperatures and, therefore deeper active layers, tend to emit heavier CH_4. Oxidation and plant transport are important processes here and enrich the soil over time with $^{13}CH_4$. Also, diffusion is much stronger if deeper active layers prevail: a strong gradient can establish and more CH_4 produced in the upper layers is transported downwards. Grid cells with lower temperature have mainly emissions by ebullition in the upper or middle layers (as soon as they enter the thawing phase), whose signature follows the layer signature it originates from. The layer signature in turn in these cells is close to the production signal. Usually, it is a bit heavier than the production signature due to oxidation in the upper layers. The grid cells with more positive emissions have plant transport as a more dominant pathway. An additional effect of a strong plant transport is that also more O_2 is transported into the soil, enriching the soil with ^{13}C. This is the case for moderate temperatures during the active phase (to prevail over diffusion) and not enough available water to trigger the ebullition and inhibit oxidation (see Tab. 2.3 and Chap. 2.6.2).

The most extreme signatures (positive and negative) can be found in grid cells with low CH_4 production and emission. They usually experience a very cold climate and only the uppermost layers thaw in the warm season and only few CH_4 is deposited in the layers. To which extreme the emissions tend, depends again on the strength of the transport pathways and oxidation. In the case of very positive emissions, the contribution of plant transport and/or oxidation is very high, while ebullition is relatively low. The signature is very negative for low temperatures combined with moderate precipitation during the active production phase. The emission is close to the production signal (which is relatively light due to the parametrization that attributes a light signature to a small production) and transported mainly by ebullition.

Note that the maps here are averages from 1991-2008. This means that it is not always possible to verify the explanation above for every grid cell: the yearly average temperature and precipitation are not exactly representative for the heat and water profile in the soil during the active phases. For a detailed illustration of the connection between heat and water profile, dominating transport pathways and resulting emission signatures, see also Chap.2.6.2 and the following section where scatter plots illustrate the correlation of climate and model variables with the resulting signature of CH_4 emissions.

Beside the fractionation effects in the CH_4 routine, the calculation of the signature of the precursor material also slightly influences the resulting CH_4 emissions. GPP in regions where mosses are dominant has a lighter signature than a GPP from a grass dominated region (see

Chap. 2.5.1). In Europe and the lower parts of North America and Siberia, the fractional cover of grasses are 40-45% and the contribution to GPP 60-65%, while in the higher parts, the partition is about 30% grass and 70% moss with a contribution from the grass PFT to the total GPP of about 45%.

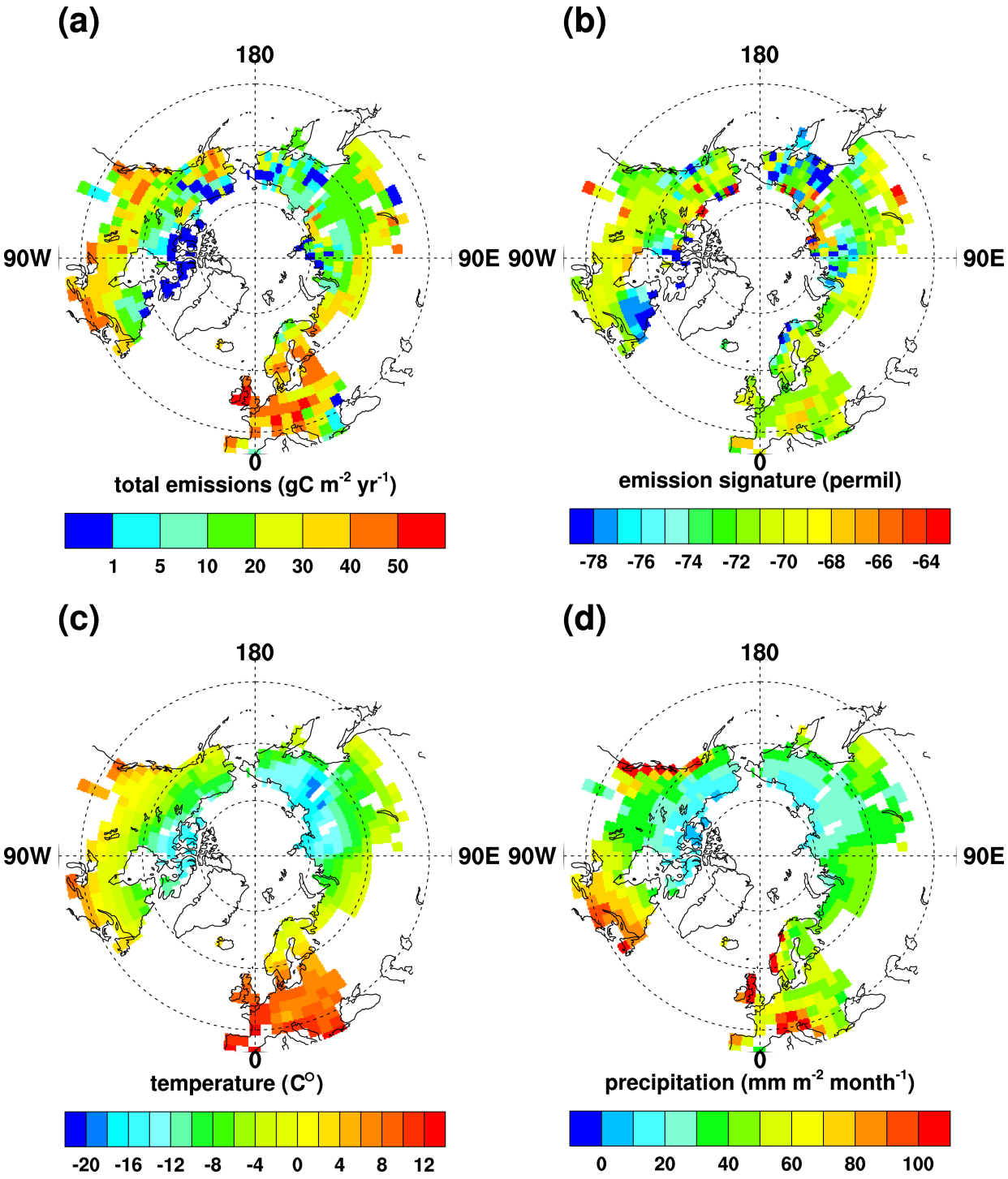

Figure 5.1: a) Simulated total CH_4 emissions per grid cell averaged over the time period 1991-2008. b) Simulated isotopic signature of CH_4 emission flux. c) Average input data for temperature. d) Average precipitation per month.

5.1.2.1 Correlation of $\delta^{13}CH_4$ with climate and model parameters

In the following, correlations between the signature of the annual emission flux of a grid cell and the respective climate variables or other model variables are presented in scatter plots. Fig. 5.2 shows the flux signature vs. the following variables: a) fraction of ebullition to the total emitted CH_4, b) fraction of plant transported CH_4 to the total emitted CH_4, c) average monthly temperature, d) average monthly precipitation, e) average CH_4 production per month, f) minimal thaw depth during June-October. All variables were averaged over the monthly output for June-October 1991-2000. This is continued in Fig. 5.3 with the flux signature vs. g) the average production signature per month, h) the total emissions and i) the fraction of GPP coming from grass (and not moss).

The correlation between the fraction of ebullition to the total emitted CH_4 and the resulting signature of the emitted CH_4 is clearly visible, and to a lesser extend as well for the fraction of plant transport. The more important ebullition events are for the total emissions, the lighter the emissions are and the more important the plant transport is, the heavier the emissions are. Cells with a higher fraction of plant transport develop more positive layer signatures and therefore more positive emissions. But there are other possibilities to have heavier emissions: grid cells with a high fraction of oxidation or diffusion through air emit isotopically more enriched CH_4 as well.

The comparison of the signature and the temperature shows as well a correlation. The warmer the average summer and autumn temperature is, the heavier the emissions. As described before, soils with an extended thawed profile over time and depth have a high production rate, an active diffusion, a considerable amount of plant transport and oxidation. Grid cells with very low temperatures and emissions tend to emit mainly in the relatively short warm phases either via large ebullition events (if enough water is available) or via diffusion in air and plant transport, therefore occupying the whole range of signatures. For the monthly precipitation, no such clear trend is visible. Grid cells with low precipitation can have signatures from the lowest simulated to the highest. While temperature scales the strength of the transportation pathways and production more directly (influencing for example the diffusion coefficients for diffusion and plant transport, RH, or the ebullition, see Chap. 2.4), the water content in the soil either serves more as a threshold (minimum water availability) or is less limiting to the processes in the CH_4 routine.

The picture of the minimal thaw depth over summer and autumn (layer 0 is the uppermost layer) does not show a clear trend. Minimal thaw depth here means that this layer and the layers above are permanently unfrozen during the active phase. There is also no clear relation visible for the fraction of GPP coming from mosses. The comparison of the average produced CH_4 with the corresponding signature of the emission shows the expected trend. The production is high in areas with a warm and long active phase and in these areas, plant transport and oxidation are high as well, leading to more positive $\delta^{13}C$. The average production signature and the average emissions signature are as well correlated. Depending on the importance of the different transportation pathways and oxidation, the emission signal is differently changed from the starting production signature. The more positive the produced CH_4 is, the more positive the signature of the emissions are. Cells with enriched produced CH_4 and emissions are mostly cells with a large amount of CH_4 emissions, warmer temperature and stronger plant transport. This even increases the effect of enrichment. The relation between the total emissions and their signature is already shown in Fig. 2.6 with a logarithmic scale for the total emissions and was used for the calibration of the production fractionation.

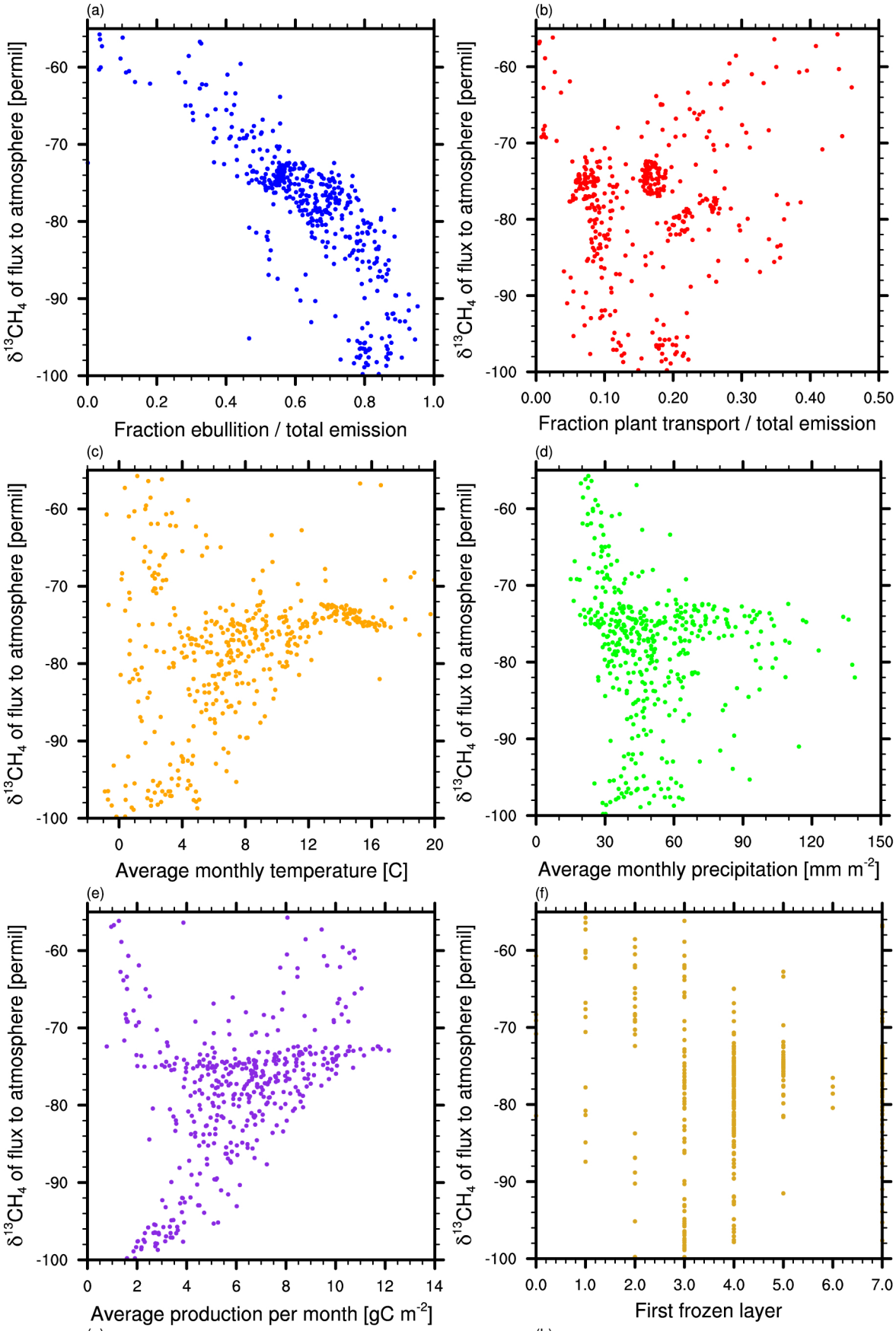

Figure 5.2: $\delta^{13}CH_4$ isotopic signature of CH_4 flux to atmosphere [permil] vs. a) fraction of ebullition to the total emitted CH_4 (R^2 = 0.71, a = -45.0, b = -49.8) , b) fraction of plant transported CH_4 to the total emitted CH_4 (R^2 = 0.16, a = 22.6, b = -84.6), c) average monthly temperature [C], (R^2 = 0.11) d) average monthly precipitation [mm m$^-$2] (R^2 = 0.04), e) average CH_4 production rate[gC m$-$2 month^{-1}] (R^2=0.16), f) average thaw depth (R^2=0.01).

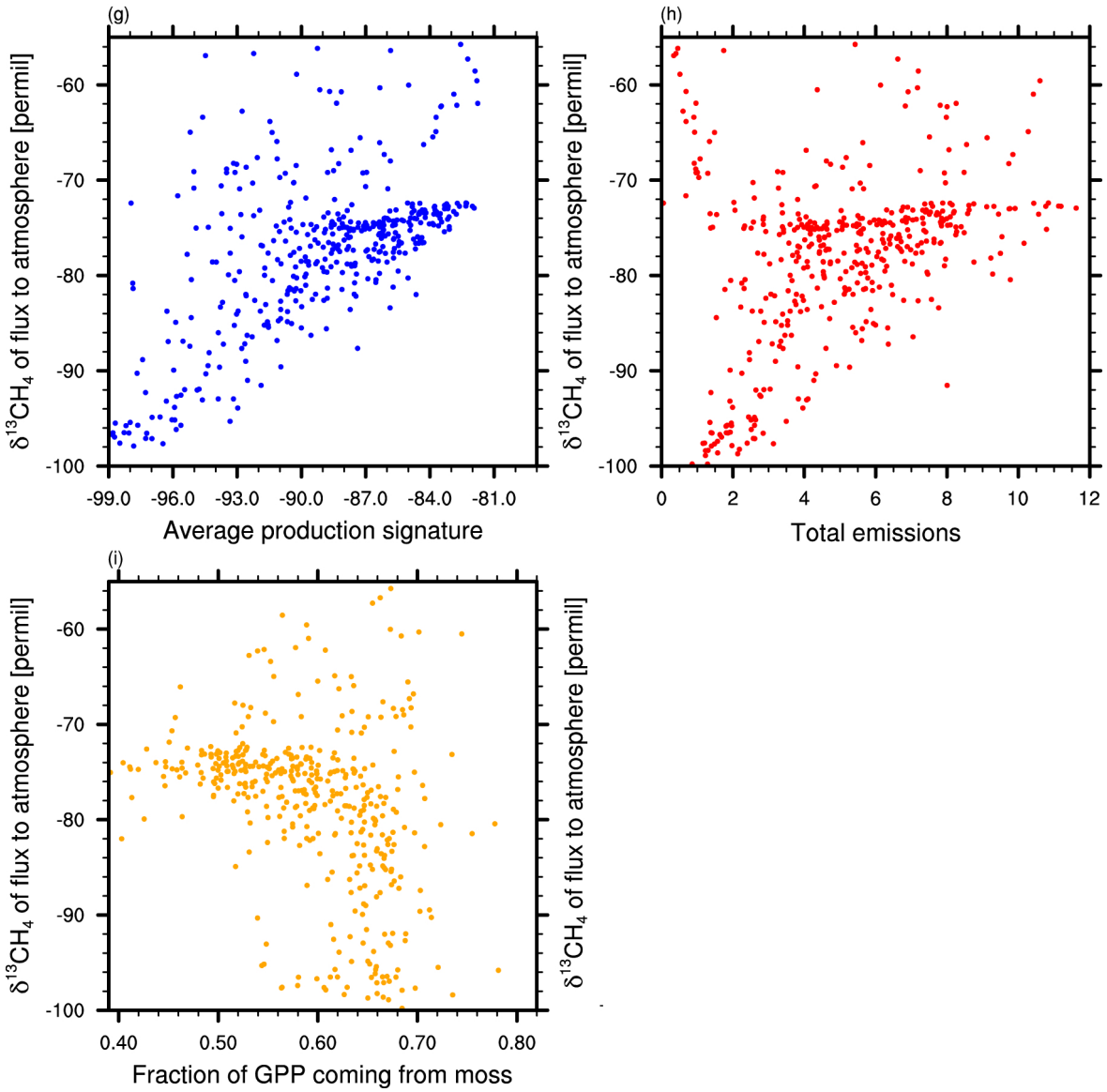

Figure 5.3: CH_4 flux signature [permil] vs. g) average production signature [permil](R^2 = 0.4, a = 1.3, b = 39), h) average emissions [gC m^{-2} $month^{-1}$](R^2 = 0.19) and i) the fraction of GPP coming from grass (R^2 = 0.06).

The strongest correlation can be found between the ebullition fraction and the emission signature with an R^2 of 0.71. All the correlation factors R^2 are summarized in the according captions. If the correlation is higher than 0.2, the according values for a and b for the regression line are given as well. Note that for this calculations, all grid cells are weighted equally.

There is no simple, clear correlation between one climate input parameter or model parameter with the signature of CH_4 emissions. The interaction between production signature, fractionation through oxidation, plant transport, diffusion and ebullition is very complex. They are influenced by the available substrate for CH_4 production, the water and temperature profile in the soil, which are in turn mainly controlled by the temperature, precipitation and atmospheric CO_2. To better constrain the LPX CH_4 routine, it would be crucial to have more site measurements of CH_4 emissions including their signatures and the corresponding temperature, water and CH_4 profile in the soil to have a better insight in actual correlations that the model should reflect.

5.2 Overview of the understanding of the atmospheric $^{12}CH_4$ and $\delta^{13}CH_4$ in the last 10'000 years

The general strong coupling between circum-N. Atlantic climate and CH_4 variations (e.g., Loulergue et al., 2008) does not hold during the Holocene: while the CH_4 record is bowl shaped and has a clear minimum around 5 ka BP, the temperature record is stable (see Fig. 5.4). As the concentration history of CH_4 is disconnected from isotope records of $\delta^{13}CH_4$ and δD_{CH4}, multiple factors seem to be needed to explain concentration and isotope records during the Holocene.

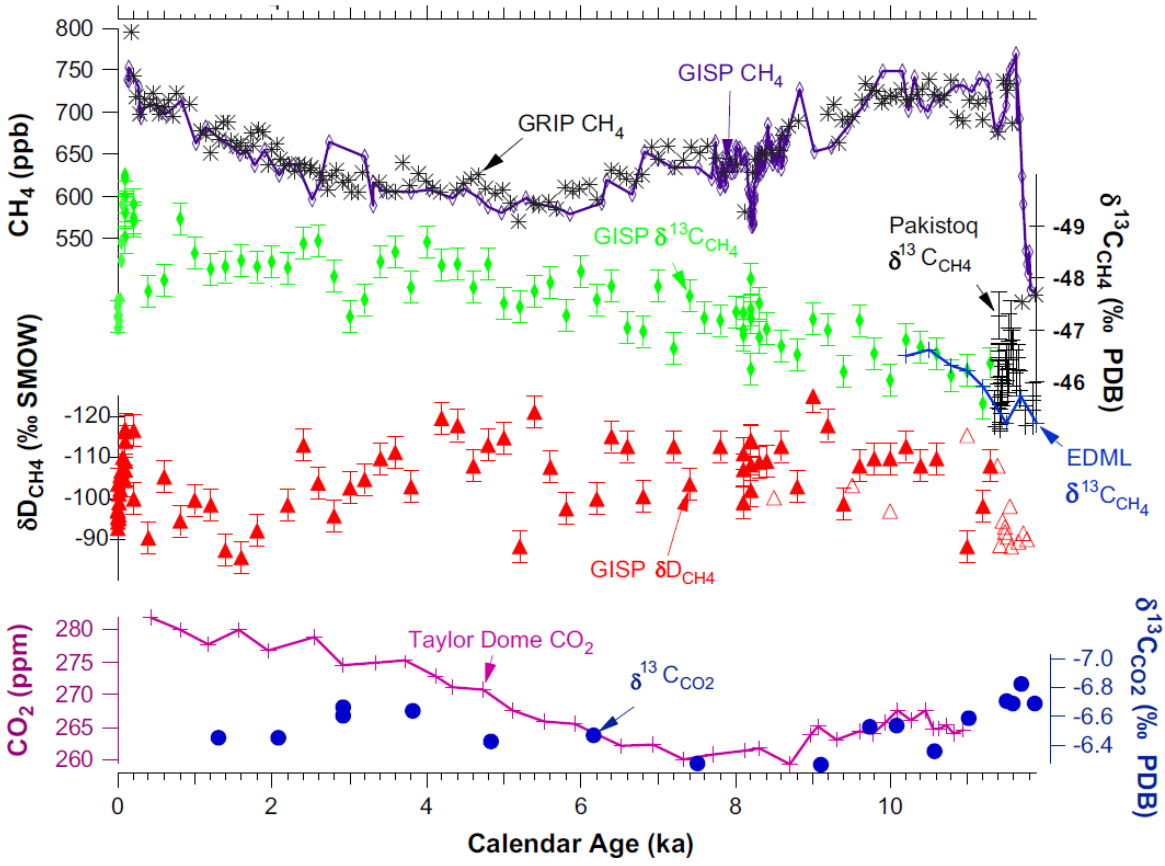

Figure 5.4: Holocene record for atmospheric CH_4 from GISP II and GRIP, $\delta^{13}CH_4$ and δD_{CH4} from GISP I, copied from Sowers (2010).

5.2.1 $^{12}CH_4$

In the early Holocene, climate in the NH experienced elevated summer insolation and increased seasonality providing ideal conditions for wetland development and high CH_4 emissions from NH wetlands. From 9 ka BP onwards, the insolation and seasonality declined again, reducing wetland emissions in the NH and SH (MacDonald et al., 2006). Desertification in the African and Asian subtropics, shifts in NH temperate forest types and modest southward migration of the Arctic tree line, as well as anthropogenic deforestation and draining of wetlands concentrated in Asia, Mediterranean and Europe would attribute the reason for the decrease of CH_4 emissions mainly to the NH (Wanner et al., 2008), while the increasing interpolar gradient in CH_4 concentration (IPG) between 10.5 and 4 ka BP suggest that SH

emissions decreased even stronger than NH emissions (Chappellaz et al., 1997). Between 4 and 1 ka BP, the IPG declined pointing to a strong increase of SH during a general rise in global emissions.

5.2.2 $\delta^{13}CH_4$

From 11 to 4 ka BP, there is an almost linear trend in $\delta^{13}CH_4$ from heavier values of -46 permil at 11 ka BP to -48 at 4 ka BP. From 4 ka BP to 1.8 ka BP, records show little change in the CH_4 concentration (Sowers, 2010). $\delta^{13}CH_4$ was relatively stable and close to present-day values from about 2 ka BP to 0.5 ka BP, then decreased to a minimum around 1700 CE, remained low until the late 18th century, and then rose exponentially to present-day values (Mischeler et al., 2009). Sowers (2010) suggest to attribute the development over the last few centuries to anthropogenic CH_4 emissions that are isotopically enriched. However, the causes are not well understood (Etheridge et al., 1998; Ferretti et al., 2005). For the time from 0 to 1000 CE, biomass burning emissions are believed to be high and then reduced by 70% in the following 700 years influenced by both natural climate change and human activities, while agricultural sources increased (Mischeler et al., 2009; Ferretti et al., 2005).

5.2.3 Different theories to explain the $^{12}CH_4$ and $\delta^{13}CH_4$ records during the Holocene

Generally, there exist various hypotheses in the recent literature to explain the CH_4 record in the Holocene. Atmospheric CH_4 levels are the result of changes in sources, sinks or a combination of the two.

Ruddiman (2003) claim that early civilizations influenced the atmospheric CH_4 concentration from 5 ka BP onwards. Rice agriculture yielded to higher CH_4 emissions and a growing anthropogenic impact on atmospheric CH_4 levels. The basis of this theory is the strong coupling between CH_4 and NH insolation seen during previous interglacial periods and the decline in the interpolar CH_4 gradient (IPG) between 4 and 0.8 ka BP that could be caused by a population increase centered on the equator. Sowers (2010) find that the Ruddiman hypothesis is not supported by isotope data of $\delta^{13}CH_4$ and δD_{CH4}. It is not possible to predict the characteristic isotope signature associated with the hypothesized agricultural emissions. Under the assumption that present day isotope values for rice and ruminants are usable for the new agricultural emissions between 4 and 1 ka BP, then these inferred isotope values are lower than the flux-weighted global emission values at 4 ka BP (see Sowers (2010)).

Singarayer et al. (2011) investigated the question whether the source of the increase in atmospheric CH_4 since the mid Holocene is due to early rice cultivation or an increase in natural wetland emissions from tropical and boreal sources. Their simulations hint to the explanation that natural changes in Earth's orbital configurations led to enhanced emission in the SH tropics.

Chappellaz et al. (1997) believe that changes in the tropical wetland emissions are the primary driving force. The broad CH_4 minimum at 5 ka BP is driven by lower tropical CH_4 emissions in this hypothesis, which are the largest natural source, while the high IPG record is driven by moderate changes in tropical emissions and subtle changes in NH wetland emissions. Between 4 and 1 ka BP, the interhemispheric gradient declined suggesting a disproportionate increase of SH emissions during the rise in global loading.

Other theories stress the importance of northern peatlands (MacDonald et al., 2006, described in Chap. 5.3), the changes in the sink term or a release of marine clathrates. If the low values of CH_4 during the mid Holocene were caused by an increase in the atmospheric sink, one would expect the isotope records to closely follow the concentration curve. As this is not the case, one can safely say other factors have had the major impact on the atmospheric loading and isotope record. A high importance of clathrates is not likely in the time from 4 to 1 ka, as no change in $\delta^{13}C$ can be seen. More details and argumentations on the different theories can be found in Sowers (2010).

Sowers (2010) used a top-down model approach with two boxes to explain the CH_4 and $^{13}CH_4$ record during the Holocene (see Fig. 5.4). He measured a $\delta^{13}CH_4$ decrease in the atmosphere throughout the Holocene of 2 permil (from -46.4 to -48.4 permil). His argumentation is fortified with data for δD_{CH4}, CH_4 and $\delta^{13}CH_4$. He believes this drop to be a combination of increased CH_4 emissions from Arctic lake ecosystems, an increase in the ratio of C_3/C_4 plants in wetlands due to an elevated atmospheric CO_2 level and newly exposed land areas north of 40°N associated with ice retreat and an increase in communities using the CO_2 reduction and not the acetate fermentation pathway and an activation of NH (see also Chap. 2.5.1).

Present day estimates of thermokarst lakes in the Arctic region are up to 20-30 $TgCH_4$ emissions per year and their isotopic signature is extremely depleted. Therefore, an increase in thermokarst CH_4 emissions could explain part of the atmospheric signal, but would also require a decline in other areas in order to maintain the total global emissions. A better constrained δD_{CH4} between 10.5 and 4 ka BP would be needed to support this theory with a more pronounced shift than it is visible in the record. Nevertheless, at the beginning of the Holocene, increased CH_4 emissions from Arctic lakes would be in line with the δD_{CH4} record that shows a slight decrease.

The ratio of C_3/C_4 increases when CO_2 is rising which holds true for the Holocene. Sowers (2010) find that in order to fully account for the 2 permil $\delta^{13}CH_4$ decrease of NH CH_4 emissions between 10.5 and 4 ka BP by a change in C_3/C_4 rates, one would need the percentage of C_4 plants to account for 40% in the early Holocene of the GPP in wetlands which then decrease to present day values of about 20%. This theory is further supported by the fact that high NH ecosystems were activated during the Holocene, where C_3 type plants are dominant. Emissions from circum-Arctic wetlands increased in a slow response to warmer, stable Holocene conditions, a mechanism that is supported by $\delta^{13}CH_4$ measurements from Greenland ice cores (Fischer et al., 2008).

In the time between 4 and 1 ka BP, the δD_{CH4} increases by 20 permil while $\delta^{13}CH_4$ remains nearly constant. A possible explanation is a shift towards the tropical emissions. This is consistent with the decreased IPG over this time. But if the CH_4 emissions shifted significantly from high latitudes to the tropics, also a shift in $\delta^{13}CH_4$ should be seen or the increased tropical emissions would need to have the same signature that from the higher latitudes. There are too few studies to verify this theory. A gradual onset of clathrate release with enriched δD_{CH4} could explain as well the records of δD_{CH4} and $\delta^{13}CH_4$ in this period.

5.3 The effect of a change in the ratio of plant functional types in peatlands

The potential effect of a shift from the peatland grass to moss PFT on atmospheric $\delta^{13}CH_4$ is investigated, simulating a process like the passage from fens to bogs.

5.3.1 Change in vegetation composition in northern peatlands

Northern peatlands have accumulated large carbon stocks since the last deglaciation acting as an important atmospheric sink. For example, Hunt et al. (2013) examined the effect of climate on vegetation composition at a peatland complex in Alaska in the last 15'000 years. They find an abundance of *Sphagnum* moss and high C accumulation typical for a warm climate during the Holocene Thermal Maximum. Throughout the mid Holocene, a wet climate prevailed. They find high organic mater deposits and a peak in *Sphagnum* at 5.8-4.6 ka BP. After 4.6 ka BP, a transition to low C accumulation rates sets in and *Sphagnum* decreases. Periods where the climate was dry and cold, led to increase in woody material and grass population. Wet regional conditions increased the moss species amount and decreased grass species. They found a recent warming in the last century leading again to an increase of *Sphagnum*. In Central Europe for example, a vegetation change from fen to ombrotrophic bog vegetation that happened 2.1 ka BP can be seen again in the last century (Dudova et al., 2013).

MacDonald et al. (2006) attribute the late-Holocene increase in CH_4 to an expansion of northern wetlands due to neoglacial climatic cooling after the Holocene thermal maximum. Based on typical peatland succession stages, higher summer insolation in the early Holocene, and evidence of peatland vegetation and type from peat cores taken in Siberia, they suggest that it is likely that many of these newly developed peatlands were warm and wet minerotrophic fens. Such fens emit CH_4 at much greater rates than the ombrotrophic *Sphagnum* bogs common in the north today. (MacDonald et al., 2006) suggest further that the observed decline in peatland initiation at 8 ka BP (while peatland area was still increasing till 6 ka BP) and the transformation from high CH_4 efflux fens to *Sphagnum* bogs to contribute to the decline in atmospheric CH_4 between 8 and 6 ka BP. Also, they used $\delta^{13}CH_4$ values of ice from the Pakitsoq outcrop in western Greenland to infer the origins of early-Holocene atmospheric CH_4. It has been suggested that major terrestrial sources contributing CH_4 during the period from 11 to 8 ka BP likely produced CH_4 with $\delta^{13}C$ values of between -50 and -60. They conclude that as northern peatlands dominated by ombrogenous bogs typically emit CH_4 with about -60 permil and as emissions of boreal fens are relatively enriched in ^{13}C (-50 to -60 permil), that these values are consistent with an early northern peatland complex dominated by minerotrophic fens.

Rapid transitions from fens to bogs can occur within a few years when the water table decreases significantly (Finsinger et al., 2012). Tahvanainen (2011) claim that dramatic changes in boreal peatlands can occur as a result of climate change: for example, temperature increase will lead to the development of raised bogs from aapa mires (a large, complex, cold-climate fen) in Finland that shift into ombrothrophic mires within a few decades in response to drainage changes.

The presented simulations with LPX should help to estimate the potential contribution of a shift from fens to bogs to a change in the atmospheric CH_4 signature.

5.3.2 LPX simulations per PFT

Two simulations were performed with LPX to test the potential effect of shifts in the contribution to the different plant types C_3 grass and moss from NH peatlands. Once, only the C_3 grass PFT was used as peatland PFT, once only the moss PFT. For the simulations with the moss PFT only, the plant transport pathway in the CH_4 routine was blocked for gas transport. The resulting signature of the emission fluxes are presented in Fig. 5.5a) and b). The total amount of CH_4 emissions (Fig. 5.5c) and d)) from moss and grass varies by about 20%. Compared to the standard simulation in Fig. 5.1, the emissions drop almost by 25% when only taking the grass PFT into account instead of both. In the simulations for both PFTs together, LPX simulates for the time period 1901-2008 a contribution to the GPP from the grass PFT of 47% and the moss PFT for 53%. Fig. 5.5e) shows the signature of the global emission flux from northern peatlands simulated for 1991-2001 for the different scenarios of the peatland PFTs growing.

The simulated signature for GPP coming from mosses is -30 permil, and -25 permil for GPP coming from the grass PFT. The fractionation of $\delta^{13}C$ during fixation in the leaf is based on a model by Lloyd & Farquhar (1994) for all PFTs except the moss PFT for which the fractionation is set to a fixed value (see Sec. 2.5.1).

If we take the two extreme scenarios 100% grass/ 0% moss and 0% grass/ 100% moss and the simulation for about 50% grass / 50% moss (this is the distribution of GPP between grass and moss if both PFTs are allowed to grow and compete in the period of 1991-2008), LPX would simulate a possible maximal change in the signature of NH peatland emissions of +1.5 permil (to grass only) and -2.5 (to moss only).

Chappellaz et al. (1997) find that during the early Holocene, the contribution from northern peatlands to the total wetland contribution may have been 30%. Assuming peatland emissions make up for 15-30% of natural CH_4 emissions (see Chap. 1.3.2), a shift from the current distribution to moss dominated peatlands could cause a shift in the signature of CH_4 emissions of about -0.35 to -0.75 permil, a shift from grass dominated peatlands to moss up to -0.6 to -1.2 permil. The simulated decrease in $\delta^{13}C$ goes into the right direction but it can only explain parts of the decrease found by Sowers (2010). Further, this value is an upper limit as it requires a transition to a completely moss vegetation and as northern peatlands could make up for less than 15-30% of natural CH_4 emissions during the Holocene. The climate in the early Holocene is thought to be much like the present (Kobashi et al., 2007), while CO_2 values were much lower. Therefore, CH_4 emission estimates from peatlands in the early Holocene are more an upper bound.

Note that even if we do not directly prescribe one PFT, only the two peatland PFTs can grow in the peatland area of a grid cell. In the remaining fraction of a grid cell, 9 natural PFTs are possible to grow. LPX's only C_4 plant is a tropical grass which does not grow in the latitudes where peatland is located if it has to compete against the other natural PFTs. If we use the PFT characteristics of the C_4 PFT and force LPX to take it as his only peatland PFT, there is almost no GPP (and therefore no RH and CH_4 emissions). Therefore a shift from C_4 plants to C_3 was not possible to estimate with this model version which is focussing on the CH_4 isotopes in NH peatlands and not all wetlands.

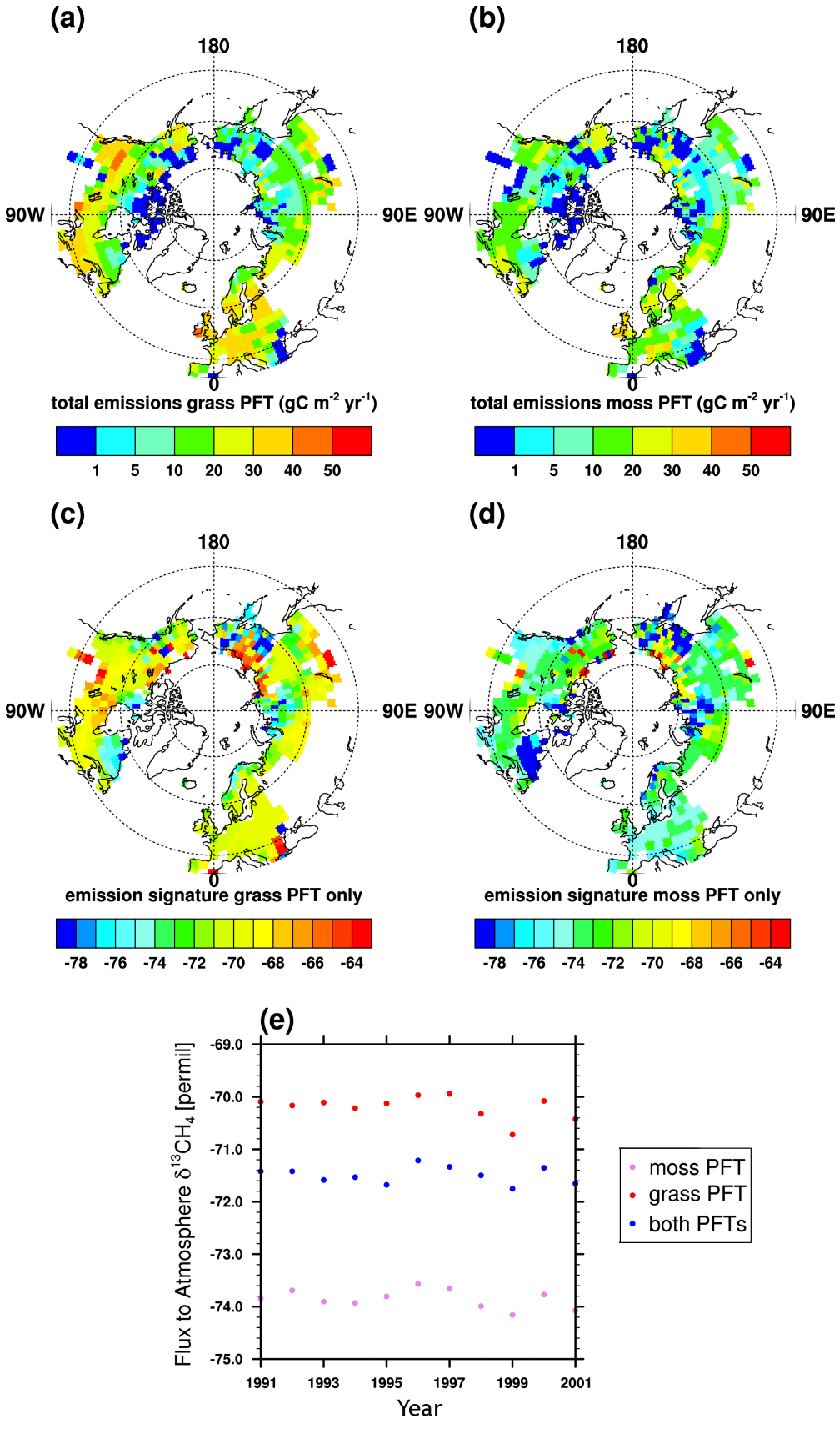

Figure 5.5: Comparison of a run with the grass PFT only and a run with the moss PFT only. a) and b) are the average weighted signatures of the total emission fluxes per grid cell for the grass PFT and the moss PFT, c) and d) the according CH_4 fluxes. Plot e) shows the global average peatland CH_4 emission signature for both scenarios and the case with both PFTs together.

5.4 NH runs over the Holocene

A simulation for the NH peatland CH_4 emissions from the LGM till present was performed to assess the variability of $\delta^{13}CH_4$ and the possible contribution of peatland emissions to the measured drop of atmospheric $\delta^{13}CH_4$ of 2 permil during the Holocene (see Chap. 5.2).

5.4.1 Input data

The setup for the simulation presented in this Section is described in Spahni et al. (2013). The goal of this work was to to simulate peatland development in the northern high-latitudes since the Last Glacial Maximum (LGM). LPX is forced by climate anomalies relative to present-day from a transient simulation since the LGM with a coupled ocean-atmosphere climate model (TraCE21ka CCSM3, Collins et al., 2006; Liu et al., 2009), the climate anomalies are simulated for every month, and added present-day observed gridded climate (CRU, Mitchell & Jones, 2005)). The climate simulation includes millennial-scale variability like the Younger Dryas. CO_2 was prescribed following ice core data (see Joos & Spahni (2008)) and LPX was run with a dynamic nitrogen cycle (see Chap. 2.3.1, Appendix and Spahni et al. (2013)). N deposition plays a crucial role for the peatland N availability and therefore for the peatland productivity. An implicit N source as N inputs and atmospheric N deposition are implemented in LPX. The N source can be interpreted as N_2 fixation and other N input processes that allow LPX to simulate different availability of nutrient sources. Modern NPP over peatlands is down-regulated by about 50% with the dynamic N cycle (Spahni et al., 2013). The spin up is 2500 yr, and an analytical solution is used to ensure that all C pools have established equilibrium conditions at the beginning of the LGM. A minimum peatland area fraction is set to 0.0001 in every grid cell.

5.4.2 Results

Fig. 5.6 shows the total simulated CH_4 flux (a) and $\delta^{13}CH_4$ (b) from NH peatlands from 14 ka BP till present day together with the climate input data, i.e. average temperature (c) and average precipitation (d) in grid cells with a peat area fraction larger than 0.0001, the modelled total peatland area (e) and the foliar projective cover fraction weighted by GPP of grasses (f). All plots show averages over ten years and the smoothed curve in Fig. b) is a running-mean average over 100 years. The time from the LGM till 14 ka BP is not shown in the Figures as the peatland area and emissions were almost zero.

CH_4 emissions start to rise at about 14 ka BP and reach annual emissions of 30 $TgC\,yr^{-1}$ at present day. The rise in CH_4 emissions is essentially driven by the simulated peatland area growth (including ice sheet retreat) and modulated with temperature. E.g., the drop in total emissions at 2 ka BP originates from a widespread emission drop over many grid cells and is reflected in the decrease of average temperature over peat land grid cells. The strong drop visible in temperature and precipitation at about 12 ka BP reflects the Younger Dryas (YD) event. The impact of climate change during the YD on CH_4 emissions is overruled by the strong peatland area growth at the beginning of the simulation.

Note that in reality, peatland emissions are not zero during the transition or glacial periods. In this simulation, only modern day peatland area is taken into account and only the ice mask is varying and the area is gradually growing from zero to present day extent. Peatlands that only existed in the past are not considered. Actual measurements suggest a southward shift from peatlands that existed during the glacial. Also, the visible climate change during the Younger Dryas would in reality decrease CH_4 emissions from peatlands existing at that

time, while in the simulation the ice mask further decreases and peatland area increases for modern peatlands (see Fig. 5.6f)).

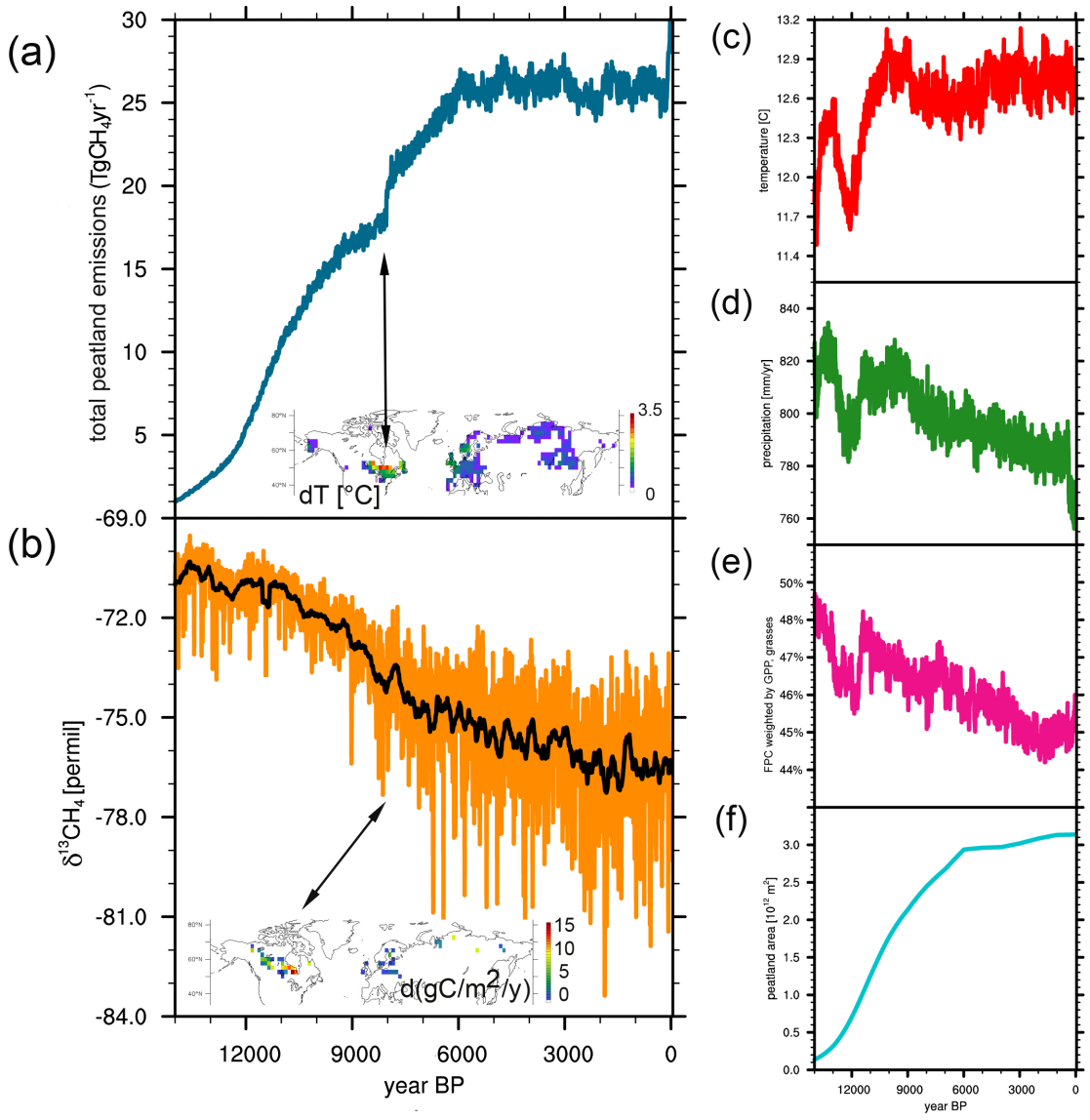

Figure 5.6: Simulated decadal CH_4 (a) and $\delta^{13}CH_4$ (b) and from 14 ka BP till present. Emissions are linearly scaled to have present day CH_4 emissions of 30$TgCH_4$ per year (see Chap. 3). The running mean was calculated over 100 years. The inlay in (a) shows δT [C] between the time slices at 7994 and 8004 BP and the inlay in (b) the change in emissions [gC m^{-2} yr^{-1}] between 6000 and 2000 BP; (c) Average annual mean temperature in all grid cells with NH peatlands. (d) Average annual precipitation over grid cells with NH peatlands. (e) Total areal extent of peatlands. (f) Foliar projective cover fraction weighted by GPP for grasses.

The sharp rise in CH_4 emissions at about 8 ka BP is a non-linear effect caused by a few grid cells in North America. The area extent does not change abruptly but the temperature in this region rises significantly (which is not visible in the average temperature signal but in the inlay plot) and the soil temperatures switch from slightly negative to positive leading to high emissions. This jump is identified as the end of the 8.2 kyr event caused by freshwater forcing in the climate model. The effect of anthropogenic N deposition towards 0 BP is visible in the total emissions (see Spahni et al. (2013); Stocker et al. (2013)).

The foliar projective cover fraction weighted by GPP contributed from grasses follows the precipitation signal. Both moss and grass GPP grow in concert with the increasing peatland area, but mosses grow faster making the relative contribution from grasses to become smaller. The simulation is therefore not a simple shift from fen to bog (as for example suggested by Sowers (2010) as a possible explanation), but there is a decrease of about -3% in the emission contribution from grasses. This effect is small compared to the effect of area growth (in the order of 0.1 permil). A decreasing grass cover fraction reduces the growth of emissions as grasses have a higher GPP than mosses (see Chap. 2.5.1), but again, the effect is to weak to be seen in the emission signal. Generally, the moss PFT is most dominant in regions more north, while the grass PFT has its highest contributions in the southern regions of NH peatlands.

The simulated δ^{13}C of NH peatlands varies over the last 14'000 years between -69.5 and -83.5 permil (Fig. 5.6). Between 14 and 11 ka BP, signatures stay in the range of -71.5 $\pm$ 2 permil, then start to drop during the Holocene till 3 ka BP to a a level of about -76 permil and fluctuate around this level till present day. Note that the short scale variations (the resolution is a decade) are of the order of the long term shifts and that variations become significantly higher with time (also true for emissions). As ice core records of atmospheric $\delta^{13}CH_4$ in the past average over many decades or more, this large fluctuations could not be seen in the ice.

The depletion in δ^{13}C in the simulation stems from the stepwise activation of some grid cells in the very North of America and Russia. They have generally a lighter emission signal than regions more south (see Chap. 5.1.2). Their contribution grows over time and becomes very high, making the overall emission signal more negative. The simulated contributions from plant transport, diffusion and ebullition to the total emissions averaged over all peat land grid cells only vary within a few percent (7.5$\pm$ 1.5% plant transport, 16$\pm$1% diffusion, 76.5$\pm$1.5% ebullition).

What effect would the simulated peatland $^{12}CH_4$ and $^{13}CH_4$ changes have on the atmospheric CH_4? The measured atmospheric CH_4 becomes steadily lighter between 11 and 4 ka BP, stays almost at a constant level from 4 to 1 ka BP and drops to a Minimum at about 1750 to rise again till present day (Fig. 5.4). The simulated NH peatland contribution drops as well during the Holocene and stays at a constant level from 3 ka BP onwards. Thus, the simulated signature from NH peatlands shows the same trend as the measured atmospheric δ^{13}C. But there are two different effects: 1) the direct shift in $\delta^{13}CH_4$ in NH peatlands and 2) the overall contribution of peatland CH_4 emissions (as a depleted source) to the total emissions and the global budget.

The effect of a shift in the peatland emission signature is weaker than the effect of the overall increase in strength of the peatland source. Assuming peatland emissions make constantly up for 15% of natural CH_4 emissions during the Holocene (see Chap. 1.3.2), a shift of 4 permil in the peatland signature causes a change in atmospheric signature of almost 0.5 permil. For an estimation of the second effect, a simple box model was used and illustrated in Fig. 5.7.

In the presented simulation, the source strength of NH peatlands grows. It gains importance to the overall mix over time when the total sources are kept constant (see Fig. 5.7) in this simple box model. The measured atmospheric CH_4 concentration in Fig. 5.4 can be translated into total atmospheric CH_4 burden M (with a unit conversion factor of 2.78 Tg CH_4 ppb^{-1}, see Chap. 3). Under the assumption of a steady state every ten years, the total source and sink strength can be calculated from the atmospheric CH_4 load with the assumption of a lifetime τ of atmospheric CH_4 of 9 years (Prinn, 1994). Assuming further that the source

mix and the fractionation of the sinks are constant, the following equation can be solved for the atmospheric $\delta^{13}CH_4$:

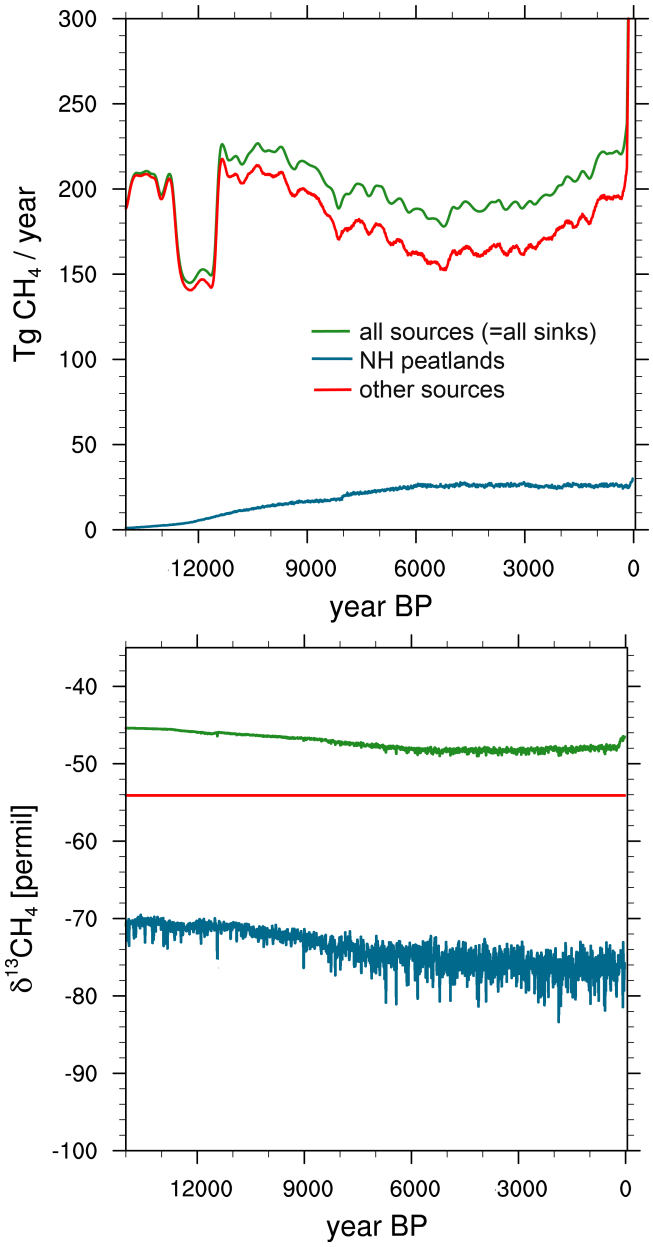

Figure 5.7: Simulated NH peatland emissions (a) and signature (b) in blue together with atmospheric $^{12}CH_4$ measurements (green, top) and assumptions for other sources (red) leading to a estimate of the resulting atmospheric $^{13}CH_4$ (green, bottom).

$$Q_{peat} \cdot \delta^{13}C_{peat} + Q_0 \cdot \delta^{13}C_0 = S \cdot \delta^{13}C_S \tag{5.1}$$

with

$$\delta^{13}C_S = \delta^{13}C_{atm} + \epsilon_S \tag{5.2}$$

$$S = \frac{1}{\tau} \cdot M \tag{5.3}$$

Q_{peat} [Tg CH_4 y^{-1}] being the peatland source, Q_0 the other sources and S the atmospheric sink. $\delta^{13}C_{peat}$, $\delta^{13}C_0$ and $\delta^{13}C_S$ [permil] the according signatures and $\delta^{13}C_{atm}$ the atmospheric signature. ϵ_S is the sink fractionation and is set to -8.8 permil (Platt et al., 2004; Brenninkmeijer et al., 1995; Gierczak et al., 1997; Quay et al., 1999), M the atmospheric burden [Tg CH_4]. Q_{peat} and $\delta^{13}C_{peat}$ were taken from the TraCE21ka simulation where CH_4 increases significantly. The atmospheric CH_4 concentration in Fig. 5.4 was used to estimate the sink strength (steady state assumption). The atmospheric concentration during 12 to 4 ka BP decreases by about 150 ppb, while the measured $\delta^{13}CH_4$ decreases by 2 permil. All other sources Q_0 were calculated as $Q_0 = S\text{-}Q_{peat}$ and their signature was set to -54 permil (the source mix is assumed to stay constant), similar to the reported emissions signatures for the largest natural CH_4 source, the tropical wetlands.

Under these assumptions, the changing contribution of peatlands, i.e. the change in peatland area extent and distribution together with the shift of the peatland emission signature can cause a change in atmospheric $\delta^{13}CH_4$ of 2 permil as shown in Fig. 5.7 and 5.8.

Fig. 5.8 shows again the simulated behavior of $\delta^{13}CH_4$ during the Holocene in more detail together with the measured atmospheric $\delta^{13}CH_4$ signal by Sowers (2010) and the projected $\delta^{13}CH_4$ signal calculated with the simple box model. Sowers (2010) explanation of the shift via a combination of increased CH_4 emissions from Arctic lake ecosystems and an increase in the ratio of C_3/C_4 plants in wetlands can not be tested with the presented simulation. However in LPX, the atmospheric shift in $\delta^{13}CH_4$ during the Holocene can be entirely explained with the development of present day peatlands.

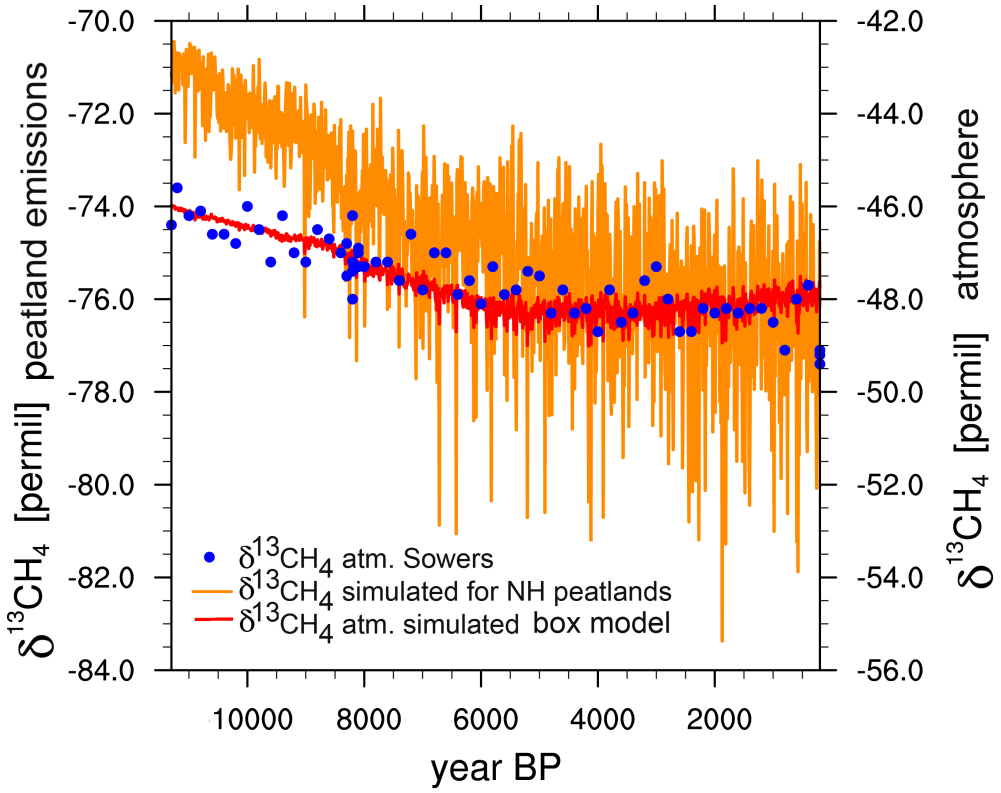

Figure 5.8: Simulated $\delta^{13}CH_4$ over the Holocene in LPX together with measurements by Sowers (2010) as shown in Fig. 5.4. Note that the source strength of NH peatlands are only about 15% of the total source strength during the Holocene (see Chap. 1.3.2). The left y-axis is valid for the NH peatland emissions (orange), the y-axis to the right for the measured (blue) and simulated (red) atmospheric $\delta^{13}CH_4$.

Bibliography

Brenninkmeijer, C., Lowe, D., Manning, M., Sparks, R., & vanVelthoven, P., 1995. The C-13, C-14 and O-18 isotopic composition of CO, CH4, and CO2 in the higher southern latitudes lower stratosphere, *J. of Geophys. Res.-Atm.*, **100**, 26163–26172.

Chanton, J., Arkebauer, T., Harden, H., & Verma, S., 2002. Diel variation in lacunal CH_4 and CO_2 concentration and delta C-13 in Phragmites australis, *Biogeochemistry*, **59**(3), 287–301.

Chappellaz, J., Blunier, T., Kints, S., Dallenbach, A., Barnola, J., Schwander, J., Raynaud, D., & Stauffer, B., 1997. Changes in the atmospheric CH_4 gradient between Greenland and Antarctica during the Holocene, *J. Geophys. Res.-Atm.*, **102**(D13), 15987–15997.

Collins, W. D., Bitz, C. M., Blackmon, M. L., Bonan, G. B., Bretherton, C. S., Carton, J. A., Chang, P., Doney, S. C., Hack, J. J., Henderson, T. B., Kiehl, J. T., Large, W. G., McKenna, D. S., Santer, B. D., & Smith, R. D., 2006. The Community Climate System Model version 3 (CCSM3), *J. Climate*, **19**, 2122–2143.

Dudova, L., Hajkova, P., Buchtova, H., & Opravilova, V., 2013. Formation, succession and landscape history of Central-European summit raised bogs: A multiproxy study from the Hruby Jesenik Mountains, *Holocene*, **23**, 230–242.

Etheridge, D. M., Steele, L. P., Langenfelds, R. L., Francey, R. J., Barnola, J. M., & Morgan, V. I., 1998. Historical co2 records from the law dome de08, de08-2, and dss ice cores. in trends: A compendium of data on global change, Research report, Carbon Dioxide Information Analysis Center, Oak Ridge National Laboratory, U.S. Department of Energy, Oak Ridge, Tenn., U.S.A.

Ferretti, D., Miller, J., White, J., Etheridge, D., Lassey, K., Lowe, D., MacFarling Meure, C., Dreier, M., Trudinger, C., van Ommen, T., & Langenfels, R., 2005. Unexpected Changes to the Global Methane Budget over the Past 2000 Years, *Science*, **309**, 1714–1717.

Finsinger, W., Schoning, K., Hicks, S., Lücke, A., Goslar, T., Wagner-Cremer, F., & Hyyppä, H., 2012. Climate change during the past 1000 years: a high-temporal-resolution multiproxy record from a mire in northern Finland, *Quat. sci. rev.*, **28**, 152–164.

Fischer, H., Behrens, M., Bock, M., Richter, U., Schmitt, J., Loulergue, L., Chappellaz, J., Spahni, R., Blunier, T., Leuenberger, M., & Stocker, T. F., 2008. Changing boreal methane sources and constant biomass burning during the last termination, *Nature*, **452**(7189), 864–867.

Gerard, G. & Chanton, J., 1993. Quantification of Methane Oxidation in the Rhizosphere of emergent aquatic macrophytes - defining upper limits, *Biogeochemistry*, **23**, 79–97.

Gierczak, T., Talukdar, R., Herndon, S., Vaghijani, G., & Ravishankara, A., 1997. Rate coefficients fot the reactions of hydroxyl radicals with methane and deuterated methanes, *J. of Phys. Chem.*, **101**, 3125–3134.

Harris, I., J. P. O. T. & Lister, D., 2013. Updated high-resolution grids of monthly climatic observations: the CRU TS3.10 Dataset, *Int. J. Climatol*.

Hornibrook, E., 2009. The stable carbon isotope composition of methane produced and emitted from northern peatlands, *Geophysical Monograph Series*, **184**.

Hunt, S., Yu, Z., & Jones, M., 2013. Lateglacial and Holocene climate, disturbance and permafrost peatland dynamics on the Seward Peninsula, western Alaska, *Quat. sci. rev.*, **63**, 42–58.

Joos, F. & Spahni, R., 2008. Rates of change in natural and anthropogenic radiative forcing over the past 20,000 years, *PNAS*, **105**(5), 1425–1430.

Kobashi, T., Severinghaus, J. P., Brook, E. J., Barnola, J.-M., & Grachev, A. M., 2007. Precise timing and characterization of abrupt climate change 8200 years ago from air trapped in polar ice, *Quaternary Science Reviews*, **26**(9-10), 1212–1222.

Liu, Z., Otto-Bliesner, B., He, F., Brady, E., Thomas, R., Clark, P., Carlson, A., Lynch-Stieglitz, J., Curry, W., Brook, E., Erickson, D., Jacob, R., Kutzbach, J., & Cheng, J., 2009. Transient Simulation of Last deglaciation with a New Mechanism for Bolling-Allerod Warming, *Science*, **325**, 310–314.

Lloyd, J. & Farquhar, G., 1994. C-13 Discrimination during CO_2 Assimilation by the terrestrial biosphere, *Oecologia*, **99**(3-4), 201–215.

Loulergue, L., Schilt, A., Spahni, R., Masson-Delmotte, V., Blunier, T., Lemieux, B., Barnola, J.-M., Raynaud, D., Stocker, T. F., & Chappellaz, J., 2008. Orbital and millennial-scale features of atmospheric CH_4 over the past 800,000 years, *Nature*, **453**(7193), 383–386.

MacDonald, G. M., Beilman, D. W., Kremenetski, K. V., Sheng, Y., Smith, L. C., & Velichko, A. A., 2006. Rapid Early Development of Circumarctic Peatlands and Atmospheric CH_4 and CO_2 Variations, *Science*, **314**(5797), 285–288.

MacDonald, G. M., Beilman, D. W., Kremenetski, K. V., Sheng, Y., Smith, L. C., & Velichko, A. A., 2006. Rapid early development of circumarctic peatlands and atmospheric CH4 and CO2 variations, *Science*, **314**(5797), 285–288.

Mischeler, J., Sowers, T., Alley, R., Battle, M., McConnell, J., Mitchell, L., Popp, T., Sofen, E., & Spencer, M., 2009. Carbon and hydrogen isotopic composition of methane over the last 1000 years, *Global Biochem. Cycle*, **23**, 3460–3473.

Mitchell, T. D. & Jones, P. D., 2005. An improved method of constructing a database of monthly climate observations and associated high-resolution grids, *International Journal of Climatology*, **25**, 693–712.

Platt, U., Allan, W., & Lowe, D., 2004. Hemispheric average Cl atom concentration from C-13/C-12 ratios in atmospheric methane, *Atm. Chem. and Phys.*, **4**, 2393–2399.

Prinn, R., 1994. The interactive atmosphere - global atmospheric-biospheric chemistry, *Ambio*, **23**(1), 50–61.

Quay, P., Stutsman, J., Wilbur, D., Snover, A., Dlugokencky, E., & Brown, T., 1999. The isotopic composition of atmospheric methane, *Global Biochem. Cyc.*, **13**, 445–461.

Ruddiman, W. F., 2003. The anthropogenic greenhouse era began thousands of years ago, *Climatic Change*, **61**, 261–293.

Singarayer, J. S., Valdes, P. J., Friedlingstein, P., Nelson, S., & Beerling, D. J., 2011. Late Holocene methane rise caused by orbitally controlled increase in tropical sources, *Nature*, **470**(7332), 82–U91.

Sowers, T., 2010. Atmospheric methane isotope records covering the Holocene period, *Quaternary science reviews*, **29**(1-2, SI), 213–221.

Spahni, R., Joos, F., Stocker, B., Steinacher, M., & Yu, C., 2013. Transient simulations of the carbon and nitrogen dynamics in northern peatlands: from the last glacial maximum to the 21st century, *Clim. Past*, **9**(3), 1287–1308.

Stocker, B., Roth, R., Joos, F., Spahni, R., Steinacher, M., Zaehle, S., Bouwman, L., Xu-Ri, & Prentice, I., 2013. Multiple greenhouse-gas feedbacks from the land biosphere unter future climate change scenarios, *Nature Climate Change*.

Tahvanainen, T., 2011. Abrupt ombrotrophication of a boreal aapa mire triggered by hydrological disturbance in the catchment, *J. of Ecol.*, **99**, 404–415.

Tarnocai, C., Swanson, D., Kimble, J., & Broll, G., 2007. Northern Circumpolar Soil Carbon Database, Digital Database, Research Branch, Agriculture and Agri-Food Canada.

Wanner, H., Beer, J., Bütikofer, J., Crowley, T. J., Cubasch, U., Flückiger, J., Goosse, H., Grosjean, M., Joos, F., Kaplan, J. O., Küttel, M., Müller, S. A., Prentice, C. I., Solomina, O., Stocker, T. F., Tarasov, P., Wagner, M., & Widmann, M., 2008. Mid- to Late Holocene climate change: an overview, *Quaternary Science Reviews*, **183**(1), 135–153.

Chapter 6

Outlook

The scope of this work was to implement a CH_4 routine with CH_4 isotopes included into a dynamic global vegetation model. The model is able to simulate peat hydrology, heat and water diffusion in the soil, peatland vegetation, permafrost distribution and peatland methane production, oxidation and transport with the according fractionation processes. The CH_4 emission fluxes and signatures were calibrated against site measurements and the model was used for the simulation of CH_4 emissions from peatlands during an abrupt climate change (Chap. 3), to reproduce reasonable soil profiles in ^{12}C and ^{13}C (Chap.2.6) and total peatland emissions (Chap.3,6). Further, it was used as a part of an inter-comparison study with 10 different wetland and wetland CH_4 4 models (Chap. 4,5). Other recent works published with LPJ-Bern or LPX are Spahni et al. (2013), where transient simulations of the carbon and nitrogen dynamics in northern peatlands, peatland development and soil-C built-up from the last glacial maximum to the 21st century are discussed, Stocker et al. (2013), where the implementation of the nitrogen cycle in the model is described and Steinacher et al. (2013), where the model is used as a part of an Earth system model to assess the future allowable carbon emissions if multiple climate targets have to be met.

As highlighted in the sections about the parameter calibration of the CH_4 routine with measurement sites (Chap. 2, 3), it would be crucial to have more site measurements with a suited resolution in time and space to calibrate the model for a better performance on the local scale, especially for the seasonality. Ideally, more data would exist from measurement sites with temperature and precipitation information, and the resulting heat and water content distribution in the soil; the CH_4 content profile in ^{12}C and ^{13}C and measurements of depth-resolved emissions from plants, by diffusion and ebullition events. This could help to reduce the discrepancies between modelled and observed site emissions, and heat diffusion and water table modelling. Effects like drainage or surface water inflow are not included in the model.

Global runs (Chap. 3, 6) and also the inter-comparison study (Chap. 4 and 5) make it apparent, that constraints for a coarser resolution - like it is used in global-scale models - are missing. Observation datasets for larger regions are not existing and the common use of intermittent and spatially non-representative chamber-based observations, without the related ecosystem measurements, is insufficient to test the mechanistically complex models used for global CH_4 emission estimates. In addition, a better knowledge of the peatland distribution or even of the partition between fens and bogs etc. would be desirable.
Spatial heterogeneity is not yet captured in the model. Such effects are only taken into account with a scaling factor for the total emissions per grid cell (see Chap. 3).

Approaches for improvements for the direct future that either could be integrated or already are worked on include:

1. Instead of prescribed maps for peatland area, a dynamical peatland area simulation will be included based on inundation

2. A differentiation between different peatland types could be integrated. For example, hummocks or hollows could be included (and separately treated) as a new topographical feature

3. Additional information on nutrient availability could be used to model pattern formation in ecosystems like peatlands

4. New PFTs as shrubs could be included as suggested by Wania (2007)

5. A better parametrization for the fractionation in the calculation of GPP for mosses could be included and the moss PFT could be limited to the uppermost soil layer instead of be treated as a grass

6. In case broader and more complete measurement data would exist for comparison, a new parameter optimization could be done. For example with Monte Carlo simulations for a broad spectrum of parameter variation

7. The simulated CO_2 emissions or the O_2 soil profile in the CH_4 routine could be investigated and used as a further constraint

8. The most important tuning parameter is the fraction of HR transformed into methane. It should be better constrained by observations

9. The model calculates the potential carbon pool for methanogenesis based on the HR which is not given per layer to the methane routine but only in total, using turnover rates that depend on the soil moisture and temperature at 25cm depth, before splitting the HR carbon into the different soil layers. A better approach would be to use the HR per layer and calculate turnover rates and actual available carbon for methanogenesis with the water content and temperature of each layer separately.

Bibliography

Spahni, R., Joos, F., Stocker, B., Steinacher, M., & Yu, C., 2013. Transient simulations of the carbon and nitrogen dynamics in northern peatlands: from the last glacial maximum to the 21st century, *Clim. Past*, **9**(3), 1287–1308.

Steinacher, M., Joos, F., & Stocker, T., 2013. Allowable carbon emissions lowered by multiple climate targets, *Nature*.

Stocker, B., Roth, R., Joos, F., Spahni, R., Steinacher, M., Zaehle, S., Bouwman, L., Xu-Ri, & Prentice, I., 2013. Multiple greenhouse-gas feedbacks from the land biosphere unter future climate change scenarios, *Nature Climate Change*.

Wania, R., 2007. *Modelling northern peatland land surface processes, vegetation dynamics and methane emissions*, Ph.D. thesis, University of Bristol.

Appendix A

Parameter Tuning for Different Versions

The adjustable parameters $f_{CH4/CO2}$, f_{O2} and f_{tiller} were optimized once for the LPJ-Bern version (see Chap. 3), and once for the LPX version with both the nitrogen cycle tuned on and off. Table A summarizes the according parameters and figure A.1 shows the site emissions for the 7 tuning sites. The threshold was in both version set to V_{gas} >0.15 $V_{available}$, in LPJ-Bern $\Delta V = 1\%$ $V_{available}$ and in LPX $f_{ebull} = 0.25$.

	$f_{CH4/CO2}$	f_{O2}	f_{tiller}	RMSE (all sites; weighted by length of measurements)
Bern-LPJ	0.17	0.5	0.0035	102.9
LPX without nitrogen	0.09	0.3	0.0035	128.9
LPX with nitrogen	0.20	0.3	0.0035	117.1

Table A.1: Overview of optimized model parameters

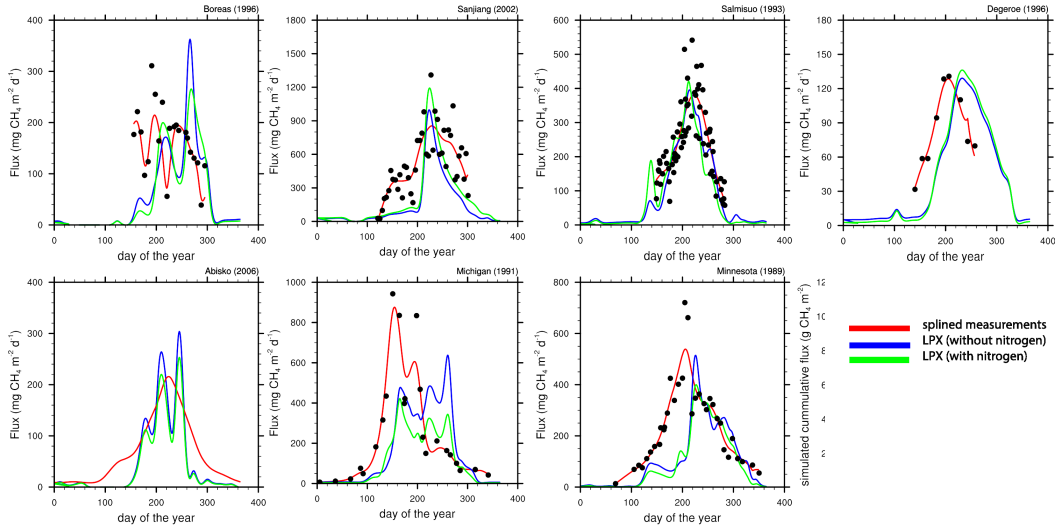

Figure A.1: Daily methane emissions measured at seven sites compared to LPX model output; analogue to the parameter optimisation done for LPJ-Bern, Fig. 2, Chap.3.

Appendix B

Source code and revision numbers

B.1 Compilation of revision numbers of LPJ-Bern and LPX used

Chapter	version	location in the subversion system in Bern
3,4,5	rev. 2471	/lpj/branches/wetland
2.5ff, 6	rev. 2598	/lpj/trunk/

Table B.1: Revision numbers of LPJ-Bern and LPX used in the different Chapters

B.2 Code of the methane routine in LPX

Revision number: 2598
The main part of the methane routine is shown here. Variable declarations, writing of output or analogue parts to already listed code are omitted and indicated with a short comment.

```
c////////////////////////////////////////////////////////////////////////////
c     SUBROUTINE METHANE
c////////////////////////////////////////////////////////////////////////////

      subroutine methane(jpngr,minit,co2_atm,ch4_atm, year)

-- arguments, include files, initialisations ---

c     ROOT DISTRIBUTION
c     ----------------------------------------------------------------------
c     The root distribution is taken from the combination of
c     Angela Gallego-Sala and Bernard & Fiala 1986 data.
        j = 1
        do i = IDX, nlayers
          depth = soil_middepth(j) / (-10.0d0) !convert from [mm] to [cm]
          b = 25.1695d0
          corr = 2.0795837d0     !with new middepth(9)=-850
          rootinit(i) = exp(depth / b) / corr
          j = j + 1
          if (depth .LT. -200.0d0) rootinit(i) = 0.0d0
        enddo

c     gas transfer velocity of SF6 [cm h-1] normalised to a Schmidt
c     number of 600: k_600 is fixed as U10 is assumed to be zero.
        k_600 = 2.07d0 + 0.215d0 * U10 ** 1.7d0

      endif
--- starting daily loop- initialisations ---

c     SET LAYER DIFFUSIVITIES
c     ----------------------------------------------------------------------
c     Calculate the diffusivity of methane in air in dependence
c     of temperature in each soil layer
c     ----------------------------------------------------------------------
c     Calculate the diffusivities for each gas and for water
c     and air once per day and then allocate it as necessary

c     From Lerman (1979) [cm2 s-1]
            D_CH4_air(i) =  0.1875d0 + 0.0013d0 * Tsoil(d,i,luwet)
#if _methane_co2_calc
            D_CO2_air(i) = 0.1325d0 + 0.0009d0 * Tsoil(d,i,luwet)
#endif
```

```
            D_O2_air(i) = 0.1759d0 + 0.00117d0 * Tsoil(d,i, luwet)

c     Method following Broecker and Peng (1974) [cm2 s-1]
            D_CH4_water(i) = (0.9798d0 + 0.02986d0 * Tsoil(d,i,luwet) +
     $           0.0004381d0 *Tsoil(d,i,luwet) ** 2.0d0) * 1.0d-5
#if _methane_co2_calc
            D_CO2_water(i) = (0.939d0 + 0.02671d0 * Tsoil(d,i,luwet) +
     $           0.0004095d0 *Tsoil(d,i,luwet) ** 2.0d0) * 1.0d-5
#endif
            D_O2_water(i) = (1.172d0 + 0.03443d0 * Tsoil(d,i,luwet)
     $           + 0.0005048d0 * Tsoil(d,i,luwet)** 2.0d0) * 1.0d-5

          enddo

c     DIFFUSIVITY IN ACROTELM
c     ------------------------------------------------------------------------
          do i = IDX, nlayers - ncatotelm
c     Use Millington and Quirk 1961 (MQ) Model tested in
c     Iiyama and Hasegawa 2005.

            Pair=Fair(d,i,luwet)-Fgas
            Ptot=acrotelm_por-Fgas
            if (Pair.gt.0.05d0) then
              D_CH4(i) = Pair ** (10.0d0 / 3.0d0) /
     $             Ptot ** 2.0d0 * D_CH4_air(i)
              f_Di(i) =  0.9825d0 !gas
#if _methane_co2_calc
              D_CO2(i) = Pair ** (10.0d0 / 3.0d0) /
     $             Ptot ** 2.0d0 * D_CO2_air(i)
#endif
              D_O2(i) = Pair ** (10.0d0 / 3.0d0) /
     $             Ptot ** 2.0d0 * D_O2_air(i)
            else

c     if Fair .le. 0.05, the slow diffusivity of water dominates the
c     overall diffusivity
              D_CH4(i) = D_CH4_water(i)
#if _methane_co2_calc
              D_CO2(i) = D_CO2_water(i)
#endif
              D_O2(i) =  D_O2_water(i)
              f_Di(i) =  0.9992d0 !water
            endif
          enddo

c     DIFFUSIVITY IN CATOTELM
c     ------------------------------------------------------------------------
c     Diffusion in water
          do i = IDX + nacrotelm, nlayers
            D_CH4(i) = D_CH4_water(i)
#if _methane_co2_calc
            D_CO2(i) = D_CO2_water(i)
#endif
            D_O2(i) =  D_O2_water(i)
            f_Di(i) =  0.9992d0 !water
          enddo
--- conversions of unities, tiller setup ---

c     ************************************************************************
c     CH4 and CO2 PRODUCTION
c     ************************************************************************

          do i = IDX, nlayers

c     Decide if ANAEROBIC CONDITIONS prevail, apply ON/OFF switch.
c     ------------------------------------------------------------------------

            anoxic = 1 - Pair

c     CH4 and CO2 PRODUCTION
c     ------------------------------------------------------------------------
c     Calculate how much CH4 and CO2 is produced CH4_prod [g CH4-C layer-1 d-1]
c     and CO2_prod [g CO2-C layer-1 d-1]. When there is more ice than water,
c     don't allow CH4 and CO2 production

            if (Fwater(d,i,luwet).lt.water_min ) then
              CH4_prod(1) = 0.0d0
#if _methane_co2_calc
              CO2_prod(1) = 0.0d0
#endif
#if compc13
              CH4_prod(2:ncvar) = MISSING_VALUE
#if _methane_co2_calc
              CO2_prod(2:ncvar) = MISSING_VALUE
#endif
#endif
            else
              CH4_prod(1) = drh(d,1) * root(i) * CH4toCO2 * anoxic

#if _methane_co2_calc
              CO2_prod(1) = drh(d,1) * root(i) - CH4_prod(1)
#endif
#if compc13

c   Fractionation during production - approach: prop. to log(prod) [Hornibrook 2009]
c   y = a log(prod) + b; Hornibrook finds for fluxes to atm. : a = 6.13, b= -100.8
c   ------------------------------------------------------------------------
c
              deltaa = 6.13 * log(CH4_prod(1)) - 25.
```

```
c              deltaa = -43 ! constant fractionation
               CH4_prod(2:ncvar) = drh(d,2:ncvar) + deltaa
#if _methane_co2_calc
               CO2_prod(2:ncvar) = drh(d,2:ncvar)
#endif
#endif
             endif

c      Add CH4 and CO2 production to CH4 pool [g CH4-C layer-1]
c      and CO2 pool [g CO2-C layer-1]
c      ------------------------------------------------------------------

             if (CH4_prod(1).gt.0.0d0) then
               call addc(
     $              CH4(d,i,:),
     $              CH4_prod(1),
     $              CH4_prod(2:ncvar)
     $              )

               call addc(
     $              dCH4_prod(:),
     $              CH4_prod(1),
     $              CH4_prod(2:ncvar)
     $              )
             dCH4_prod_l(i,:) = CH4_prod(:)

             endif

#if _methane_co2_calc
             if (CO2_prod(1) .gt. 0.0d0) then
               call addc(
     $              CO2(d,i,:),
     $              CO2_prod(1),
     $              CO2_prod(2:ncvar)
     $              )

               call addc(
     $              dCO2_prod(:),
     $              CO2_prod(1),
     $              CO2_prod(2:ncvar)
     $              )
             endif
#endif
           enddo

c      ************************************************************************
c      DIFFUSION OF OXYGEN
c      ************************************************************************
c      ************************************************************************
c      PLANT TRANSPORT OF OXYGEN
c      ************************************************************************
---both analogue to diffusion and plant transport of CH4 and CO2---

c      ************************************************************************
c      DIFFUSION OF METHANE: PART 1
c      ************************************************************************

c      Caculate Schmidt number and gas transfer velocity in the top soil
c      layer. For another way to calculate k for CH4 look at
c      Happell et al. (1995). They used -2/3 for ngtrans.
c      ------------------------------------------------------------------
           if (Tsoil(d,IDX,luwet).le.49.0d0) then
             ScCH4 = 1898.0d0 - 110.1d0 * Tsoil(d,IDX,luwet)
     $            + 2.834d0 * Tsoil(d,IDX,luwet)**2.0d0
     $            - 0.02791d0 * Tsoil(d,IDX,luwet)**3.0d0
           else
             ScCH4 = 23.950d0
           end if

           kCH4 = k_600 * (ScCH4 / 600.0d0) ** ngtrans
c      Go from cm h-1 to m d-1
           kCH4 =kCH4 / 100.0d0 * 24.0d0
c      Tpos(:) =  0.0d0

           do i = IDX, nlayers
             k_henry_ln_CH4 = -68.8862d0 + 101.4956d0 * 100.0d0 /
     $            (Tpos(i) + 273.15d0) + 28.7314d0 *
     $            dlog((Tpos(i) + 273.15d0) / 100.0d0)      ![ml g/ ml w] (Bunsen)
             k_henry_CH4(i) = 1.0d0 / dexp(k_henry_ln_CH4) ![ml w/ml g]
             k_henry_CH4average(i)= k_henry_CH4average(i)+ k_henry_CH4(i)/365.0d0
           enddo

      henry_coeff = k_henry_CH4(IDX)/(8.314d0*(273.15d0+Tpos(IDX)))    ![ml w/ml g] -> [l atm mol-1]

c      pp_CH4 [micro-atm] / 1E6 to get [atm] Ceq is in [mol C L-1]
c      Convert Ceq from [mol C L-1] to [mmol C m-3]
c      * 1000 to get to [mmol]
c      * 1000 to get from [L-1] to [m-3]
c      => Ceq /1E6 *1000 *1000 = Ceq
c      ------------------------------------------------------------------
           Ceq(1) = pp_CH4 / henry_coeff ![mmol m-3]
#if compc13
           Ceq(2:ncvar) = ch4_atm(2:ncvar)
#endif

c      convert concentration from [g C layer-1] to [mmol m-3]:
c      / cmass to get mol, / V_water to get per m-3,
c      * 1000 to get mmol
c      for isotopes get from [permil] to [mmol m-3]
```

```
c     ------------------------------------------------------------------
          waterheight = 0.0d0
          mycounter = 0

          do i = IDX, nlayers

cc      start separation dissolved/gas
cc      ------------------------------------------------------------------
cc      partition of the available CH4 for diffusion
cc      in dissolved and gaseous part
cc      when diffusion coefficient is taken in water,
cc      dissolved part diffuses, otherwise all
cc      ------------------------------------------------------------------
cc      pV = nRT
cc      H = c_g / c_w (dimensionless Henry constant version bunsen)
cc      H / RT = c_w / Pgas
cc      P_tot / RT = n_CH4 / (v_g + v_w / H_CH4) + n_CO2 / (v_g + v_w / H_CO2) + n_N2 / (v_g + v_w / H_N2)
cc      -> cubic equation for v_g(i)
cc      given: Rstd, P_tot (assumption: equilib. with external pressure), Tpos(i)+ 273.15d0,
cc      k_henry_N2/CH4/CO2, V_water(i)
cc              n = m / M

             waterheight = waterheight + Total_water(i) ! [m]
             hydro_press = rho_H2O * grav * waterheight ! [Pa]
             P_tot = atm_press + hydro_press ! total partial pressure of CH4,CO2 and N2 [Pa]

             k_henry_ln_N2 = -59.6274d0 + 85.7661d0 * 100.0d0 /
     $            (Tpos(i) + 273.15d0) + 24.3696d0 *
     $            log((Tpos(i) + 273.15d0) / 100.0d0)
             k_henry_N2 = 1.0d0 / (dexp(k_henry_ln_N2)) ![ml w/ml g]

             k_henry_ln_CO2 = -58.0931d0 + 90.5069d0 * 100.0d0 /
     $            (Tpos(i) + 273.15d0) + 22.294d0 *
     $            log((Tpos(i) + 273.15d0) / 100.0d0)
            k_henry_CO2(i) = 1.0d0 / ( dexp(k_henry_ln_CO2) ! [ml w/ml g]
     $          / 101.325d0 *  Rgas*(273.15d0+Tpos(i)) )

            if (CH4(d,i,1).gt.0.0d0) then
               n_CH4 = CH4(d,i,1) / cmass ! from g to mol
               n_CO2 = CO2(d,i,1) / cmass
               vol_gas(i) = 0.01d0*V_water(i) ! [m3]
               Vtot = V_water(i)+Fgas*Dz(i)- 0.01d0*V_water(i) ![m3]

               n_N2 = P_tot /((Tpos(i)+273.15d0)*Rgas)*(0.01d0*V_water(i)
     $              + V_water(i) / k_henry_N2) !    [mol]

               ptot = P_tot
               L=3

               var_A = 0.0d0 !n_CH4
               var_B = 0.0d0 !n_CO2
               var_C = n_N2*0.01 !arbitrary!

               ptot = (var_C/(V_water(i)/k_henry_N2))
     $              * (Rgas * (Tpos(i)+273.15d0))

               var_D = ptot / (Rgas * (Tpos(i)+273.15d0))
               var_E = V_water(i) /  k_henry_CH4(i)
               var_F = V_water(i) /  k_henry_CO2(i)
               var_G = V_water(i) /  k_henry_N2

               v_g_lsg(i) = 0.0d0
               v_g_old = 0.0d0

               do step=1,10

                 var_A = var_A + n_CH4*0.1d0
                 var_B = var_B + n_CO2*0.1d0
                 var_C = var_C + n_N2*0.1d0

                 var_input(4) = 1
                 var_input(3) = var_G+var_F+var_E - (var_A+var_B+var_C)/var_D
                 var_input(2) = var_G*var_F + var_E*var_G + var_E*var_F -
     $                (var_A*var_F+var_A*var_G+var_B*var_E+var_B*var_G+var_C*var_E
     $                +var_C*var_F) / var_D
                 var_input(1) = var_E*var_F*var_G - (var_A*var_F*var_G +
     $                var_B*var_E*var_G + var_C*var_E*var_F) / var_D


ccc       SUBROUTINE CUBIC(A,X,L)
cC      A(0:3)       (i)  vector containing the polynomial coefficients
cC      X(1:L)       (o)  results
cC      L            (o)  number of valid solutions (beginning with X(1))
cC      ================================================================
c      a*x^3 + b*x^2 + c*x + d = 0
c             var_input(4) = 1   ! a
c             var_input(3) = -2  ! b
c             var_input(2) = -1  ! c
c             var_input(1) = 2   ! d

                 call CUBIC(var_input, v_g(i,:), L)

                 diff = 0.2d0*V_water(i)
                 v_g_old = v_g_lsg(i)
                 do los=1,3
                   if (v_g(i,los).gt.0.0d0) then
                     tmpdiff = abs(v_g_old-v_g(i,los))
                     diff2 = min(tmpdiff,diff)
                     if (diff2.lt.diff) then
```

```
                        v_g_lsg(i) = v_g(i,los)
                        diff = diff2
                      endif
                    endif
                  enddo

                  if (v_g_lsg(i) .le. 0.0d0) then
                    v_g_lsg(i) = 0.0d0
                    n_CH4_gas(i) = 0.0d0
                    n_CO2_gas(i) = 0.0d0
                  else
                    if (v_g_lsg(i) .ge. 0.2d0*V_water(i)) then
                      v_g_lsg(i) = 0.2d0*V_water(i)
                    endif
                    n_CH4_gas(i) = n_CH4/(1.0d0+V_water(i)/v_g_lsg(i)/k_henry_CH4(i))
                    n_CO2_gas(i) = n_CO2/(1.0d0+V_water(i)/v_g_lsg(i)/k_henry_CO2(i))
                  endif

                  ptot = (var_A/(v_g_lsg(i)+V_water(i)/k_henry_CH4(i))
     $                 + var_B/(v_g_lsg(i)+V_water(i)/k_henry_CO2(i))
     $                 + var_C/(v_g_lsg(i)+V_water(i)/k_henry_N2))
     $                 * (Rgas * (Tpos(i)+273.15d0))

                  var_D = ptot / (Rgas * (Tpos(i)+273.15d0))

                  mycounter = mycounter+1

                enddo              ! while loop

                dCH4_gas(d,i,1) = n_CH4_gas(i) *  cmass
                dCO2_gas(d,i,1) = n_CO2_gas(i) *  cmass
                dCH4_water(d,i,1) =  CH4(d,i,1)- dCH4_gas(d,i,1)
                dCO2_water(d,i,1) =  CO2(d,i,1)- dCO2_gas(d,i,1)

                dCH4_diss_l(d,i,1:ncvar) = dCH4_water(d,i,1:ncvar)

c [partition is in average about 25% of mass in dissolved form, 75% in gas]
c end partition dissolved/gas
c-----------------------------------------------

c note: with the new partition, actually more diffusion can take place
c because of a stronger gradient between the layers. To use to old version,
c uncomment the following line
          dCH4_water(d,i,1) = CH4(d,i,1)

             CH4diffbefore(i,:) =  CH4(d,i,:)
             CH4diffbefore(i,2:ncvar) = (CH4diffbefore(i,2:ncvar) / 1000.0d0 + 1.0d0) *
     $                R_std(2:ncvar) * CH4(d,i,1)

             CH4diffafter(i,:) =  CH4diffbefore(i,:)

              if ((Fair(d,i,luwet)-Fgas) .gt. 0.05) then !gas dominant; whole content diff.
                C(i,1) = CH4(d,i,1) / cmass / V_water(i) * 1000.0d0
             else                                        !water dominant; only water part diffuses
                if ((CH4(d,i,1) - dCH4_water(d,i,1)) .ge. 0.0d0) then
                  CH4(d,i,1) = CH4(d,i,1) - dCH4_water(d,i,1) ! saving gas part; untouched; same sign.
                  dCH4_water(d,i,2:ncvar) = CH4(d,i,2:ncvar)
                  C(i,1) = dCH4_water(d,i,1) / cmass / V_water(i) * 1000.0d0
                  else
                     stop
                  endif
          endif

#if compc13
             if (C(i,1).gt.0.0d0) then
               if ((Fair(d,i,luwet)-Fgas) .gt. 0.05) then
                 C(i,2:ncvar) = (CH4(d,i,2:ncvar) / 1000.0d0 + 1.0d0) *
     $                R_std(2:ncvar) * C(i,1) ! [mmol m-3]
               else
                 C(i,2:ncvar) = (dCH4_water(d,i,2:ncvar) / 1000.0d0 + 1.0d0) *
     $                R_std(2:ncvar) * C(i,1) ! [mmol m-3]
               endif
             else
               C(i,2:ncvar) = 0.0d0
             endif
#endif
               Di(i) = D_CH4(i)  ! [m2 d-1]
             enddo

c      Set the boundary condition on the top of the soil
c      ------------------------------------------------------------------------

c      When the water table rises above the surface, then the CH4
c      concentration in the surface layer is suddenly very low as it
c      didn't have a concentration allocated. Therefore, I'll add
c      the water volume of the standing water to the top layer and
c      spread the methane concentration over 2 layers now. This will
c      mean that you'll see a drop in CH4 concentration in the top
c      soil layer when the wtp goes above the surface.

           surf_conc(1:ncvar) = C(IDX,1:ncvar) ! [mmol m-3]

c      Do one timestep of the Crank-Nicholson method. The CN solver is an
c      approximation and doesn't give exact results in terms of conservation,
c      i.e. when having a total C content summed over all layers of e.g.
c      248.149216 before calling cnstepgas, I end up with a total C content of
c      248.149368 after calling it.
c      ------------------------------------------------------------------------
           if (Fwater(d,IDX,luwet).gt.water_min.or.
```

```
      $          Fwater(d,IDX+1,luwet).gt.water_min.or.
      $          Fwater(d,IDX+2,luwet).gt.water_min) then

              csum1a = 0.0d0
              csum1b = 0.0d0
              csum1c = 0.0d0
              do i = IDX, nlayers
                csum1a = csum1a + C(i,1) * V_water(i) !* cmass / 1000.0d0
#if compc13
                csum1b = csum1b + C(i,2) * V_water(i) !* cmass / 1000.0d0
#if compc14
                csum1c = csum1c + C(i,3) * V_water(i) !* cmass / 1000.0d0
#endif
#endif
              enddo

              time=0.0d0
              do while (time.lt.1.0d0)
                call cnstepgas(IDX, C(:,1), Di, Dz, surf_conc(1),Dt)
#if compc13
                call cnstepgas(IDX, C(:,2), Di*f_Di, Dz, surf_conc(2),Dt)
#if compc14
                call cnstepgas(IDX, C(:,3), Di*f_Di, Dz, surf_conc(3),Dt)
#endif
#endif
                time=time+Dt
              enddo

              csum2a = 0.0d0
              csum2b = 0.0d0
              csum2c = 0.0d0
              do i = IDX, nlayers
                C(i,1) = max(C(i,1),0.0d0) ! prevent numerical negative results
                csum2a = csum2a + C(i,1) * V_water(i) !* cmass / 1000.0d0
#if compc13
                C(i,2) = max(C(i,2),0.0d0) ! prevent numerical negative results
                csum2b = csum2b + C(i,2) * V_water(i) !* cmass / 1000.0d0
#if compc14
                C(i,3) = max(C(i,3),0.0d0) ! prevent numerical negative results
                csum2c = csum2c + C(i,3) * V_water(i) !* cmass / 1000.0d0
#endif
#endif
              enddo

              if (csum2a.le.0.0d0) then
                csum1a = 1.0d0
                csum2a = 1.0d0
              endif

              if (csum2b.le.0.0d0) then
                csum1b = 1.0d0
                csum2b = 1.0d0
              endif

              if (csum2c.le.0.0d0) then
                csum1c = 1.0d0
                csum2c = 1.0d0
              endif

              do i = IDX, nlayers

                C(i,1) = C(i,1) * csum1a / csum2a
#if compc13
                C(i,2) = C(i,2) * csum1b / csum2b
                C(i,3) = C(i,3) * csum1c / csum2c
#endif

              if ((Fair(d,i,luwet)-Fgas) .gt. 0.05) then !gas
                CH4(d,i,1) = C(i,1) * cmass * V_water(i) / 1000.0d0
              else !water
                dCH4_water(d,i,1) = C(i,1) * cmass * V_water(i) / 1000.0d0
              endif

#if compc13
                if (C(i,1).gt.0.0d0) then

                  if ((Fair(d,i,luwet)-Fgas) .gt. 0.05) then !gas
                  CH4(d,i,2:ncvar) = ( (C(i,2:ncvar) / C(i,1)
      $                / R_std(2:ncvar)) - 1.0d0) * 1000.0d0 ![permil]
                  else              !water
                  dCH4_water(d,i,2:ncvar) = ( (C(i,2:ncvar) / C(i,1)
      $                / R_std(2:ncvar)) - 1.0d0) * 1000.0d0 ![permil]
                  endif
                else
                  if ((Fair(d,i,luwet)-Fgas) .gt. 0.05) then !gas
                    CH4(d,i,2:ncvar) = MISSING_VALUE
                  else              !water
                    dCH4_water(d,i,2:ncvar) = MISSING_VALUE
                  endif
                endif
#endif
          enddo
            endif ! water in upper layers

            do i = IDX,nlayers

          if ((Fair(d,i,luwet)-Fgas) .gt. 0.05) then !gas
                          !
          else                      !water
```

```
            if (dCH4_water(d,i,1) .gt. 0.0d0) then
              call addc(
     $             CH4(d,i,1),
     $             dCH4_water(d,i,1),
     $             dCH4_water(d,i,2:ncvar)
     $             )
            else

            endif
          endif

          CH4diffafter(i,1) =  CH4(d,i,1)
          CH4diffafter(i,2:ncvar) =  (CH4(d,i,2:ncvar) / 1000.0d0 + 1.0d0) *
     $                R_std(2:ncvar) * CH4(d,i,1)

          dCH4_difflay(d,i,1:ncvar) = CH4diffbefore(i,1:ncvar) - CH4diffafter(i,1:ncvar)

        enddo
          enddo

c     ************************************************************************
c     CH4 OXIDATION
c     ************************************************************************

          dCH4_oxid(1) = 0.0d0
          dCH4_oxid(2:ncvar) = MISSING_VALUE

          do i = IDX, nlayers

c     Assume that 1/2 of the O2 is utilized by other electron acceptors
            O2(d,i) = oxid_frac*O2(d,i)

c     O2 is in [mol layer-1], 2 moles of O2 per 1 mol of CH4 are needed
c     convert O2 from [mol layer-1] to [g C layer-1]
            CH4_oxid(1) = min(CH4(d,i,1), 0.5d0 * O2(d,i) * cmass)

            if (CH4_oxid(1).gt.0.0d0) then
#if compc13
              CH4_oxid(2) = CH4(d,i,2)+f_ch4_oxid
              CH4_oxid(3) = CH4(d,i,3)+f_ch4_oxid*2.0d0
#endif
             CH4old(:) = CH4(d,i,:)
             CH4(d,i,1) = CH4old(1)-CH4_oxid(1)

            if ( CH4(d,i,1) .gt. 0.0d0) then
             CH4(d,i,2:ncvar) = (CH4old(1)*CH4old(2:ncvar)-CH4_oxid(1)
     $           *CH4_oxid(2:ncvar))/CH4(d,i,1)
            else
             CH4(d,i,2:ncvar) =    MISSING_VALUE
             CH4_oxid(2:ncvar) = CH4old(2:ncvar)
             endif

              call addc(
     $             dCH4_oxid(:),
     $             CH4_oxid(1),
     $             CH4_oxid(2:ncvar)
     $             )

              dCH4_oxid_l(i,:)= CH4_oxid(:)

c     2 moles of O2 per 1 mol of CH4 are needed
            O2(d,i) = max(0.0d0,O2(d,i)-2.0d0*CH4_oxid(1)/cmass) ! [mol layer-1]

#if -methane_co2_calc
             call addc(
     $            CO2(d,i,:),
     $             CH4_oxid(1),
     $             CH4_oxid(2:ncvar)
     $             )
#endif
            endif

          enddo

c     ************************************************************************
c     turn on/off:
c     daily check if layer is frozen. If so, 90 % of content is added to the layer
c     above. If surface layer is frozen, the leaving flux is added to ebullition.
c     ************************************************************************

          do i =  nlayers, IDX-1, -1
            if (frozen(i)) then
              CH4(d,i-1,1) = CH4(d,i-1,1)+ 0.9d0*CH4(d,i,1)
              CH4(d,i,1) = 0.1d0*CH4(d,i,1)
              CH4(d,i,2:ncvar) =  CH4(d,i,2:ncvar)
              if ((CH4(d,i-1,1)+0.9d0*CH4(d,i,1)).gt.0.0d0) then
                CH4(d,i-1,2:ncvar) = (CH4(d,i-1,2:ncvar)*CH4(d,i-1,1)+
     $               0.9d0*CH4(d,i,2:ncvar)*CH4(d,i,1))/
     $               (CH4(d,i-1,1)+0.9d0*CH4(d,i,1))
              else
                CH4(d,i-1,2:ncvar) = MISSING_VALUE
              endif
            endif
            if (frozen(IDX)) then
              call addc(
     $             CH4_ebull(d,:),
     $             0.9d0*CH4(d,IDX,1),
     $             CH4(d,IDX,2)
     $             )
```

```
              CH4(d,IDX,1) = 0.1d0*CH4(d,IDX,1)
              CH4(d,IDX,2:ncvar) = CH4(d,IDX,2:ncvar)
            endif
          enddo

c     ************************************************************************
c     DIFFUSION OF METHANE: PART 2
c     ************************************************************************

c     Set the boundary condition on the top of the soil
c     ------------------------------------------------------------------------
c     F = k (Cm - Ce) in
c     UNITS: k [m d-1], surf_conc and Ceq [mmol m-3]
c     [mmol m-3] multiplied by [m d-1] gives
c     flux units of [mmol m-2 d-1]
c
c     Here, an analytical solution is used to calculate in one step
c     how much gas diffuses in or out from a layer within 1 day.
c     C(t+1) = Ceq + (C(t) - Ceq) * e(-k/dz)
c     dz is replaced by V_water[m3]/Area[m2], where Area is 1m2
c
c     Water content must be larger than a threshold (water_min) to allow
c     methane diffusion into the top layer.
c     ------------------------------------------------------------------------
          if (Fwater(d,IDX,luwet).gt.water_min) then

            C(IDX,1) = CH4(d,IDX,1) / cmass / V_water(IDX) * 1000.0d0
            CH4old(:) = CH4(d,IDX,:)
#if compc13
            C(IDX,2:ncvar) = CH4(d,IDX,2:ncvar)
#endif
            Cnew(1) = C(IDX,1) * exp(-kCH4*dTschmidt/V_water(IDX))
#if compc13
            Cnew(2:ncvar) = C(IDX,2:ncvar)
#endif

            call addc(
     $           Cnew(:),
     $           Ceq(1) * (1.0d0-exp(-kCH4*dTschmidt/V_water(IDX))),
     $           Ceq(2:ncvar)
     $           )


c     A) Flux from top layer to the atmosphere
c     ------------------------------------------------------------------------
            if (C(IDX,1).gt.Cnew(1)) then

c     Cnew(1) [mmol m-3] to Cnew(1) in [gC layer-1]
              call addc(
     $             CH4_diff(d,:),
     $             (C(IDX,1)-Cnew(1))* cmass * V_water(IDX) / 1000.0d0 ,
     $             C(IDX,2:ncvar) + f_ch4_airwater
     $             )

              dCH4_diff_l(d,IDX,:) = CH4_diff(d,:)
            else

c     B) Flux from atmosphere into the top layer
c     ------------------------------------------------------------------------
c     Cnew(1) and C(IDX,1) [mmol m-3] to Cnew(1) in [gC layer-1]

              call addc(
     $             CH4_uptake(d,:),
     $             (Cnew(1)-C(IDX,1)) * cmass * V_water(IDX) / 1000.0d0, ![g layer-1 d-1]
     $             ch4_atm(2:ncvar) - f_ch4_airwater
     $             )
            endif

            CH4(d,IDX,1) = Cnew(1) * cmass * V_water(IDX) / 1000.0d0
#if compc13
            if (C(IDX,1).gt.Cnew(1)) then
c            CH4(d,IDX,2:ncvar) = Cnew(2:ncvar)
            CH4(d,IDX,2:ncvar) = (CH4old(2:ncvar)* CH4old(1) -
     $          ((C(IDX,1)-Cnew(1))*cmass*V_water(IDX)/1000.0d0)*
     $          (C(IDX,2:ncvar) + f_ch4_airwater)) /
     $           CH4(d,IDX,1)

            else
              if (CH4(d,IDX,1) .gt. 0.0d0) then
                CH4(d,IDX,2:ncvar) =  (CH4old(2:ncvar)* CH4old(1)+
     $               (ch4_atm(2:ncvar) - f_ch4_airwater)* (Cnew(1)-C(IDX,1)) *
     $               cmass * V_water(IDX) / 1000.0d0)/CH4(d,IDX,1)
              else
                 CH4(d,IDX,2:ncvar) = MISSING_VALUE
              endif
            endif

c     ************************************************************************
c     PLANT TRANSPORT OF CH4
c     ************************************************************************

          do i = IDX, nlayers

c     convert concentration from [g C layer-1] to [mmol m-3]
c     / cmass to get mol
c     / V_water to get per m-3
c     * 1000 to get mmol

c     Weight plant transport by the area of porous root cross-sections.
```

```
c      plant_trans(i) [mmol layer-1 d-1]
c      ------------------------------------------------------------------------

              if (Fwater(d,i,luwet).gt.water_min) then

                C(i,1) = CH4(d,i,1) / cmass / V_water(i) * 1000.0d0
#if compc13
                C(i,2:ncvar) = CH4(d,i,2:ncvar)
#endif
                Cnew(1) = C(i,1) * exp(-kCH4*dTschmidt/(V_water(i)/tiller_area(i)))
#if compc13
                Cnew(2:ncvar) = C(i,2:ncvar)
#endif
                 call addc(
      $              Cnew(:),
      $              Ceq(1) * (1.0d0 - exp(-kCH4*dTschmidt / (V_water(i)
      $              / tiller_area(i)))),
      $              Ceq(2:ncvar)
      $              )


c      A) Flux from layer i to the atmosphere
c      ------------------------------------------------------------------------
                if (C(i,1).gt.Cnew(1)) then

                  call addc(
      $               CH4_plant(d,:),
      $               (C(i,1)-Cnew(1)) * cmass * V_water(i) / 1000.0d0, ![g layer-1 d-1]
      $               C(i,2:ncvar)+f_ch4_plant(1)
      $               )

          dCH4_plant_l(d,i,1) =(C(i,1)-Cnew(1))*cmass*V_water(i)/1000.0d0
          dCH4_plant_l(d,i,2:ncvar) = C(i,2:ncvar)+f_ch4_plant(1)

                else

c      B) Flux from atmosphere into the top layer
c      ------------------------------------------------------------------------
c      Cnew(1) and C(i,1) [mmol m-3] to Cnew(1) in [gC layer-1]

                  call addc(
      $               CH4_uptake(d,:),
      $               (Cnew(1)-C(i,1)) * cmass * V_water(i) / 1000.0d0, ![g layer-1 d-1]
      $               ch4_atm(2:ncvar)
      $               )

                endif

                CH4(d,i,1) = Cnew(1) * cmass * V_water(i) / 1000.0d0
#if compc13

              if (C(i,1).gt.Cnew(1)) then

                CH4(d,i,2:ncvar) = ( C(i,1)*C(i,2:ncvar) - (Cnew(2:ncvar)
      $            +f_ch4_plant(1:2)) *(C(i,1)-Cnew(1)) )/Cnew(1)
              else
                if (Cnew(1) .gt. 0.0d0) then
                 CH4(d,i,2:ncvar) = ( C(i,1)*C(i,2:ncvar) +
      $            ch4_atm(2:ncvar)  *(Cnew(1)-C(i,1)) )/Cnew(1)
             else
c              no change
              endif
            endif
#endif

        endif
            enddo

c      ************************************************************************
c      DIFFUSION OF CO2: PART 1 & 2
c      ************************************************************************
c      ************************************************************************
c      PLANT TRANSPORT OF CO2
c      ************************************************************************

---analogue to CH4, with different constants----

c      ************************************************************************
c      EBULLITION OF CH4 & CO2
c      ************************************************************************

c      Using the relations
c      P_tot = P_CH4 + P_CO2 + P_N2
c      C_x = P_x * V_g /R*T + P_x / H_x * V_w / R*T  (eq.1) [Tokida et al., 2003]
c      P_x : partial pressure of a gas
c      V_g : gas volume (all gases)
c      V_w : water volume
c      H_x : dimensionless Henry constant for gas x in Bunsen version (gas per liquid)
c      C_x : # [mol] (total mass of a gas species)
c      scz : Equations correct for H in unit gas per liquid; Diss Zuercher:
c      H defined as liquid per gas (normal definition for unitless Henry const.) and
c      equations different therefore (H instead of 1/H)

#if _methane_co2_calc
#else
            CO2(:,:,1) = 0.3d0     ! [gC per layer]
#endif
            waterheight = 0.0d0
```

```
          do i = IDX, nlayers

c     if (Fwater(d,i,luwet).gt.water_min) then
            if (Fwater(d,i,luwet).gt. 0.3d0 .and. Tpos(i) .gt. 0.0d0) then

              waterheight = waterheight + Total_water(i) ! [m]
              hydro_press = rho_H2O * grav * waterheight ! [Pa]

              vol_gas(i) = 0.01d0*V_water(i) ! [m3]
              Vtot = V_water(i)+Fgas*Dz(i)-vol_gas(i) ![m3]

              P_tot = atm_press + hydro_press ! total partial pressure of CH4,CO2 and N2 [Pa]

              k_henry_ln_N2 = -59.6274d0 + 85.7661d0 * 100.0d0 /
     $             (Tpos(i) + 273.15d0) + 24.3696d0 *
     $             log((Tpos(i) + 273.15d0) / 100.0d0)
              k_henry_N2 = 1.0d0 / (dexp(k_henry_ln_N2)) ![ml w/ml g]

            k_henry_ln_CO2 = -58.0931d0 + 90.5069d0 * 100.0d0 /
     $           (Tpos(i) + 273.15d0) + 22.294d0 *
     $           log((Tpos(i) + 273.15d0) / 100.0d0)
            k_henry_CO2(i) = 1.0d0 / ( dexp(k_henry_ln_CO2) ! [ml w/ml g]
     $           / 101.325d0 *  Rgas*(273.15d0+Tpos(i)) )

            if (CH4(d,i,1).gt.0.0d0) then
              n_CH4 = CH4(d,i,1) / cmass ! from g to mol
              n_CO2 = CO2(d,i,1) / cmass
              vol_gas(i) = 0.01d0*V_water(i) ! [m3]
              Vtot = V_water(i)+Fgas*Dz(i)- 0.01d0*V_water(i) ![m3]

              n_N2 = P_tot /((Tpos(i)+273.15d0)*Rgas)*(0.01d0*V_water(i)
     $             + V_water(i) / k_henry_N2) !    [mol]

              ptot = P_tot
              L=3

              var_A = 0.0d0 !n_CH4
              var_B = 0.0d0 !n_CO2
              var_C = n_N2*0.01!arbitrary...

              ptot = (var_C/(V_water(i)/k_henry_N2))
     $             * (Rgas * (Tpos(i)+273.15d0))

              var_D = ptot / (Rgas * (Tpos(i)+273.15d0))
              var_E = V_water(i) /  k_henry_CH4(i)
              var_F = V_water(i) /  k_henry_CO2(i)
              var_G = V_water(i) /  k_henry_N2

              v_g_lsg(i) = 0.0d0
              v_g_old = 0.0d0

              do step=1,10

                var_A = var_A + n_CH4*0.1d0
                var_B = var_B + n_CO2*0.1d0
                var_C = var_C + n_N2*0.1d0

c                v_g_old(i) = v_g_lsg(i)

                var_input(4) = 1
               var_input(3) = var_G+var_F+var_E - (var_A+var_B+var_C)/var_D
               var_input(2) = var_G*var_F + var_E*var_G + var_E*var_F -
     $              (var_A*var_F+var_A*var_G+var_B*var_E+var_B*var_G+var_C*var_E
     $              +var_C*var_F) / var_D
               var_input(1) = var_E*var_F*var_G - (var_A*var_F*var_G +
     $              var_B*var_E*var_G + var_C*var_E*var_F) / var_D


ccc       SUBROUTINE CUBIC(A,X,L)
cC     A(0:3)       (i)  vector containing the polynomial coefficients
cC     X(1:L)       (o)  results
cC     L            (o)  number of valid solutions (beginning with X(1))
cC     ================================================================
c     a*x^3 + b*x^2 + c*x + d = 0
c              var_input(4) = 1   ! a
c              var_input(3) = -2  ! b
c              var_input(2) = -1  ! c
c              var_input(1) = 2   ! d

                call CUBIC(var_input, v_g(i,:), L)

                diff = 0.2d0*V_water(i)
                v_g_old = v_g_lsg(i)
                do los=1,3
                  if (v_g(i,los).gt.0.0d0) then
                    tmpdiff = abs(v_g_old-v_g(i,los))
                    diff2 = min(tmpdiff,diff)
                    if (diff2.lt.diff) then
                      v_g_lsg(i) = v_g(i,los)
                      diff = diff2
                    endif
                  endif
                enddo

                if (v_g_lsg(i) .le. 0.0d0) then
                  v_g_lsg(i) = 0.0d0
                  n_CH4_gas(i) = 0.0d0
                  n_CO2_gas(i) = 0.0d0
                else
```

```
                  if (v_g_lsg(i) .ge. 0.2d0*V_water(i)) then
                    v_g_lsg(i) = 0.2d0*V_water(i)
                  endif
                  n_CH4_gas(i) = n_CH4/(1.0d0+V_water(i)/v_g_lsg(i)/k_henry_CH4(i))
                  n_CO2_gas(i) = n_CO2/(1.0d0+V_water(i)/v_g_lsg(i)/k_henry_CO2(i))
                endif

                ptot = (var_A/(v_g_lsg(i)+V_water(i)/k_henry_CH4(i))
     $               + var_B/(v_g_lsg(i)+V_water(i)/k_henry_CO2(i))
     $               + var_C/(v_g_lsg(i)+V_water(i)/k_henry_N2))
     $               * (Rgas * (Tpos(i)+273.15d0))

                var_D = ptot / (Rgas * (Tpos(i)+273.15d0))

                mycounter = mycounter+1
              enddo              ! while loop


              if (v_g_lsg(i) .gt. 0.15*V_water(i)) then

                P_par_CH4 = (var_A/(v_g_lsg(i)+V_water(i)/k_henry_CH4(i)))* (Rgas * (Tpos(i)+273.15d0))
                P_par_CO2 = (var_B/(v_g_lsg(i)+V_water(i)/k_henry_CO2(i)))* (Rgas * (Tpos(i)+273.15d0))

                delta_vol = (v_g_lsg(i) -0.15d0*V_water(i)) * ebullmodul  ! [m3]
                delta_CH4 = delta_vol*P_par_CH4/ (Rgas*(Tpos(i)+273.15d0)) ![mol]
                delta_CO2 = delta_vol*P_par_CO2/ (Rgas*(Tpos(i)+273.15d0)) ![mol]

                if (delta_CH4 .le. 0.0d0) then
                  delta_CH4 = 0.0d0
                  delta_CO2 = 0.0d0
                endif
              endif

                call addc(
     $               CH4(d,i,:),
     $               - delta_CH4* cmass, ! [g m-2 d-1]
     $               1.0d0*CH4(d,i,2:ncvar)
     $               )

                call addc(
     $               CH4_ebull(d,:),
     $               delta_CH4* cmass, ! [g m-2 d-1]
     $               1.0d0*CH4(d,i,2:ncvar)
     $               )

                dCH4_ebull_l(d,i,:)=  CH4_ebull(d,:)
#if _methane_co2_calc
                call addc(
     $               CO2(d,i,:),
     $               - delta_CO2* cmass, ! [g m-2 d-1]
     $               1.0d0*CO2(d,i,2:ncvar)
     $               )

                call addc(
     $               CO2_ebull(d,:),
     $               delta_CO2* cmass, ! [g m-2 d-1]
     $               1.0d0*CO2(d,i,2:ncvar)
     $               )
#endif
              else
                delta_CH4 = 0.0d0
#if _methane_co2_calc
                delta_CO2 = 0.0d0
#endif
              endif
            endif               !water_min
          enddo

c     Calculate monthly totals
c     ------------------------------------------------------------------------
c     Fluxes are in g C d-1 (daily fluxes) and g C month-1 (monthly fluxes)

          call addc(
     $          mCH4_plant(jpngr,m,:),
     $          CH4_plant(d,1),
     $          CH4_plant(d,2:ncvar)
     $          )
--- done for all transport fluxes (total and per layer)---

          if (dCH4_difflay(d,i,1) .ne. 0.0d0) then

          mCH4_lay_difflayold(:) = mCH4_lay_difflay(jpngr,m,i,:)

          mCH4_lay_difflay(jpngr,m,i,1)=mCH4_lay_difflay(jpngr,m,i,1)+
     $           dCH4_difflay(d,i,1)

          if ((mCH4_lay_difflayold(1)+dCH4_difflay(d,i,1)) .ne. 0.0d0) then
            mCH4_lay_difflay(jpngr,m,i,2:ncvar)=
     $          (mCH4_lay_difflayold(2:ncvar)* mCH4_lay_difflayold(1)+
     $          dCH4_difflay(d,i,1)*dCH4_difflay(d,i,2:ncvar))/
     $          (mCH4_lay_difflayold(1)+dCH4_difflay(d,i,1))
          else

          endif
        else
       endif
         enddo                  ! day loop

      end if                    ! frozen(IDX)
```

```
c      ***************************************************************************
c      END OF THE YEAR
c      ***************************************************************************

---Save concentrations for next year and calculate annual fluxes-----
       return
       end subroutine methane


c//////////////////////////////////////////////////////////////////////////////
c*****************************************************************************
!-----------------------------------------------------------------------------
!
!      SUBROUTINE cnstepgas
!
!      Crank-Nicholson timestepper for temperature diffusion equation.
!      This routine performs a single timestep (of length dt) of the heat
!      diffusion equation
!
!                          6 T    6   /       6 T \
!                          --- = --- | D(z) --- |
!                          6 t    6 z \       6 z /
!
!      where here, T(z, t) is the temperature, the '6's represent partial
!      differentiation, and D(z) is the (depth-dependent) diffusion
!      constant.  The boundary conditions are a prescribed surface
!      temperature, and no heat flow at the bottom of the solution domain.
!
!      INPUT PARAMETERS:
!
!       nlayers       Total number of layers represented in temp, d and
!                     dz arrays.  Not all of the layers have to be active
!                     at one time, but this parameter is used to constrain
!                     the sizes of the depth-based arrays.
!
!       layer0        Index of the first active layer.  The diffusion
!                     equation will be solved for all layers in the range
!                     layer0 - nlayers inclusive, and the surface temperature
!                     boundary condition will be applied to the top of layer
!                     index layer0.
!
!       conc          The concentrations in each layer at the start of the
!                     timestep.
!
!       d             The diffusivities for the tracer in each layer.
!
!       dz            The thickness of each layer.
!
!       surf_conc     The surface concentration boundary condition.
!
!       dt            The timestep.
!
!
!      NOTE ON UNITS: no units are specified here for any of these
!      inputs; the only constraint on units is that the layer
!      thicknesses, the diffusion constant and the timestep should be
!      measured in consistent units.  For instance, if the layer
!      thicknesses are measured in metres, and the timestep in days, then
!      the diffusion constants should have units of m2 / day.
!
!      OUTPUT PARAMETERS
!
!       conc          The concentrations in each layer at the end of the
!                     timestep.  Only layers layer0 - nlayers will have
!                     valid concentrations values after a call to cnstep.
!                     All layers with index less than layer0 will have
!                     missing value set (a value of -1.0E35).
!
!-----------------------------------------------------------------------------

       subroutine cnstepgas(layer0, conc, Di, dz, surf_conc, dt)

       IMPLICIT NONE

#include "para.inc"
#include "soil.inc"


       ! --- PARAMETERS ---

       INTEGER layer0             ! Index of first active layer.
       REAL*8 conc(nlayers)         ! Layer concentrations.
       REAL*8 Di(nlayers)           ! Layer diffusion constants.
       REAL*8 dz(nlayers)           ! Layer thicknesses.
       REAL*8 surf_conc             ! Surface concentration forcing.
       REAL*8 dt                    ! Timestep.


       ! --- LOCAL VARIABLES ---

       ! Layer counters: note that there are two different layer counting
       ! schemes used, one for the input and output parameters (vectors of
       ! length nlayers) and one for the values used in the Crank-Nicholson
       ! solver (vectors of length active_layers)
       INTEGER layer, lidx, active_layers

       ! Diffusion constants averaged over adjacent layers.
       REAL*8 dplus, dminus
```

```
      ! Layer-dependent weighting factors in Crank-Nicholson scheme.
      REAL*8 dz_factor, Cplus, Cminus
      REAL*8 dzhere, dzminus, dzplus
      REAL*8 chere, cominus, coplus

      ! Leading diagonal, left and right subdiagonals for Crank-Nicholson
      ! matrix.
      REAL*8 diag(nlayers - layer0 + 1)
      REAL*8 left(nlayers - layer0 + 1)
      REAL*8 right(nlayers - layer0 + 1)

      ! Right hand side vector for Crank-Nicholson scheme equations.
      REAL*8 rhs(nlayers - layer0 + 1)

      ! Solution vector for Crank-Nicholson scheme equations.
      REAL*8 solution(nlayers - layer0 + 1)

      REAL*8 MISSING_VALUE
      PARAMETER (MISSING_VALUE = -9999.0d0)

      ! --- CODE STARTS HERE ---

      ! Not all layers in the input arrays are actually used.  Calculate
      ! how many layers we have to deal with here.

      active_layers = nlayers - layer0 + 1

      !-----------------------------------------------------------------
      !
      !    BUILD TRIDIAGONAL MATRIX AND KNOWN RIGHT HAND SIDE
      !

      ! End members for off-diagonal elements.
      left(1) = 0.0d0
      right(active_layers) = 0.0d0

      ! Process the active layers.
      do lidx = 1, active_layers
         ! Deal with different layer counting schemes.
        layer = lidx + layer0 - 1

         ! Calculate diffusion constants averaged over adjacent layers.
         ! The diffusion constant at the bottom layer is clamped to zero
         ! to enforce the no conc flow boundary condition there.
        if (layer .eq. nlayers) then
            dplus = 0.0d0
         else
            dplus = 0.5d0 * (Di(layer) + Di(layer + 1))
         end if
         if (layer .eq. layer0) then
            dminus = Di(layer)
         else
            dminus = 0.5d0 * (Di(layer) + Di(layer - 1))
         end if

         ! Extract sensible values to use for concentration and
         ! thickness of the current layer, the layer above and the layer
         ! below, taking account of padding layers and end cases.
         dzhere = dz(layer)
         chere = conc(layer)
         if (layer .LE. nlayers - 1) then
            dzplus = dz(layer + 1)
            coplus = conc(layer + 1)
         end if


c         if (layer .eq. 1) then
         if (layer .eq. layer0) then
            dzminus = dz(layer)
            cominus = conc(layer)
         else if (layer .LE. nlayers + 1) then
            dzminus = dz(layer - 1)
            cominus = conc(layer - 1)
         end if


         ! Calculate layer-dependent weighting factors.
         dz_factor = 0.25d0 * (dzplus + 2 * dzhere + dzminus)
         Cplus = dplus * dt / dz_factor / (dzplus + dzhere)
         Cminus = dminus * dt / dz_factor / (dzhere + dzminus)

         ! Fill in matrix diagonal and off-diagonal elements.
         ! Setting the diag(1) to 1.0 and right(1) to 0.0 means
         ! that the surface concentration is allocated to the top
         ! layer.
         if (lidx .eq. 1) then
            diag(lidx) = 1.0d0
         else
            diag(lidx) = 1.0d0 + Cplus + Cminus
         end if
         if (lidx .gt. 1.0d0) left(lidx) = -Cminus
         if (lidx .lt. active_layers) then
            if (lidx .gt. 1.0d0) then
               right(lidx) = -Cplus
            else
               right(lidx) = 0.0d0
            end if
         end if
```

```
         ! Calculate right hand side vector values.
         if (lidx .eq. 1.0d0) then
            rhs(lidx) = surf_conc
         else if (lidx .eq. active_layers) then
            rhs(lidx) = (1.0d0 - Cminus) * chere + Cminus * cominus
         else
            rhs(lidx) = (1.0d0 - Cplus - Cminus) * chere +
     $           Cplus * coplus + Cminus * cominus
         end if
       end do


      !-----------------------------------------------------------------
      !
      !   SOLVE TRIDIAGONAL SYSTEM
      !
      call tridag(active_layers, left, diag, right, rhs, solution)


      !-----------------------------------------------------------------
      !
      !   FORMAT OUTPUT PARAMETERS
      !

      ! Transfer the solution to the concentration array.
      do lidx = 1, nlayers
         if (lidx .lt. layer0) then
            conc(lidx) = MISSING_VALUE
         else
            conc(lidx) = solution(lidx - layer0 + 1)
         end if

      end do

      end subroutine cnstepgas

c subroutine: solving cubic equation for partition dissolved and gas CH4
c-------------------------------------------------------------------------------
C     Solution of a cubic equation
C     ************************************************************
C     A(0:3)       (i)  vector containing the polynomial coefficients
C     X(1:L)       (o)  results
C     L            (o)  number of valid solutions (beginning with X(1))
C     ============================================================
      SUBROUTINE CUBIC(A,X,L)
      IMPLICIT NONE

c     Arguments
      REAL*8 A(0:3),X(3), L

c     Local Vars
      REAL*8 PI, THIRD
      PARAMETER(PI=3.14159265358979 32d0,THIRD=1.d0/3.d0)
      REAL*8 U(3), W, P, Q, DIS, PHI
      INTEGER I

c     Function Value
      real*8 CBRT

C     ===== determine the degree of the polynomial =====
C
      IF (A(3).NE.0.d0) THEN
C
C       cubic problem
        W=A(2)/A(3)*THIRD
        P=(A(1)/A(3)*THIRD-W**2)**3
        Q=-.5d0*(2.d0*W**3-(A(1)*W-A(0))/A(3))
        DIS=Q**2+P
        IF (DIS.LT.0.d0) THEN
C         three real solutions!
C         Confine the argument of ACOS to the interval [-1;1]!
          PHI=ACOS(MIN(1.d0,MAX(-1.d0,Q/SQRT(-P))))
          P=2.d0*(-P)**(0.5d0*THIRD)
          DO I=1,3
            U(I)=P*COS((PHI+DBLE(2*I)*PI)*THIRD)-W
          ENDDO
          X(1)=MIN(U(1),U(2),U(3))
          X(2)=MAX(MIN(U(1),U(2)),MIN(U(1),U(3)),MIN(U(2),U(3)))
          X(3)=MAX(U(1),U(2),U(3))
          L=3
        ELSE
C     only one real solution!
          DIS=SQRT(DIS)
          X(1)=CBRT(Q+DIS)+CBRT(Q-DIS)-W
          L=1
        END IF
C
      ELSE IF (A(2).NE.0.d0) THEN
C
C     quadratic problem
        P=0.5d0*A(1)/A(2)
        DIS=P**2-A(0)/A(2)
        IF (DIS.GE.0.d0) THEN
C     two real solutions!
          X(1)=-P-SQRT(DIS)
          X(2)=-P+SQRT(DIS)
          L=2
        ELSE
```

```
C     no real solution!
          L=0
        END IF
C
      ELSE IF (A(1).NE.0.d0) THEN
C
C     linear equation
        X(1)=-A(0)/A(1)
        L=1
C
      ELSE
C       no equation
        L=0
      END IF
C
C     ==== perform one step of a newton iteration in order to minimize
C          round-off errors ====
c      DO 110 I=1,L
c        X(I)=X(I)-(A(0)+X(I)*(A(1)+X(I)*(A(2)+X(I)*A(3))))
c     *        /(A(1)+X(I)*(2.d0*A(2)+X(I)*3.d0*A(3)))
c  110 CONTINUE
      RETURN
      END

c     Function CBRT - cubic root
c     --------------------------
c
      real*8 function CBRT(Z)

      implicit none

c     Arguments
      real*8 Z

c     Local Vars
      real*8 THIRD
      parameter(THIRD=1.d0/3.d0)

c     define cubic root as statement function
      CBRT(Z)=SIGN(ABS(Z)**THIRD,Z)

      end

cc Note: The boundary conditions in the heat diffusion
cc dT/dz -> 0 at the bottom of the computational domain is
cc ok as dT in the deepest layer is in the region of 0.5 - 2
cc Watt; therefore the boundary condition T -> 0 is valid and
cc the geothermic flux small.
```

Acknowledgements

I would like to thank

- Fortunat Joos and Hubertus Fischer, my supervisors. I am very grateful for their guidance and mentorship during the last four years
- Renato Spahni for introducing me to LPJ, CH_4, Fortran, Debugging, NCL and his never ending patience and support
- Marco Steinacher, Kay Bieri and René Bleisch for solving all computer problems
- Doris Rätz and Sue Nydegger for the impeccable administration and constant encouragement
- Stefan Ritz, Johannes Rempfer, Anil Bozbiyik, Beni Stocker and Roman Schmid for providing a wonderful habitat in 014e
- Kathrin Keller, Valentina Cocco, Daiana Leuenberger, Christoph Raible, Kay Bieri, Suzanne Wyss, Shyam Ranjan and Sarah Hangartner for the good times on and off the work
- Rita Wania, Jochen Schmitt and Michael Bock for broadening my knowledge and providing data
- Thomas Stocker, Martin Grosjean and all colleagues at KUP
- My family and friends, especially my father for his endless support
- *Darko*, my best friend, beloved husband, sword master and my Prostetnic Vogon Jeltz - s'isch äben ä Mönsch uf Ärde, dass i möcht bi-n-ihm sii.

Publications

Melton, J. R., Wania, R., Hodson, E. L., Poulter, B., Ringeval, B., Spahni, R., Bohn, T., Avis, C. A., Beerling, D. J., Chen, G., Eliseev, A. V., Denisov, S. N., Hopcroft, P. O., Lettenmaier, D. P., Riley, W. J., Singarayer, J. S., Subin, Z. M., Tian, H., Zürcher, S., Brovkin, V., van Bodegom, P. M., Kleinen, T., Yu, Z. C., & Kaplan, J. O., 2013. Present state of global wetland extent and wetland methane modelling: conclusions from a model inter-comparison project (wetchimp), *Biogeosciences*, **10**(2), 753–788.

Wania, R., Melton, J. R., Hodson, E. L., Poulter, B., Ringeval, B., Spahni, R., Bohn, T., Avis, C. A., Beerling, D. J., Chen, G., Eliseev, P., Hopcroft, Riley, W., , Subin, Z. M., Tian, H., van Bodegom, P., Kleinen, T., Yu, Z., Singarayer, J., Zürcher, S., Lettenmaier, D. P., Beerling, D., Denisov, S., Prigent, C., Papa, F., & Kaplan, J. O., 2013. Present state of global wetland extent and wetland methane modelling: methodology of a model inter-comparison project (wetchimp), *Geosci. Model Development*, **6**, 617–641.

Zürcher, S., Spahni, R., Joos, F., Steinacher, M., & Fischer, H., 2013. Impact of an abrupt cooling event on interglacial methane emissions in northern peatlands, *Biogeosciences*, **10**, 1963–1981.

Erklärung

gemäss Art. 28 Abs. 2 RSL 05

Name/Vorname:	Zürcher Sibylle
Matrikelnummer:	02–906–725
Studiengang:	Physik
	Bachelor ☐ Master ☐ Dissertation ☒
Titel der Arbeit:	Methane Emissions and Isotopes of Northern Peatlands in a Global Vegetation Model
Leiter der Arbeit:	Prof. Dr. Fortunat Joos und Prof. Dr. Hubertus Fischer

Ich erkläre hiermit, dass ich diese Arbeit selbständig verfasst und keine anderen als die angegebenen Quellen benutzt habe. Alle Stellen, die wörtlich oder sinngemäss aus Quellen entnommen wurden, habe ich als solche gekennzeichnet. Mir ist bekannt, dass andernfalls der Senat gemäss Artikel 36 Absatz 1 Buchstabe o des Gesetzes vom 5. September 1996 über die Universität zum Entzug des auf Grund dieser Arbeit verliehenen Titels berechtigt ist.

Bern, 27. August 2013

Curriculum vitæ

Personal Data

Name	Sibylle Zürcher
Date of birth	September 10, 1982
Place of birth	Trubschachen (BE), Switzerland

Education

2009–2013	Ph. D. thesis at the division of Climate and Environmental Physics, Physics Institute, University of Bern, Switzerland (Thesis advisors: Prof. Dr. Fortunat Joos and Prof. Dr. Hubertus Fischer)
2008	Diploma thesis in Physics, ETH Zürich (Thesis advisor: Prof. Dr. G. Dissertori)
2002–2008	Studies in Physics at the ETH Zürich
1994–2002	Matura Type B, Kantonsschule Solothurn
1988–1994	Primary School in Luterbach (SO)

Attended Events

April 2009	ETH and University of Bern exchange meeting (oral presentation)
May 2009	EGU, Vienna, Austria (poster presentation)
December 2009	LPJ Development Meeting, Bern, Switzerland (oral presentation)
October 2011	WETCHIMP workshop, Hamburg, Germany
June 2012	LPJ Development Meeting, Bern, Switzerland